Adsorption and Desorption of Gases in Porous Silicon

PATHMA V.GUNASINGAM

School of Engineering Systems

Middlesex University

August 2001

A thesis submitted in partial fulfilment of the requirements of

Middlesex University for the degree of Doctor of Philosophy

Synopsis

This research was undertaken to provide an understanding of the nature, origin and desorption mechanism of species found on the porous silicon (PS) surface and the changes that occur when PS is stored under varying conditions.

The PS used in this work was produced from p^-, high-resistivity FZ c-Si substrates. Three types of commonly used HF-based electrolytes were chosen for anodisation, under the same process conditions. With the resulting samples, temperature programmed desorption (TPD) coupled with mass spectrometry were used to identify species liberated at different temperatures. FTIR was also used to investigate the nature of surface species on PS and hence to infer how these give rise to the observed volatile products. After various modifications, the TPD system with the custom-made heating unit and the appropriate methodology were developed to suit the present work.

Freshly anodised PS in the vacuum chamber at room temperatures gave somewhat enhanced peaks due to air components (O^+, N_2^+ and/or CO^+, O_2^+ and CO_2^+) and, most significantly, an increase in F-containing species (e.g. F^+), derived from the electrolyte.

On heating, the main desorbed species were found be hydrogen, silane, $Si\text{-}F_x$ species, and $H_x\text{-}F_x$ species. TPD spectra for hydrogen showed two peak maxima with a "hump". This implies two types of hydrogen environments; these were assigned as Si-H (lower temperature peak) and $Si\text{-}H_2$ (higher temperature peak) species on the PS surface. The temperature difference between the two peaks was similar (~100K) in all three cases. This shows that hydrogen desorption occurs similarly from PS prepared using the three different electrolytes. It also suggests that hydrogen adsorption during PS formation occurs analogously in the three electrolytes.

Silane was observed to desorb at 575K. It is proposed that this comes from $-SiH_3$ groups on the PS surface, possibly after reaction with sorbed water. A mechanism is suggested. In contrast, desorption of $Si\text{-}F_x$ species was found to be sensitive to the nature of the electrolyte. The lower temperature peaks from the TPD experiments are assigned to H_2SiF_6, SiF_4 and perhaps H_2SiF_2 (by-products from anodisation) sorbed on PS. They are

held relatively weakly by electrostatic and/or van der Waals forces. The higher temperature peak assigned to SiF_3^+ may be explained in terms of migration of F atoms followed by Si-SiF_3 bond breakage. The various H_x-F_y products derive from species present in the HF electrolytes.

To investigate changes in PS under typical storage conditions, samples were kept in (i) a blue wafer box, (ii) a screw-top white box and (iii) a similar box in a vacuum desiccator. The PS was then analysed by FTIR after various time intervals. After one month, only PS stored under condition (iii) was unchanged. The other samples showed evidence of oxidation, attributed to hydrolysis, formation of silanol (SiO-H) species, and back-bond oxidation of Si-H_x groups. Further ageing revealed inclusion of C-H species on PS.

This work is a contribution to understanding of PS behaviour, and is relevant to its applications in electronic devices and sensors.

Acknowledgements

I would like to express my thanks and gratitude to Professor Bernard Aylett for his advice and never-ending support, as well as for tirelessly reading and editing this work. His encouraging e-mails and phone calls particularly during the times when the progress was relatively slow served as a remarkable source of stimulation.

My thanks also go to Middlesex University for allowing me to do a PhD programme of study and giving me extended time to complete this work.

I would like to thank John Keen for the provision of grant, and Drs. Leigh Canham and Armando Loni at DERA, Malvern UK, for their support during this work.

Professor John Butcher acted as my Director of Studies until his retirement, giving me all the necessary support I needed; Keith Pitt in his role as my supervisor made valuable suggestions and corrections; Professor George Goldspink who succeeded John Butcher as my Director of Studies has been very understanding of the problems I faced from time to time; Professor Tony White, School of Engineering System, sorted out many of the administrative problems caused by my redeployment. Thank you all for your support and encouragement.

My thanks are also due to my colleagues at CCSS, Marva Gabbidon, Brian Fuller, Dervish Mono, Stuart Scattergood, Simon Hinks, Gwo-Huey Ling, Robert Crouch and those from the Helpdesk for their encouragement, solving software problems and having smiling faces whenever I discussed about my PhD work.

Finally, I want to thank my husband for having been a constant source of inspiration to me and my darling sons, Aran and Aayan, for their much needed computer-based support and understanding of the priority this work has received for some years over many other things at home.

Contents

Table of Figures

List of Tables

Abbreviations

AES	Auger Electron Spectroscopy
CMOS	Complementary Metal Oxide Semiconductor
c-Si	Crystalline silicon
CZ	Czochralski mehod
EL	Electroluminescence
EPR	Electron Paramagnetic Resonance
ERDA	Elastic Recoil Detection Analysis
FIPOS	Full Isolation by Porous Oxidised Silicon
FTEMIRS	Fourier Transform Electron Modulated Infrared Specroscopy
FTIR	Fourier Transform Infrared Specroscopy
FZ	Float Zone method
HF	Hydrofluoric acid
HREELS	High Resolution Electron Energy Loss Spectroscopy
HRSEM	High Resolution Scanning Electron Microscopy
IPOS	Insulation by Porous Oxidised Silicon
ITO	Indium Tin Oxide
LED	Light Emitting Diodes
LEED	Low Energy Electron Diffraction
LOCOS	Local Oxidation of Silicon
MOS	Metal Oxide Semiconductor
NRA	Nuclear Reaction Analysis
PANI	Polyaniline
PIGME	Particle Induced Gamma Emission
PL	Photoluminescence
PS	Porous Silicon
RBS	Rutherford Backscattering Spectroscopy
RIE	Reactive Ion Etching
SEM	Scanning Electron Microscopy
SIMS	Secondary Ion Mass Spectrometry
SOI	Silicon On Insulator
SRAM	Static Random Access Memory
TEM	Transmission Electron Microscopy
TPD	Temperature Programmed Desorption spectroscopy
XPS	X-ray Photoelectron Spectroscopy
XRD	X-ray Diffraction

Chapter 1 Introduction

Porous silicon (PS) is an important and versatile electronic material in microelectronic fabrication technology. It is produced by electrochemical etching of crystalline silicon (c-Si) in hydrofluoric acid (HF) based electrolytes. The discovery of PS dates back to 1956, when Uhlir (1956) was electrolytically polishing germanium and silicon to eliminate the damage produced by mechanical polishing. He found that, under certain conditions of electrolysis below the voltage required for electropolishing, there was a localised anodic dissolution of the substrate which led to the formation of porous silicon and germanium. The research into this material has come a long way since Uhlir's discovery and now covers the areas of formation mechanisms, material characterisation and the realisation of devices.

Applications of this material are various. Because of its very thin open microstructure, the material can be oxidised throughout the whole pore volume independently of layer thickness, allowing the formation of thick silicon dioxide (SiO_2) layers unlike the case of c-Si where the oxide formation is diffusion limited. The low temperature oxidation of PS (Tsao 1987, Benjamin et al 1986, Imai et al 1984, Unagami 1980, Yon et al 1987) and the electrochemical conversion of PS to oxide (Yamana et al 1990) has already been utilised in Silicon On Insulator (SOI) and Fully Isolated Porous Oxidised Silicon (FIPOS) processes, although commercial devices are yet to come. Silicon displacement reactions in the PS network have been used to produce buried conductor regions (Yamana et al 1990, Ito 1989). SOI structures can be obtained by oxidising buried layers of PS which can be formed selectively under silicon islands of low doping levels because of the strong doping dependence of the anodisation process. Because of its extreme reactivity, due to the large surface area of the pores, PS has been used as a useful sacrificial material in micromachining processes for the production of sensors (Lang et al 1994a, 1994b, 1995)

Crystalline silicon, which is the basis for the majority of integrated electronic devices, is extremely inefficient in emitting light under electrical or optical excitation as it has a relatively small ($\approx$1.1 eV) and indirect bandgap. In 1990, Canham demonstrated tunable strong visible photoluminescence in porous silicon at room temperature. Recent data shows that the PL peak can be tuned right from the bulk Si bandgap in the near infrared

through the visible range to 400 nm in the violet. Since 1990, there has been a rising level of research work focussed on the understanding of the origin of photoluminescence (PL) in PS, but none so far provides a complete picture of the mechanism of light emission.

This research was funded by Defence Research Agency (DRA) under the contract number 2249/001/ RSRE to provide an understanding of the nature, origin and mechanisms of the adsorbed "foreign" species that are found in the pores and hence the "ageing" mechanism.

Freshly prepared PS is in a metastable condition and is very reactive towards the gases in the ambient air. This produces slow oxidation of the pore surface (aging process) as well as adsorption of gases on to the dangling bonds of the surface silicon atoms. As a result, most of the properties of PS, including luminescence, degrade slowly with time (the ageing phenomenon). Furthermore, luminescence peak wavelength shift is observed with any change in composition of the anodising electrolyte (Canham 1990). These factors point to the importance of the surface chemistry of PS in the luminescence processes.

1.1 Objectives

An understanding of the surface chemistry of freshly anodised PS and the ageing process of PS is very important in predicting the behaviour of the devices which are to be realised in PS as well as in the understanding of the PL mechanism. The current project was undertaken to investigate the gas adsorption processes on the surface of the pores of PS. Time-varient adsorption studies also formed a part of this work. Many, mainly surface analytical techniques, have been used in analysing the composition of PS and H,C,O,F have been found to be the main "impurity" elements.

A review of the compositional analyses of PS is presented in section 2.4. Most of the techniques used sputtering techniques and analysed the sputtered species. These analytical results provide mainly elemental information. There is a limited amount of information available on the nature of the bonding of the various gaseous species to the PS surface using Raman and FTIR techniques. The pore walls of PS adsorb the gaseous species from the environment it is placed in and the ions from the electrolyte that is used

for its preparation. It was intended to investigate the adsorbate-substrate system using Temperature Programmed Desorption Spectroscopy (TPD) and FTIR in a detailed manner with the following objectives.

a) The modification of the anodising procedures and the storage technique for PS samples
b) Temperature Programmed Desorption Spectroscopic analysis of the porous silicon sample to provide information on the binding energies and structure of adsorbates and adsorption sites. The adsorbates in the case of PS are the "contaminants" formed from various gaseous species; and
c) Fourier Transform Infrared Spectroscopic (FTIR) analysis to be used as a complementary technique to support the TPD findings, as well as to investigate the bonding characteristics of the gaseous species that are found in PS.

Chapter 2 Literature Review

Research into PS has received considerable attention for the last ten years since the discovery that PS structures emit visible photoluminescence (PL) (Canham, 1990). At present, most of the solid state light emitters such as LEDs and lasers are made from direct bandgap materials such as GaAs/AlGaAs. Direct integration of these materials with silicon electronics is extremely difficult because of the incompatibility of material characteristics and processing requirements.

PS is a potential candidate for many applications, since it is found to retain the crystalline characteristics of bulk silicon and it is easier to integrate PS with silicon electronic devices. However, before PS can be successfully used for commercial devices, a better understanding of the material is needed. Numerous papers have been published on its preparation, material characterisation and application.

This chapter reviews the areas of research on PS which are relevant to the present work and will cover the following areas:

a) Formation mechanisms
b) Material properties
c) Compositional analysis
d) Applications

2.1.Formation mechanism of PS

PS is prepared by anodic electrochemical etching of single crystal silicon (c-Si) in HF based electrolytes. The formation of PS depends critically on the doping level of c-Si and the electrochemical parameters, mainly HF concentration and current density applied. By controlling the parameters it is possible to create reproducible structures with pore diameters ranging from less than 2nm to greater than 10^3nm and densities from near bulk value of 2.33g cm^{-3} to less than 0.2g.cm^{-3}. The porous layers formed from

c-Si exhibit surface areas in the range of 200-250m^2 cm^{-3} for n^+ and p^+ substrates and of the order of 600m^2 cm^{-3} for p^- wafers (Herino 1987).

Beale et al (1985) have characterised PS layers obtained from different substrates and using a wide range of anodisation conditions. The layers obtained from heavily doped silicon (< 0.05Ω.cm) either p^+ or n^+, have dentritic-like pores with the preferential orientation normal to the surface and a pore diameter is in the range of 4-12 nm. For the lightly doped Si, the situation is different. The growth of the pores is isotropic whereas that in n^+ or p^+ are anisotropic. In the case of p^- silicon, the porous layer consists of random arrays of very small voids (~ 3 nm diameter) and is microporous.

2.1.1. Silicon Dissolution Chemistry

There are two separate questions to be answered in the formation of PS layers. The first one concerns the anodic dissolution of silicon in an HF solution. The second is to explain why this dissolution becomes localised under certain conditions, leading to the formation of the porous structure.

The exact dissolution process of silicon atoms during anodisation is still not clear, although it is accepted generally that holes are required in the initial step for both electropolishing and pore formation (Memming et al 1966, Searson et al 1990). This means that, for n-type silicon, significant dissolution occurs only under illumination, high fields or other hole generation conditions.

During pore formation, only two of the four available electrons of a silicon atom participate in the direct charge transfer process. It has been shown that, during pore formation, hydrogen gas evolves in a 2 : 1 atomic ratio to silicon (Memming et al 1966, Pickering et al 1984). Current efficiencies have been measured at 2 electrons per dissolved silicon atom during pore formation (Beale et al 1985, Memming et al 1983). The overall reaction can be written as ,

$Si + 2HF + 2h^+ \rightarrow SiF_2 + 2H^+$ (h^+ - defined as positive hole)

The subsequent reactions can be written as,

$SiF_2 + 4F^- \rightarrow SiF_6^{2-} + 2e^-$

$2H^+ + 2e^- \rightarrow H_2 \uparrow$

Memming and Schwandt (1966) suggested a number of subsequent chemical disproportionation reactions occur in which the unstable SiF_2 species is transformed into tetravalent H_2SiF_6 and molecular hydrogen.

$2SiF_2 + 2F^- \rightarrow Si + SiF_6^{2-}$ (Disproportionation reaction)

This mechanism assumes that the silicon surface is fully fluorinated at the beginning of the reaction. However, it has been shown by Ito et al (1988), using an infrared technique, that anodised PS is saturated with Si-H bonds. Another mechanism was put forward by Lehmann and Gösele (1991), which assumes that the silicon surface fluctuates between hydride and fluoride coverage at each pair of electron / hole exchanges. There are various models presented in the literature and which was well reviewed by Smith and Collins (1992).

It is clear that the formation of PS is an extremely complicated process involving many chemical and electrochemical reactions, which occur simultaneously. More work is required to understand the complex nature of the dissolution process.

2.1.1. Localised pore formation

It is very important to understand why anodic dissolution should produce localised pore formation, leading to the formation of porous structures displaying very different morphologies.

Unigami (1980) proposed that PS results from the formation of insoluble silicates which passivate the pore walls. However, such a phenomenon can hardly explain the difference in microstructures observed when Si doping is changed. Theunissen (1972) proposed that PS formation in n-Si results from the reverse bias breakdown resulting from high fields concentrated at the pore tips. Dubin (1992) proposed another model based on silicon dissolution taking place at active impurity sites which are responsible for local electric field enhancement resulting in the breakdown of the depletion charge layer and the initiation of pores.

So far, few models have been proposed to explain the differences in the microstructures of PS from different types of silicon substrate. Three of the most probable models are reviewed here. They are,

(a) the Beale model

(b) the Diffusion limited model

(c) the Quantum-based model

Presently, the Beale model is the accepted standard for PS formation. Several reports, however, have noted some inconsistencies in the Beale model (Smith et al 1990, Zhang et al 1989, Bomcil et al 1989)

The Beale model

This proposes that a semiconductor depletion layer is responsible for controlling the electric field density in both n- and p-type material (Beale 1985). There is a large number of experimental facts indicating that at equilibrium the silicon surface in contact with an HF solution is depleted. Thus a Schottky barrier must exist at the interface. At the beginning of the reaction, the surface potential is modulated by ionic absorption at the silicon surface and this can cause a large difference in the current flow at the interface. The interface can no longer be considered as planar, but more or less spherical. In such a case, the surface potential, which is inversely proportional to the radius of curvature, would be higher at the depressions. Therefore the current density and the dissolution rate will be locally enhanced, leading to the formation of pores.

Diffusion Limited model

The diffusion limited model, proposed by Smith and co-workers (1988, 1990) explains pore formation as resulting from the diffusion of an electroactive species (holes or electrons) to or from the silicon surface. During pore formation, a hole diffuses to the silicon surface and removes an electron from a silicon atom (oxidation). Alternatively, the process can be described as an injected electron diffusing away from the silicon. The nature of the random walk indicates the pore tips as the most likely contact sites for a particle diffusing from the bulk semiconductor (Smith, 1988) and provides a similar selective dissolution at the surface irregularities as does the Beale's model (Beale 1985).

The diffusion-limited model avoids a number of uncomfortable assumptions, such as the diode model, associated with Beale's model and provides a simple understanding of pore formation in terms of basic semiconductor electrochemistry. The computer simulation of PS using the diffusion limited model shows a very good resemblance to TEM information (Figure 2-1) for both n- and p-type PS, providing strong verification of the model's validity.

Quantum Model

This model was proposed by the Lehmann group (1991) and Föll (1991) to explain pore formation in terms of increasing bandgap due to quantum charge confinement within the small dimensions of the silicon "wires" formed in PS. The increased bandgap causes a decrease in the concentration of the mobile carriers and creates a depletion region similar to the depletion layer proposed by the Beale group (1985)

The average spacing between the pores in p-type silicon is of the order of magnitude where quantum effects for electrons are expected, i.e. tens of Å. Although quantum effects are very likely for p^- type silicon, it is unlikely that the same effects regulate pore formation in p^+- or n-Si where the interpore dimensions can be as high as several micrometres.

It is clear that the formation of PS is an extremely complicated process involving chemical, electrochemical and physical processes. Both Beale's and the diffusion-limited models predict a fractal pore structure which is a collection of "pores on top of pores" within certain upper and lower bounds. The upper bound for the pore dimension is determined by the depletion or diffusion length depending on the model used. The lower bound for the pore dimensions is of the quantum dimensions as outlined in quantum model of pore formation.

None of the above models deals with the physical aspects of pore formation and no account is taken of the specific surface chemistries that give rise to the dissolution chemistries.

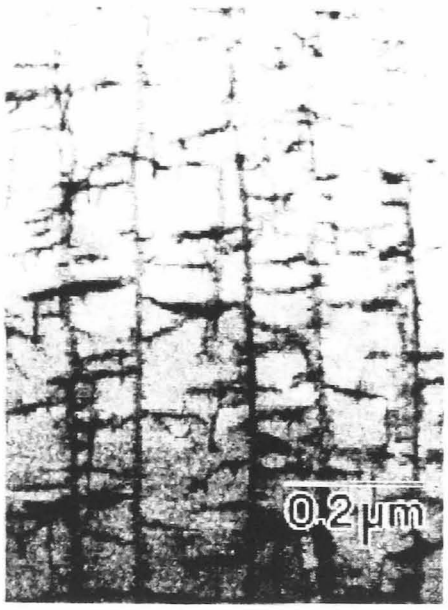

(a)

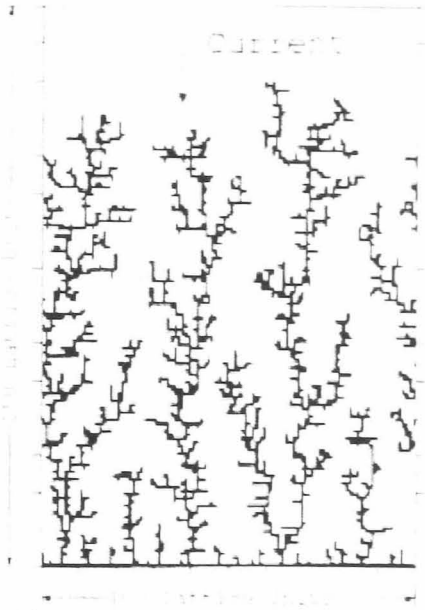

(b)

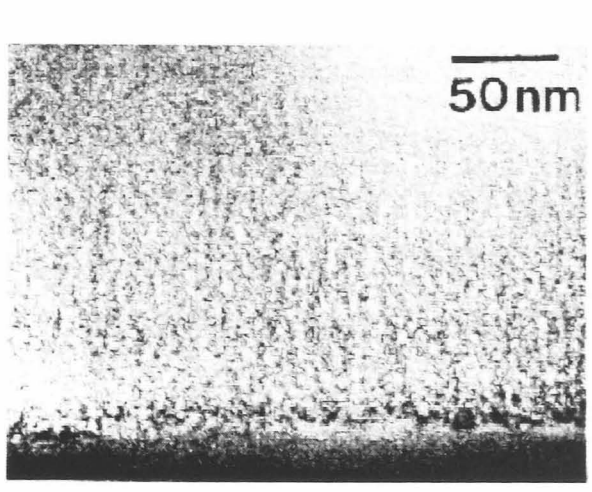

(a)

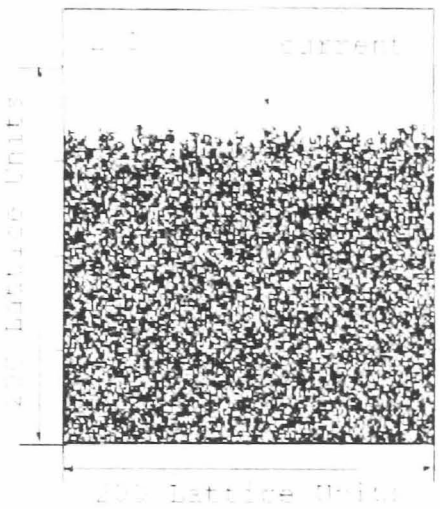

(b)

FIGURE 2- 1 Comparison of diffusion-limited models to PS

(top) high resistive c-Si

(bottom) low resistive c-Si

The figures marked (a) are TEM sections from PS samples and those marked (b) are the respective simulated models (Smith et al., 1988)

2.2.Material Properties of PS

This section will review

a) porous microstructures,

b) crystalline properties and

c) the heating effects of PS.

2.2.1. Porosity and pore size of PS

The formation of PS depends critically on the type and doping level of the Si substrate (refer to section 2.1) as well as the electrochemical parameters such as HF concentration and current densities (Beale et al 1985, Bomchill et al 1988). For a given HF-based electrolyte, the average porosity increases to a limit with current density and electropolishing occurs beyond a certain value of current density (Beale et al 1985, Bomchil et al 1989). An increase in HF concentration results in a decrease of the porosity (Herino 1987). This was found experimentally by comparing gravimetric porosity as a function HF concentration.

Herino et al (1987) used a gas adsorption isotherm technique to establish the surface area, pore size and pore distribution of the PS layer. The PS film on heavily doped silicon exhibits a specific surface area in the range of $200m^2cm^{-3,}$ while the PS layer on lightly doped p- Si has an area of the order of $600m^2cm^{-3}$. These results agree with the IUPAC convention for mesoporous structures (~2 nm -50 nm) observed in n^+ and p^+ Si wafers and less with the microporous (<2 nm) structures observed with p^- Si. This is due to the fact that this technique requires a minimum pore volume for an adequate accuracy and therefore a layer of PS several microns thick is needed. For this reason, this method is not applicable to very small pores of radii below 2 nm.

The influence of the anodisation time on some structural characteristics such as dissolved mass, maximum porous layer thickness, porosity and crystalline size were investigated with p-type silicon (Pascualet al. 2002). Equations based on pore nucleation and growth processes explain well the evolution of the maximum layer thickness with anodisation time. It was shown that chemical dissolution of the porous layer during the anodisation must be taken into account in order correct some of the experimental data.

Transmission electron microscopy (TEM) and high resolution scanning microcopy (HRSEM) were used to study the structural properties of PS layers (Beale et al 1985, Gonchond et al 1991). In p^+ or n^+type Si, the PS films consisted of many large voids running perpendicular to the surface. In addition, there were small "buds" on the sides of the pores and occasional branches emerged at wide angles to the main pores. In lightly doped p^- or n^- films, the pore structures were found to consist of random arrays of fine holes markedly different from the heavily doped structure. As the electrolyte must be able to penetrate the structures for the removal of Si to occur, it is evident that the pores must be continuous from the surface. Also, the Beale group (1985) reported that the interface between the PS layer and the silicon substrate is well defined and was locally planar on the scale of the pore dimensions for films formed on both heavily and lightly doped substrates.

2.2.2. Crystalline Properties of PS

Crystalline properties of PS have been investigated by means of X-ray diffraction techniques (XRD) (Barla et al 1984, Sugiyama et al 1990, Young et al 1985,) and Raman spectroscopy (Goodes et al 1988, Gregora et al 1994, Jardin et al 1995, Zhang et al 1994)

.

XRD Analysis

Barla et al (1984) used double crystal diffractometry to measure the lattice parameter of c-Si and PS on 0.01Ω cm p-type Si (100). Their findings are summarised as follows:

a) The crystalline quality of PS depends on the porosity. For porosities less than 35%, the crystalline quality of the PS is very good and similar to that of silicon substrate. When the porosity increases, the crystalline quality decreases.
b) The lattice parameter increases with the porosity and the mean pore radius. It appears that the lattice expansion is a genuine effect and not an artefact resulting from stress caused by lattice misfit between the PS layer and the Si. Another explanation is that the lattice expansion results from an intrinsic effect of a silicon network consisting of small particles. In fact PS could be considered as an assembly of small particles (nanocrystallites) diffracting coherently.

Young et al (1985) also used a double crystal diffraction method to measure the changes in lattice parameter on anodisation. The X-ray diffraction results for the PS layers formed on heavily doped and lightly doped Si substrates were found to differ significantly. They have reported that the crystal lattice of a porous layer was tetragonally distorted and the change in lattice spacing of the PS layer was about ten times smaller on the heavily doped wafers than on the lightly doped wafers. The samples analysed showed no systematic dependence of doping levels on the lattice spacing or on the anodising conditions. It was concluded that the main factor responsible for the interplanar spacing is the type of PS which in turn depends on the substrate dopant concentration.

The role of oxygen in the increase of lattice parameter was considered by Young et al 1985. Calculations of the order of magnitude of the oxidation induced stress have been made and it was found to be sufficient to cause the observed changes in lattice parameter. The greater surface area of the lightly doped PS results in greater oxygen incorporation and is consistent with the greater observed increase in the lattice parameter.

Sugiyama et al (1989a, 1989b, 1990) studied the microstructure of PS layers produced on p-Si wafers with various resistivities using X-ray multicrystal diffractometry, TEM, IR spectroscopy and gas adsorption methods. The summary of their finding is as follows.

a) The crystalline quality of as-prepared PS is inferior to that of c-Si, but is not strongly degraded. The lattice spacing of PS layer was found to be slightly larger than that of c-Si. This was due to Si-Si becomes Si-O-Si to some extent during the anodisation/storage processess.
b) The lattice distortion of as-prepared PS was shown (Sugiyama et al 1990) to be related to the difference of pore morphology, which in turn can be related to the dopant concentration as shown by the Young group (1985). The degradation of the crystalline quality of the PS layer takes place secondarily as a result of oxidation of the pore surfaces. This is due to the compressive stress created by the formation of the native oxide.

c) The crystal lattice of a PS layer is distorted elastically in the direction normal to the wafer surface without any regard to its crystal orientation.

Sugiyama and co-workers ((1990) have shown also that lattice contraction takes place as a result of desorption of hydrogen during heating as most of the PS surface is covered with H atoms. Their samples were heated stepwise in 50°C intervals and the lattice spacing was measured. The lattice contraction took place at about 350°C. Above this temperature, the wafer bending was found to reverse, indicating that the PS layer was under compression before annealing. It was confirmed (Sugiyama et al, 1989) with an IR technique that the number of Si-H bonds decreases with annealing and Si-O related absorption increased with temperature. Figure 2-2 illustrates the effects of annealing on a PS layer. Their conclusion was that the distortion of the PS layer is influenced strongly by the chemisorbed H-atoms as well as by pore morphology and that the crystalline quality of the layer is degraded as a result of oxidation of the pore walls.

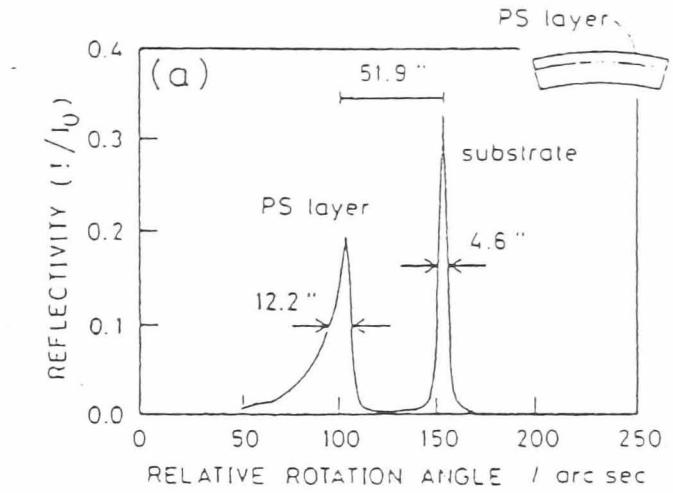

(a)

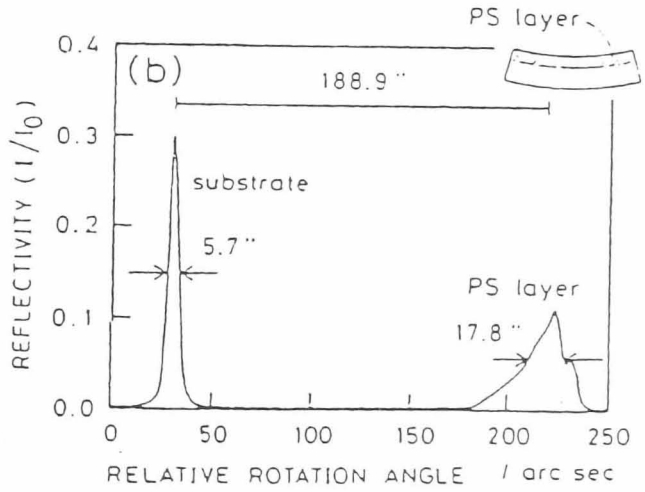

(b)

FIGURE 2- 2 Effects of thermal annealing of PS using XRD analysis

(Relative rotation angle/arc sec.is a measure of angular separation between 2 peaks to determine the degree of wafer bending)

a) **Lattice contraction at about 350°C**
b) **Lattice expansion above 350°C**
(Sugiyama et al., 1989)

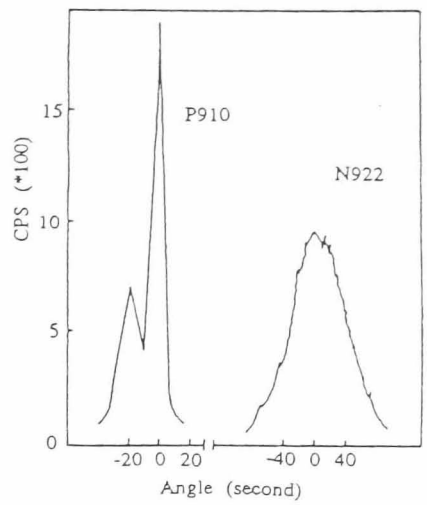

FIGURE 2- 3 XRD showing the effects of electrolytes on the crystallinity of PS P910 – 1:1 HF:C_2H_5OH and N922 – 9:1 HF:C_2H_5OH (Qing-Shan Li, 1995)

The Qing-Shan Li group (1995) have shown using an X-ray diffraction technique, that the electrolyte concentration has an effect on the crystalline properties of PS. Figure 2-3 shows X-ray diffraction rocking curves for PS at room temperature in HF:ethanol in 1:1 ratio (P910) and in HF: ethanol in 9:1 ratio (N922). P910 shows, besides the main peak which is due to c-Si, a small peak with a small angle which corresponds to a very small lattice expansion. N922 shows a broad angle which originates from the reduction of the lattice parameter.

A high resolution X-ray technique was used to examine the variations in the lattice parameter of PS formed on p-type Si, produced by pentane wetting and vapour adsorption (Dolino et al 1995). The interactions between PS and liquids play a key role during the formation of the PS layer itself. For example PS layers of high porosity (90%) often break during drying under the action of capillary forces. A homogeneous lattice expansion is observed during wetting, while for vapour adsorption there is first a lattice contraction, followed by a lattice expansion. This was explained by the variation in surface stress and the existence of van der Waals interactions between the pore walls. The presence of a thin adsorbed liquid film increases the attractive forces.

Raman spectroscopy

Raman spectroscopy is one of the most suitable methods for investigating and characterising semiconductor microstructures. In c-Si, an optical phonon is observed in the centre of the Brillouin zone with an energy of 520 cm^{-1}. This is a consequence of the conservation of quasimomentum in crystals. Phonons in nanocrystallites, however, are localised and this induces a shift in the Raman signal to lower energies accompanied by a broadening effect. This technique is very useful for investigating crystallinity, and the dimensions of microcrystallites in PS.

Goodes et al (1988) obtained data for PS from degenerate (0.01Ωcm) and non-degenerate (5 and 25Ωcm) p-type Si. They associated the observed Raman features with an amorphous component in the PS film, although a similar spectrum may be obtained from the interface region between the silicon pores and their oxides.

Shu-Lin Zhang et al (1994) analysed p-type PS samples in the region of 50-1050 cm^{-1}. Raman spectra from free standing PS films and PS films on silicon substrate were compared. In addition to the first order Raman peak at 510cm^{-1} associated with optical phonons, additional peaks were observed at 147, 632 and 956 cm^{-1}. These were identified with the PS layer itself. No substantial amorphous silicon (a-Si) component in p-type PS was found confirming the results shown for the first order Raman investigation of PS by Goodes et al (1988).

Jardin et al (1995) estimated the dimensions of the silicon crystallites from the shift and the half width of the one-phonon Raman peak detected near 520 cm^{-1} for Si. Assuming columnar morphology for the Si crystallites, an average diameter of 4-5nm was estimated from the shift value. The weak bands observed at 150, 310, 480 and 630 cm^{-1} were attributed to a-Si. The dimensions of the Si crystallites were found to be reduced when the porosity of the layer was increased. The a-Si contribution was not observed for PS on n-Si and the crystallites were deduced from the Raman spectra to be larger than 10nm.

Sasaki et. al. (1994) carried out Raman scattering on PS samples anodised in electrolytes of various HF concentrations. The size of the Si particle (or column) was estimated to be a few nanometers for samples anodised with solutions of HF : H_2O in

the ratio of 1:1 and it decreased with decrease in the HF concentration. No silicon nanostructures were detected from Raman data for the case of HF : H_2O : C_2H_5OH in the ratio of 1 : 1 : 8.

Gregora et al (1994) used p^- (1.0 Ωcm) and p^+ (~ 0.01 Ωcm) PS for their measurements. A sizeable fraction of a highly disordered a-Si phase in the p-type sample was detected. Also, it was found that the frequency shift and the line shape of the Raman peak in PS (p^+) corresponded to an average crystallite diameter of 4-5 nm.

Kozlowski et al (1994) have shown that there are two types of PS layers which can be distinguished by the existence of different Raman spectra. The top layer of the PS film may consist of oxidised nanoparticles with constricted wires (type I) as the current paths which were assumed to be the origin of electroluminescence(EL). Type II PS consists only of silicon nanocrystallites and no oxide and is PL active but with no EL properties. The nanocrystals were associated with Raman peak or shoulder at 510 - 513 cm^{-1} and a half width of 10 - 40 cm^{-1}. It was observed (Kozlowski et al 1992) that oxidation deactivates the nanocrystal structure.

This phenomenon was also observed by Münder and co-workers (1993). It was shown that the laser beam which is the source used in Raman spectroscopy should be kept at about 1 mW power to avoid local heating. During microRaman measurements, the sample temperature in the laser focused area can rise by a few hundred Kelvin depending on the laser power, on the topology and on the porosity of the sample. It was observed that at moderate temperatures (< 350°C) hydrogen starts to desorb and leads to destabilisation of pores and a reduction in the number of nanocrystals with diameters below 3 nm. In the temperature range of 450 - 500°C the PS loses its nanocrystalline nature and a-Si is formed. Also, it was shown that for the PS prepared from p^+ Si, the diameter of the nanocrystals was found to be 2.5 nm and about 4 nm and for p^- Si the nanocrystals were found to be smaller than 3 nm.

Feng et al (1994) used PS membranes for Raman studies. These were prepared from p^+ Si (111) with 0.02-0.04 Ωcm resistivities, anodised in electrolyte containing HNO_3, HF and CH_3COOH in the ratio of 5 : 3 : 3 respectively. Their Raman features are markedly distinct from those of crystalline, microcrystalline and a-Si

2.3. Thermal effects of PS

It is very important to know the effects of heating on PS as it is a part of the processing steps in the applications of PS in SOI technology (Zhao 1990), and sensor technologies (Steiner 1995). A review of the applications of PS is presented in the following sections SOI islands are produced from PS in two different ways

i. Devices are made in islands of the original Si wafer and the surrounding areas are selectively anodised and oxidised ;
ii. The second method is to grow an epitaxial layer over PS. The required islands can be produced in the epilayer by photolithographic techniques. The PS can be selectively oxidised.

Both oxidation of PS and epitaxial growth of silicon over PS involve thermal treatment of PS. The heating effects of PS have been studied by techniques such as X-ray diffraction (Labunov et al 1986, 1987), scanning electron microscopy (SEM) (Unagami et al 1978, 1980, Herino et al, 1984), Raman spectroscopy (Münder et al, 1993) and thermal desorption studies (Gupta et al, 1988a, 1988b).

The structure and lattice deformation of PS layers with high temperature treatment in hydrogen ambient at 900 - 1200°C were investigated. It was found that heat treatment at temperatures between 300 - 900°C induces a slight change in the PS structure (Unagami 1978). Labunov et al (1986) have shown that heat treatment at 1000 - 1200°C leads to a significant decrease in the specific surface area to $10m^2\ cm^{-3}$.

2.3.1. X-ray Diffraction Methods

Double crystal X-ray diffractometry was used (Labunov, 1987) to measure the lattice parameter of as-anodised PS of different thickness as well as high temperature treated PS samples of different thickness. The observations can be summarised as follows.

a) When the thickness of PS increases, the intensity of the PS peak increases but the position of the peaks is changed significantly (Figure 2-4). Also, the relative deformation Z_s, which is $\Delta a/a$, where a is the lattice constant and Δa is the change in a, increases with thickness of the PS layer. It was observed that there is an additional

peak shift towards smaller reflection angles. This is assumed to be connected with the decrease in porous volume density in the thickness direction.

b) After the heat treatment, an additional peak was found at larger reflection angle i.e. on the right hand side of the main Si peaks (Figure 2-5). This is evidence of the change of sign of the stress as well as a decrease in the lattice parameter with respect to unanodised silicon.

Labunov et al (1987) explained the structural changes during thermal treatment by a model based on the sintering process in powdered substances. (Figure 2-6). The spherical shape of the pores is due to "spheroidisation" - flattening of various protrusions to produce spherical shapes that provides the smallest surface free energy at a given pore volume. The real process of PS sintering is complicated by the presence of gas in the pores which may hinder their contraction. The formation of cavities instead of channels may be one of the reasons for the slowness of thermal oxidation of PS at high temperature (Unagami, 1978).

Muller et al. (2000) have shown the changes in the morphology of PS during thermal treatment. A 2-D model was used to simulate the annealing behaviour of PS. This model explained the closing of pores and a formation of a separation layer during annealing. Their simulations and measurments reveal the formation of voids that are bounded by low-energy facets.

The Herino group (1984) reported that at temperatures above 400°C under moderate vacuum (10^{-7} Torr), coarsening of the porous structures was observed. On heating to 900 °C for one hour, large voids of ~ 1 nm were observed. This was related to the instability caused by hydrogen desorption between 200 - 400°C . The stabilisation of the pores was successfully carried out by heating the PS sample at 300°C in dry oxygen (preoxidation). It was shown by the Herino group (1984) that 12% of silicon atoms in the layer had been oxidised in two hours. This corresponds roughly to the growth of one monolayer of oxide over the whole surface of the sample. This structure was found to be stable for hours when it was heated to 900°C, so long as no reducing ambient was present. Densification at temperatures higher than 1000 °C was needed to obtain non-porous oxide. Figure 2-7 shows the pore size distribution of PS as prepared (1) and after the above treatment (preoxidation at 300°C and 800°C vacuum anneal for one hour).

Large differences were observed in the densification times of different porous structures. The very fine structures of p^- layers were densified an order of magnitude quicker than p^+ layers, although the initial porosity was the same.

Sabet - Dariani et al (1994) used HRSEM to study the changes in the structure of PS with heating. Structural changes were observed at temperatures of 50, 150, 250, 350 and 500°C It was found that the heat treatment at 150°C and above showed a gradual improvement in the sharpness of images and below 150°C the images were not sharp. It was deduced that the fresh PS contains a large fraction of spheroidal silicon particles, each of which is surrounded by a coating of some material, of irregular thickness and of high resistance. The coating is removed by the annealing treatment above 150°C.

Münder et al used Raman spectroscopy to study the thermal effects of PS (1993). The Raman spectrum of as-anodised PS shows a typical asymmetric broadening . This is an indication of inelastic scattering from nanocrystallites. At temperatures around 350°C, drastic changes occur in the morphology which cause a reduction in the amount of nanocrystallites with a diameter below 3 nm. In a temperature range of 450 - 500°C, the PS layer loses its nanocrystalline nature and amorphous silicon is formed.

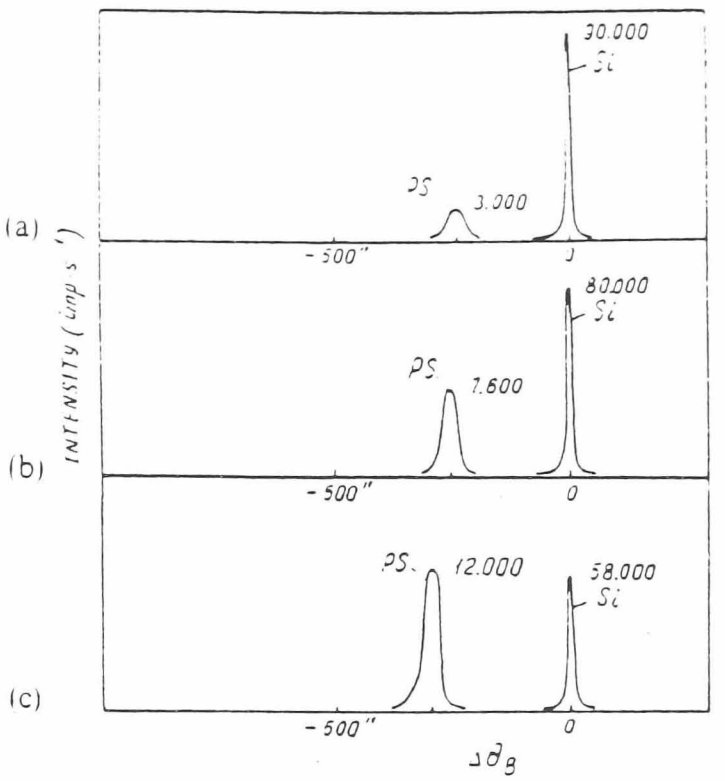

FIGURE 2- 4 XRD analysis showing lattice variation with respect to PS thickness variation ($\Delta\theta_B$ – angle of diffracion)
a) 2um, b)10um and c) 35um thick PS (Labunov et al., 1987)

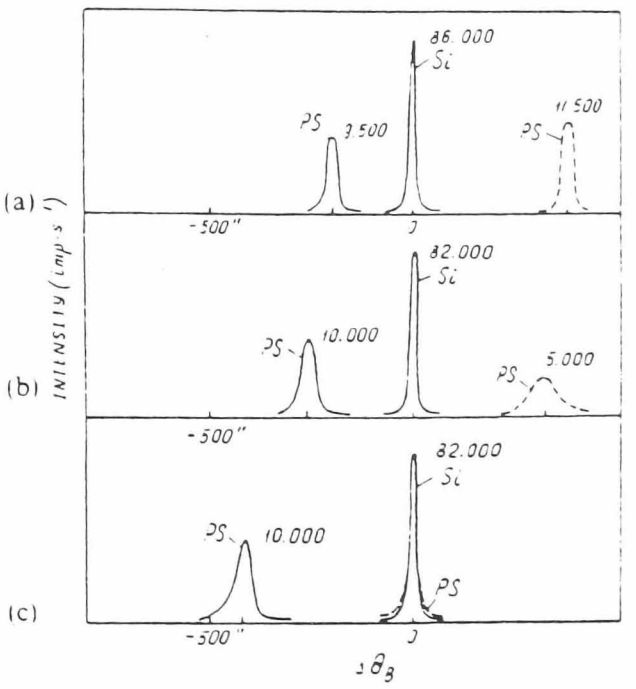

FIGURE 2- 5 Heating effects on PS using XRD analysis ($\Delta\theta_B$ – angle of diffracion)

PS thickness- 10um in all cases As-grown PS (solid line);heat treated PS dotted line ((Labunov et al., 1987)

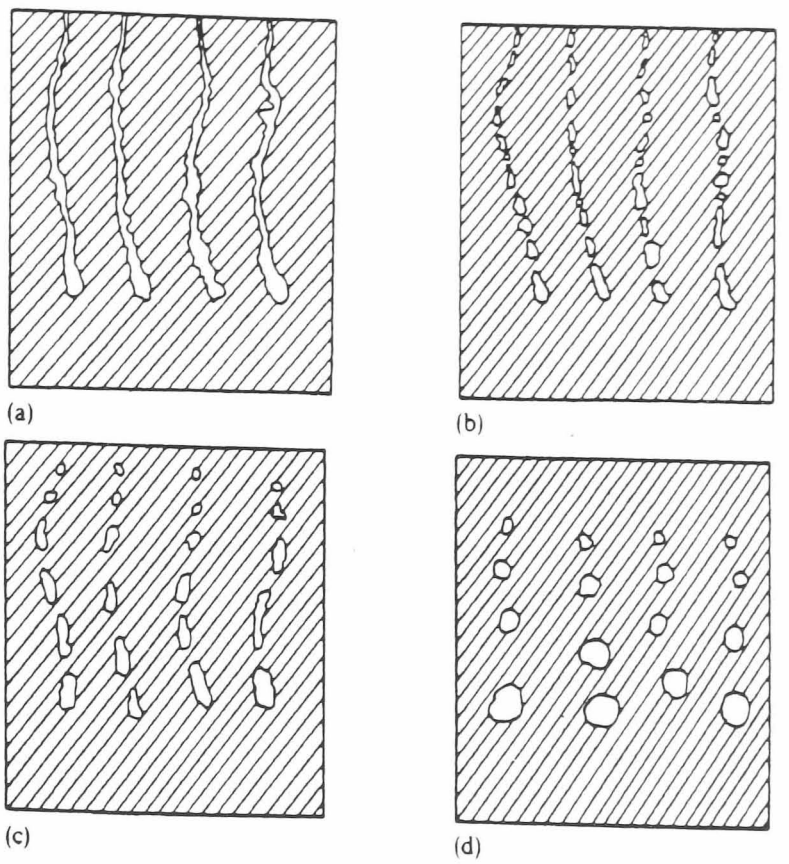

FIGURE 2- 6 A model of the pores going through sintering process

a) as-grown, b) to d) increase in temperature. (Labunov et al., 1986)

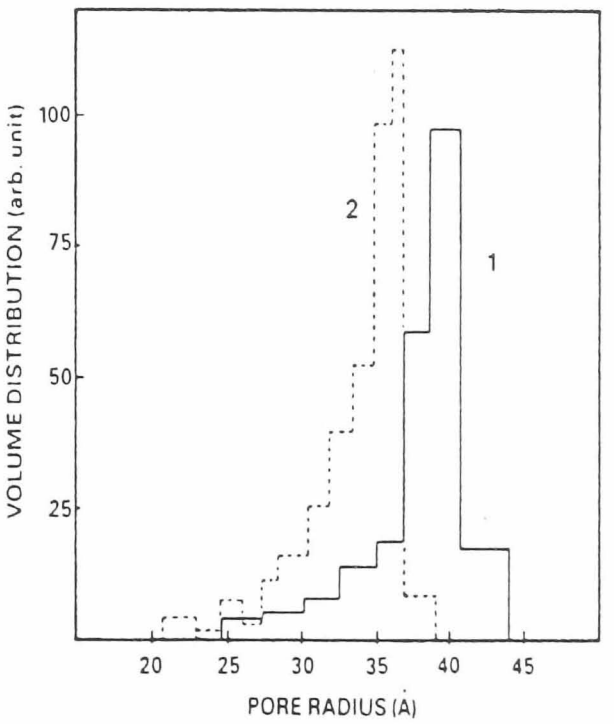

FIGURE 2- 7 Pore size distribution of (1) as-anodised and (2) oxidised PS

(Bomchil et al., 1988)

2.4. Compositional Analysis

The large surface area (200 - 600m^2 cm^{-2}) and the metastable nature of the freshly anodised PS attracts many "contaminants" from the electrolyte solution as well as from the ambient gases. Compositional semi- quantitative analyses of PS have been carried out using surface techniques such as SIMS, RBS, NRA, ERDA, etc. FTIR and EPR were used to evaluate the structural and bonding characteristics. The main contaminants were found to be H, O, F and C. The most significant analyses are reviewed in this section.

2.4.1. Effects of HF on c-Si

Extensive work has been carried out on the effects of HF on c-Si surfaces (Comello 1990, Chabal et al 1989, Hirose et al 1991, Grundner et al 1991, Pietsch et al. 1994). It was found that dipping c-Si in HF leaves the wafer surface terminated by about 0.85 monolayer (ML) of silicon hydrides, about 0.1ML of fluoride and about 0.05ML of oxide or hydroxide with silicon bonding mainly to single fluorine or oxygen atoms (Comello 1990). The main conclusion from the Chabal group was that a Si (100) surface is microscopically rough after HF treatment with mono-, coupled mono -, di - and trihydride termination.

The Hirose group (1991) found that the fluorine coverage on an HF-cleaned silicon surface depends upon the HF concentration in the solution as well as the on the water rinse time. A two-order variation of HF concentration causes a little change in the fluorine coverage. Exceptionally, high fluorine coverage was observed with 50% HF cleaning without a water rinse. This was attributed to the adsorbed HF molecules on the surface because it is dramatically reduced by a one second water rinse.

Grundner et al (1991) used X-ray photoelectron spectroscopy (XPS) and high resolution electron energy loss spectroscopy (HREELS) to analyse the chemical composition of HF-treated surfaces. It was found that the fluorine coverage was a function of HF concentration. On a Si(100) surface, the coverage ranged from $3x10^{13}$ to $1x10^{14}$ atoms cm^{-2} with an approximate logarithmic dependence on HF activity. It was found also (Grundner 1991) that the surface of silicon is by no means saturated by fluorine as was reported previously by Krasinski (1986). HREELS spectra of Si (100) and (111)

surfaces after a 1 min. 40% HF dip revealed that the Si (100) surface corresponded closely to that of a dihydride-covered Si (1x1) surface and the Si (111) showed mainly monohydride covered surface (Watanabe et.al., 1991).

2.4.2. Si-H_x Species from PS

The inner surface of the as- prepared PS layer is almost fully covered with chemisorbed hydrogen during the anodisation process. Nascent hydrogen is produced during anodisation at the Si anode and the dangling bonds of freshly etched silicon accommodate these hydrogen atoms(Gupta et al 1988, Beckmann 1965).

FTIR Analyses of Si-H_x Species

Environments of different species on the surface of PS have been extensively investigated by the FTIR method (Beckmann 1965, Anderson et al 1994, Kato et al 1988, 1989,Ogata et al 1995, Feng et al 1994). Unigami (1980) observed IR absorption peaks at 2128, 907 and 625cm^{-1} and assigned them to Si-H, Si-H_2 and Si-Si vibration modes. Gupta et al (1988) observed a doublet at ~ 2000cm^{-1} and assigned 2110cm^{-1} and 2087cm^{-1} to Si-H and Si-H_2 stretching modes of vibration. Also, 910cm^{-1} to the Si-H_2 scissors mode and 666cm^{-1} and 625cm^{-1} to the Si-H and Si-H_2 deformation modes were assigned. Their assignments rely on the measurement of thermal desorption of hydrogen from PS.

Kato et al (1988) used a self supporting PS film which was separated from c-Si by a sudden increase of the current density during the anodisation process. A triplet was observed at 2090, 2110, 2140cm^{-1} and was assigned to the stretching modes for Si-H, Si-H_2 and Si-H_3 respectively. The assignment of FTIR peaks for Si-H_x raised some controversy. Gupta et al (1988) assigned 2110 and 2089cm^{-1} to Si-H and Si-H_2 stretching modes and others (Beckmann 1965, Ogata 1995) have assigned the stretching modes in a different way : 2090, 2110 and 2140cm^{-1} to Si-H, Si-H_2 and Si-H_3 respectively. The latter assignments are being used in thiswork and the reasons were discussed in the Discussion chapter.

Ogata et al (1995) used an *ab inito* molecular simulation method to assign various peaks of the FTIR spectrum of PS. To simulate various states of hydrogen in PS, $SiH(SiH_3)_3$, $SiH_2(SiH_3)_2$ and $SiH_3(SiH_3)$ were employed as cluster models for local structures of

SiH, SiH_2 and SiH_3 respectively. The calculated vibrational frequencies and the measured IR spectrum of PS were compared. The triplet that was observed with PS at 2142, 2108 and 2087cm^{-1} was assigned to Si-H_3 Si-H_2 and Si-H stretching vibrations respectively. The close resemblance between the IR spectra of hydrogen on a PS surface and hydrogen on Si (100) 2x1 surface suggests that the surface of PS is very similar to a Si (100) 2x1 surface (Chabal 1985).

Some work has been done to investigate the effects of the ageing process in PS using the FTIR method (Kato et al 1988, 1989, Ito et al 1993) They observed shifted signals in aged samples of PS. These were deconvoluted to give four peaks at 2130, 2165 2200, and 2260cm^{-1}. The Kato group (1989) concluded that during ageing process, oxidation proceeds through breaking selectively the backbonds of Si-H bonds without any dissociation of the Si-H bonds. Once a Si atom is oxidised, the remaining backbond of the Si atom can be easily attacked by other oxidants.

Dynamic secondary ion mass spectroscopy (Dynamic SIMS)

In dynamic SIMS, a focused ion beam is used to sputter material from a specific location on a solid surface in the form of neutral and ionised atoms and molecules. The ions are then accelerated into a mass spectrometer and separated according to their mass-to-charge ratios. SIMS provides a measurement of elemental impurity as a function of depth with detection limits in the ppm range. Quantification requires the use of standards.

SIMS was used by Canham et al (1991) to analyse the impurities in as-anodised and aged PS wafers of p^- (20-50 Ωcm), p^+ (0.01-0.04Ωcm) and n+ (0.012Ωcm) CZ silicon. The negative ions monitored were $^1H^-$, $^{12}C^-$, $^{16}O^-$, $^{19}F^-$, $^{30}Si^-$ and $^{28}Si\ ^{14}N^-$ The samples were analysed after 15 mins., 5 hrs, 5 days and 10 weeks storage in air. Small changes were noticed in hydrogen content up to 10 weeks in air and after 10 weeks, its concentration has approximately doubled. The remarkable stability of H content with low temperature annealing in air had been noted already from infrared absorption spectra (Kato 1989). The increase in the hydrogen content during lengthy storage of PS was explained by the room temperature oxidation of PS pores by hydrogen-containing species such as water vapour, methane, molecular hydrogen, hydrogen sulphide and organic vapours, all of which were found in the ambient air.

Elastic Recoil Detection Analysis (ERDA)

ERDA was used for the determination of hydrogen in PS prepared from p type Si (100) with 10Ωcm resistivity. Calibration was carried out on a polyimide film of known composition and H concentration (Sabet-Dariani 1993). The analysis of a 4 days old film prepared from 50% HF solution yielded a H concentration of 20 ± 2 atomic %. The analysis assumed that the concentration was uniform to a depth of at least 10^3 nm.

Grosman et al (1992) also used the ERDA technique to analyse PS layers on p^+ and n^+ Si substrates. A HF and C_2H_5OH mixture in the ratio of 1 : 1 was used as the anodising electrolyte. In this case, the reference sample for the analysis was spin-coated with a solution of polystyrene $(C_8H_8)_n$ in toluene. It was found that similar quantities of hydrogen were present in different PS layers except in the n^+ PS layers, in which a higher concentration of hydrogen was found.

Earwaker et al (1985) used ERDA for the analysis of PS on "low" resistive Si wafers and found hydrogen up to 50 atomic %. The preparation details of the PS were not given for comparison.

2.4.3. Fluorine (F) content in PS

A freshly anodised PS film produced in 50% HF can have a relatively high level of fluorine take up. The reaction mechanism studies suggest that the fluorine adsorption is at least as important as hydrogen in the formation of PS (Lehmann et al 1991). The bond energy for Si-F is the highest on all possible PS surfaces, Si-F (129.3 kcal mol^{-1}) > Si-O (88.2 kcal mol^{-1}) > Si-H (70.4 kcal mol^{-1}) > Si-Si (42.2 kcal mol^{-1}), indicating that the fluorine adsorption should be prevalent on the Si surface since it is the most thermodynamically stable bond.

By contrast, it was shown that the Si-H bond energy is enhanced with increase of the external current used in the preparation process of PS. It was shown also that the strength of the Si-F bond is weakened (Bi-cai 1993). Bi-cai had shown, by computational methods that, with increasing anodising currents, the Si-F bond is gradually weakened and the Si-H bond is strengthened. At some threshold current

value, the Si-H will be as strong as Si-F and beyond this level Si-F becomes weaker than Si-H. It was concluded that there would be more Si-F in the samples produced with lower current density than in the PS samples produced with larger current density.

Canham et al (1991) reported that a freshly anodised microporous film, produced in 50% HF, had a relatively a high level of fluorine incorporation. The fluorine level by the SIMS method of analysis showed a monotonic decrease with time. This was attributed to the hydrolysis of $Si\text{-}F_x$ by atmospheric moisture to give Si-OH species. These findings give only a trend for the distribution of fluorine as the SIMS analysis requires internal calibration standards of similar composition and porosity to avoid matrix effects.

There is evidence of fluorine found both on external surface of PS from Auger (AES) and X-ray photoelectron spectroscopy (XPS) analysis (Earwaker et al 1983, Harderman et al 1985) and throughout the layer from nuclear reaction analysis (NRA) at a level of 1-2 atomic % (Earwaker 1983). Analysis of fluorine was carried out by particle induced gamma emission (PIGME) on 14 days old PS and it was found to be 265 ± 6ppm, i.e. ~ 0.03 atomic % (Sabet-Dariani 1993).

Detailed infrared adsorption studies are needed to demonstrate conclusively that the majority of the fluorine is chemisorbed, rather than some form of etch residue trapped in the micropores. A number of IR studies of PS have not identified the stretch mode characteristic of Si-F bonding (Chabal 1989, Kato 1988). This may be due to (a) the low oscillator strength of the bond and (b) hydrolysis of Si-F bonds by water vapour.

2.4.4. Carbon (C) content in PS

It is very difficult to have any material with no carbon adsorbed on the surface. The principal carbon bearing species in the ambient air are carbon dioxide (CO_2) carbon monoxide (CO) methane (CH_4) and various organic vapours. Many vacuum based surface analytical systems that are used for compositional analysis use pumps with carbon based vacuum oil unless specifically modified. Therefore it is difficult to be confident in the values for the carbon content in PS.

SIMS analysis of as-anodised wafers shows a carbon concentration lower than the fluorine level (Canham 1991). Exposure of PS to the ambient air shows an increasing carbon content as expected. After 10 weeks in air, the PS layer was found to have about 20 times more carbon than a freshly prepared sample. It was found also that the carbon content near the surface was constant for all the samples exposed to air for 15mins. to 10 weeks.

Grosman et al (1993) reported that the atomic ratio of C/Si is 10% to 20% in PS samples prepared from p^+ and n^+ substrates with porosity ranging from 47% to 80%. The origin of carbon was found not to be ethanol of the ethanol-HF electrolyte system as the same level of carbon was found in water-HF anodised PS. They were in agreement with the Canham group (1991) that the carbon content increases during ambient storage, confirming that the carbon present in PS is from carbon-bearing species in the atmosphere. Also it was confirmed that the carbon is not from CO_2 and CO adsorption since the oxygen content was found to be one order of magnitude lower than the carbon content indicating that the origin is probably from the organic vapours in the ambient air (Sabet-Dariani 1993). In freshly prepared PS samples, H was found to be the main impurity but there is some discrepancies in the levels of C, O and F. The Canham group (1991) found the impurity levels increased in the order C < O < F which is exactly the reverse of the findings of the Grosman group. This was explained by (a) the samples being different in the two studies and (b) the sputtering yields corresponding to the negative ion monitored (C^-, O^-, F^-) might have been different. Earwaker et al (1983, 1985) found carbon at 3 atomic % which is lower than found by the Grosman group (1993).

Oxygen (O) content in PS

The principal oxygen-bearing species in ambient air are molecular oxygen, water vapour, carbon dioxide and monoxide, nitrous oxide, sulphur dioxide and ozone. Canham et al (1991) reported that there was a dramatic increase in the oxygen content of a microporous layer during storage in air at room temperature. While it is present as a uniformly distributed minor impurity (< 1 atomic %) in a freshly anodised layer, after a week the oxygen content has risen an order of magnitude throughout the layer and there is an enhanced concentration near the external surface. They observed also that after 10 weeks in air, the oxygen content throughout the PS layer was 35 times that

immediately after anodisation. This was attributed to a gradual oxidation of the PS skeletal structure.

A summary of the compositional analyses of PS using different techniques is presented in Table 2-1. It should be noted that the compositional variations are dependent on the preparation method as well as on the type of Silicon used. Sabet-Dariani et al (1993) analysed PS for oxygen using the NRA technique with single crystal SiO_2 (quartz) as their standard for oxygen. The analysis was based on knowing the stopping power of PS which was calculated using the data from the standards.

2.5.Porous Silicon Applications

PS possesses unique optical, chemical and electronic properties that can be used in Si device applications. Besides its exciting electro-optical properties, PS shows some interesting features for micromechanical applications. For many micromachining applications, cantilevers and bridges are needed. In contrast to the surface micromachining method, where a thin film of SiO_2 (< 10nm) is dissolved, a sacrificial layer (up to 10^4 nm) can be produced with PS technology (Steiner 1995). The dissolution of this thick layer results in a large distance between membranes and bridges and the bulk Si. This is an important aspect for the sensitivity of thermal transducers.

Thermal oxidation of PS is a promising technique for the fabrication of high quality SOI and is in contrast to other SOI methods because the silicon islands formed are undamaged monocrystalline silicon.(Bondarenko et al 1995)

The three main areas where PS has found applications are:

i. SOI Technologies;
ii. Sensor Technologies
iii. Optoelectronics

TABLE 2- 1 Comparison of the effects of anodising conditions of PS to compositional variation

Type of Silicon	Anodising conditions	Method	Compositiom	references
p-Si (100) 1 - 2 Ωcm	10N HF /H_2O	**IR**	$H_1 Si_1 O_{1.5}$ $H_2 Si_1 O_1$	Beckmann,1965
p-Si (100) 1-5 Ωcm	HF : H_2O : C_2H_5OH 1 : 1 : 4; 11mA cm^{-2}	**FTIR**	SiOH, SiO_2, Si_3 - SiH, SiO_2, O_2-SiH	Borghesi *et al*,1993
p-Si (100) 0.5 Ωcm	HF : H_2O : C_2H_5OH 1 : 1: 4; 200mA cm-2; 15sec.	**FTIR**	SiH, SiH_2	Gupta *et al*,1988
p-Si $10^{16}cm^{-3}$	HF : H_2O ; C_2H_5OH 2 : 2 : 1	**FTIR**	SiH_x (x = 1, 2, 3)	Xie *et al*,1992
p, n-Si $10^{15}cm^{-3}$	H_2O : HF :C_2H_5OH 1 : 1 : 1	**FTIR**	SiH_x	Rao *et al*,1991
p-Si (100) 10 Ωcm	40 -50 % HF/H_2O 10mA cm^{-2}, 3min.	**NRA, ERDA, RBS, PIGME**	$Si_{2.5} O_{1.2} C_{1.3} H_{1.2}$	Sabet-Dariyani *et al*1993
p-Si (100) 0.01-700 Ωcm	HF/H_2O 10 -300mA cm^{-2}	**RBS, NRA**	0 - 5 at.% O, 1 -2 at.% F, 20 - 50 at.% H and ~ 3 at.% C	Earwaker et al,1985
p^+, 0.01 Ωcm	HF : H_2O ;C_2H_5OH 1 : 1 : 2; 1-50mA cm^{-2}	**NRA,ERDA, RBS**	$Si_{5.4} C_{0.8} O_{0.1} H_{3.6} F_{0.1}$ - Lum. PS $Si_{7.2} C_{0.5} O_{0.1} H_{2.1} F_{0.1}$ - Non-lum PS	Grosman *et al* 1994
p^-, 30 Ωcm p^+, 0.01 Ωcm	20 - 50 % HF/H_2O 20%HF/H_2O/C_2H_5OH	**SIMS**	H : F : O : C = 50 : 26 : 3 : 1 – Fresh PS H : F : O : C = 17 : 1 : 15 : 5 - Aged PS	Canham *et al* 1991

2.5.1. SOI Technologies

The SOI fabrication methods are classified into two main categories:

a) Buried PS formation. This is done by selective formation of buried PS underneath islands, which will eventually contain the devices. It exploits the strong dependence of the rate of PS formation on Si dopant and concentration (Tsao 1987)

b) Epitaxial deposition on PS. This is carried out by direct epitaxial deposition of Si on a previously formed PS layer. This process relies on the fact that the remaining porous silicon skeleton is a single crystal.

Imai et al (1979, 1981) developed a method for isolation of MOS IC's. This method is called IPOS (Insulation by Porous Oxidised Silicon) which was an alternative to the LOCOS (Local Oxidation of Silicon) isolation technique. The LOCOS method gives a rigid structure which protrudes above the original Si surface and the IPOS method has the advantage of having the thick oxide fully recessed by producing PS and oxidising it (Figure 2-8). The main problem with the IPOS method was large leakage current. Imai found that the leakage current decreased with the HF concentration of the electrolyte. Figure 2-9 shows the I-V characteristics of a reverse biased P-N junction made by the IPOS method for different HF concentrations and also by the LOCOS method. The next advance in device isolation using the FIPOS (Full Isolation by Porous Oxidised Silicon) process came about in 1984 (Imai et al). The process is shown in Figure 2-10. The key features of this process are proton implantation and the formation of thick oxidised layers. A FIPOS / CMOS logic array with 1300 gates was successfully fabricated and was shown to have a higher speed and lower power dissipation than the equivalent fabricated by bulk CMOS technology (Imai, 1984). The main disadvantage of Imai's FIPOS method was that a thick oxidised PS layer is needed to isolate even small islands. For example, a 7μm thick layer is needed to isolate 8μm wide islands. Wafer warpage was found to be the other problem and was due to the oxidation of PS on one side of the wafer. Despite these problems, 64K CMOS-SOI SRAM (Static Random Access Memory) were produced by Ehara and co-workers (1985) The structures used in the above applications have mainly used n / p structures where n islands were implanted in a p-Si substrate with PS formed only in the p regions.

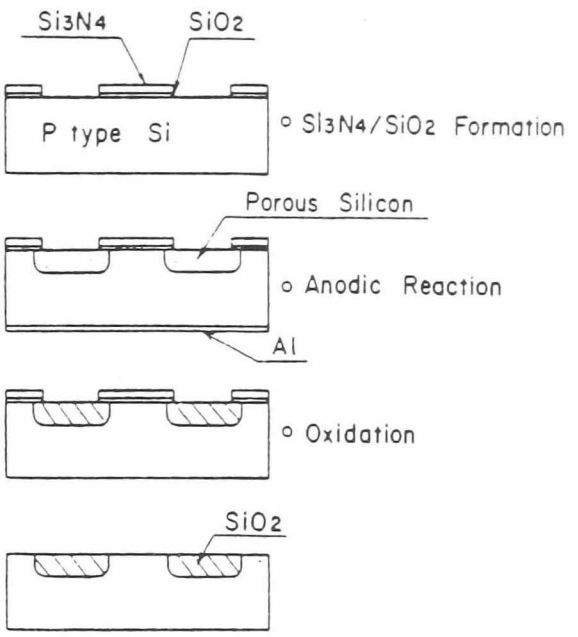

FIGURE 2- 8 IPOS processing method

(Imai et al., 1976)

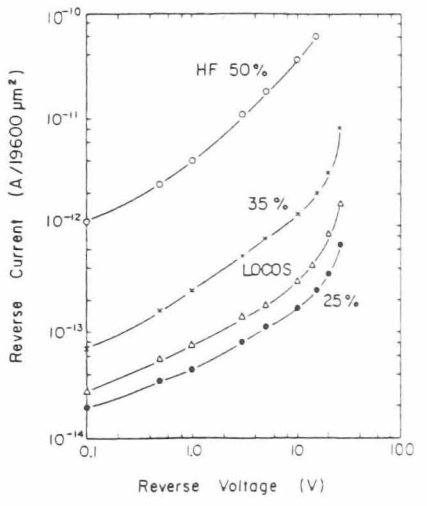

FIGURE 2- 9 I-V characteristics of reverse biased P-N junction- LOCOS and IPOS methods

(Imai et al., 1978)

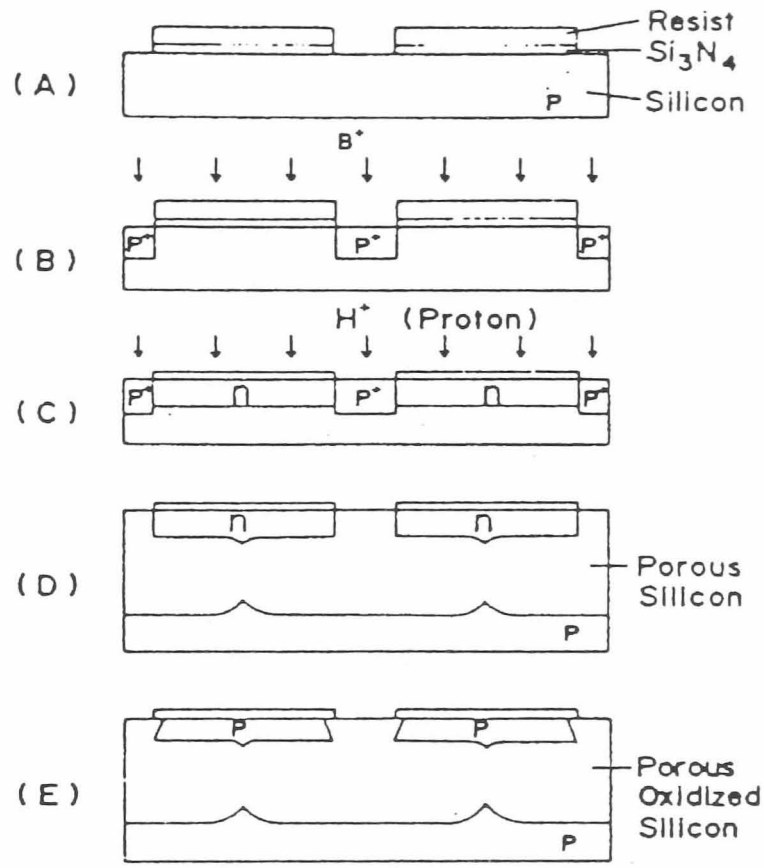

FIGURE 2- 10 FIPOS method of processing

(Imai et al., 1984)

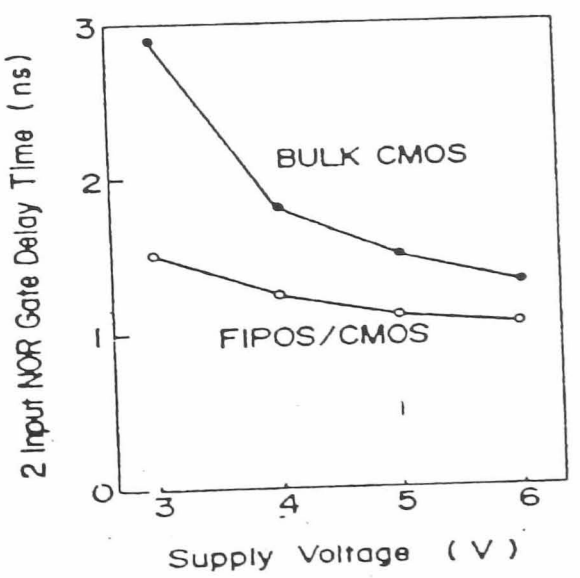

FIGURE 2- 11 Comparison of FIPOS/CMOS and bulk CMOS

(Imai et al., 1984)

The most promising approaches are those based on structures such as $p/p^+/p$ or $n/n^+/n$ (Tsao 1987, Holmtrom 1983) where PS is formed only in a thin (10-30 μm) heavily doped buried layer accessible through the upper layer (Figure 2-11). The processing details for the above structures are given in the above references. The disadvantage of this technique is the need for a good thin epitaxial layer with a sharp interface. The Barla group (1986) fabricated a 3nm CMOS in the SOI islands and their results show mobilities of 540 $cm^2V^{-1}s^{-1}$ and 180 $cm^2V^{-1}s^{-1}$ for N-channel and P-channel transistors with very low leakage currents, $<10^{-13}$ A /μm width.

Zorinsky et al 1986), at Texas Instruments, developed a method called ISLANDS (Isolation by Self-Limiting Anodisation of an N^+ Epitaxially Defined Sublayer). This method uses RIE (reactive ion etching) to form trenches of several microns deep, to exposing n^+ anodisable layer. This gives the process the added flexibility to isolate layers of any desired thickness while at the same time making it possible to anodise either from a top surface or from the side walls (Figure 2-12). The minimum pitch achieved to date is roughly 2.8μm (1μm islands separated by a 1.8μm wide trench), but a pitch of 2μm or less are possible (Zorinsky, 1986). The main advantage of this method is the self-limiting nature of the anodisation process, which allows the thickness and the uniformity of the SOI layer to be controlled accurately. Thomas et al (1989) used the ISLANDS method to produce fully depleted thin film CMOS-SOI devices and circuits in silicon islands 100nm thick with performance comparable to SIMOX (Separation by Implanted Oxygen) processed on the same line. This technology for the production of SOI-CMOS offers all the advantages over bulk CMOS of SOI produced by oxygen implantation, including simpler processing, reduced short-channel effects and reduced parasitic capacitance (Figure 2-13).

Epitaxial deposition techniques on PS are attractive owing to the uniformity of thickness of the PS layer in the isolated island. Epitaxial growth is performed at a relatively low temperature (< 850°C) to avoid PS restructuring. Low-temperature epitaxy techniques such as PECVD (Plasma enhanced chemical vapour deposition) of silane (SiH_4) at ~ 750°C (Takai 1983) and MBE (molecular beam epitaxy) at ~ 770°C (Beale 1985, DÁvitaya 1985) are used. Residual defects such as microtwins and dislocations originating from PSL/epitaxial silicon interface are observed with TEM (Beale 1985).

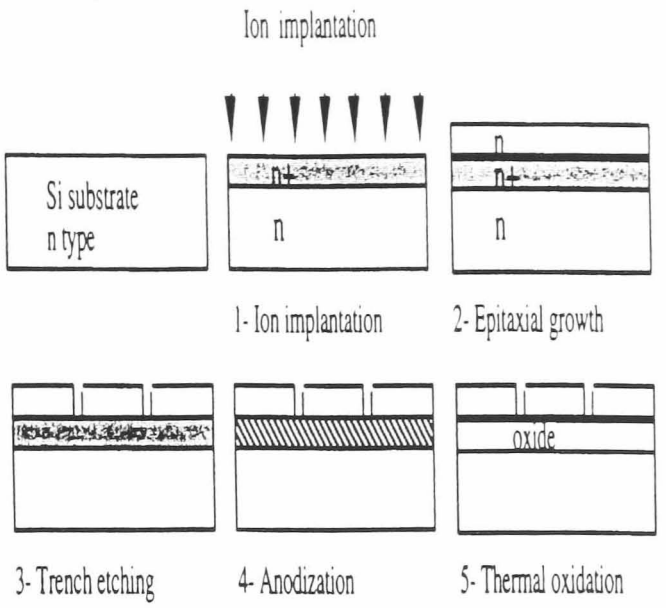

FIGURE 2- 12 Trench etching for SOI structures

(Tsao et al., 1987)

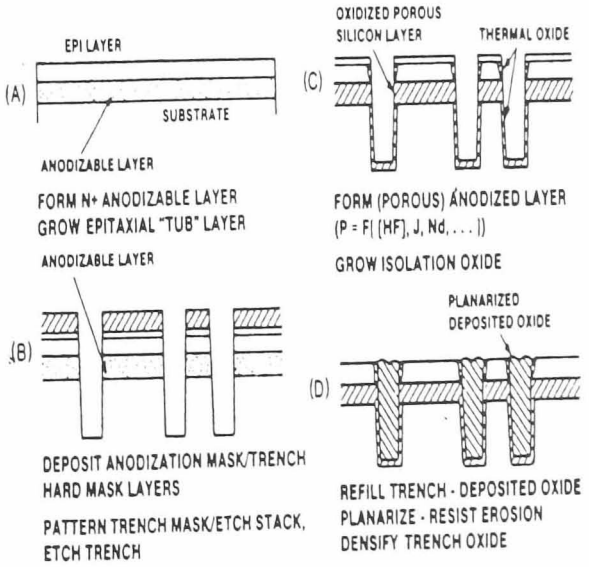

FIGURE 2- 13 Island method to form SOI structures

Zorinsky et al., 1986)

Oules et al (1989) found that epitaxial silicon films grown on PS layers on lightly doped wafers exhibited a large defect density (10^{10} cm^{-2}). It was shown that the defect density was reduced by a fraction of 10^2 to 10^3 by the use of silicon channelled implantation and susequent annealing (Oules et al 1992). Also, it was observed that if the epitaxial layer was deposited on PS formed from a p^+ Si substrate, the epitaxial quality was equivalent to the homoepitaxy of Si on c-Si. So far, the crystalline quality of Si overlayers fabricated with epitaxial techniques have been inferior to those fabricated by the selective buried anodisation method. However, reasonably good device characteristics have been obtained using these epitaxial techniques, since the bottom of the epilayer which is found to be the most defective region of the island (Oules, 1992), is also oxidised during the PS oxidation. An initial low temperature oxidation ($\approx$ 450°C) to stabilise the pores, followed by higher temperature oxidation has been reported to reduce warpage and defects in the epitaxial Si layer (Lin et al 1986)

2.5.2. Sensor Applications

PS possesses unique optical, chemical and electronic properties that can be used in device applications. Owing to its very large surface area to volume ratio (> 500) and small characteristic dimensions, PS can be dissolved quickly by certain etchants which attack bulk Si to a negligible degree (Barret 1992)

The formation of PS is dependent on the type and the level of the silicon doping and the material can be formed selectively on particular regions of a wafer which has appropriate doping characteristics. The selectivity of PS formation and its extreme reactivity due to the large surface area of its pores can be used in microsensor technology. Also, PS can be selectively dissolved in dilute KOH solution and silicon micromachining can be achieved by appropriate localisation of PS formation followed by chemical etching. Various micromechanical structures such as holes, trenches and membranes can be obtained by these means.

Some of the interesting properties of PS are summarised below:

a) Silicon can be etched to form thick layers of PS. (Barret, 1992);
b) An etch stop in silicon can be obtained by selective doping (Steiner 1993);
c) It can be removed easily with very weak KOH solution(Lang 1994)

d) Anodisation is a CMOS compatible process and is exploited in SOI (Bondarenko 1995) and optoelectronic applications (Kozlowski, 1994);
e) PS has a thermal conductivity of less than 2W mK^{-1} and is a good material for thermal sensors (Drost 1995)

A few selected examples of the use of PS in sensor applications are presented.

Thermal Sensors

A large number of physical parameters can be measured by thermal sensors. Besides temperature, the thermal measurement is relevant to fluid flow, IR and UV radiation, high frequency power and gas analysis. A small amount of thermal energy should cause a large temperature variation of the thermal structure to realise an efficient thermal sensor. This means that the heated body must be small and well isolated from its support, which is normally a Si substrate. Two examples are given for the application of PS in thermal sensors.

A thin film bolometer

A bolometer is a thermal sensor for the measurement of infrared radiation. Figure.2-14 shows a 3-D sketch of a such a bolometer which consists of free standing membrane with a zig-zag resistor (NiCr 15nm and Au 500nm widths) on it (Steiner et al 1995). When the self-supporting membrane is heated externally by IR radiation or the surrounding medium, the resistivity of the metal resistor changes and this change is measured.

Crystalline silicon is not a suitable membrane because of its high thermal conductivity ($\approx$ 150W mK^{-1}) and silicon nitride (Lang et al 1990) or silicon carbide (Klumpp et al. 1994) were used. These membranes have thermal conductivities of the order of 2.25W mK^{-1}. The only disadvantage is the vulnerability to breakage. Drost et al (1995) showed that the thermal conductivity of PS is very small ($\approx$ 0.025W mK^{-1}) and they avoided the use of a free standing PS film for bolometer application. Instead, the sensor was placed on a thick PS layer (>30μm). Convection was prevented by the pore structure and it was found to be a good isolation layer.

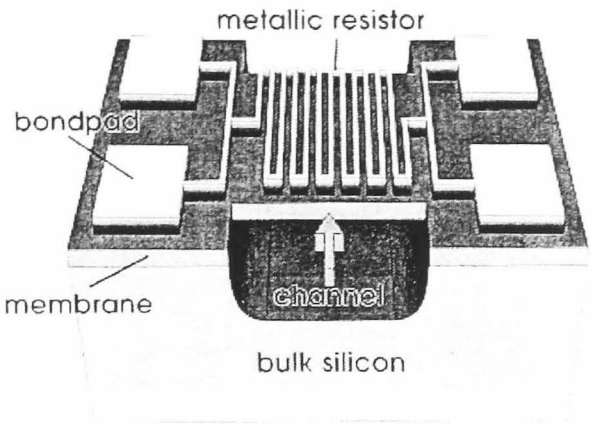

FIGURE 2- 14 A 3-D sketch of a bolometer

(Steiner et al., 1995)

Hot Wire Anemometer

A sketch of a polysilicon hot wire anemometer showed in Figure 2-15. A polysilicon bridge of cross section 0.5 x 2 μm and 600 μm long was fabricated over a wide groove of 80μm width, forming the hot-wire anemometer in a flow channel (Steiner 1993). The gas or liquid medium flowed round a heated bridge. Depending on the velocity and the density of the medium, the bridge was cooled by heat dissipation. The change in temperature was detected by the change in the resistance of the wire. The flow rate was thus measured indirectly.

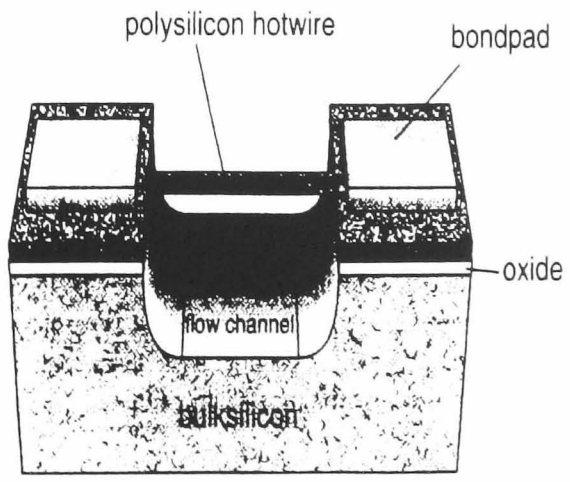

FIGURE 2- 15 Hot wire anemometer

(Steiner et al., 1993)

Humidity Sensors

PS has a high surface to volume ratio. Therefore a capacitance-based moisture sensor can be realised using the change of relative permittivity when moisture is absorbed on the oxidised pore walls. A thin gold film is sputtered on to the porous layer, allowing a good electrical conductivity (Steiner et al. 1995).

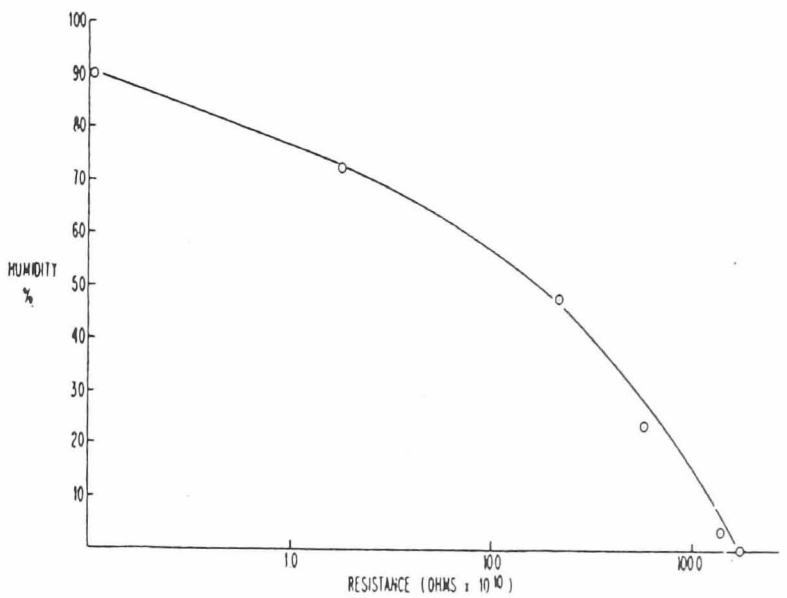

FIGURE 2- 16 Performance of a PS-based humidity sensor

(Burkhardt, 1975)

The Anderson group (1994) reported a similar device with aluminium metallisation. Mesa structures of 200 μm width were produced. The range of capacitive response between a dry ambience and 100% humidity at 25°C for 20min. was assessed. A large change in capacitance (440%) from 0-100% relative humidity was observed, much larger than the response of previous state-of-the-art humidity sensors. A patent was published in 1977, (Burkhardt et al) describing a method using porous silicon moisture sensors for a manufacturing process. The devices were subjected to various relative humidities for a period of several minutes and the resistances were measured. Figure 2-16 gives a plot of the relative humidity versus the resistance.

A review on miniaturised humidity sensors was reported by Rittersma (2002). This reviews capacitive-, hygrometric-, gravimetric-, optical- and integrated sensors. A summary of all the reviewed devices was given in a table format.

Gas Sensors

The high surface area of PS was taken into account in the application of gas sensors. A gas sensor for the detection of NO_2 was developed by Bartato et al. In 2001. This was done by depositing a free standing PS film on alumina substrate, thus removing the Si substrate that is inactive in gas detection. This sensor was able to detect very low concentration of NO_2 (100 ppb) with no interference with ozone, benzene (20 ppm), CO (1000ppm) and organic vapours. This was shown to operate at room temperature. Another sensor was produced for the detection of HCl, NH_3 and NO at the 10 ppm level (Seals et al. 2002). This was fabricated from mesoporous PS structure through electroless gold plating. The response of this device, which operates at a bias voltage of 1-10 mV, was reported to be rapid and reversible.

Biosensors

The role of Si structures in medicine has taken a new dimension. In particular porous silicon produced with nanometer size holes can be "biocompatible and "biodegradable". There are some interesting papers that have been published on this subject (Canham et al., 1997, 2001).

An optical interferometric biosensor was developed by Tinsley-Bown et al. (2000) for immunoassays. For this model system, the pores should be > 50nm in diameter to allow easy ingress of reagents and the layer must also display Fabry-Perot optical cavity modes. The detection antibody was rabbit IgG and the analyte was a-rabbit Ige conjugated to horseradish peroxidase (HPR).

Another biosensor was reported for detecting life threatening micro-organisms such as E.Colii using PS (Misra et al. 2001). This sensor was produced by vacuum deposition of polyaniline films on macroporous PS structures. The response time was found to be 5s. The fabrication process, morphological, structural and electrical characterisation of this sensor have been described in this paper.

The characteristics of urea sensor based on platinum deposited PS was described by Jin et al.(2001). Platinum deposited PS and polypyrrole (Ppy) films were characterised by SEM and energy dispersive X-ray spectroscopy. The sensitivity of this sensor was found to be ~800mA/decade in the range of 10mM-100mM.

Chan et al. (2001) reported the design and testing of a biosensor for DNA testing. This device structure consists of a microcavity resonator made of PS layers. When a luminescent PS layer is inserted between two Bragg reflectors (also from PS), the broad luminescence band is altered and multiple and very small narrow peaks is detected. The position of these peaks is very sensitive to a small change in refractive index. It was demonstrated that this sensor displayed sensitivity, selectivity and response speed. Bengtsson et al. Reported to have produced enzyme microreactors by homogenous PS carrier matrix. The production of PS micro enzyme reactors (mulMER) was described. The mulMERs were evaluated by immobilising two types enzymes, glucose oxidase (Gox) and trypsin and the resulting catalytic turnover was monitored by a calorimetric assay.

2.6.Applications in Optoelectronics

It was reported in 1990, that when PS is further etched chemically in HF for several hours after anodisation to give fine "quantum wires" of Si; (< 5nm diameter), it emits bright red light under excitation with blue or shorter wavelength light (Canham 1990). It was reported that the quantum efficiency, which is defined as the fraction of electrons and holes that emit light during recombination, is as high as 10% i.e., 10^5 times higher than that of c-Si. The luminescence of PS covers three characteristic regions: (a) the red-green region around 1.4 -2.2 eV (b) the blue region of 2.3 -2.6 eV and (c) the IR region which is around 0.8eV (Pavesi 1996,437-48). Research into the luminescence of PS is concentrated in two main areas: (a) understanding of the origin of luminescence; and (b) fabrication of electroluminescent (EL) devices.

Many theories have been put forward to explain the origin of photoluminescence (PL) in PS. Excellent reviews are given by Jung et al (1993) and Pavesi (1996). The origin of PL was explained by different models and the main models will be discussed briefly here. Also, some examples of the applications of PS in the areas of EL and photovoltaics will be reviewed in this section.

2.6.1. Origin of Luminescence

Although, the exact mechanism of emission of light is still unclear and highly controversial, the most common proposed mechanism in the literature centres around

quantum size effects of the Si "quantun wires" formed in high porosity PS layers (Canham 1990, Lehman et al. 1991). The contradictory observations reported in the literature may be due to the fundamental differences in the preparation methods adopted by various groups in this field. The following four proposed models are briefly discussed here.

(a)quantum confinement model

(b)disordered silicon surface model

(c)amorphous silicon model

(d)siloxene model

Quantum Confinement model

This model was put forward by Canham (1990) using the concept of a "quantum wire". He suggested that, as porosity increases, the feature size of the Si skeleton decreases and a dramatic quantum size effect should occur if the diameter of the Si wire is significantly less than the dimensions of the free exitons (~ 5nm). An exciton is a bound electron-hole pair. It was shown by Canham that, by changing the anodising conditions to obtain finer quantum wires, the PL peaks were shifted to lower wavelengths (Figure 2-17). This suggests that the quantum confinement plays a significant role in the PL mechanism. Lehman and Göslele (1991) reported that there was an increase in the bandgap with increase in porosity of PS. This observation supports the quantum confinement model.

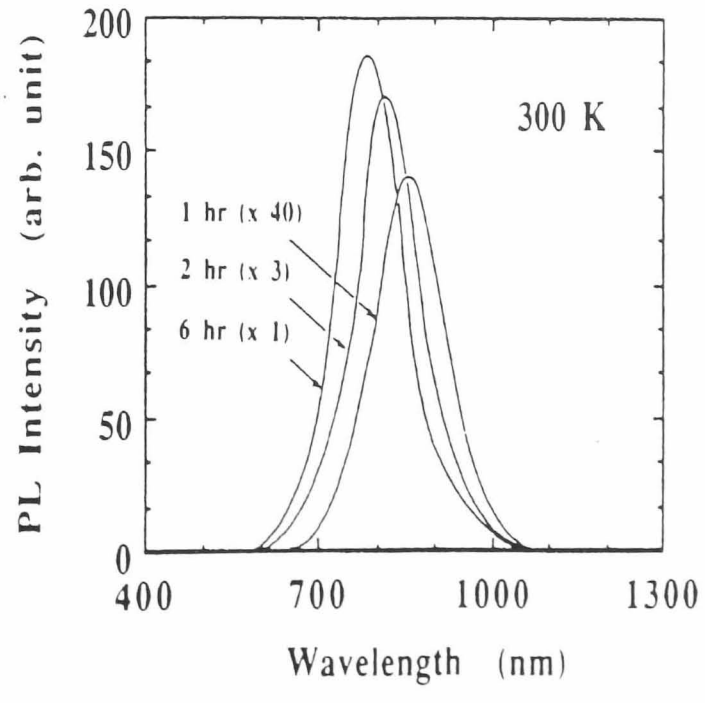

FIGURE 2- 17 Observed blue shift with thinning of Si wires

(Canham, 1990)

However, this does not by any means imply that PS is a direct bandgap material. In a direct bandgap semiconductor, the luminescent decay time is typically not more than a few microseconds. In PS, however, this lifetime can be of several tens of microseconds, which suggests that the mechanism is most likely an indirect transition. (Iyer et al 1993).

Read et al (1992) have calculated the properties of quantum wires and used the results to analyse the PL phenomenon. They modelled PS as an assembly of Si wires of rectangular cross section with thickness of 1.2-2.3 nm and employed a first-principles pseudo-potential technique. Also, they assumed that the surface of the Si wire of PS is saturated with hydrogen atoms. Their calculations suggest that the fundamental bandgap of a Si wire structure of PS is both "direct" and larger than the bandgap in c-Si which is "indirect". The difference between the theoretical phonon emission peak (1.8 eV) and experimental phonon emission peak (1.48 eV) for ~ 3 nm quantum wires produced from 80% PS was explained by the binding and localisation energies of the luminescence excitons.

There are a few controversies that do not support this model entirely. It was shown by Canham (Canham 1990) that further pore widening or reducing the diameter of the Si wires (by chemical etching for longer hours) of PS leads to blue shift. However, Prokes et al (1992) found that there was no blue shift, but only a change in the PL intensity. Figures 2-17 and 2-18 illustrate both findings. These results indicate that the blue shift of the PL as a function of particle size or pore widening is not a universal phenomenon.

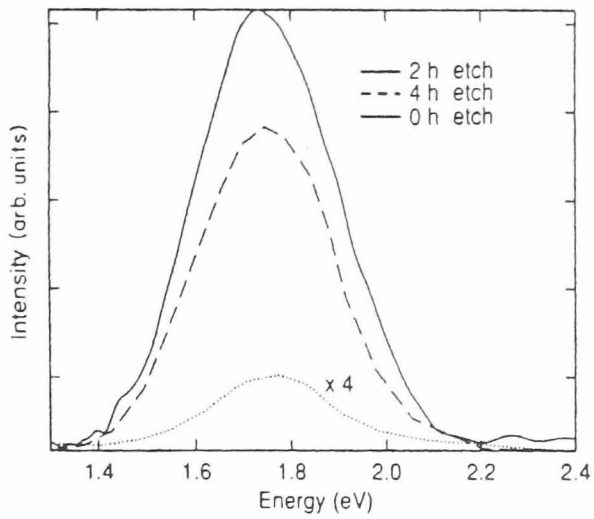

FIGURE 2- 18 No blue shift with thinning of Si wires

(Prokes et al., 1992)

Disordered Si Surface Model

It was proposed by the Koch group 1993) that the carriers were created within quantum confined Si nanocrystallites, but that the recombination leading to light emission occurs at the surface. The recombination at the surface was assumed to originate from Si band tail states created at the surface by strain and disorder. It is accepted by the Koch group that the enlarged bandgap of PS is a quantum size effect but they suggest that the c-Si skeleton of PS has imperfectly passivated surfaces as a result of its irregular shape and strained bonds between Si atoms and the surface. They argue that this might lead to surface states which are the cause of the PL in PS.

The surface state mechanism can account for the observed sensitive dependence of the emission on photochemical treatment reported by Kux and coworkers (1993). It was shown by the Kux group that, by dipping in propanol and HF based electrolytes under UV light, the PL changed from green to red, a shift of up to 0.6 eV. There is no logical way to account for this in terms of the quantum size effect (Figure 2-19).

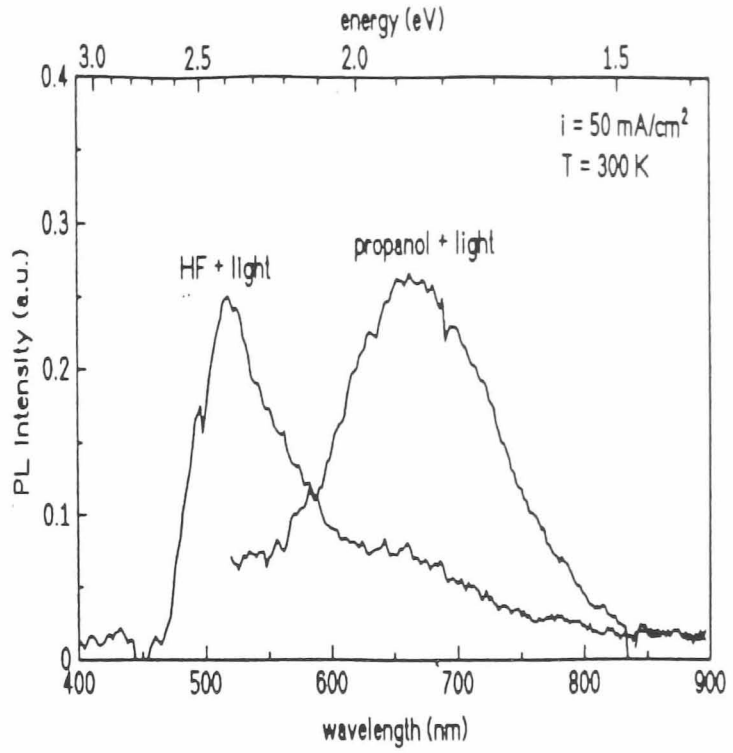

FIGURE 2- 19 Effects of different electrolytes on PL spectra

(Kux et al., 1993)

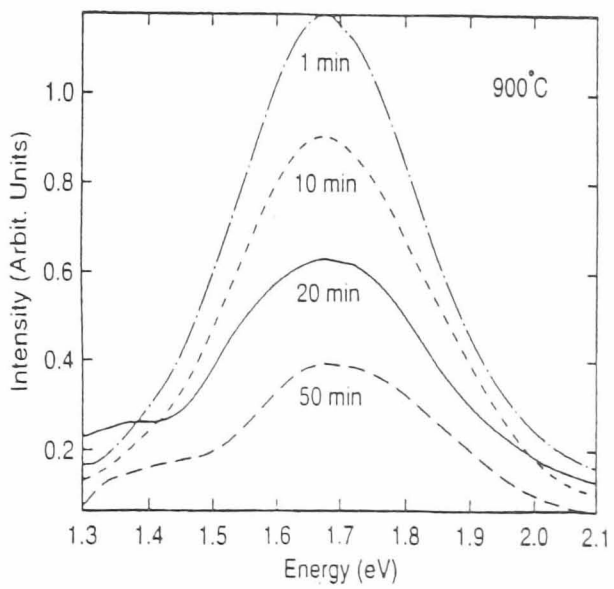

FIGURE 2- 20 PL spectra as a function of oxidation times

(Fisher, 1979)

One of the problems with this model is the fact that the red PL in oxidised PS does not shift in energy after a prolonged heating at high temperature (Figure 2-20). At high temperatures, hydrogen desorbs from the PS surface and the surface states should be

different from those at room temperature, i.e. PS should be temperature sensitive as is amorphous Si (Fisher 1979), and thus the PL frequency is expected to shift. Figure 2-21 shows that it is not the case.

Amorphous Silicon Model

There have been reports of the presence of amorphous Si in the PS network (Pickering et al 1984, Cullis et al 1991, 1998, Prokes 1994, Pavesi 1996). In PS samples, the Si "wires" was found to consist of nanocrystalline Si particles embedded in amorphous Si or oxide (Cullis 1991). Jung et al (1992) have analysed luminescing PS using TEM, and have found a structure containing Si nanocrystals and an amorphous phase. Figure 2-22 gives a schematic of this proposed structure.

One of the drawbacks of this model is that there is no PL peak energy shift observed at elevated or room temperature. This means that the PL mechanism is not related to c-Si or a-Si as they are sensitive to temperatures. It is a well-established fact that the a-Si crystallises at temperatures as low as 450°C (Csepregi 1984) so it is very unlikely that the a-Si component of PS can exist after heating and oxidation at 800°C.

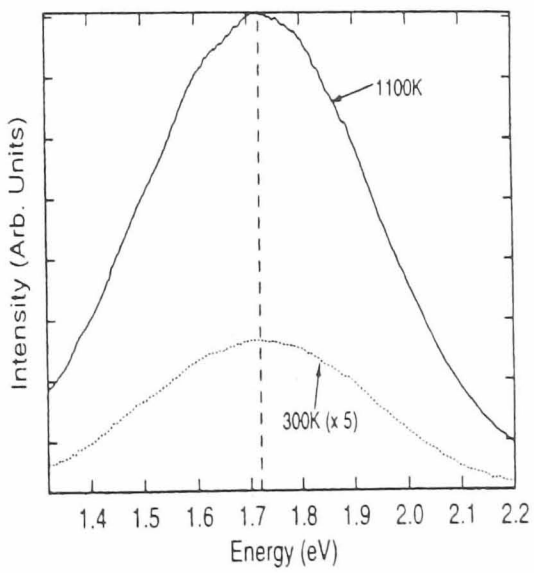

FIGURE 2- 21 PL spectra of laser annealed PS at 1000K and at 300K

(Prokes et al., 1995)

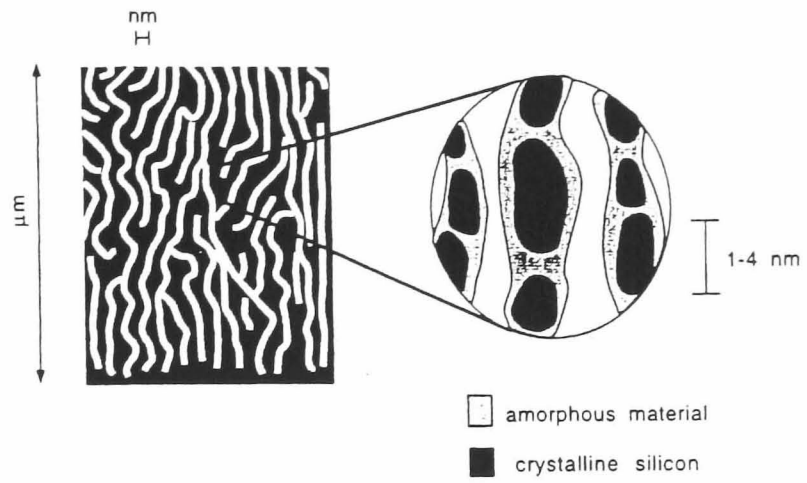

FIGURE 2- 22 Schematic of a PS layer showing Si nanocrystals in amorphous matrix (Pavesi, 1996)

Siloxene Model

This model was suggested by Brandt et al (1992) and it relates the origin of PS to a polymeric Si-O-H compound called siloxene $(Si_6O_3H_6)_n$. This consists of linear Si chains interconnected by oxygen or Si layers with alternating OH or H terminations. The luminescence energy of this material can be tuned over a large spectral range, including the visible region, by substituting different ligands such as OH group, alhohols or halogens in the place of H.

During annealing, siloxene goes through a dehydrogenation process to give Si_2O, as the temperature approaches 600°C.

$Si_6H_3(OH)_3 + H_2O \rightarrow Si_6H_{3-x}(OH)_{3+x} + x\ H_2$

$Si\text{-}OH + HO\text{-}Si \rightarrow Si\text{-}O\text{-}Si + H_2O$

This is no longer a siloxene structure, and this material is not luminescent. However, luminescent PS can survive oxidation at temperatures as high as 950 to 1050°C (Petro-Koch et al 1992). Heating of the freshly etched PS at these temperatures in oxygen would have driven off all the H atoms and replaced them with oxygen. This cast doubt on models based on a-Si and siloxene. Also, efficient PL is observed from as-anodised structures, where there is negligible oxygen on the surface and there is no chance of having siloxene compounds.

2.6.2. Electroluminescent (EL) Devices

There have been many reports published on the EL observed from PS and its applications to produce LED's. These are very simple structures with a conducting material on a PS layer. EL is observed (a) in solution with liquid or wet contacts and (b) in structures using a number of different solid state contacts such as gold or indium tin oxide (ITO). The LED's produced from PS show very low efficiency ($\leq 10^{-2}$ %) compared to its high quantum efficiency for PL ($\approx$10%) (Steiner et al 1995).

The EL was detected during anodic oxidation in the electrochemical cell containing solutions of KNO_3 or HCl (Billet al 1992, Halimaoui et al 1991). The EL excited in this manner is short lived, lasting only a few minutes. This was attributed to the oxidation of the c-Si/PS interface which electrolytically isolates the PS layer. However, more stablity was reported using an aqueous electrolyte containing persulphate ions ($S_2O_8^{2-}$) with the PS layer biased negatively (Beale et al 1993). The EL produced by liquid contacts is very efficient but for practical LED's solid state contacts are essential.

EL devices with solid state contacts have been demonstrated using conductors such as a semitransparent layer of gold (Richter et al 1991, Koshida et al 1992, 1992, 1995), transparent ITO Indium tin oxide (ITO: 91% In_2O_3, 9% SnO_2) (Kalkhoran et al 1992), microcrystalline silicon carbide (μc-SiC) (Mimura et al 1993) and conducting polymers such as electropolymerised polypyrrole (Koshida et al 1995, Cottrell et al 1993), and polyaniline, PANI (Bsiesy et al 1995).

The first LED made of PS consisted of an Au/PS/c-Si structure similar to a Schottky diode (Kalkhoran 1992). Although this device showed EL, its efficiency at room temperature was of the order of 10^{-4}-10^{-5} %. The threshold voltage for observable EL was ~ 10V. Another version of the diode mentioned above was fabricated on a PS layer produced from n-Si and the anodisation was carried out under illumination. A thin (12nm) film of gold was sputtered on the PS layer, It was found that the intensity of light is linear with the current through the device (Lang et al 1993). This behaviour is similar to that observed with LED's in GaAs technology. The quantum efficiency was found to be of the order of 10^{-4} to 10^{-3} %. The onset voltage was found to be less than 2V.

Gold absorbs some of the emitted light and is semitransparent and the the quantum efficiency is observed to be low when gold is used for the metal contacts. ITO makes a better top contact because it is transparent to all wavelengths of visible light. Even though ITO does not form a good junction to PS, the p-n junction that ITO forms injects carriers more effectively into the luminescent layer than does a Schottky contact and it is possible to improve EL characteristics by the ITO method. Maruska et al (1993) fabricated a n-p heterojunction LED based on p-type PS and transparent n-type ITO. It was reported (Maruska,1993) that, under forward bias, a light emission at ~580nm was observed with an onset voltage lower than 2V.

Loni et al (1995) produced an PS based EL device with an external quantum efficiency greater than 0.1% under CW operation. The structure that was used in the study was ITO/PS/c-Si/Al. External efficiency was defined as the ratio of the total number of photons emitted and the number of electrons flowing through the external circuit. Loni *et al* found that, for an applied bias of 9V, the ratio of forward to reverse current was 10^4. The EL was orange in colour. The device was found to show quantum efficiency between 0.1 to 0.18 for an applied current density in the range of 0.2 - 7.0 Am^{-2}. This corresponds to an applied bias in the range of 4-6V. It should be noted that this efficiency is achieved at biases compatible with the operation of CMOS circuitry. Also, it was found that the output efficiency fell by a factor of 4 over a period of 5 hours when the device was in a vacuum system under a pressure of 10Pa. However, in ambient air at a pressure of 1000Pa, the efficiency fell by a factor of 100 in a few minutes.

Another type of heterojunction approach used wide bandgap semiconductors such as microcrystalline silicon carbide (μc-SiC) to improve carrier injection which was believed to be the mechanism for EL in PS. This method was used by the Futagi group (1993, 389-93). This device had a ITO/μc-SiC/PS/c-Si/metal structure. Red to orange EL was observed under an electrical bias of ~20V, which is very high for practical purposes.

The colours achieved from PS-based EL devices were reported by Kozlowski et al (1994). It was demonstrated that by illuminating n-type PS samples with light of different wavelengths during anodisation, the colours of EL from n-PS could be modulated. Kozlowski reported that the devices produced from UV-illuminated PS

samples produced blue and green EL and the visible illumination of PS produced orange EL.

The method of using an optical micro-cavity technique to control spontaneous emission is well known in lll-V semiconductor optoelectronics. The idea of using both a p-n junction for carrier injection and a micro-cavity to control the spontaneous emission was shown to produce a very efficient LED based on PS (Pavesi et al 1995). The key problems with the PS-based LED's which are still to be solved for optical interconnections are their stability and switching speed in the Gbit/sec. range. Thus, for interconnects, the best hope seems to be the blue luminescence. For optical display applications such as flat panel displays, better efficiencies are required. This means that better material is needed for the solid state contacts to increase carrier injection efficiency.

2.6.3. Photovoltaics

PS is shown to be useful in transforming optical absorption into electricity. The applications of PS to photovoltaics such as solar cells are reviewed here. The potential advantages of using PS in solar cells are listed below.

a) The network morphology of PS can be used to enhance trapping.
b) The bandgap of PS may be adjusted for optimum sunlight absorption by controlling the Si skeletal size. The maximum solar cell efficiency vs. bandgap curve peaks at ~1.5eV.

The application of PS in photovoltaics can be traced back to 1982, when Prasad et al (1982) formed a SiO_2 layer with an oxidised PS layer on the front surface of a solar cell to form an antireflection (AR) coating. In experiments by Prasad et al, p^+n diffused junction solar cells of relatively low conversion efficiency were used. A PS layer was produced on p^+ Si and it was oxidised at 500 to 600°C. This caused the average reflectance of the solar cell surface (in the wavelength range of 300 - 800nm) to decrease from 37% to 8%. Also, the conversion efficiency was found to be improved and this was due to a combination of light trapping and passivation of the surface. Some of the solar cells were exposed to a normal terrestial environment for several months and showed no degradation of the AR coating (Prasad 1982)

More recently, photoelectrochemically-etched PS was used to reduce surface recombination and this was found to improve both the efficiency and the stability of the cell (Lévy-Clément 1991). Tsuo et al (1993), in their study, found that the PS-covered c-Si showed an integrated reflectance of only 1.4% at 500nm compared with about 40% for the polished Si surface. They also investigated the efficiency of a PS anti-reflection layer (ARL) on polycrystalline Si in HF/methanol electrolyte. It was found to produce a much more uniform etch and a much brighter PL than the HF/ethanol system. The average reflectance of PS-etched poly-Si in the range of 500 to 850nm was about 10%. Other methods such laser texturing has a loss of 5% and mechanical grooving with a 6.6% loss over a similar wavelength range (Tsuo 1995). Smestad et al (1992) studied the photoresponse of a Pt probe/PS/c-Si structure . They reported that, under simulated sunlight, the open circuit voltage was approximately 0.36V and the photocurrent was about 2μA. However, the series resistance was found to be high (1 mega-ohm) in all cells. With little known presently about the charge carrier transport mechanisms and the photocarrier generation, it is difficult to determine the origin of this high resistance and to design high-efficiency solar cells that use PS as the light absorbing layer.

It was reported (Unal et al. 2001) that a sandwiched structure device in which semi-transparent continuous gold electrodes were deposited on stain-etched PS showed high efficiency in photocurrent under visible light exposure. It was shown that metal coated PS devices have great potential for application in solar cells and photodetectors. This process was is also more cost-effective than current technologies since there is no need for antireflection coatings.

2.6.4. Photodetectors

There have been reports of photodetectors fabricated using PS. Yu et al (1992) fabricated a PS metal-Si-metal (MSM) device using a micromachined Si mask instead of photolithography. A responsivity of 0.5 A/W at 628nm and a dark current of 950nA at 10V were reported. Zheng et al (1992) fabricated Al/PS/Al photodetectors. The spectral response was measured for the wavelength range of 400nm – 1075nm. Near unity quantum efficiency for light converted to electrical energy was obtained in the wavelength range of 600 - 900nm. The metastable state and the high resistivity of PS restrict the utility of as-anodised PS for optoelectronic devices. Tsai et al (1993) applied rapid thermal oxidation to PS to fabricate MSM photoconductors and p-n photodiode.

The MSM was found to have responsivity greater than 6.4 A/W at 810nm and to exhibit strong responsivity in the UV region. The photodiode was found to exhibit 75% efficiency at 740nm

A porous silicon based UV detector was reported by Min et al. in 2001. This device was based on stain-etched PS and pn junction. To increase detection efficiency, the peak spectral response wavelengh of the pn junction diode is matched with the peak wavelength of PL emitted from PS. It was found that the diodes showed no sensitivity to UV light on their own but with the PS the detector was very sensitive to UV light. The differntial sensitivity was calculated as 2.9 mA/mW.

Chapter 3 Experimental Methods

The development of the TPD system, as well as methodologies of characterising the adsorbates on PS are discussed in this chapter. The developments of these techniques are as important as the results obtained from them for this work since the system was developed and built in the Middlesex university Microelectronics Centre and was not a commercial system. The following three main areas are considered here.

a) Development of the TPD vacuum system
b) Development of the heating unit
c) Development of a suitable technique for the preparation of PS samples with a minimum exposure to the environment,
d) Development of FTIR analytical technique for the characterising adsorbates on PS substrates,

3.1 Development of the TPD system

The development of the TPD system falls into two categories. One is to choose a suitable pumping station that gives minimum contamination and the other is the development of a compatible heating method for the PS wafer and the measurement of temperature of the PS sample. It is found that PS is a material which has lower thermal conductivity than c-Si (Drost et al., 1995)

3.1.1 Development of the Vacuum System

The vacuum chamber for the TPD system was built as "6-way crosses" with three rotable flanges. The pumping system comprised of three sorption pumps connected in series with an ion pump. This arrangement was selected in order to provide a contamination free vacuum system. It was found that this pumping system was incapable of handling the upsurge in pressure caused by the gases released during the heating of a PS sample.

The system was modified to a turbomolecular pumping station. This consists of a turbomolecular pump (Edwards 250EXT model) backed by a two-stage rotary pump. The EXT models are hybrids, have a facility of preventing backstreaming of oil into the vacuum system. This means that any carbon contamination from the pumping oil

vapour is avoided. It is achieved by having the high pressure end of the pump, which is connected to the backing pump, with oil lubricated bearings and the lower pressure end, which is connected to the vacuum chamber, with ceramic based oil-free magnetic bearings. A molecular sieve based trap was set up between the turbo molecular pump and the backing pump as an additional precaution to trap any oil molecules from the backing pump..

A VG Monitorr 100 quadrupole mass spectrometer (QMS) was connected to the chamber with the detector head line of site of the PS sample. The distance between the analyser head of the QMS and the sample is approximately 6mm. This arrangement avoids the analysis of the target gas being swamped by the background gases which could desorb from the vacuum chamber walls. The schematic diagram of the TPD system is given in Figure 3-1.

3.1.2 Development of the heating unit

Uniform heating of porous silicon is essential in TPD analysis as the desorption of the adsorbed species occurs at a narrow range of temperature. It is a well known fact that uniform heating of c-Si presents a difficult problem. c-Silicon exhibits negative resistance characteristics, that is, the resistance of the sample decreases with increasing temperature. Therefore direct heating of porous silicon or c-silicon needs a very high output impedance power supply to swamp the negative impedance of the sample and prevent thermal runaway. Thermal runaway is caused by higher current passing through low resistance spots present on the material and results in higher degree of localised heating. In the case of low resistance c-silicon (e.g. 2Ω cm), a low voltage is sufficient to start the heating current, but with the high resistance c-silicon (e.g. 50Ω cm.) a high voltage (~ 500 volts) is required. In both cases the current requirement is high when the sample reaches higher temperature. Also, the direct resistive heating, would involve large "feed throughs" to the vacuum system for the reasons discussed above.

Such a power supply was built in-house. The temperature of the sample was controlled by feedback from a thermocouple. Localised spots on the wafer exhibited slightly lower resistance and current flowed preferentially through these spots.

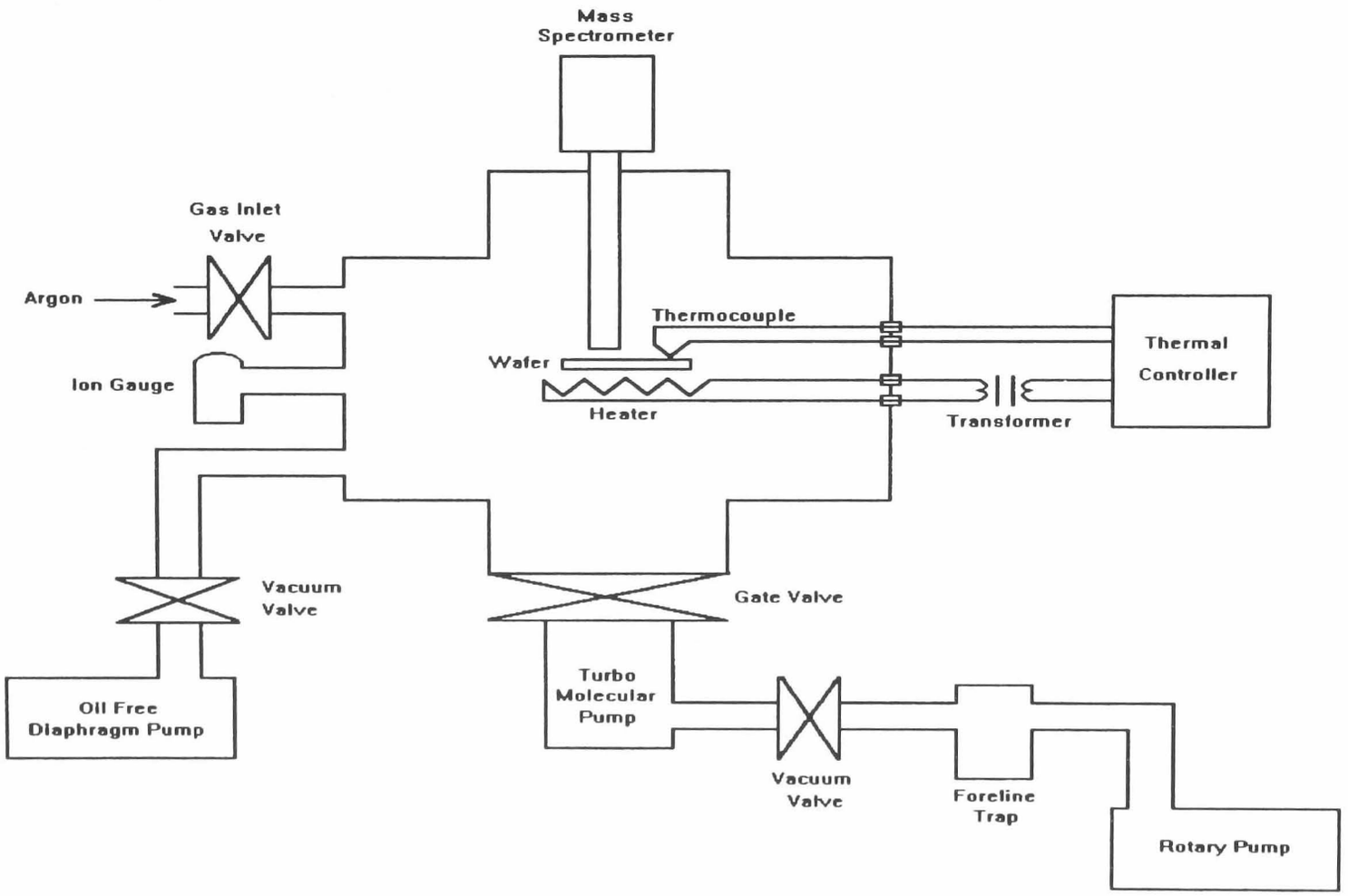

FIGURE 3- 1 Schematic of the TPD system

This caused current flow through interlinked areas of spots forming a narrow track clearly visible at higher temperatures. This phenomenon is known as "tracking".

E-beam Heating Method

In view of the preceding problems, an electron-beam heating system was built which consisted of a heating filament held at a negative voltage from the silicon which was earthed. The silicon wafer was held on a tungsten mesh, and the voltage of the electron beam supply was controlled by a thermocouple which allowed the temperature to be slowly increased.

Due to the limited space available in the vacuum chamber, it proved to be impossible to produce an electron beam that was to some extent not focused ,and as a result, uniform heating of the wafer was not obtained.

A molybdenum (Mo) disc 1inch in diameter and 1/8 inch thickness was used to hold the porous silicon slice. The lack of close thermal contact between the silicon and molybdenum prevented the silicon wafer from heating up except at the minute spots where it actually was in contact with the disc. The wafer melted at these spots. Molybdenum (Mo) mesh was used in an effort to remedy this problem but did not improve the situation.

Also, a few other problems were encountered with this method. The stray or the scattered electrons from the e-beam that are not focused were found to heat the chamber walls, thereby increasing the background effects during the measurement of the desorbed gases from PS. Also, it was observed that the thermal controller (Neutronic, Micro96) used for controlling the heating rate was subjected to random electronic failure during e-beam heating. This phenomenon was not explainable, even by the manufacturers concerned. However, it was thought to be a function of the stray electrons that were not focused on the sample, probably due to the generation of a plasma which caused an electrical breakdown.

Development of the Present System

Even though e-beam heating is a very efficient way of heating, it has many side effects which are undesirable for this work. The adopted method is to use a 100 μm thick tantalum foil (Ta) sandwiched between a sapphire plate (1mm x 5mm x 1mm) which acts as a support and the PS sample (19mm x5mm). The assembly is clamped at the edge with stainless steel plates. The current is passed through the Ta foil as well as the PS sample, which is in parallel to the current flow. The very low resistance of the Ta foil swamps the local variations of resistance of the silicon wafer, even with the low resistance c-silicon, so that the "tracking" observed with the direct heating method, was avoided. The PS is heated by the radiant heat emitted by the heated Ta foil as well as the direct heating by a small ratio of the current passing through it. The exploded view of the arrangement of the heating system used in this work is presented in Figure 3-2

The transparency of silicon to infrared radiation and its variable emissivities with temperature caused difficulties in using an infrared pyrometer for measuring the temperature. The other alternative is to use thermocouples and the possibility was investigated. The present solution is to use thermocouples of the smallest diameter that can be practicable for handling in order to minimise the heat loss through conduction. Unsheathed fine gauge K type (nickel-chromium\nickel-aluminium) thermocouples of diameter 76.2 μm with "beaded" junction are used in this work. The output of the thermocouple is fed to a thermal controller (Newtronic Micro96) which has a cold junction compensating facility. The thermocouple is connected to a short solid nickel leadthrough A compensating cable is used to connect the leadthrough to the thermal controller Good contact between the thermocouple and the silicon wafer was obtained by sandwiching the thermocouple between the sample and a piece of very high purity c-silicon that was cleaned beforehand by heating repeatedly to 1000°C.

3.2 Development of FTIR Technique for PS Application

FTIR is used as the primary source of information about the chemical nature of the bonding between the PS and the adsorbed gases in this work. The FTIR Model that was used in this work provides a scan range of 4400 to 400 cm^{-1} with a resolution of 2 cm^{-1}. It was observed that the highly doped Si wafers (> 0.006 Ωcm) that were used routinely for producing PS showed very low transmittance in the infrared region compared with

"normal" wafers of resistivity in the range of 2-15Ωcm. Figure 3-3 and 3-4 show FTIR spectra of low and high resistivity wafers respectively. The interference observed in lower resistance silicon wafers is due to free carrier absorption. When dopant atoms are introduced into intrinsic Si, additional levels are created in the energy band structure, usually within the bandgap. When highly doped c-Si is exposed to infrared radiation, a range of free carriers in excited states are created, leading to plasma absorption. It has been established by J.R.Ferraro et al.in 1990 that, the low transmittance is due to free carriers in the highly doped silicon and not due to scattering effects caused by the pores of the PS.

An option of thinning the wafer to reduce the free carrier absorption due to high dopant density proved to be difficult. This is because

a) it is difficult to etch a Si wafer uniformly even though the overall etch rate can be controlled and
b) wafer handling during the anodisation was difficult because the thinned wafer was found to be very fragile.

An investigation of the possibility of using reflectance mode FTIR did not provide a satisfactory solution. It was therefore decided to use p-type high resistive Si back implanted wafers for transmission mode FTIR analysis and this method was developed successfully. The back implantation is needed to provide uniform anodisation and is discussed in section 4.4.

3.3 Preparation of PS Samples

PS is formed during electrochemical dissolution of silicon in HF electrolytes. This dissolution takes place when a Si wafer is used as an anode and platinum (Pt) is used as a cathode in a simple electrolytic cell. The drawback of this simple cell system is the observed non-uniformity in both the porosity and thickness characteristics of the PS layer.

The anodisation process for this work is carried out by using a specially enclosed double cell which was developed and built by the Defence Research Agency (DRA) . The cell body is made of highly HF acid resistant polymer PTFE (polytetrafluoroethylene).

This cell consists of two half cells in which Pt electrodes are placed (Figure 3-5). The Si wafer is placed in between the two cells and this arrangement isolates the two half-cells. A viton "O" ring between the front half cell and wafer provides a good leak-tight seal.

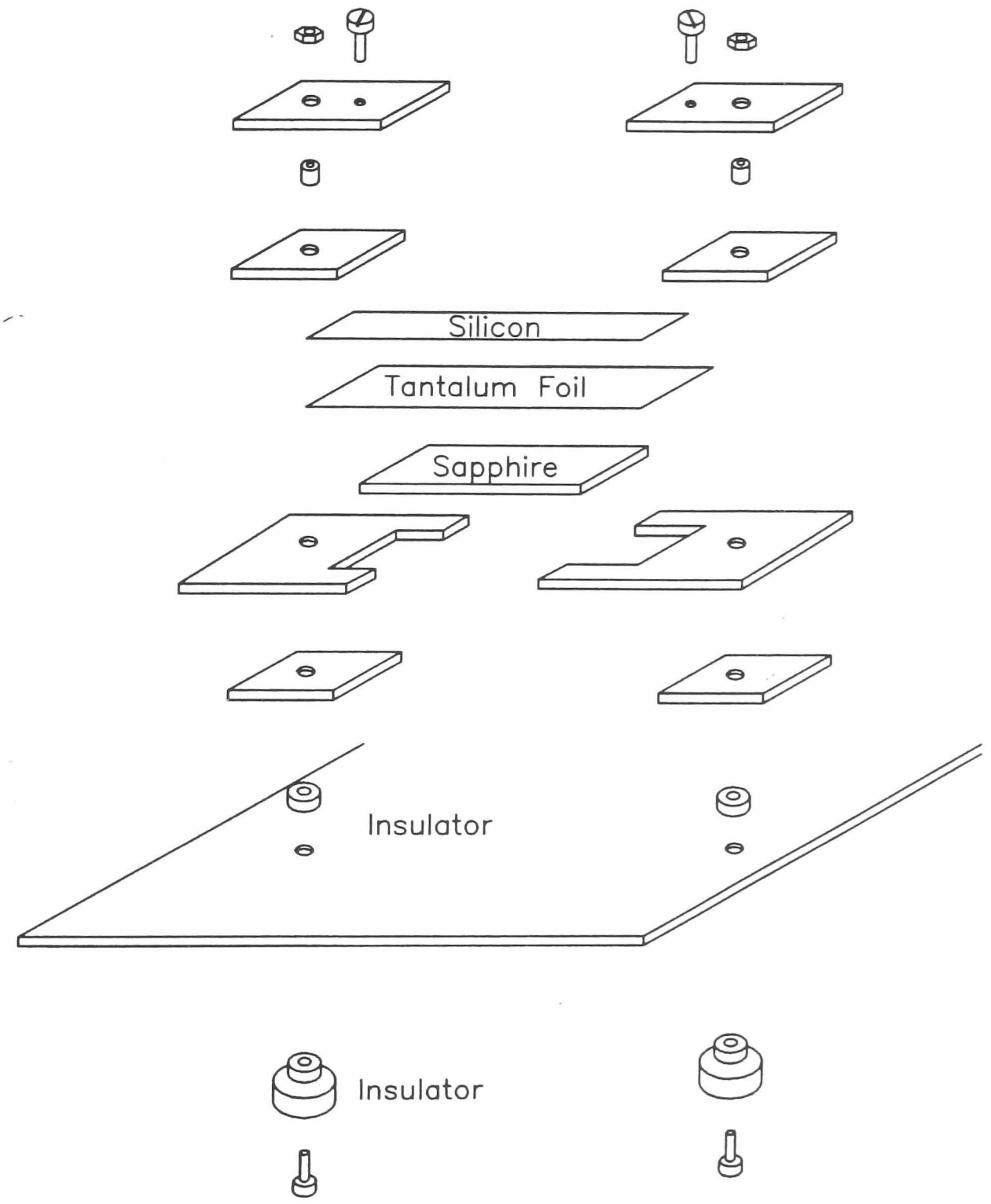

FIGURE 3- 2 Exploded view of the heating unit

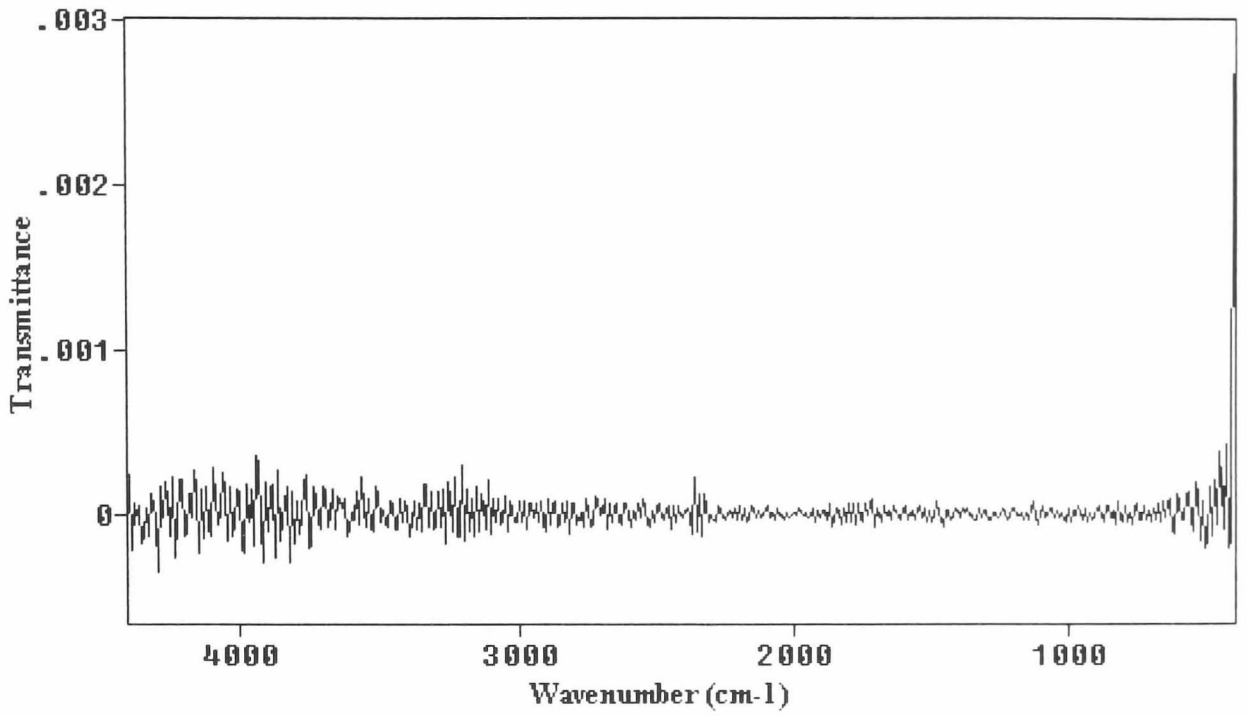

FIGURE 3- 3 FTIR of a high resistivity (~ 0.006 Ω cm) c-Si wafer

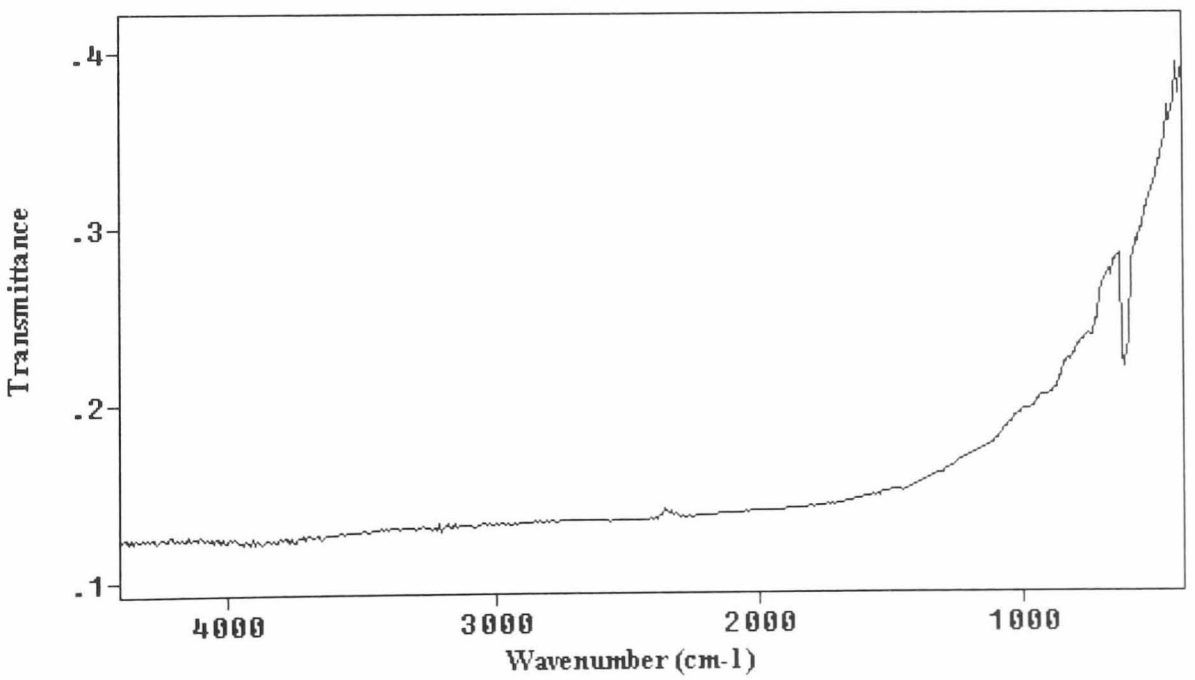

FIGURE 3- 4 FTIR of medium- resistivity (2-6 Ω cm) B-doped wafer

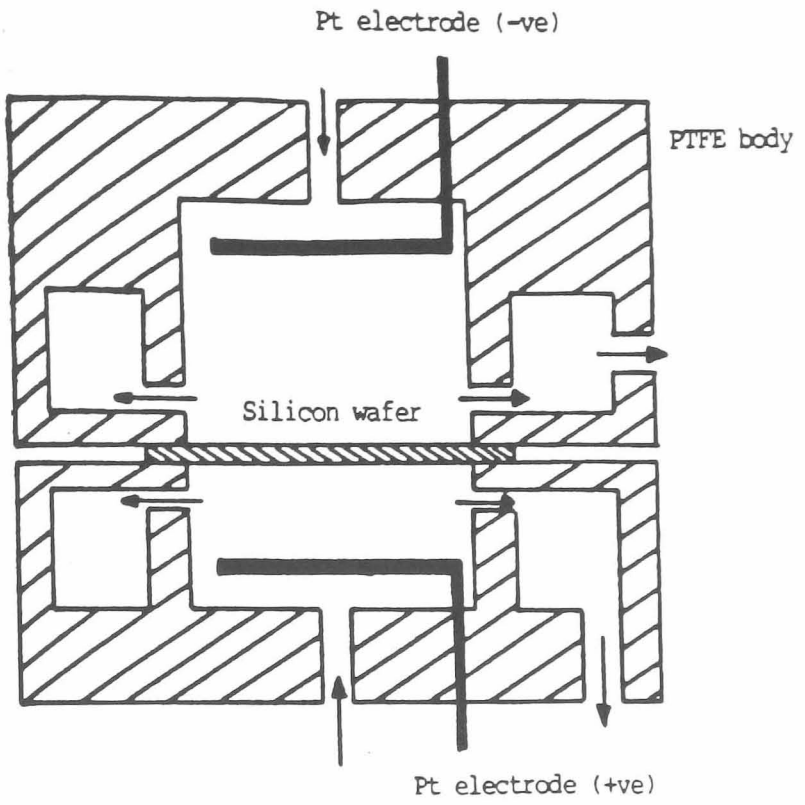

FIGURE 3- 5 Cross section of anodising cell

(Obtained from DRA, Malvern, UK.)

The HF electrolyte is used in both half-cells and was continuously circulated by two peristaltic pumps which are also protected by a PTFE lining. This pumping action helps to provide fresh electrolyte species to the anodising face of the wafer as well as to remove gases that are produced during anodisation (mainly hydrogen).

The Pt electrodes are circular and of similar diameter to the half cells. This arrangement helps to provide a better uniformity. These electrodes are connected to a constant current power supply and the current flows from one half cell to the other through the Si wafer. The back side of the Si wafer acts as a secondary cathode where proton reduction takes place leading to hydrogen evolution. The front side of the wafer acts as a secondary anode and PS forms on this side. It should be noted that, for safety reasons the HF was drawn rather than forced at pressure through the anodising cell.

The PS samples used in this work were produced from p^- (50-100 Ω cm) FZ silicon wafers for the reason mentioned above (Section 3.3). The backs of the wafers were implanted with $1x10^{15}$ boron/cm^2 at 40 KeV. This is to overcome the reverse biased nature of the back interface, providing ohmic contact and allowing uniform anodisation

on the front face of the wafer. This was followed by a nitrogen anneal (with 1% oxygen) at 1050°C for 30 minutes. After the anodisation, the sample was removed from the cell in an argon atmosphere. It was spin dried without dipping in deionised (DI) water to minimise contamination and possible partial oxidation with water.

The porosity and the thickness of the PS layer can be varied by adjusting the electrochemical parameters such as current density, anodisation time, resistivities of the Si wafer and the HF concentrations. The adopted method of anodisation for this work is to anodise the silicon wafer with 20 mA/cm^2 current density in 40% HF electrolyte for 2 minutes. The porosity and the thickness of the PS layer produced under these conditions were 52% and $2x10^3$nm respectively. These parameters were calculated using a gravimetric method published by Herino et al (1987). The details of the method are given in Appendix 1

3.4 Sample Storage

Since the freshly anodised PS is in a metastable condition, the storage of the porous silicon is very important. The effects of storage in different environments, on porous silicon were investigated. An as-anodised porous silicon wafer was divided into four quarters for this evaluation.

a) The first quarter was placed in a wafer rack and kept in a blue wafer box. This storage technique is the standard practice used by the process engineers in the microelectronics industry.
b) The second quarter was stored in a white wafer box. This type of box can hold a single wafer and has a screw top. This type of box is used for transporting wafers.
c) Third quarter was placed in a vacuum desiccator. The desiccator was filled with inert argon first to displace the air and it was evacuated to around 10^{-4} torr pressure, with a roughing pump attached to a sieve filled filter unit.
d) The fourth piece was kept in the vacuum desiccator as it was in (c) but the wafer was kept in a white wafer box

FTIR spectra were obtained on all four quarters of porous silicon after 7, 15,40, 60,70,80,90, 106, 113, and 145 days being kept in the above-described environments. It is important to mention here that every time the wafer was removed for the FTIR analyses they were exposed to the air for about two minutes. The slow oxidation

process (ageing process) will be discussed in Chapter 5 in detail. This investigation concentrated on the formation of oxide layer on porous silicon walls with respect to days and the environments they were kept under.

Figure 4-23 shows a typical FTIR spectrum of as-anodised porous silicon. It shows a triplet at 2140, 2115, 2089 cm^{-1}a doublet at 668 and 626 cm^{-1} and singlets at 910, 816, 735 and 512 cm^{-1}. No peak was observed with as anodised porous silicon in the region of 1100 cm^{-1}, where Si-O-Si symmetric vibration occurs, (W.A. Pliskin, 1977). This can be interpreted as showing there are no Si-O bonds present in as-anodised porous silicon (or that they are not detectable with FTIR technique).

Figures 3-6, 3-7, 3-8 and 3-9 show FTIR spectra of porous silicon samples kept in a blue wafer box, a white screw top wafer box, in a vacuum desiccator and in a white wafer box in the vacuum desiccator for 7 days and 145 days respectively. For clarification, the FTIR spectra are split into regions 3200 to 2000 cm^{-1} and 2000 to 400 cm^{-1}.

3.4.1 Blue wafer box

Figure 3-6 shows a broad peak has developed in the region of 1102 cm^{-1} to 1059 cm^{-1} with porous silicon kept in the blue wafer box for 145 days, which is due to Si-O bond vibrations. The typical "shoulder" at 1102 cm^{-1} is typically observed with SiO_2 grown on Si with steam as a part of microelectronic processing. Also the triplet observed with as-anodised porous silicon has changed to a broad single peak. Also two small peaks due to C-H vibrations have appeared at 1515 and 1463 cm^{-1}. The blue wafer box is not air-tight enough to keep the wafers free of hydrocarbon-contaminated air of the cleanroom.

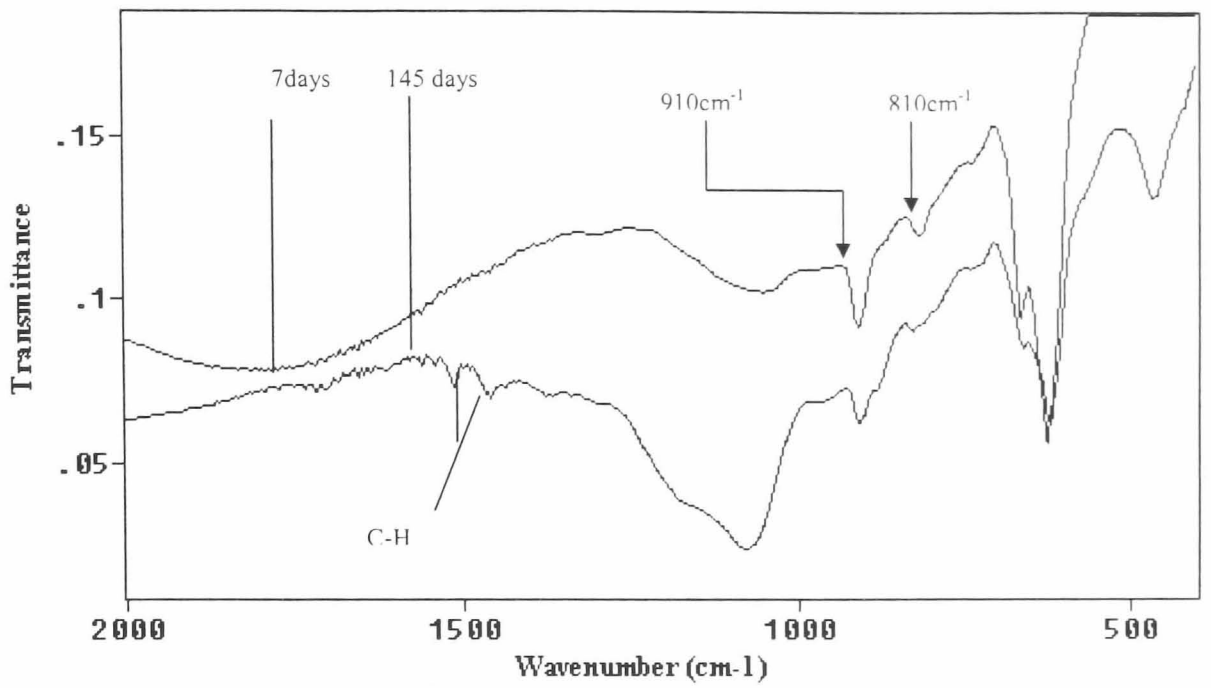

FIGURE 3- 6 FTIR spectra of PS samples kept in a blue box

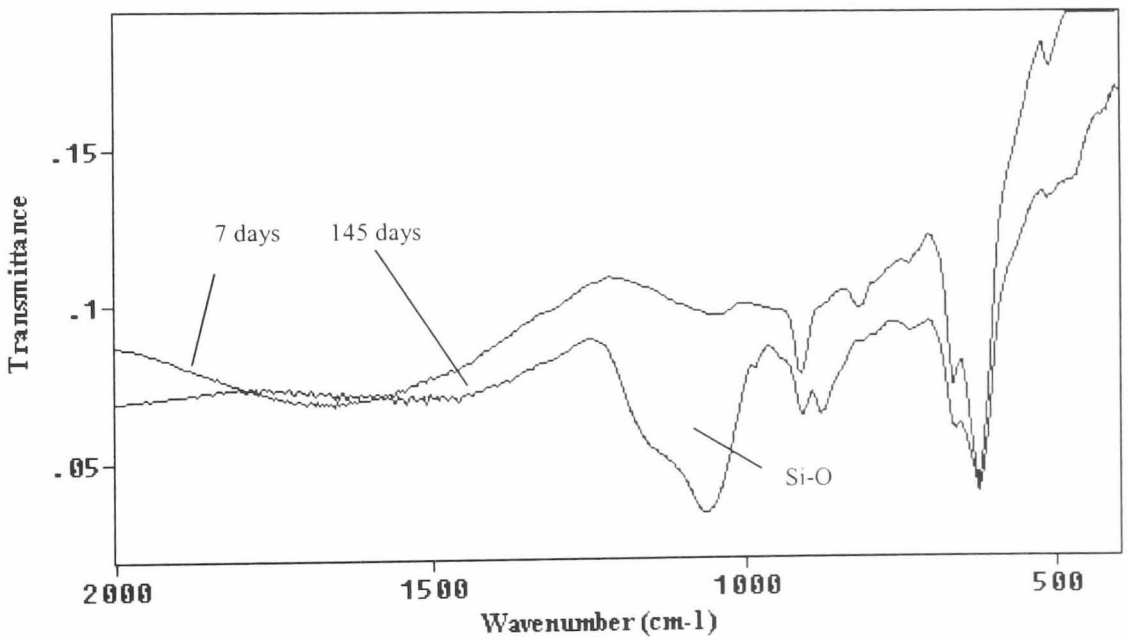

FIGURE 3- 7 FTIR spectra of PS samples kept in a white screw-top box

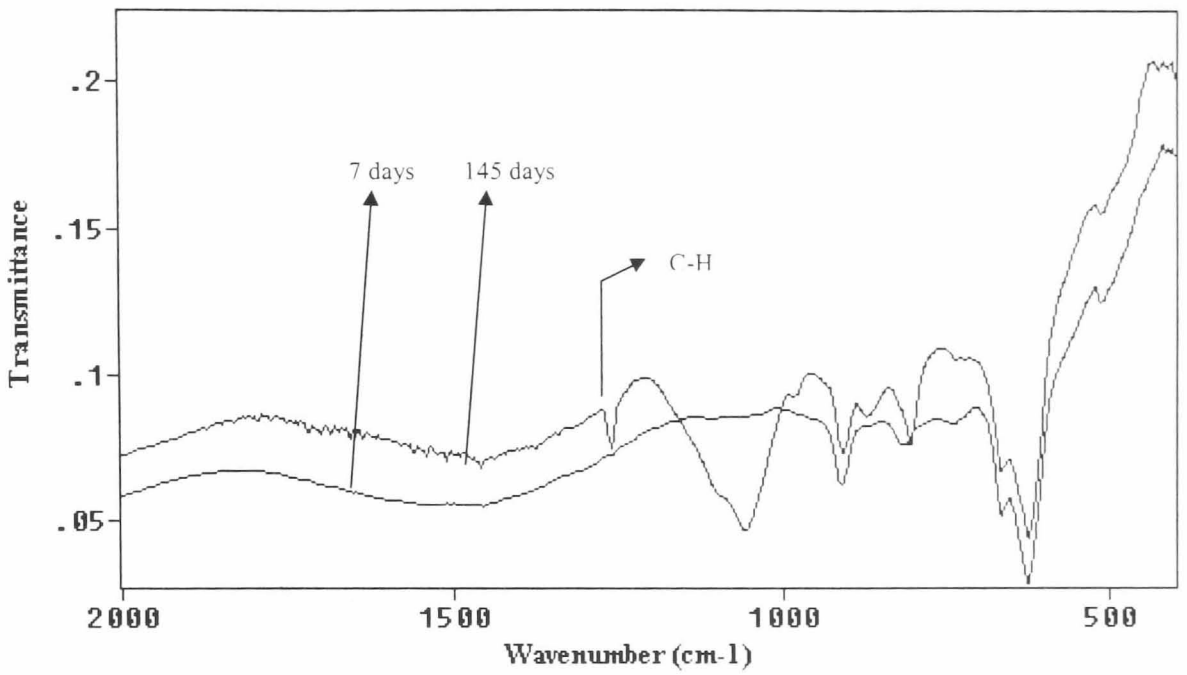

FIGURE 3- 8 FTIR spectra of PS samples kept in a vacuum desiccator

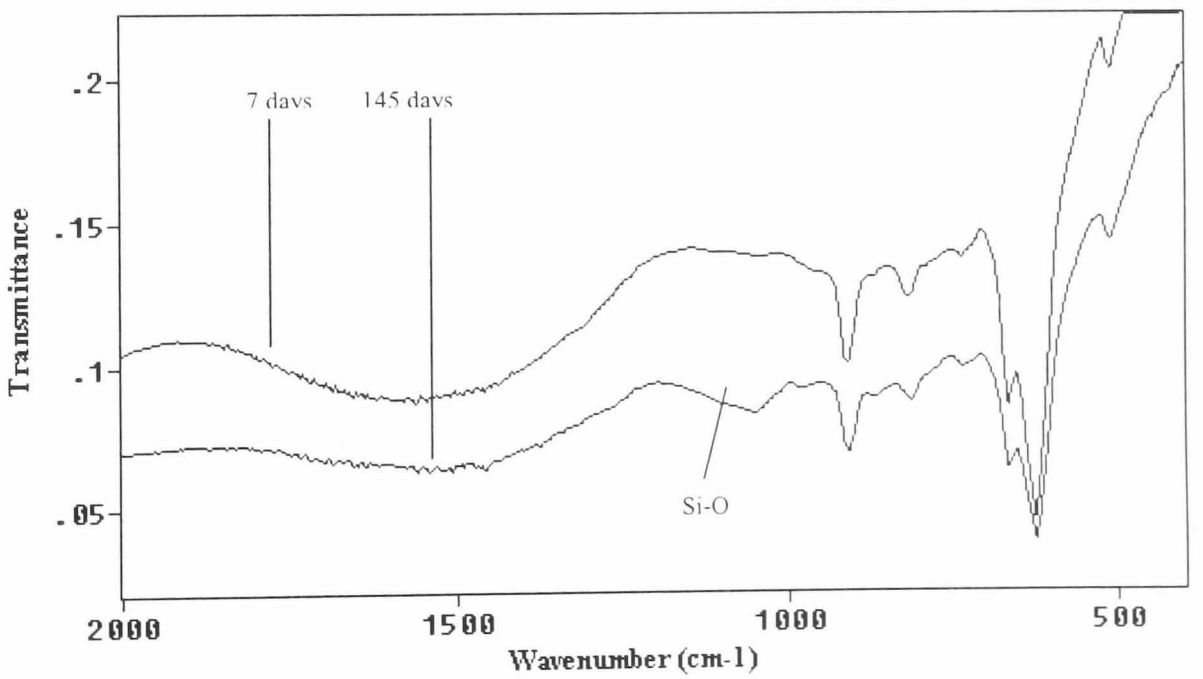

FIGURE 3- 9 FTIR spectra of PS samples kept in a white box/vacuum desiccator

3.4.2 White wafer box

Figure 3-7 shows the FTIR spectra of 7 and 145 days-old samples. These are similar to those from the blue box environment except that no C-H contamination was observed with this environment.

3.4.3 Vacuum Desiccator

Figure 3-8 shows the FTIR spectra of 7 and 145-days old samples. The Si-O peak at ~1100 cm^{-1} is now sharper. The slow oxidation process presumably involved less moisture, understandable with a vacuum desiccator. Also peak at 1267 cm-1 due to C-H bonds started to appear after around 90 days in the vacuum desiccator. The only explanation for this observation involves the silica gel used as a drying agent. The manufacturers were contacted and they agreed that there was possibility of carbon contamination.

3.4.4 White box kept in vacuum desiccator

A very small oxide peak was observed with the 145 day-old sample. Up to 16 days, the sample resembled an as-anodised porous silicon sample. No C-H peak was observed with this method of storage (Figure 3-9).

As a result of the above experiments, a routine procedure was established for storing the PS wafers. The adopted procedure was to spin dry after anodisation without the DI water rinse and to store in a vacuum desiccator. The vacuum desiccator was successively filled with argon and then pumped twice to remove most of the ambient air.

3.4.5 Observed "Peeling Effect"

It was observed that the PS layer developed 'cracks' and peeled off from the underlying silicon in narrow strips during the vacuum heating process. Figure 3-11 shows two SEM micrographs of different magnifications of the PS layer displaying this effect. This effect had found to be dependent upon the details of the thermal cycle which the PS sample had undergone and also on the resistivity of the PS. The gas evolution from all PS samples is similar in its composition but the peeling effect was noticed only for high resistivity silicon.

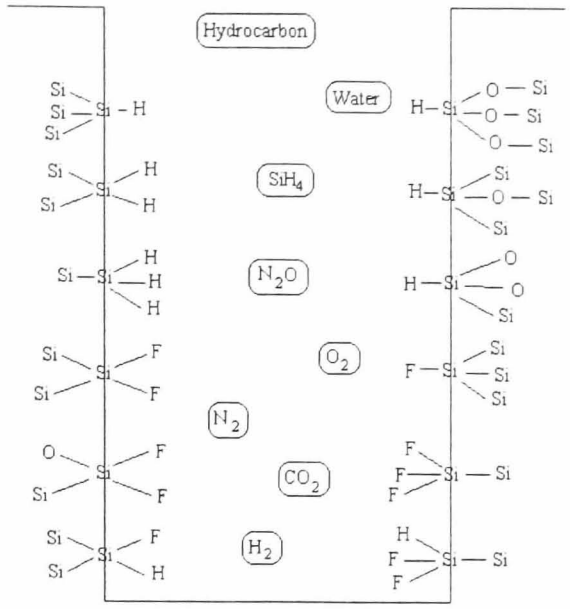

FIGURE 3- 10 Idealised pore wall with some possible chemical species

High resistive porous silicon gives rise to microporous silicon on anodisation (Beale, 1985). If an "idealised" pore is magnified, the following possible structures may be observed (figure 3-10). The pore walls consists of freshly etched silicon atoms with dangling bonds which would be passivated by hydrogen species while oxygen would have reacted with the back bonds. The void space of the pores will have fluorine species from electrolytes, HF, H_2O and gases produced during electrochemical processes in the cell, N_2 and other air components etc. The pores have multilayers of adsorbed species on the pore walls and molecular gases in the pore cavities. During heating, physisorbed gaseous species and the trapped gas molecules that come out of the pores at lower temperature cause the cracked appearance of the porous silicon surface. Microporous structure of porous silicon also contributes to this cracked surface.

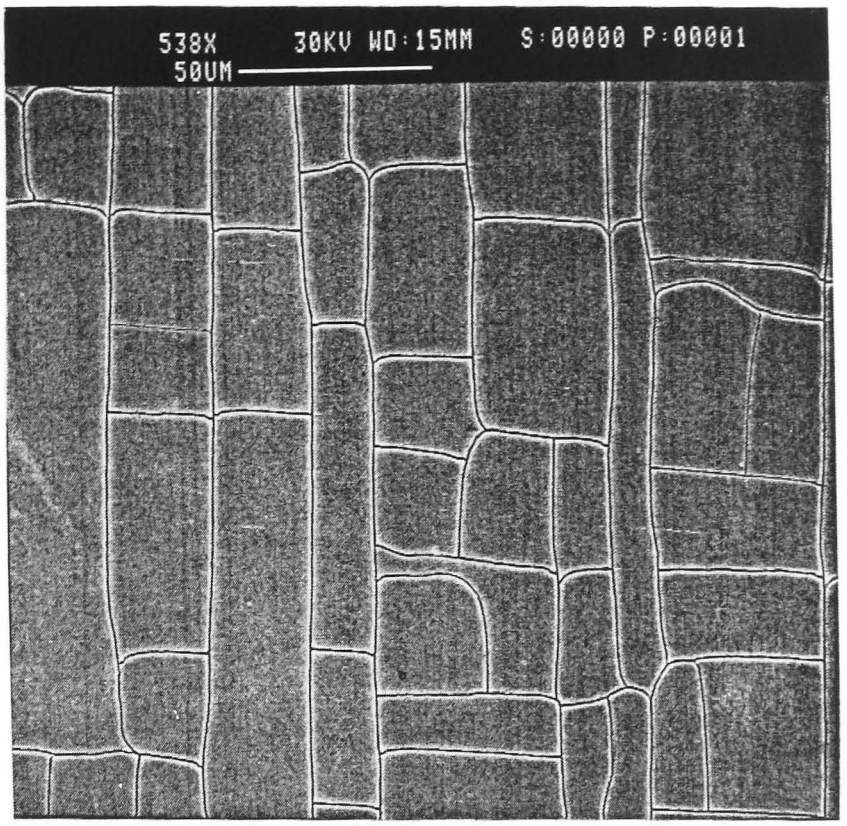

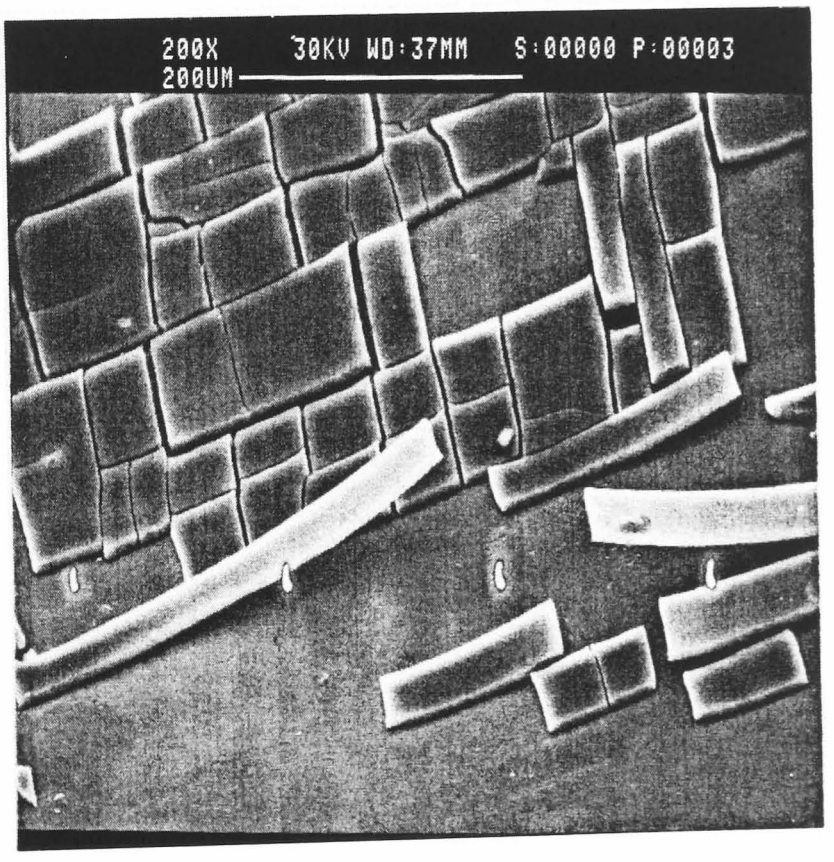

FIGURE 3- 11 SEM micrographs of heated PS sample

(Shows the peeled-off PS strips)

This problem was overcome by heating the samples to 50°C and keeping them at this temperature for 5 minutes before the temperature ramping was carried out. This produced crackfree samples for the TPD analysis.

3.5 Summary

1. The TPD system was built with a turbomolecular pump (Edwards 250EXT hybrid model), backed with a two-stage rotary pump and a molecular sieve based trap. A quadrupole mass spectrometer was used as a detector and placed ~6mm distance from the samples.
2. A heating unit was developed. K-type thermocouples with "beaded" junctions were used for measuring temperature. A programmable thermal controller was used for ramping the sample temperature.
3. High-resistive p- FZ wafers were used for producing porous silicon. These samples were found to be the best for FTIR work.
4. A vacuum desiccator flushed with argon was used for storing porous silicon samples.
5. The problem of "cracking" during the heating of porous silicon samples for TPD work was solved. The sample is heated to 50°C for 5 mins. before applying the linear temperature increase needed for the TPD analysis.

Chapter 4 Results

4.1 Introduction

The main thrust of the work undertaken is to establish the nature of the porous silicon surface using TPD and FTIR techniques. The development of these techniques to suit microporous silicon was discussed in Chapter 3. This Chapter is divided into the following three main categories:

a) TPD analysis of the desorbed gaseous species during the linear heating of porous silicon samples.
b) FTIR analysis of the effects of heating porous silicon
c) Study of gradual modification of the pore walls during the "ageing" process (slow oxidation) using FTIR technique.

4.2 Results from TPD Analysis

The quadrupole mass spectrometer used as a detector in this work is a VG Monitorr 100. Two of its facilities were utilised in this work.

a) MIM (Multiple Ion Monitoring) mode facility.

   This particular system uses software which is capable of monitoring up to 16 individual masses in a tabulated or graphical form. Background subtraction, relative sensitivities can be programmed in this mode. This facility was used for obtaining TPD spectra which are graphical representations of partial pressure versus temperature.

b) Analogue mode facility

   This mode provides for the analysis of species with m/z values of 1-100, versus intensity. A scan in the analogue mode provides a snapshot of these volatile species present in the system at that time,

The analogue mode of analysis was used to identify the dominant species desorbed from porous silicon when it is heated. The sample was heated linearly at a heating rate of 1.5 Ks^{-1} in the TPD vacuum chamber at a starting base pressure of $< 10^{-8}$ mbar while the desorbed species were scanned. Table 4-1 gives the details of the findings.

m/z	Assumed Species	
1	H^+	H_2 based
2	H_2^+	
19	F^+	HF based species
20	HF^+	
38	F_2^+/ $(H_3O)F^+$	
39	HF_2^+	
40	$H_2F_2^+$	
28	Si^+, N_2^+	Silyl based species
29	SiH^+	
30	SiH_2^+	
31	SiH_3^+	
32	SiH_4^+	
85	$^{28}SiF_3^+$	Fluorosilyl based species
86	$^{29}SiF_3^+/^{28}SiHF_3$	
87	$^{30}SiF_3^+/^{29}SiHF_3^+$	
33	$^{28}SiF_2^{++}$	
66	$^{28}SiF_2^+$	
47	$^{28}SiF^+$	

TABLE 4- 1 The main species that were observed with the analogue mode scan

The TPD results are categorised in the following order:

a) Background Studies

b) Analysis of porous silicon samples prepared in three different electrolytes

   i. Aqueous 40% HF electrolyte. (Electrolyte A)

   ii. "20% ethanoic HF". It is a 1:1 ratio of ethanol and 40% HF mixture. (Electrolyte B)

   iii. Aqueous 40% HF electrolyte followed by a 4-hour period of chemical etching - by standing in the same electrolyte for four hours without applied potential. (Electrolyte C).

4.2.1 Background Studies

The following background investigations were carried out before the analysis of porous silicon

   i. Study of the vacuum chamber

ii. Analysis of a c-silicon wafer (p^-, FZ, 20-50 Ω cm.) which was placed in an electrolyte solution similar to that for producing porous silicon but with no current applied to the system.

iii. The same type of c-silicon, dipped in 2% HF, rinsed with deionised water and dried, was used as a blank in the TPD analysis.

Vacuum System

Figure 4-1 shows a mass spectrum of the volatiles in the vacuum chamber of the TPD system which is normally pumped down to about 10^{-9} mbar pressure. The TPD chamber was scanned through 1-100 amu (atomic mass unit) using the analogue mode facility available with the quadrupole mass spectrometer. A similar investigation was carried out with the vacuum system containing the porous silicon sample (from Electrolyte A) and pumped overnight (Figure 4-2). The observed minimum pressure with the porous silicon sample was 5x 10^{-8} mbar. The observed increase in base pressure indicates that gaseous species were given out from the porous silicon sample during pumping. The observed species in both systems are given in the Table 4-2

TABLE 4- 2 Observed species in the vacuum System (with PS and with no PS)

m\z	Assumed Species	Vac.system with no porous silicon	Vac. System with porous silicon
1	H^+	Yes	Yes
2	H_2^+	Yes	Yes
16	O^+	Yes	Yes-larger
17	OH^+	Yes	Yes
18	H_2O^+	Yes	Yes
19***	F^+	No	Yes
28	N_2^+ and/or CO^+	Yes	Yes-larger
32	O_2^+	Yes	Yes-larger
44	CO_2^+	Yes	Yes-larger

*** *Fluorine species are found in the vacuum chamber with porous silicon sample.Refer to Figure 4-2*

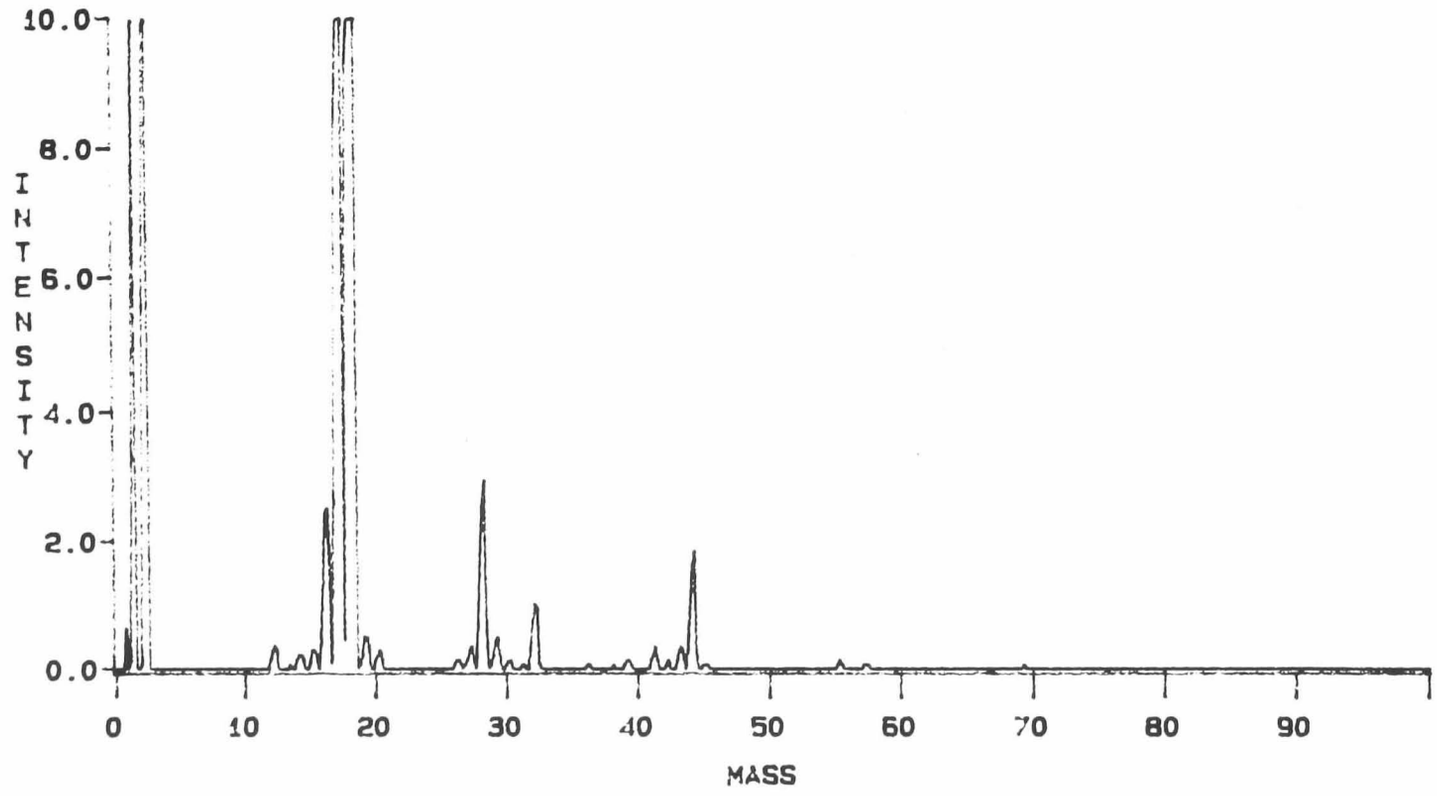

FIGURE 4- 1 Analogue mode MS scan of the TPD vacuum chamber

(Base pressure $5x10^{-9}$ mbar)

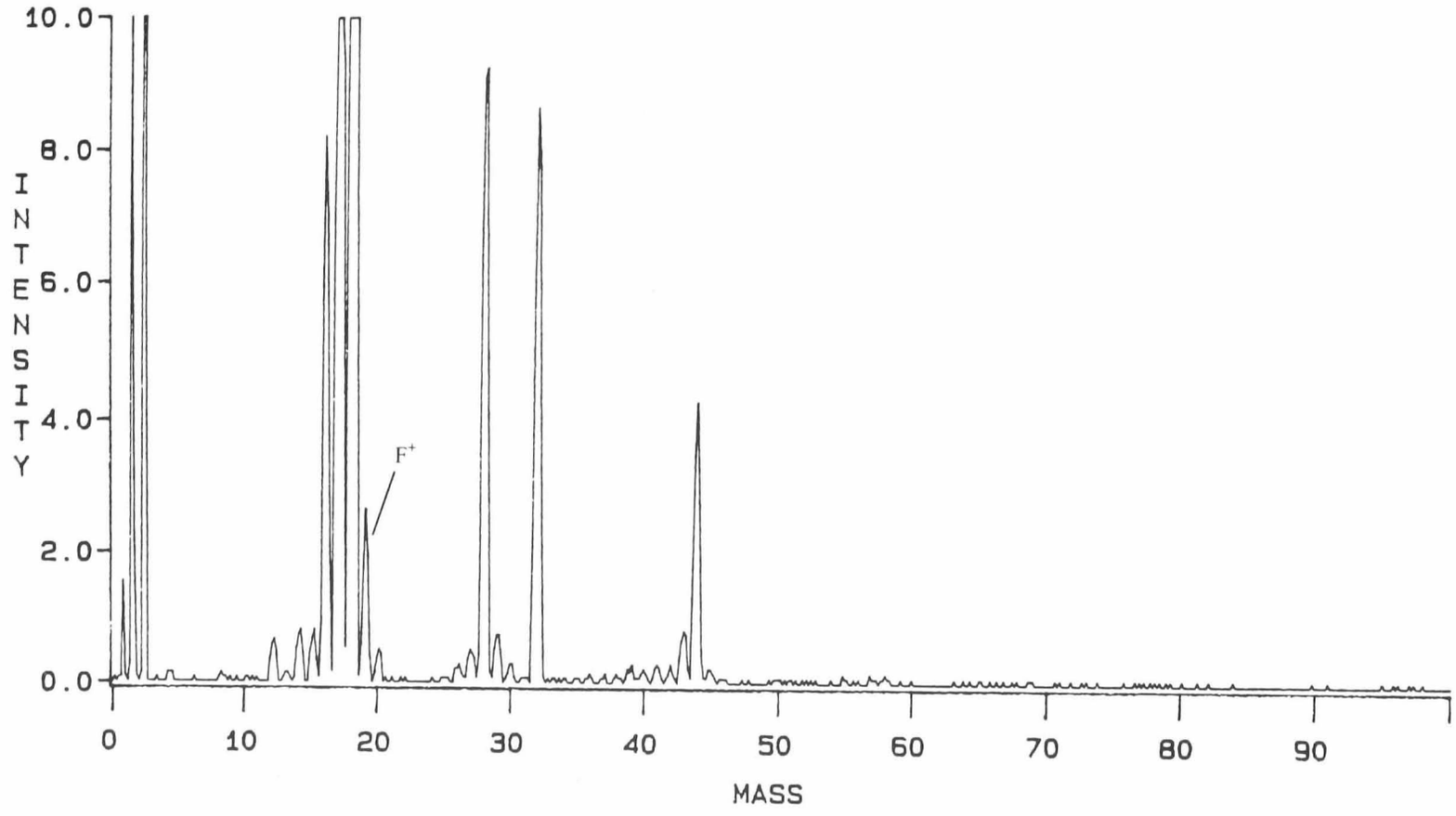

FIGURE 4- 2 Analogue mode MS scan of TPD chamber showing additional F^+ species

(Base pressure of the chamber with PS $5x10^{-8}$ mbar)

4.3 TPD analyses of a blank c-Si and a HF exposed c-Si wafer

The elimination of background effects from the heating of the c-Si and from the heating units were investigated. The heating unit with Ta foil and sapphire plate with c-Si piece as a blank was heated in the vacuum chamber with a 1.5°C/s heating rate. The thermocouple wires were sandwiched between the PS sample and c-Si pieces of 19mmx5mm dimensions.

Another analysis was carried out to investigate the effect of HF on crystalline Si surface in the same way. Figures 4-3 and 4-4 show the TPD spectra for the two types of samples. Species with m/z values 2, 18, 19, 20, 85, 31 (H_2^+, H_2O^+, F^+, HF^+, SiF_3^+, SiH_3^+ respectively) were selected for this analyses.

Analysis of c-Si (Figure 4-3) shows no detectable amounts of the above mentioned species. The HF-covered c-Si surface shows small peaks for SiH_3^+(31) and SiF_3^+(85). These are the main fragmentation products for SiH_4, silane and SiF_4, silicon tetrafluoride respectively (Figure 4-4). The peak temperature for SiF_3^+ was found to be lower than that observed with porous silicon sample which will be discussed in Chapter 5.

It is important to mention here that the TPD analyses with blank specimens suffer from the disadvantage that this technique when set up for porous silicon allows the use of small sample size (19 x 5 mm) as porous silicon has a very large surface area cm^{-2} (~200-600 m cm^{-2}). Investigation of the blanks was carried out with the same size sample as it would be for porous silicon. This is to establish that the nature of desorbed species are from porous silicon and not from blank Si.

4.3.1 TPD Analyses of Porous Silicon

As discussed in Review Chapter, the type of photoluminescence or other properties of porous silicon depends on many processing conditions, including the type of electrolyte used for the preparation of the material. Porous silicon samples prepared from three different electrolytes were chosen for this work. The wafers used for the anodisation in this work are p^- type, FZ and of resistivity 20-50 Ω cm. The silicon wafers were anodised with 20mA/cm^2 current density and spin-dried. No rinsing in deionised (DI)

water was involved at any stage of preparation. These conditions were adopted throughout the work. The porous silicon wafer was then cut to the right size (19 x 5 mm) using a diamond scriber which was dedicated to this work only. The cut sample was fixed to the heating unit and the system was pumped overnight. The sample was then linearly heated at a heating rate of 1.5 Ks^{-1} in the TPD vacuum chamber.

The TPD analyses were repeated with five samples from porous silicon prepared from each of the three different electrolytes. The average values of their peak temperatures were given in this work.

Four types of gaseous species and their fragmentation products were identified when porous silicon was heated in the TPD vacuum chamber. They were:

i. Hydrogen
ii. Silane and its fragmentation products
iii. Si-F_x species
iv. H_xF_y species

Hydrogen Formation

Figures 4-5, 4-6, 4-7 show the TPD spectra for H_2 desorption obtained from Electrolyte A, Electrolyte B and Electrolyte C respectively. All of them show two"humps" which are due to two types of detectable hydrogen environments.

The temperature differences between the two peaks of hydrogen TPD spectra are all similar. This suggests that there is no difference in the way hydrogen desorption occurs in porous silicon prepared from the three electrolytes.

The fragmentation pattern of hydrogen on the mass analyser head of quadrupole mass spectrometer with ionisation voltage of 70 eV is given below.

TABLE 4- 3 Fragmentation pattern of H_2

m/z	AssumedSpecies	% Abundance
2	H_2^+	100%
1	H^+	2%

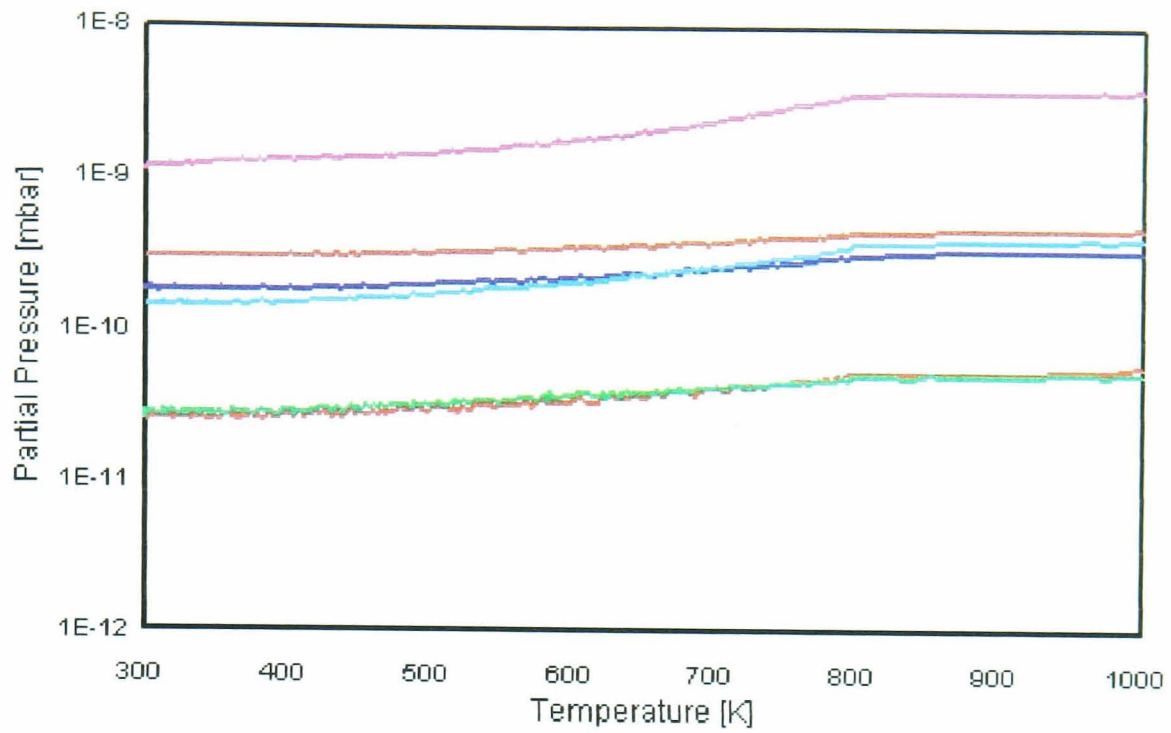

FIGURE 4- 3 TPD spectrum of blank c-Si wafer heated in the TPD chamber

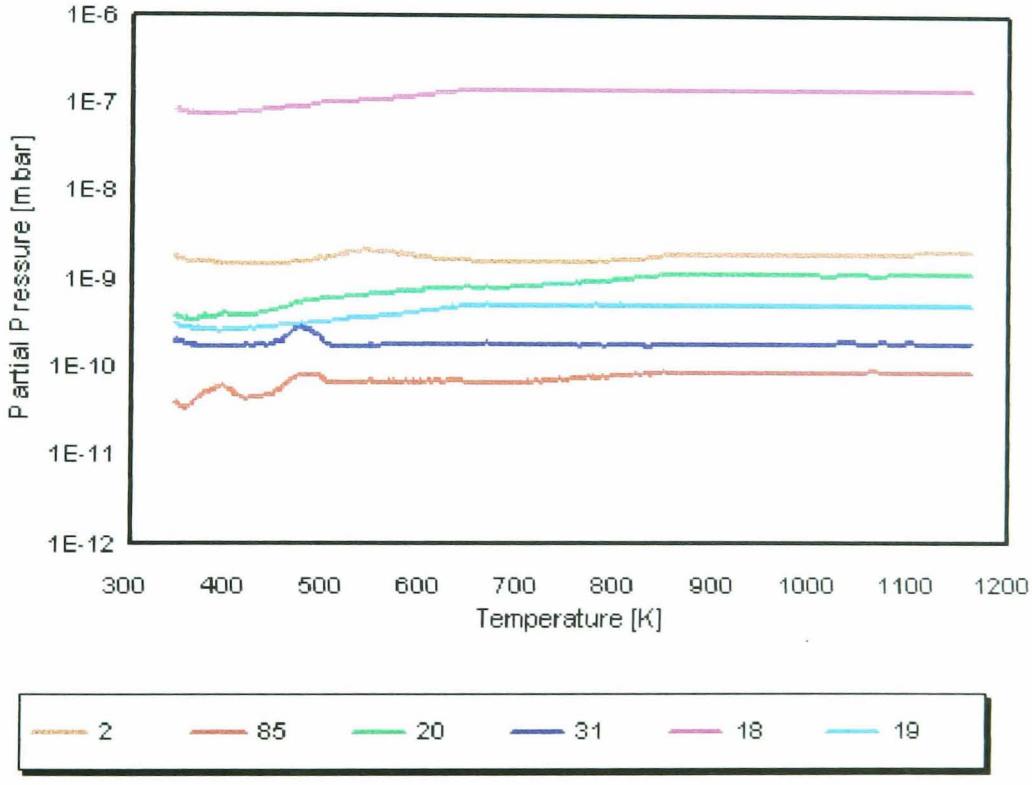

($2\text{-}H_2^+$, $85\text{-}SiF_3^+$, $20\text{-}HF^+$, $31\text{-}SiH_3^+$, $18\text{-}H_2^+$, $19\text{-}F^+$)

FIGURE 4- 4 TPD spectrum of a blank c-Si wafer immersed in electrolyte with no current

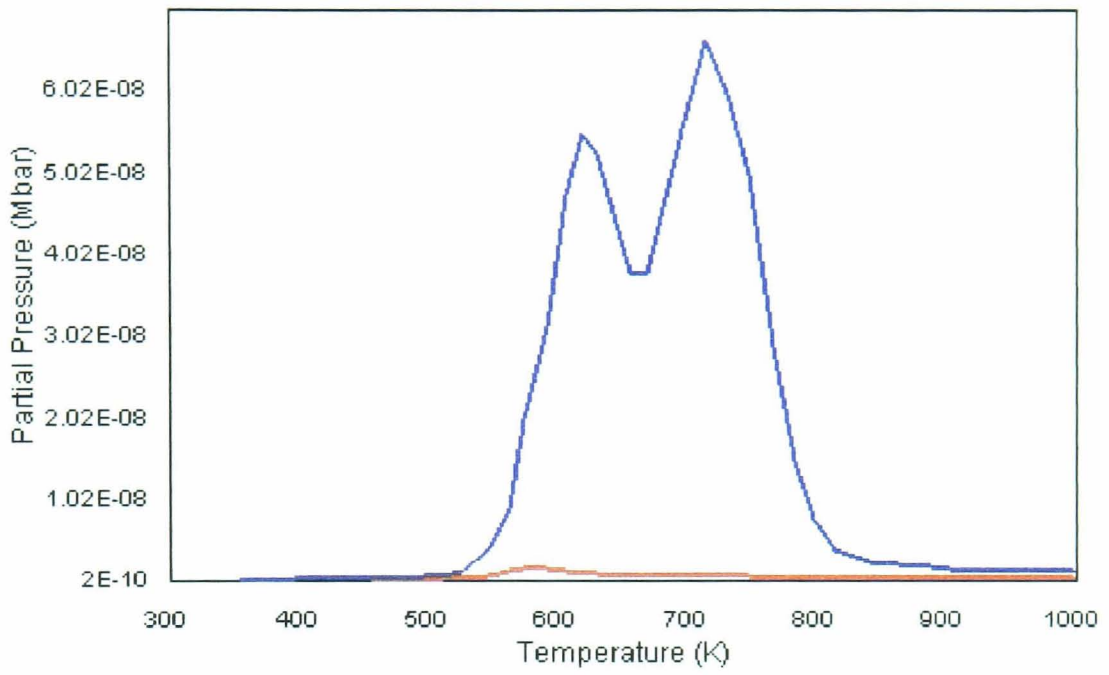

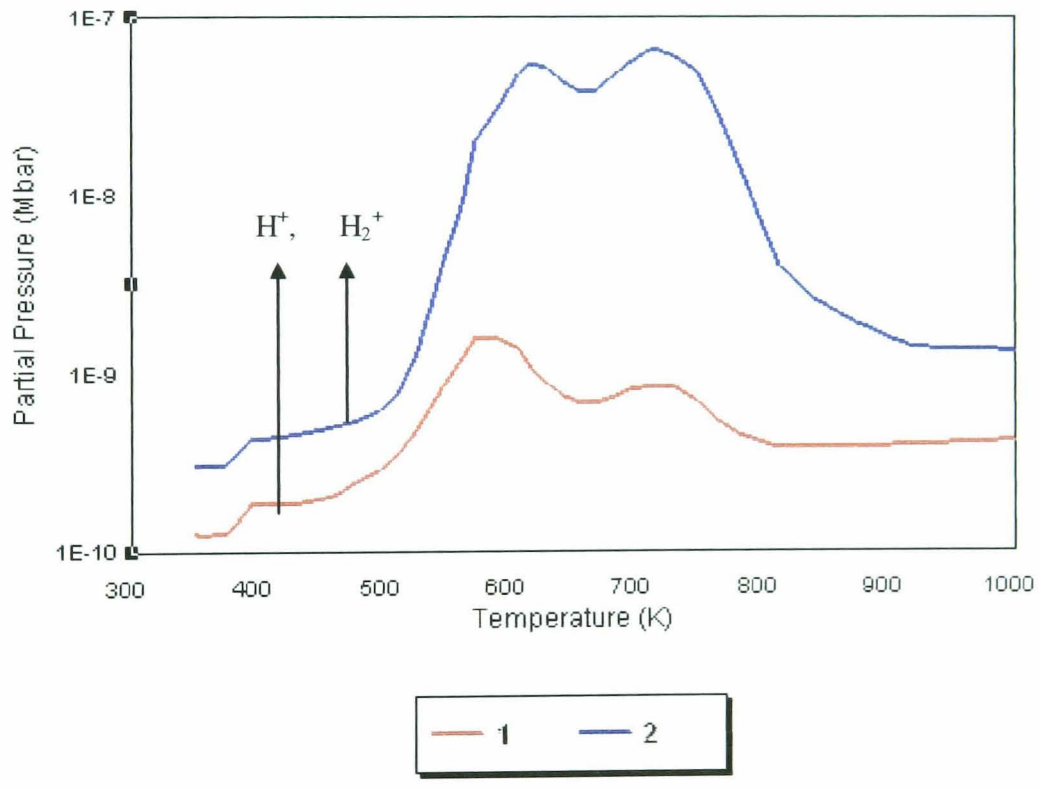

FIGURE 4- 5 H_2 desorption spectra of PS prepared from Electrolyte A

(Note – linear and log scales on partial pressure axes)

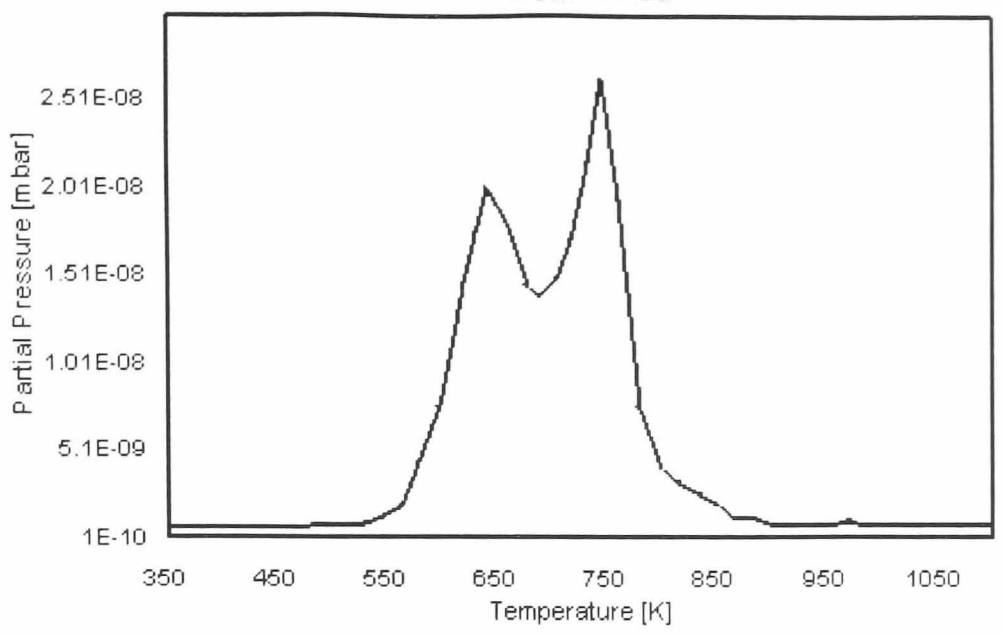

FIGURE 4- 6 H_2 desorption spectra of PS prepared from Electrolyte B

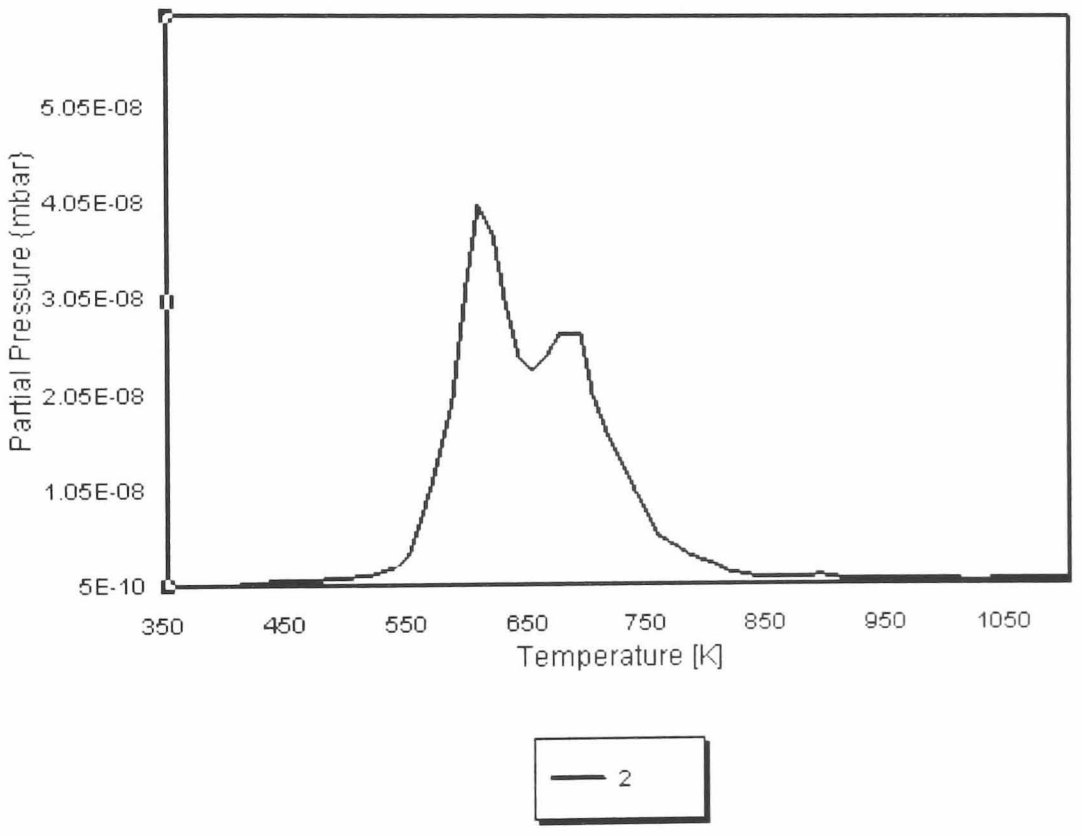

FIGURE 4- 7 H_2 desorption spectra of PS prepared from Electrolyte C

Silane and Silyl groups

Figures 4-8, 4-9 and 4-10 show TPD spectra of silyl related fragmentation products from all three electrolytes. All three spectra show very similar peak temperatures of 575-585K. The desorbed species observed at this temperature were 28, 29, 30, 31 and 32 which are identified as the fragmentation products of silane (Si^+, SiH^+, SiH_2^+, SiH_3^+ and SiH_4^+ respectively) (Potzinger et al.).

The TPD desorption peaks of samples prepared from electrolytes B and C appeared to be broader than those of sample prepared from electrolyte A. Also, a second peak at 425K ± 5K was seen at m/z 29 (SiH^+) with porous silicon from electrolyte A.

Si-F_x and H_xF_y species

Three types of fluorine-based species were observed. They were:

i. Fluorosilyl species - F (fluorine) atoms bonded to Si atoms
ii. Fluorohydrides - F atoms bonded to H atoms
iii. Non-bonded fluorine

Fluorosilyl Species

Eight fluorosilyl species, Si-F_x were observed during the desorption process. Four of them were identified as SiF_3^+, SiF_2^+, SiF_2^{++} and SiF^+, which correspond to m/z values of 85, 66, 33 and 47 respectively. The fragmentation pattern, for SiF_4 itself is given in Table 5-7. It can be seen from the table that the doubly ionised SiF_2^{++} species is four times more abundant than the singly ionised SiF_2^+ species. Also, the SiF_3^+ species distinctively shows considerable amount of its isotopic counterparts ($^{29}SiF_3^+$ and $^{30}SiF_3^+$ - 5.24% and 3.4% respectively)

The desorption spectrum at m/z 85, SiF_3^+ shows three distinctive peaks with the porous silicon prepared from electrolyte A (Figure 4-11). This suggests that the SiF_3^+ species originated from three different sites within the porous silicon. The porous silicon prepared from alcoholic electrolyte (Electrolyte B) shows a broad single peak and a larger well defined peak at higher temperature (figure.4-12). The porous silicon prepared from Electrolyte C shows three peaks but the first and second peaks are not

well resolved and the second peak is larger than the third high temperature peak (Figure 4-13).

Fluorohydrides and F^+ species

The TPD spectra for H-F species are presented (Figures 4-17, 4-18 and 4-19) for porous silicon samples anodised in all three electrolytes. Please note that the partial pressures of the desorbed species are presented in linear and log scales to illustrate the differences.

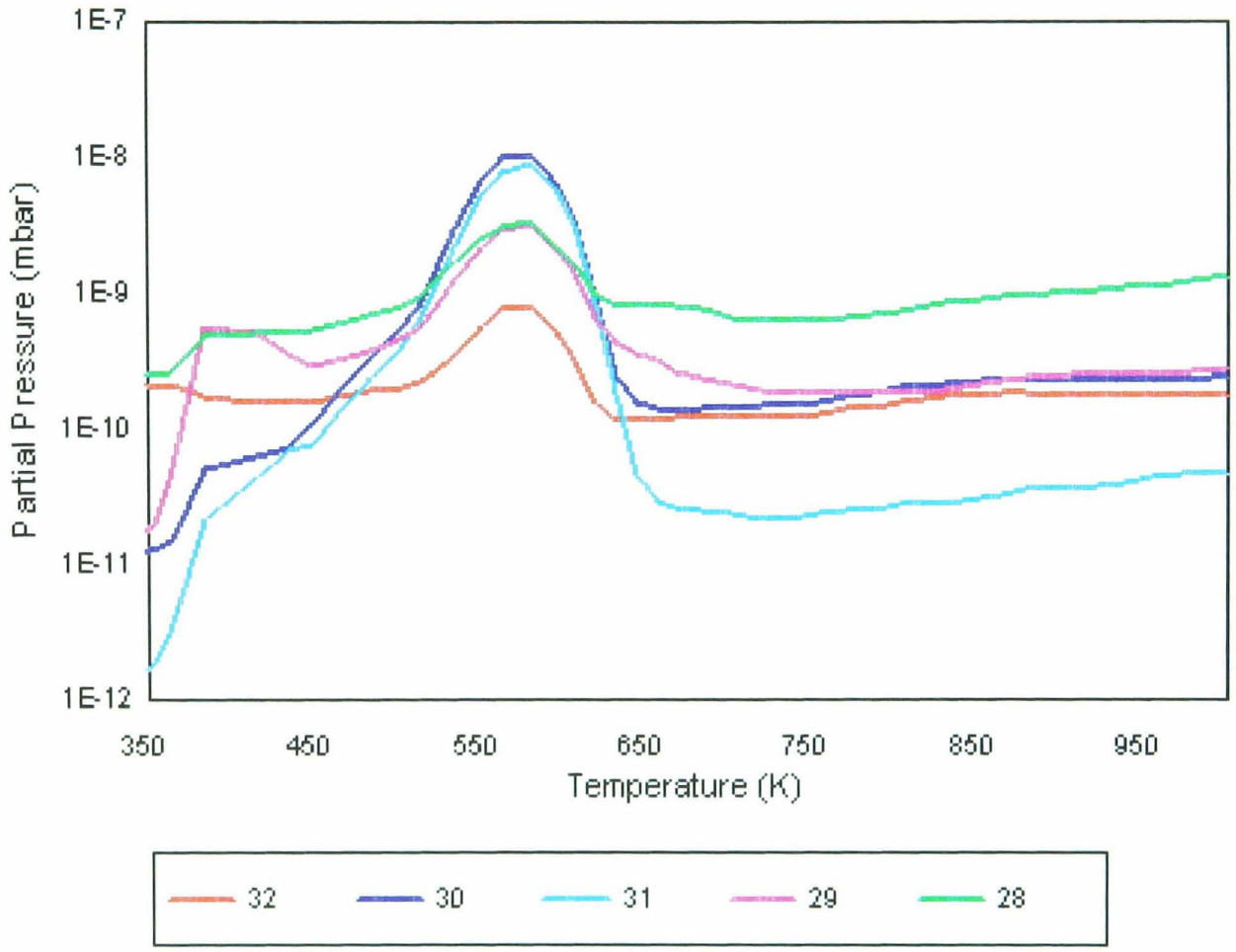

(32-SiH_4^+, 31-SiH_3^+, 30-SiH_2^+, 29-SiH^+, 28-Si^+)

FIGURE 4- 8 TPD spectrum showing fragmentation products of SiH_4 from PS (Electrolyte A)

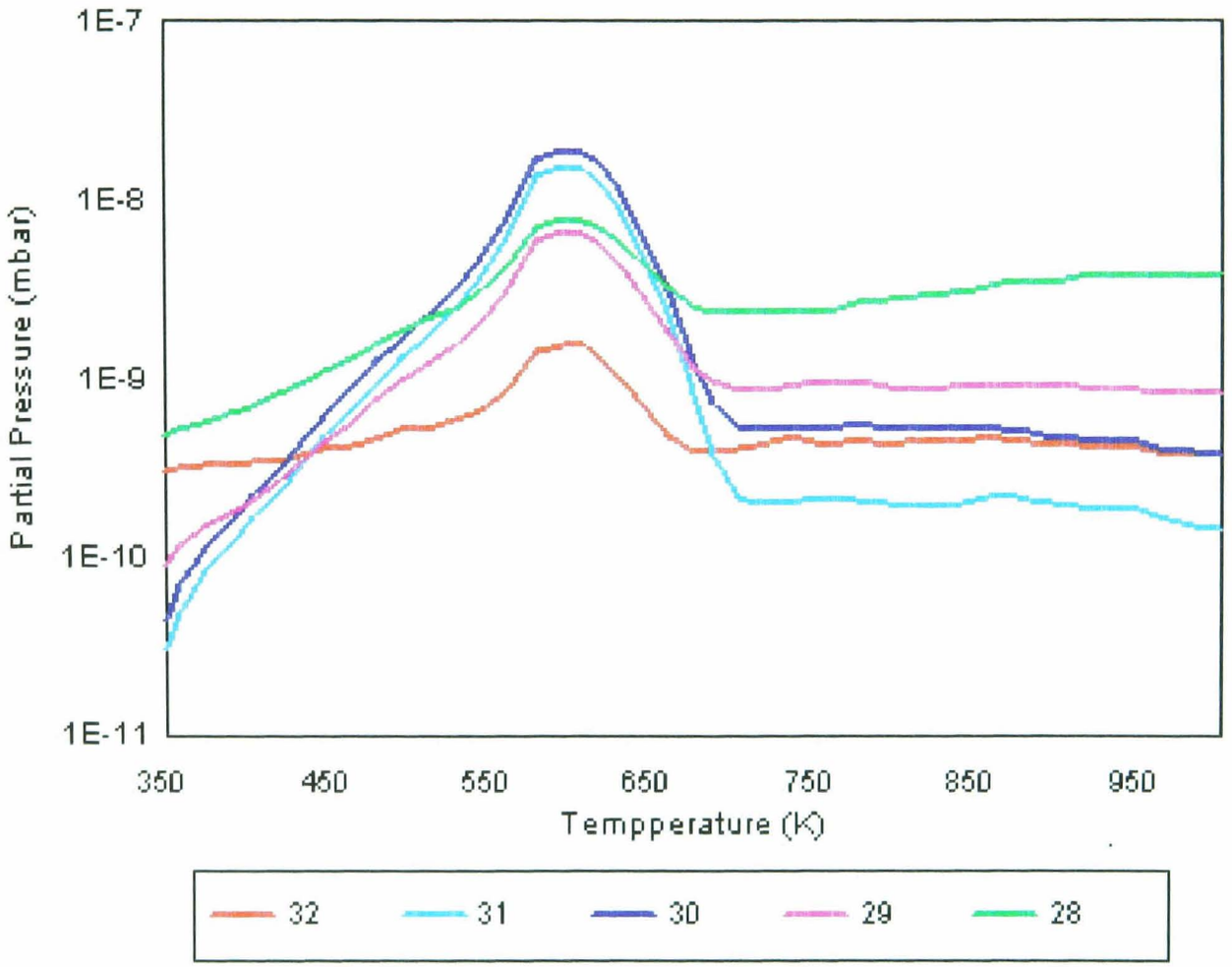

($32\text{-}SiH_4^+$, $31\text{-}SiH_3^+$, $30\text{-}SiH_2^+$, $29\text{-}SiH^+$, $28\text{-}Si^+$)

FIGURE 4- 9 TPD spectrum showing fragmentation products of SiH_4 from PS (Electrolyte B)

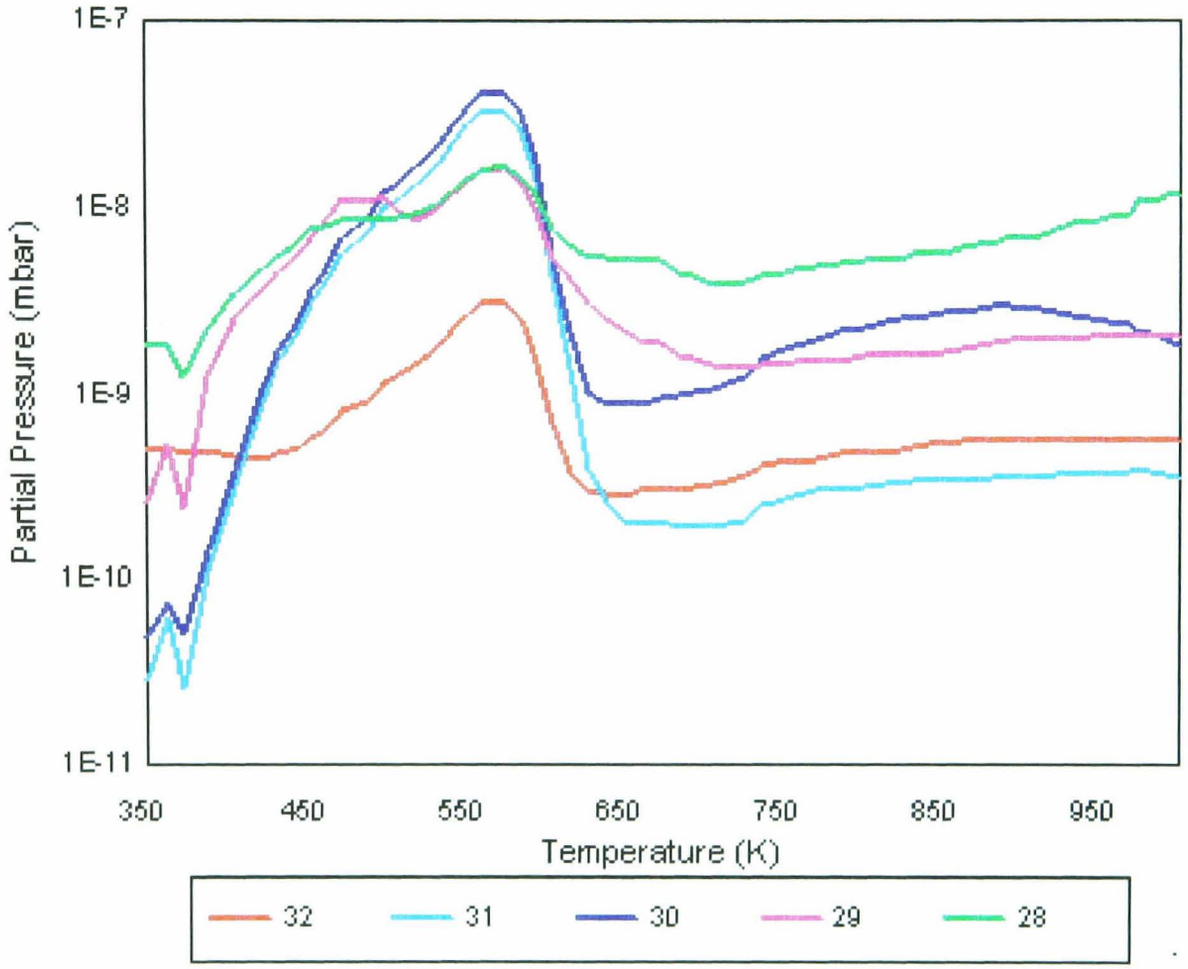

(32-SiH_4^+, 31-SiH_3^+, 30-SiH_2^+, 29-SiH^+, 28-Si^+)

FIGURE 4- 10 TPD spectrum showing fragmentation products of SiH_4 from PS (Electrolyte C)

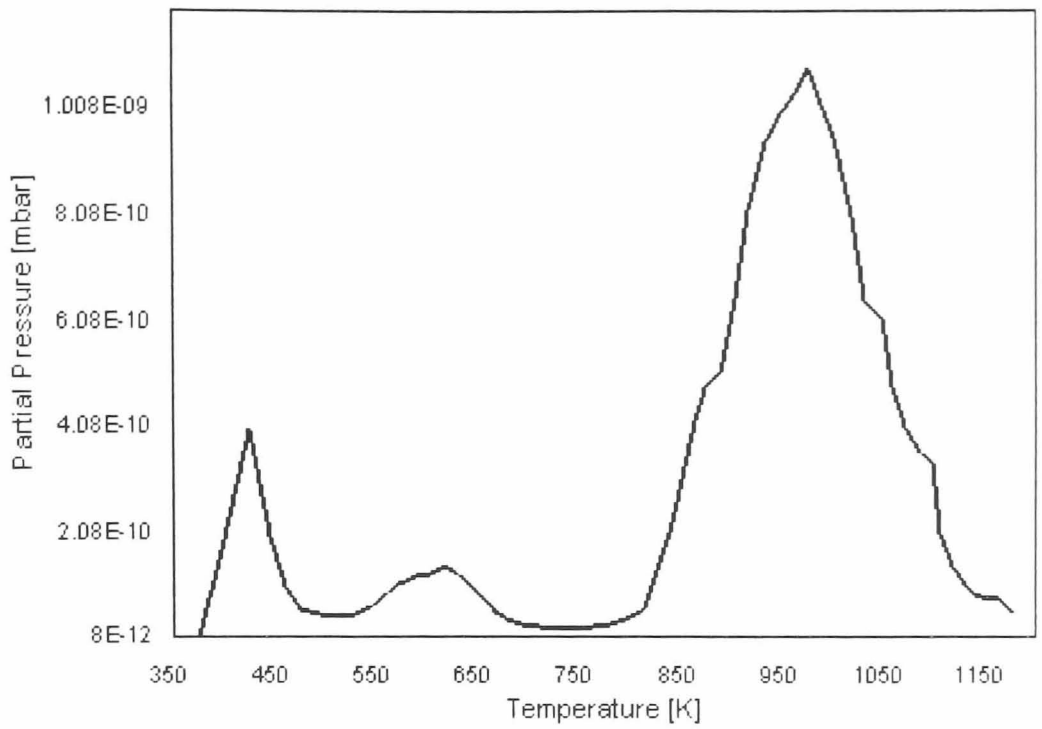

(a)

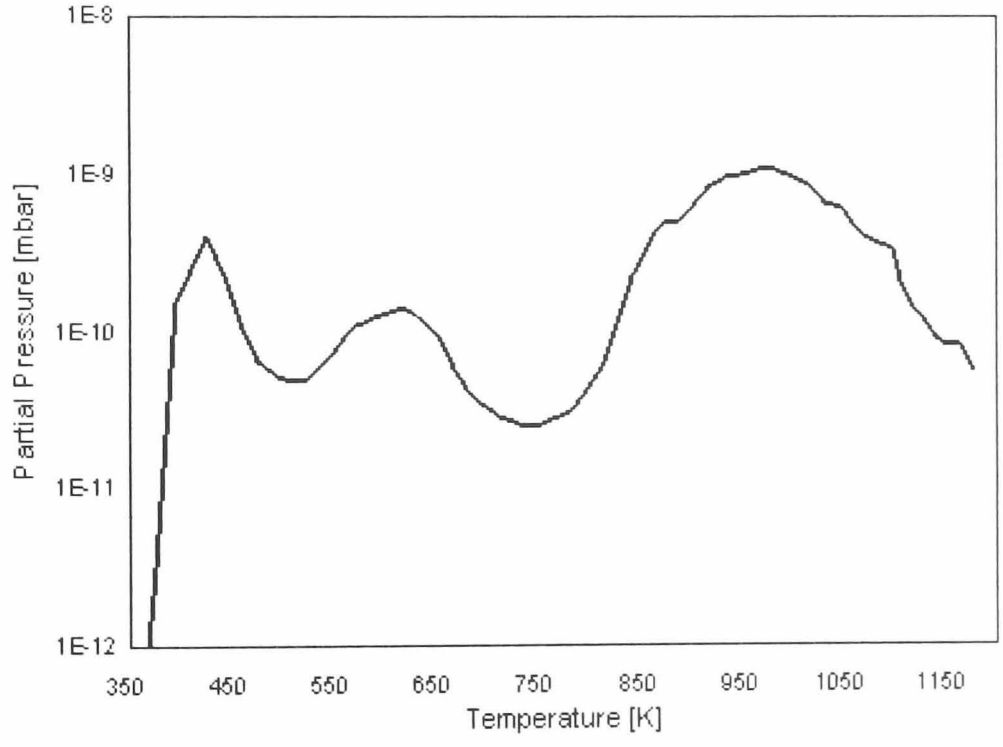

(b)

FIGURE 4- 11 TPD desorption spectrum of SiF_3^+ species from PS (Electrolyte A)

Partial pressure scale is linear in (a) and log in (b)

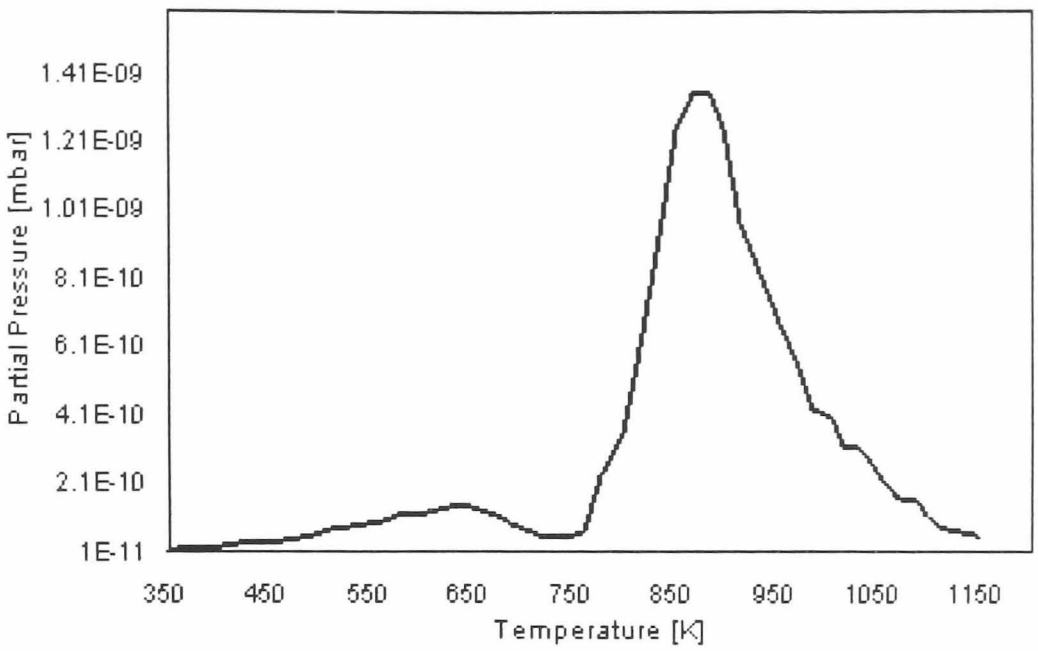

(a)

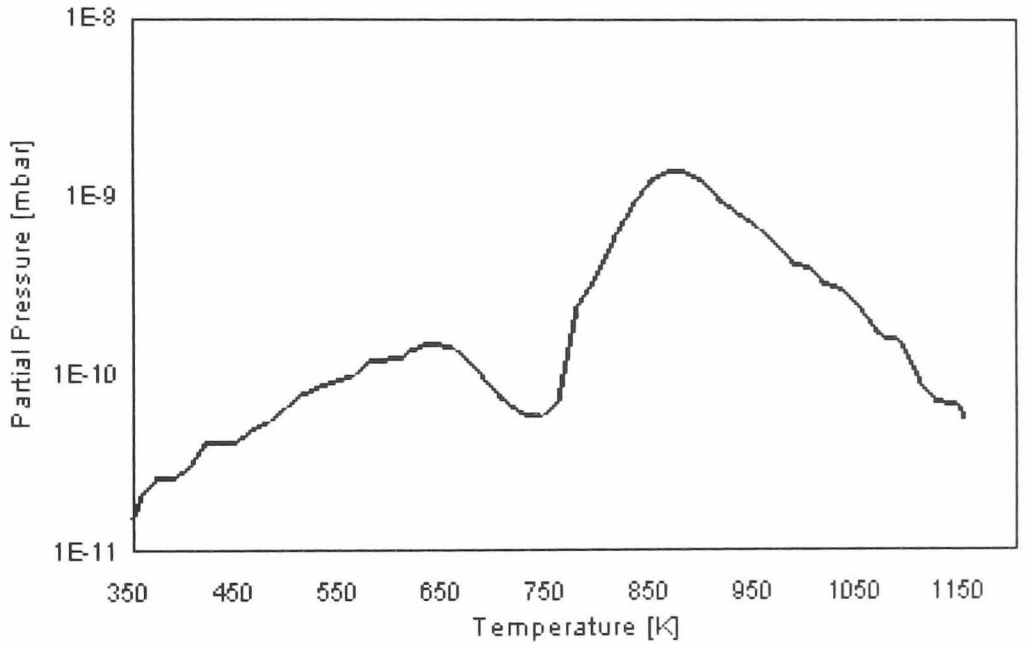

(b)

FIGURE 4- 12 TPD desorption spectrum of SiF_3^+ species from PS (Electrolyte B)

Partial pressure scale is linearin (a) and is log in (b)

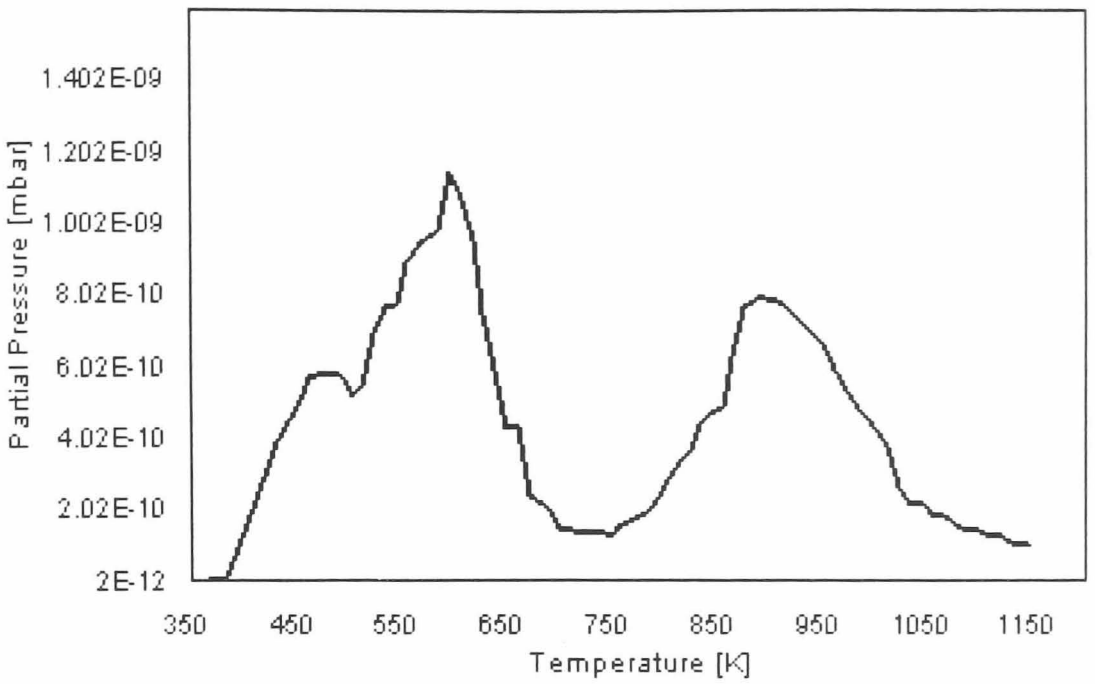

(a)

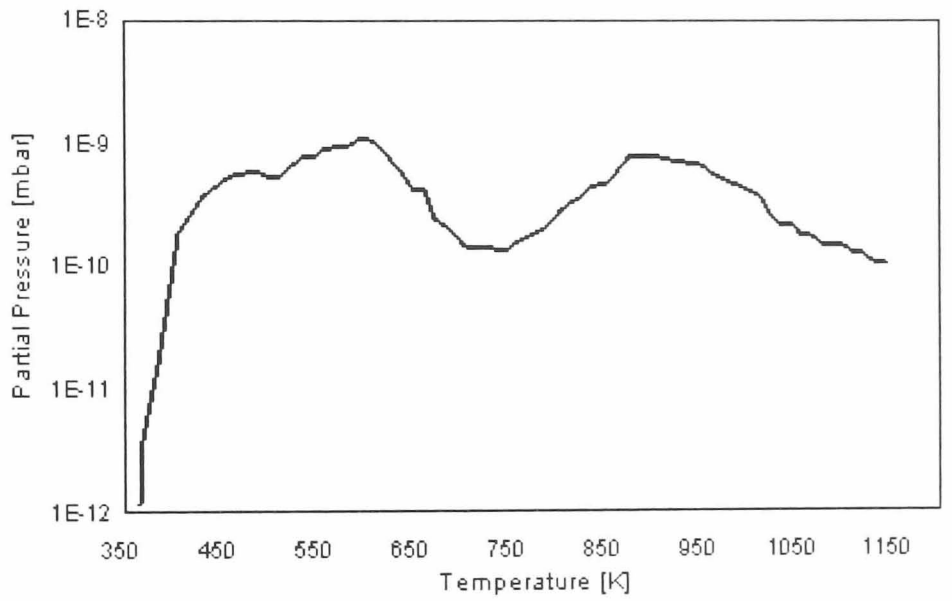

FIGURE 4- 13 TPD desorption spectrum of SiF_3^+ species from PS (Electrolyte C)

Partial pressure scale is linear in (a) and is log in (b)

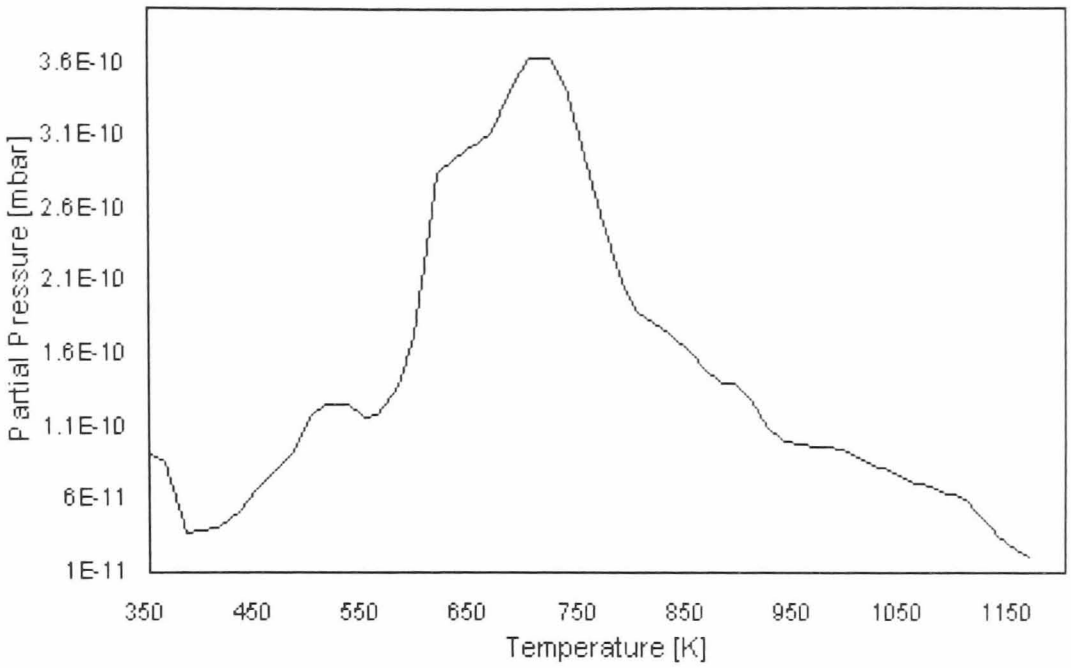

(a)

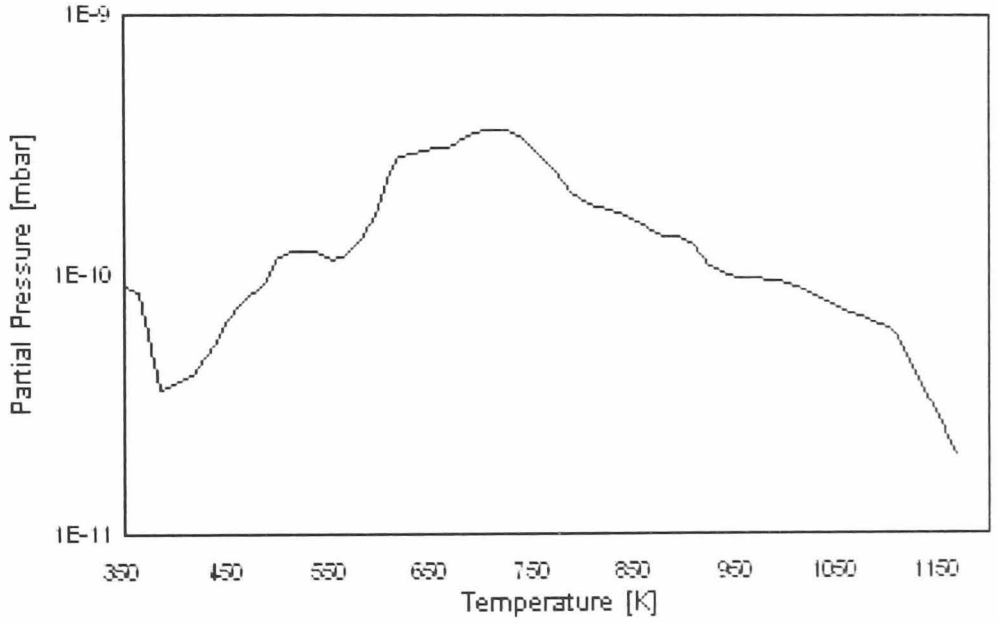

(b)

FIGURE 4- 14 Desorption spectra of F^+ of PS from Electrolyte A

Please note- the partial pressure axis in (a) is linear and in (b) is log

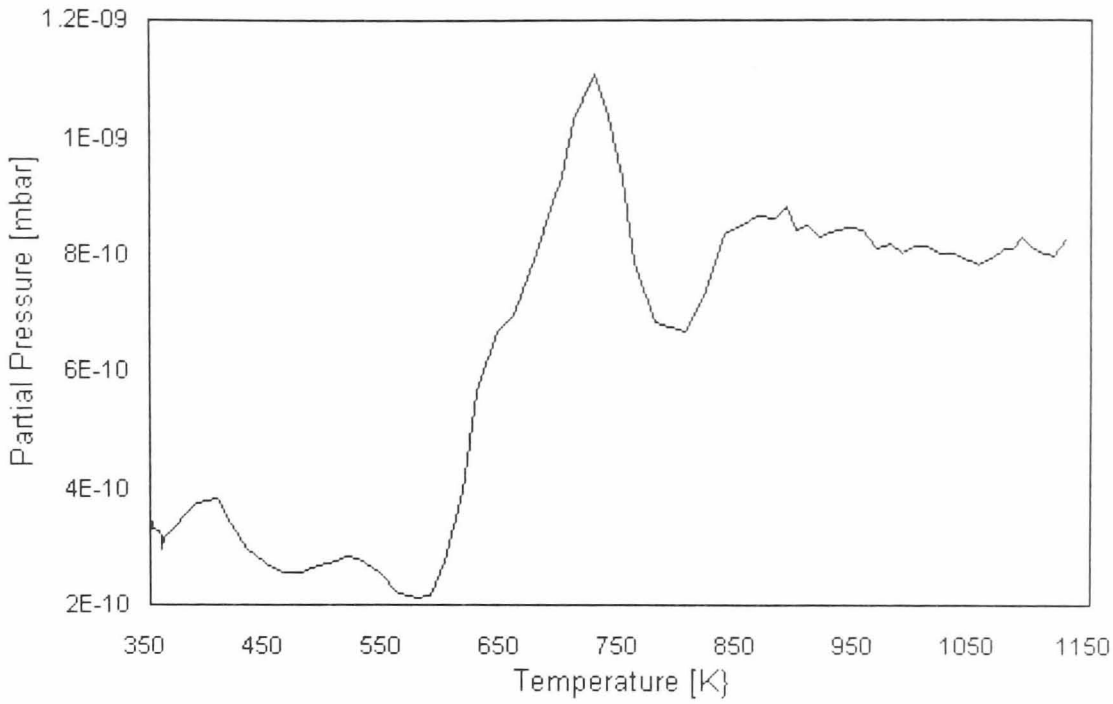

(a)

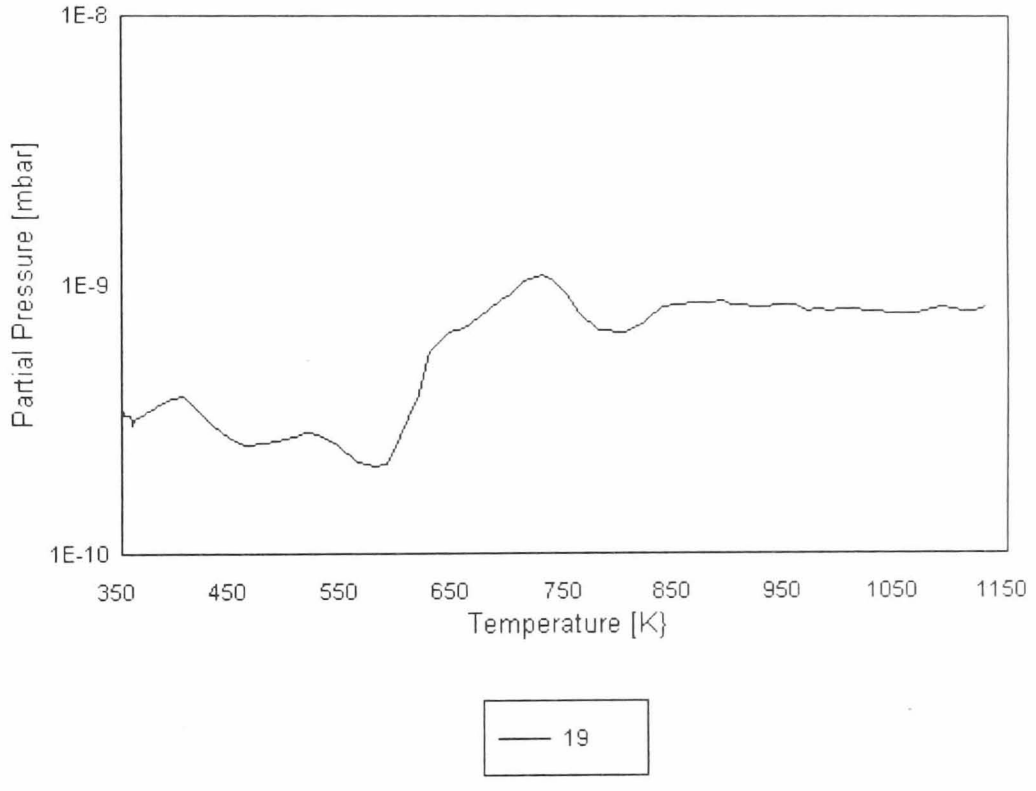

(b)

FIGURE 4- 15 Desorption spectra of F^+ of PS from Electrolyte B

Please note- the partial pressure axis in (a) is linear and in (b) is log

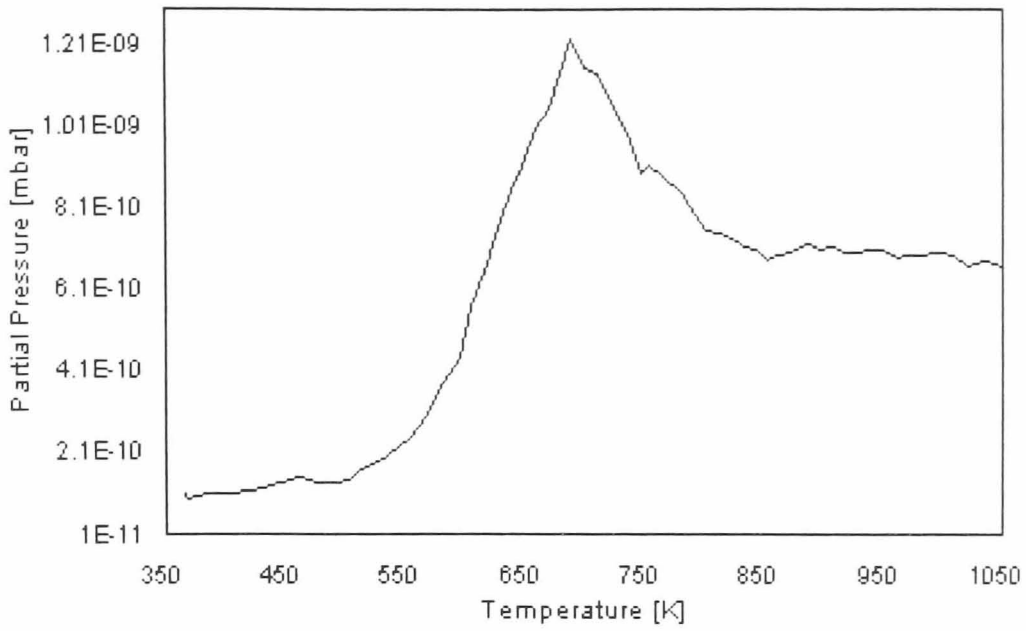

(a)

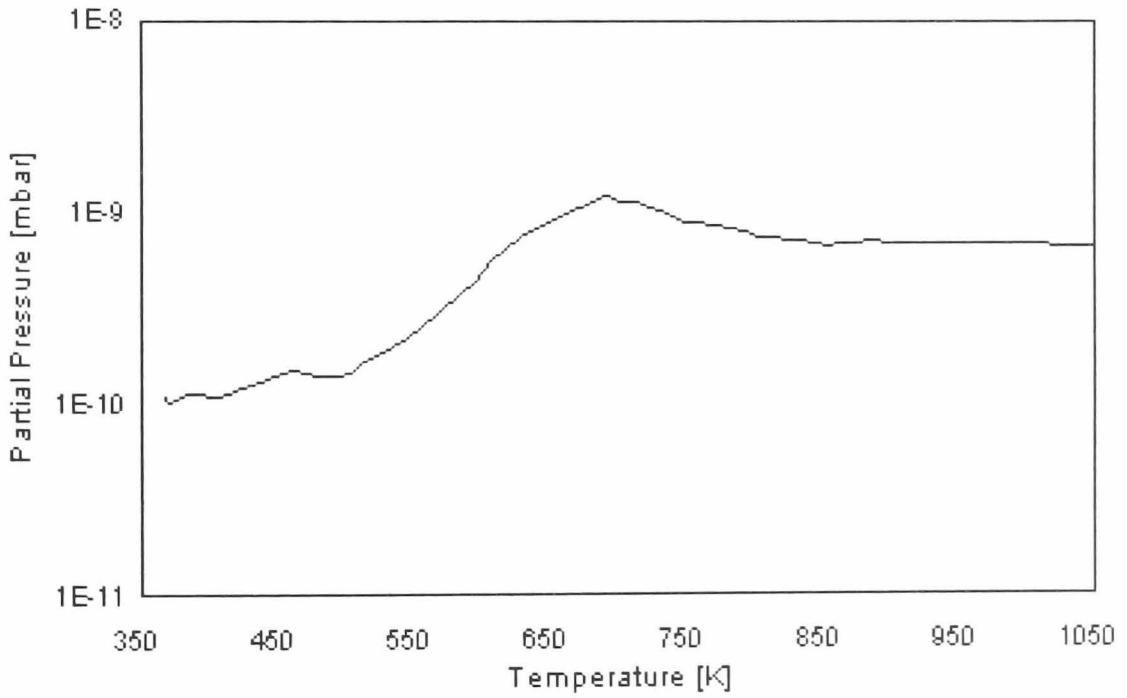

(b)

FIGURE 4- 16 Desorption spectra of F^+ of PS from Electrolyte C

Please note- the partial pressure axis in (a) is linear and in (b) is log

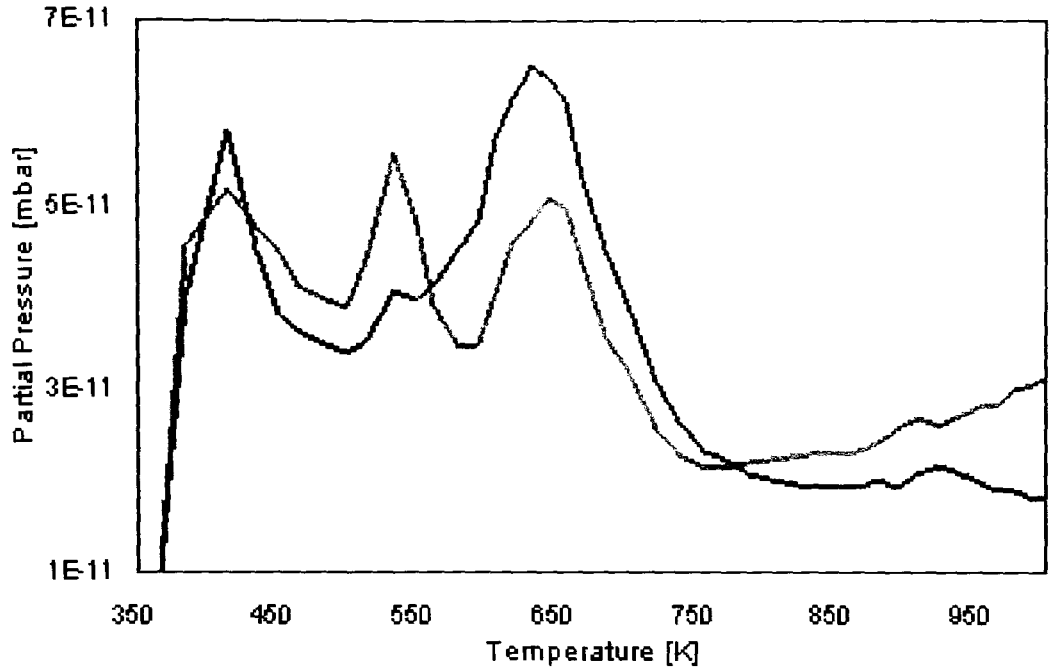

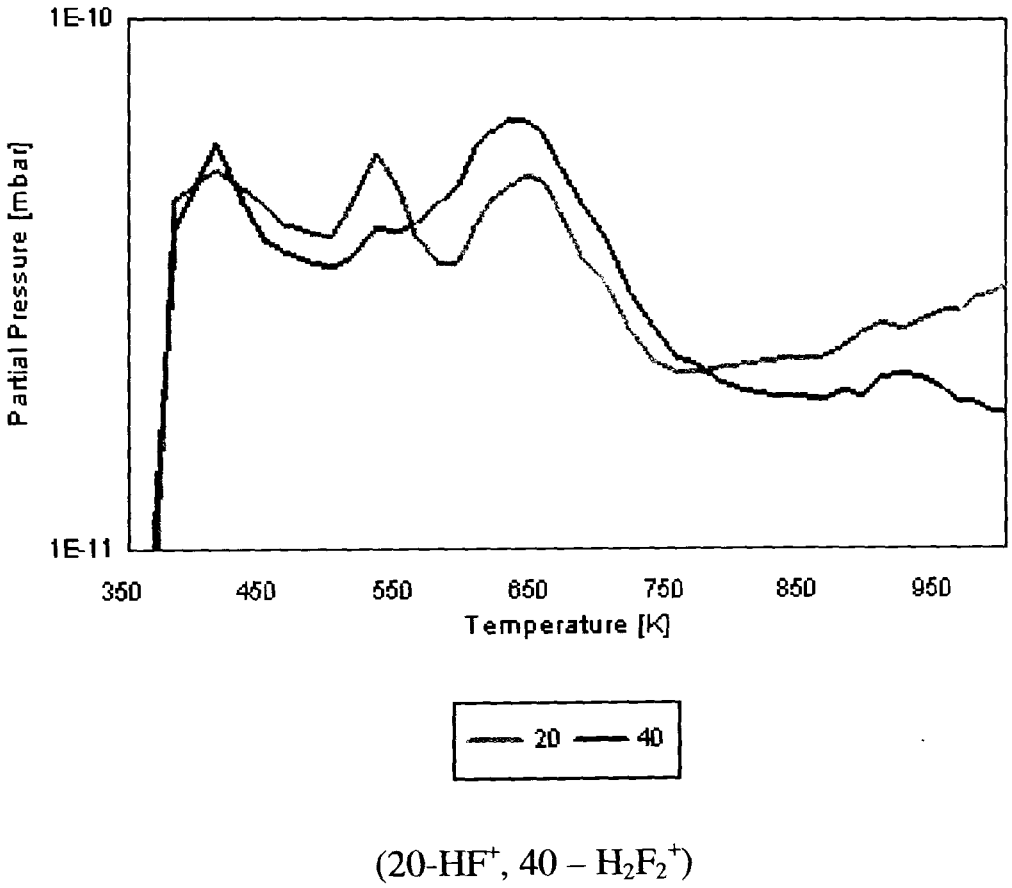

$(20\text{-}HF^{+}, 40 - H_2F_2^{+})$

FIGURE 4- 17 Desorption spectra of HF^{+} and $H_2F_2^{+}$ from PS (Electrolyte A)

(Note- log and linear scales for the partial pressure)

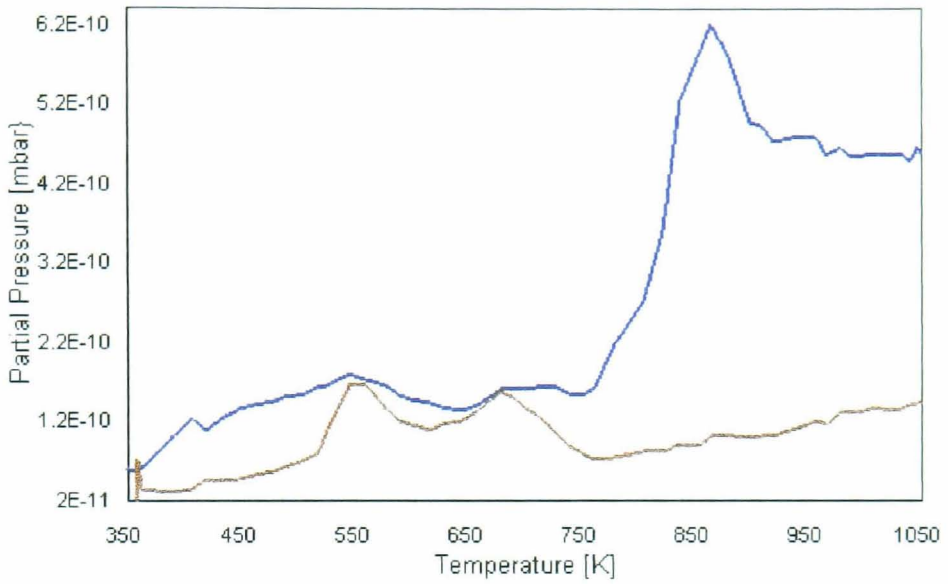

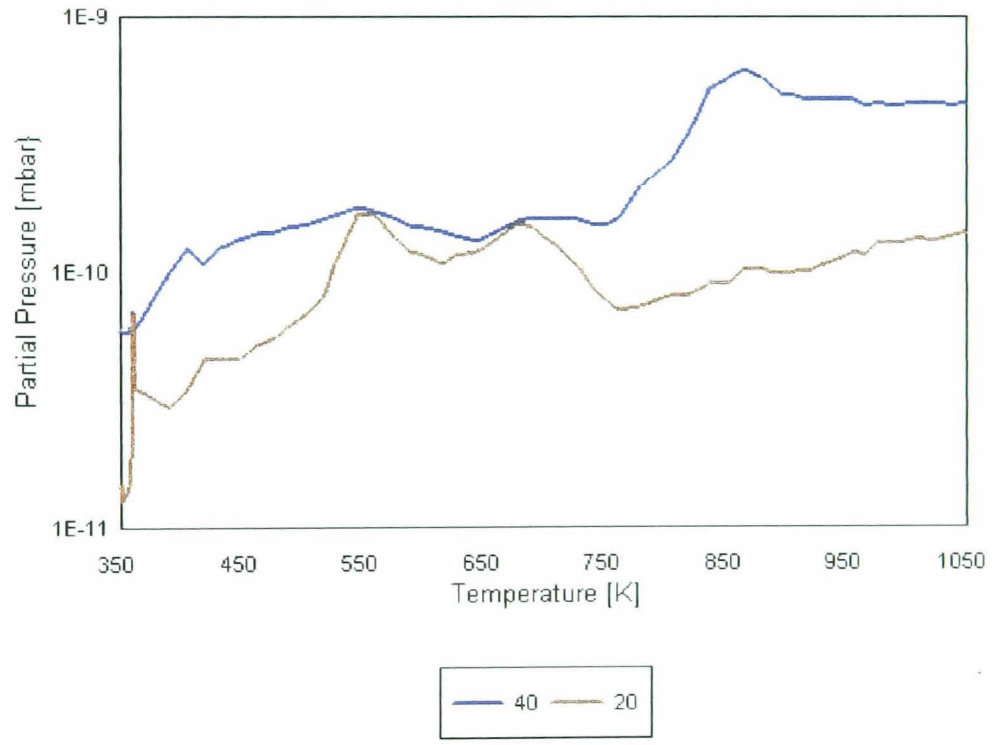

$(20\text{-}HF^{+},\ 40 - H_2F_2^{+})$

FIGURE 4- 18 Desorption spectra of HF^{+} and $H_2F_2^{+}$ from PS (Electrolyte B)

(Note- log and linear scales for the partial pressure)

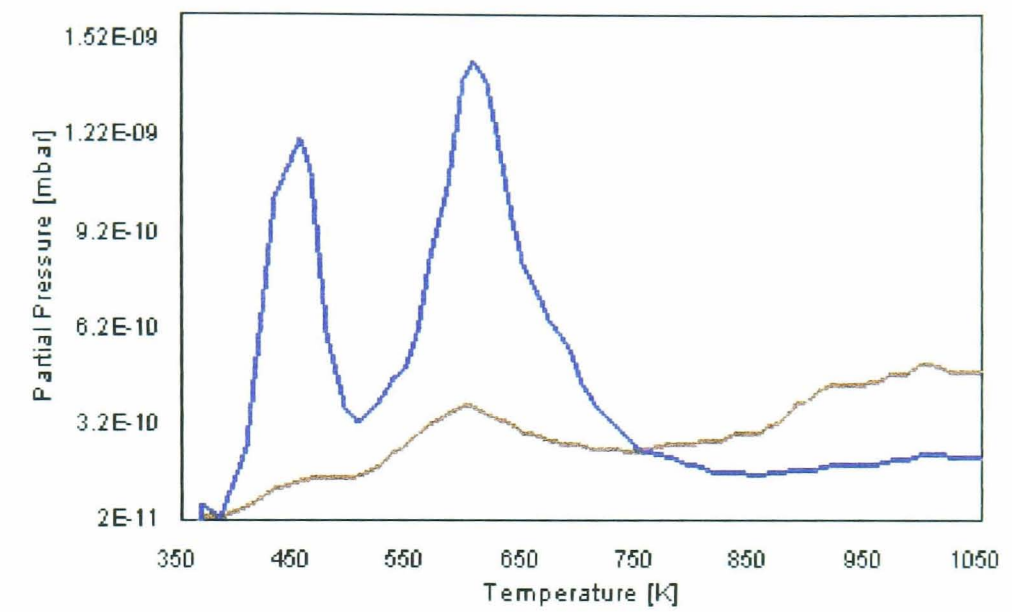

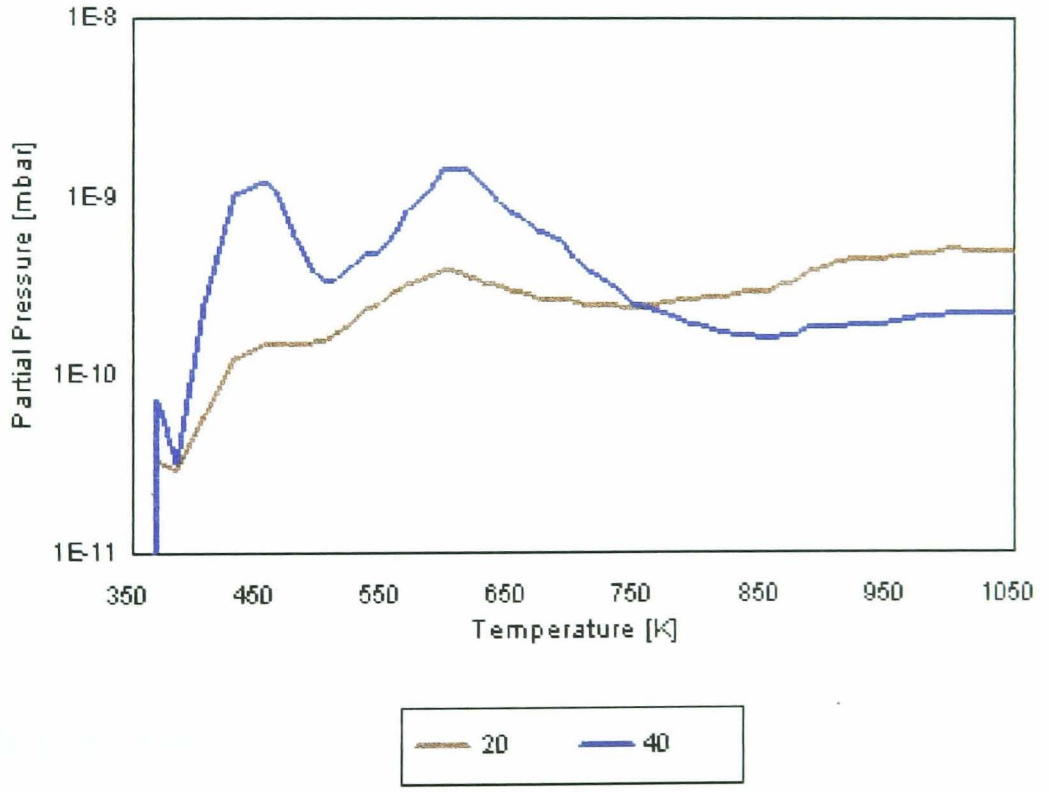

(20-HF^+, 40 – $H_2F_2^+$)

FIGURE 4- 19 Desorption spectra of HF^+ and $H_2F_2^+$ from PS (Electrolyte C)

(Note- log and linear scales for the partial pressure)

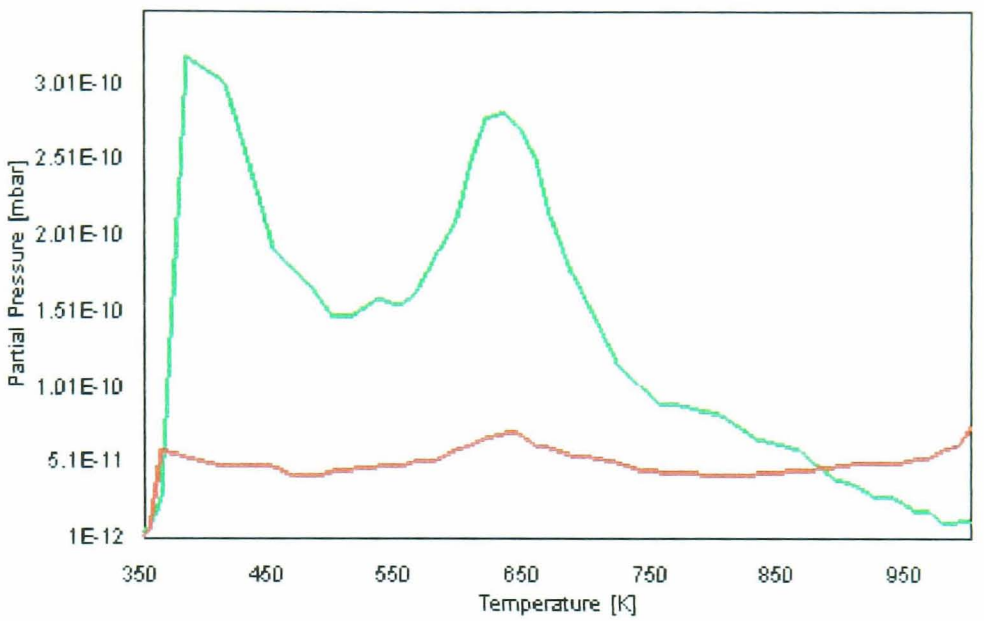

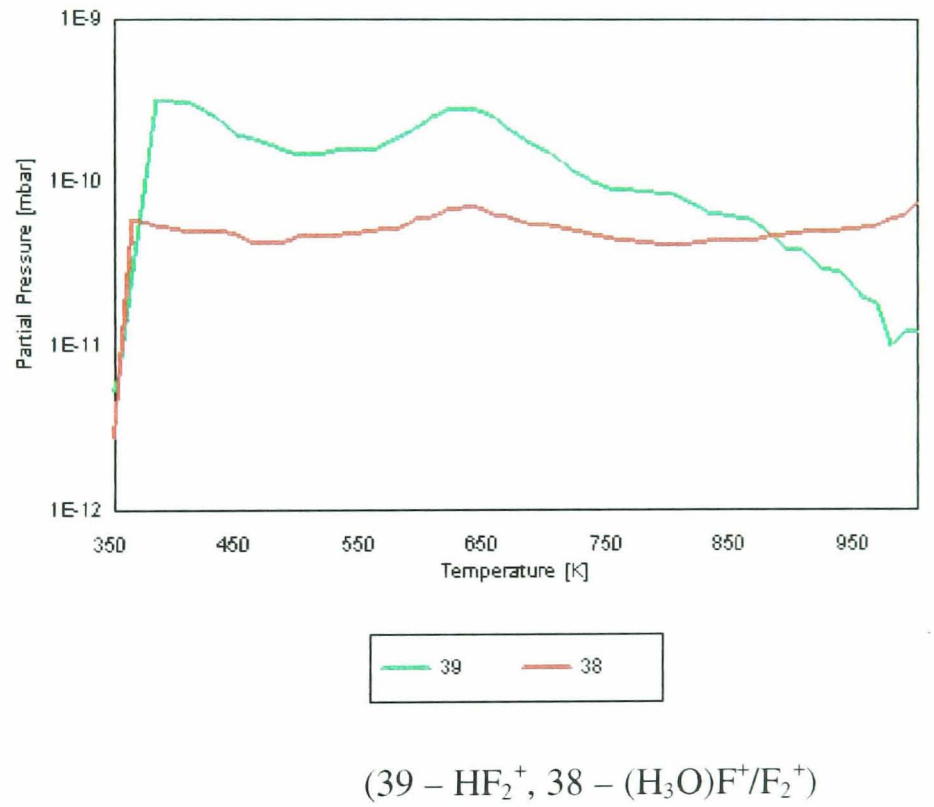

$(39 - HF_2^+, 38 - (H_3O)F^+/F_2^+)$

FIGURE 4- 20 Desorption spectra of HF_2^+ and $(H_3O)F^+$ and/or F_2^+ from PS (Electrolyte A)

(Note- log and linear scales for the partial pressure)

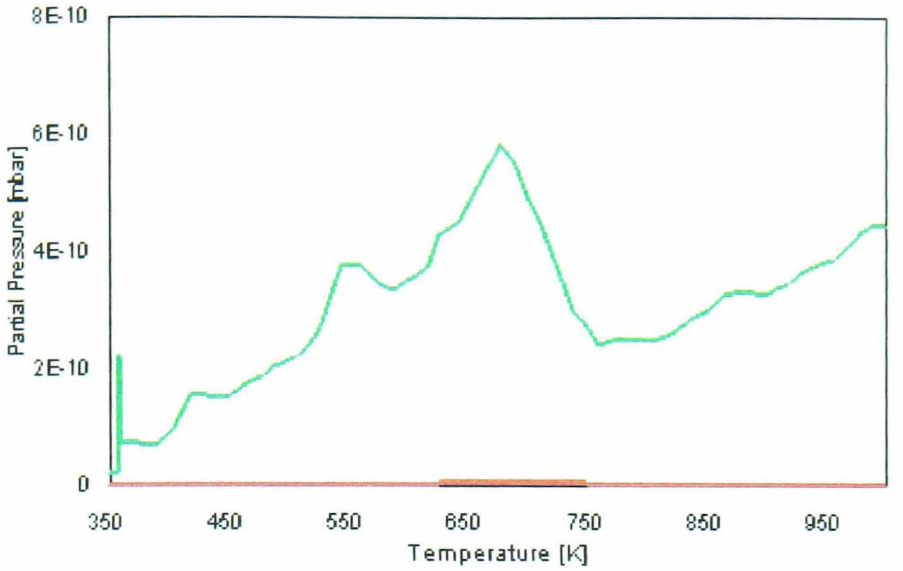

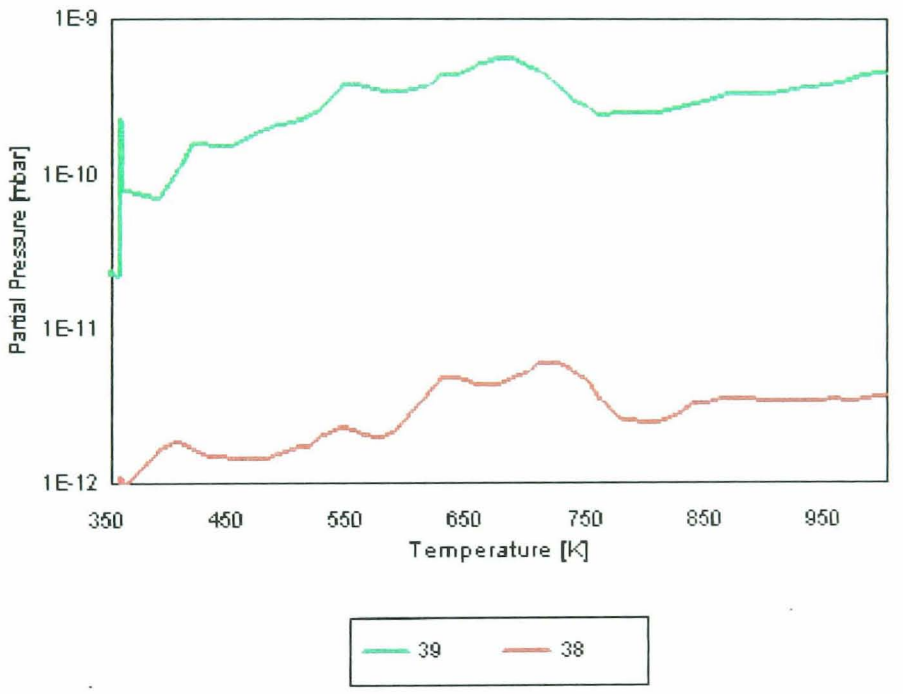

$(39 - HF_2^+, 38 - (H_3O)F^+/F_2^+)$

FIGURE 4- 21 Desorption spectra of HF_2^+ and $(H_3O)F^+$ and/or F_2^+ from PS (Electrolyte B)

(Note- log and linear scales for the partial pressure)

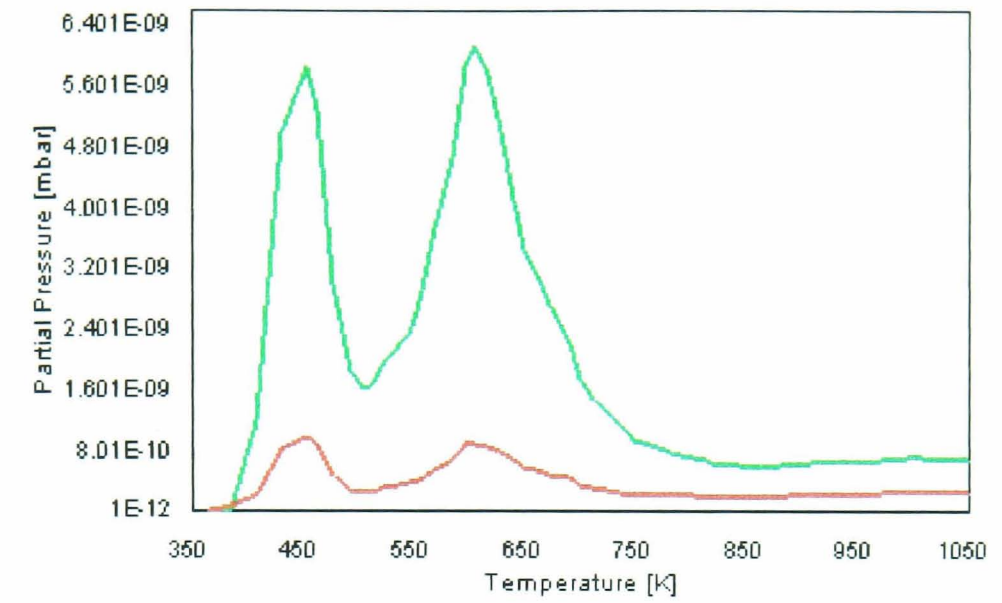

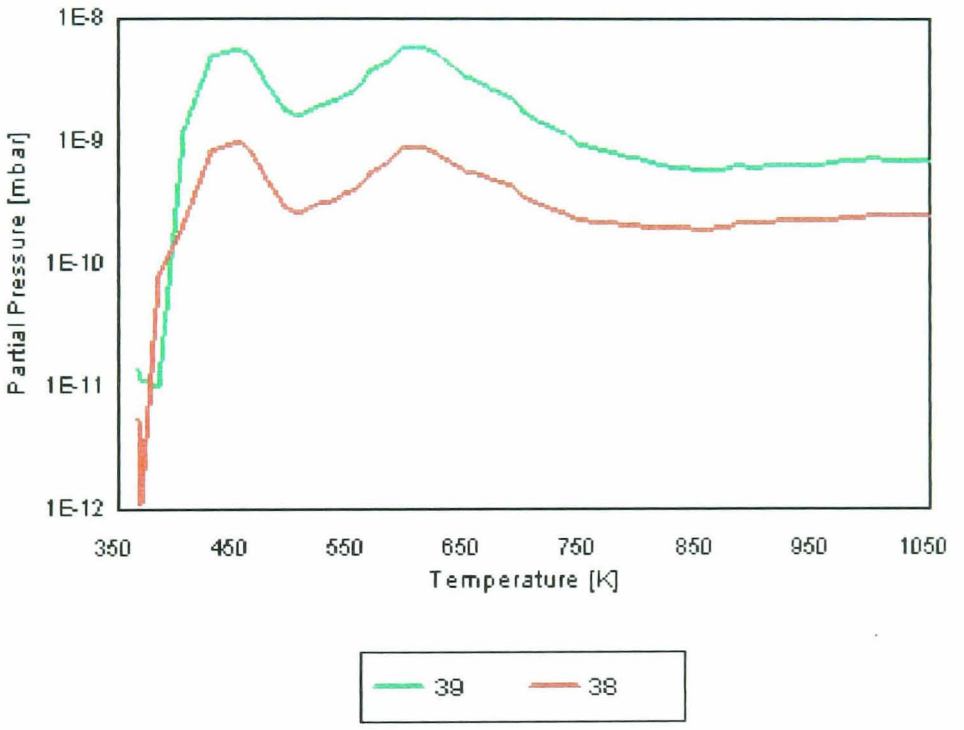

$(39 - HF_2^+, 38 - (H_3O)F^+/F_2^+)$

FIGURE 4- 22 Desorption spectra of HF_2^+ and $(H_3O)F^+$ and/or F_2^+ from PS (Electrolyte C)

(Note- log and linear scales for the partial pressure)

4.4 The effects of Heating Porous Silicon from FTIR Analysis

FTIR Spectroscopy is one of the primary sources of information about the chemical nature of the bonding between the porous silicon and the adsorbed species.

A range of as-anodised porous silicon samples were heated in the vacuum chamber to 375K, 425K, 525K, 550K, 575K, 600K, 625K, 650K, 675K, 700 and 875K. FTIR analyses were carried out on them. These results were found to support the TPD spectra in identifying the desorbed species at different stages of heating

4.4.1 FTIR Spectrum of As-anodised Porous Silicon

Figures 4-23 and 4-24 show the FTIR spectra of as-anodised PS from FZ and CZ c-Si at 300K within 20 minutes of preparation. An additional peak at 1107cm^{-1} was observed with PS sample prepared from CZ silicon. This is due to the interstitial oxygen concentrated during the manufacturing process for CZ Si (Oates et. al.). In this work FZ silicon is used.

100 scans were used to obtain FTIR spectra in order to maximise signal to noise ratio. For clarification and for the detailed analytical purposes, these spectra were obtained with short ranges of wave numbers. Figures 4-25 and 4-26 show the ranges of 2300cm^{-1} to 2000 cm^{-1} and 1800 cm^{-1} to 400cm^{-1}The FTIR spectrum shows clearly a partially resolved triplet in the region of 2100 cm^{-1}, a doublet at 662 cm^{-1} and 629 cm^{-1} and singlets at 909, 822, 734, 515 and 412 cm^{-1}.

The porous silicon FTIR spectrum from 4400 cm^{-1} to 400 cm^{-1} also shows well-defined interference fringes resulting from the difference in refractive indices at the PS layer /Si substrate interface.

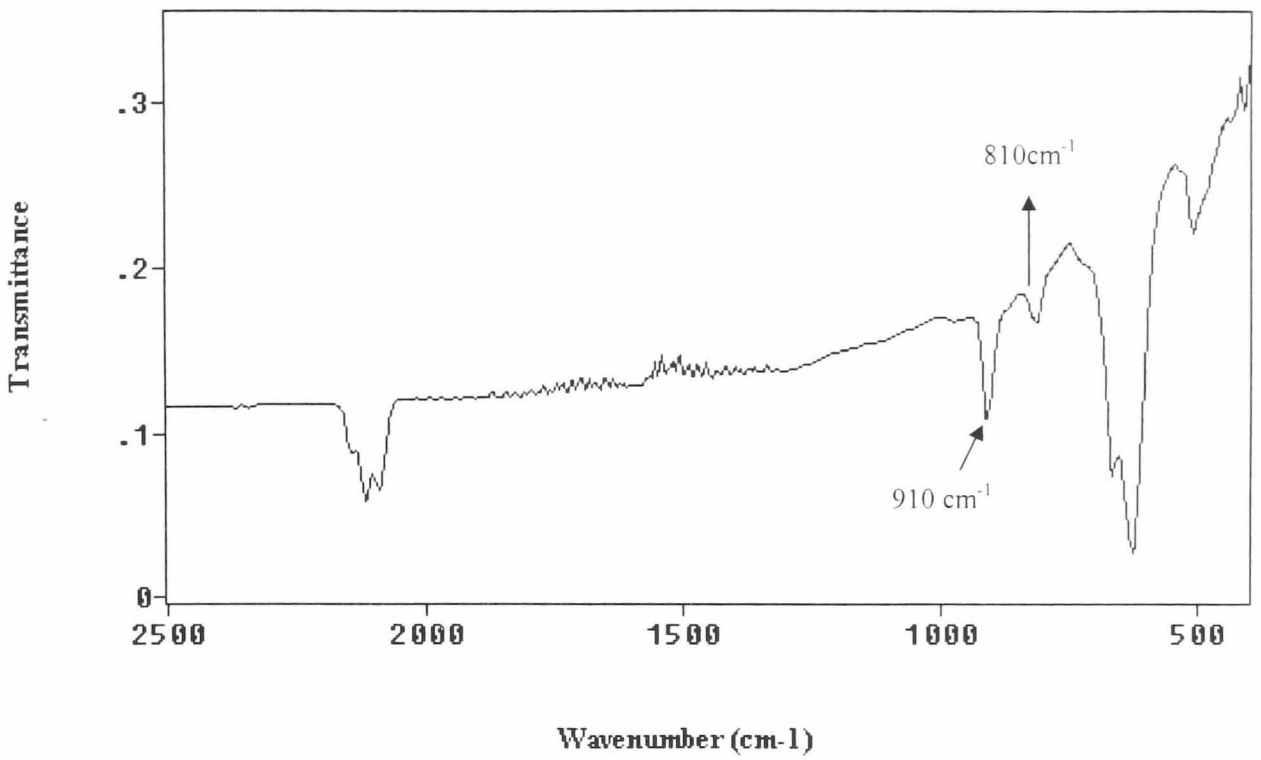

FIGURE 4- 23 FTIR spectrum of 2μm as-anodised PS from c-Si(100), FZ, 20-50 Ω cm

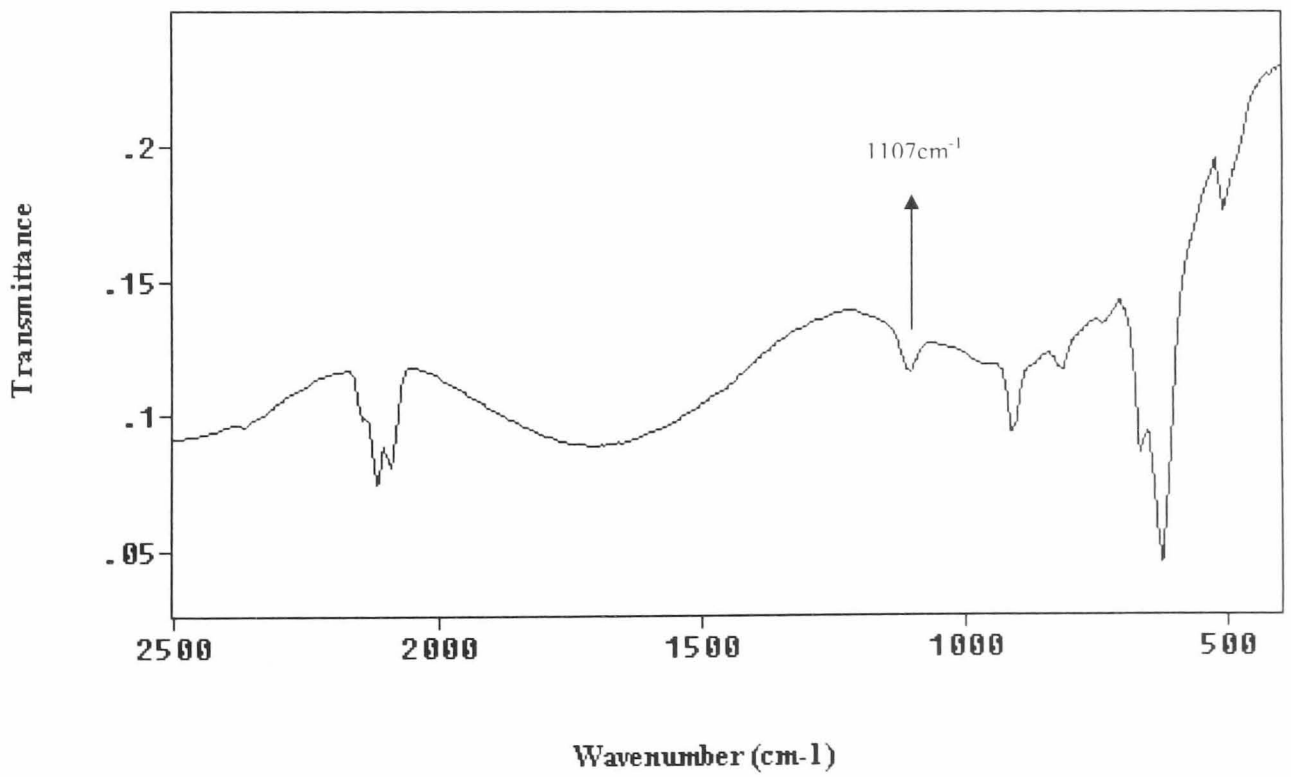

FIGURE 4- 24 FTIR spectrum of 2μm as-anodised PS from c-Si(100), CZ, 20-50 Ω cm

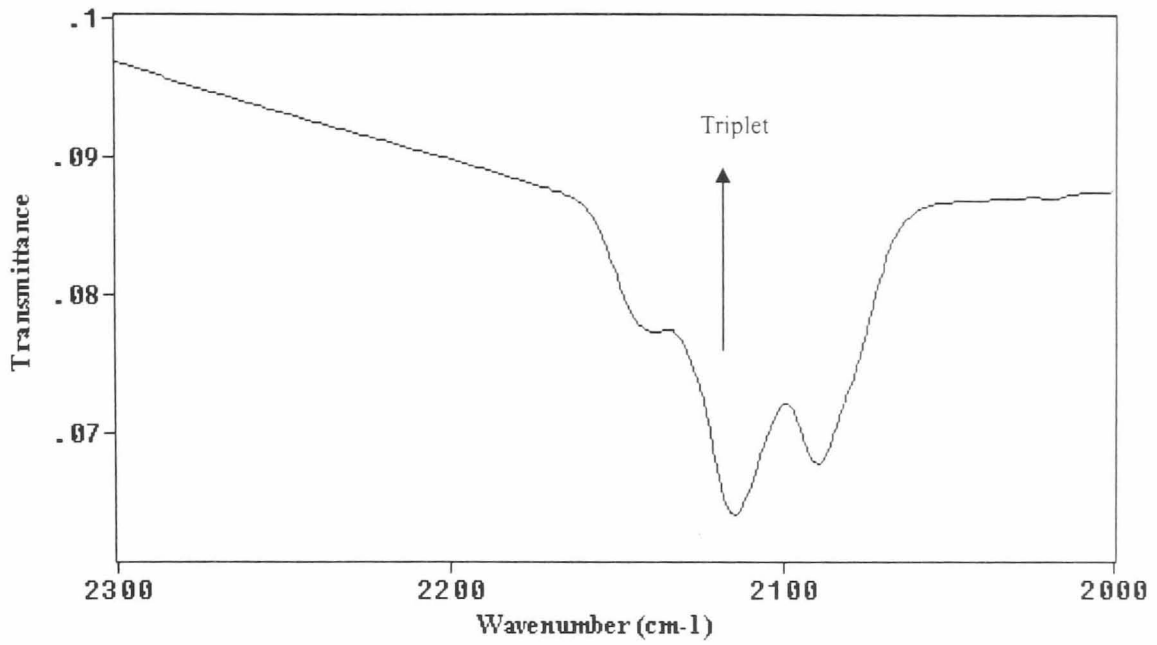

FIGURE 4- 25 FTIR spectrum of the region 2300cm^{-1}-2000 cm^{-1} showing triple peaks due to Si-H$_x$

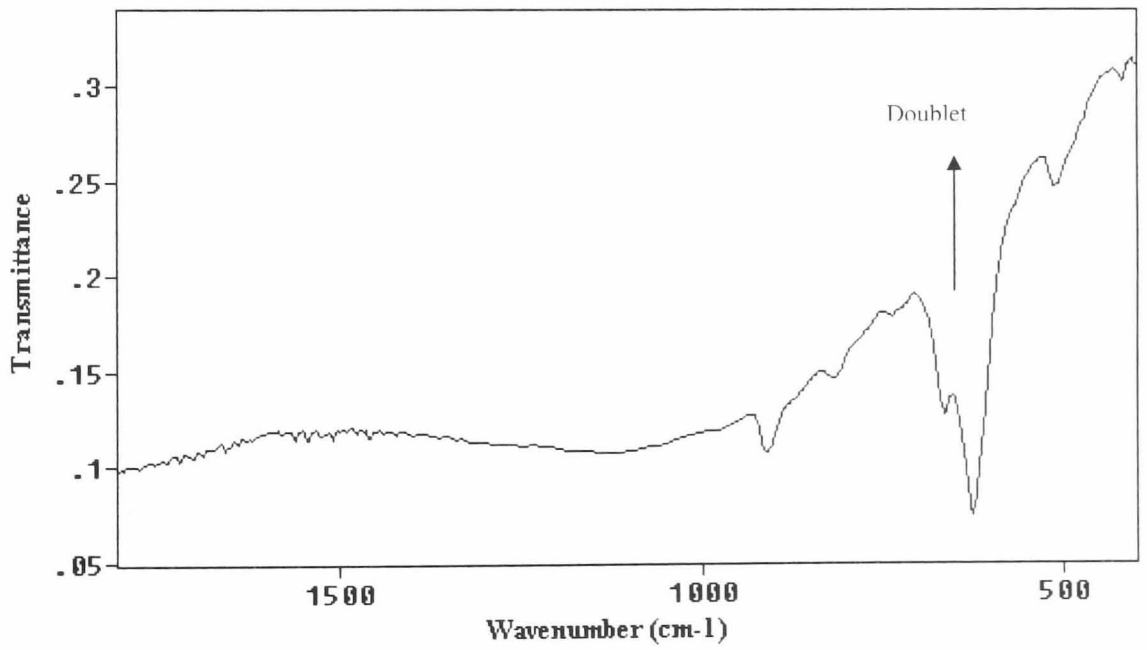

FIGURE 4- 26 FTIR spectrum of the region 1800cm^{-1} to 400 cm^{-1} showing Si-H$_x$ deformation modes

The detailed analysis of the triplet, Figure 4-25, shows three distinct peaks at 2141, 2115 and 2090 cm^{1}. These were assigned to asymmetric vibrations of Si-H bonds in the group SiH_x (x=1, 2,or 3). As the mass of the atoms bonded to silicon decreases, the vibrational IR frequency increases, i.e. the wave number increases. Therefore, the Si-H oscillators attached to hydrogen atoms (eg. H_2Si-H) are observed at higher wave numbers than Si-H oscillators with bonded silicon atoms (Si_2Si-H). Therefore, the triplets at 2141, 2115 and 2090 cm^{-1} are assigned to -H_2Si-H, -HSiSi-H and -Si_2Si-H groupings respectively.

The FTIR range of 1800 to 400 cm^{-1} range (Figure 4-26) show single and a double peak. The assignments of the singlets in the region of 909 to 412 cm^{-1} is quite difficult as Si-H bending modes and Si-F both antisymmetric and symmetric vibrations occur in this region.

4.4.2 Effects of heating in the range 2300 cm^{-1} – 2000 cm^{-1}

The triplets were found to persist up to 525K. At 550K most of the peak assigned to –SiH_3 disappeared and a shoulder was observed. FTIR spectrum at 575K shows only a doublet at 2107 and 2090 cm^{-1} with decreased intensities.

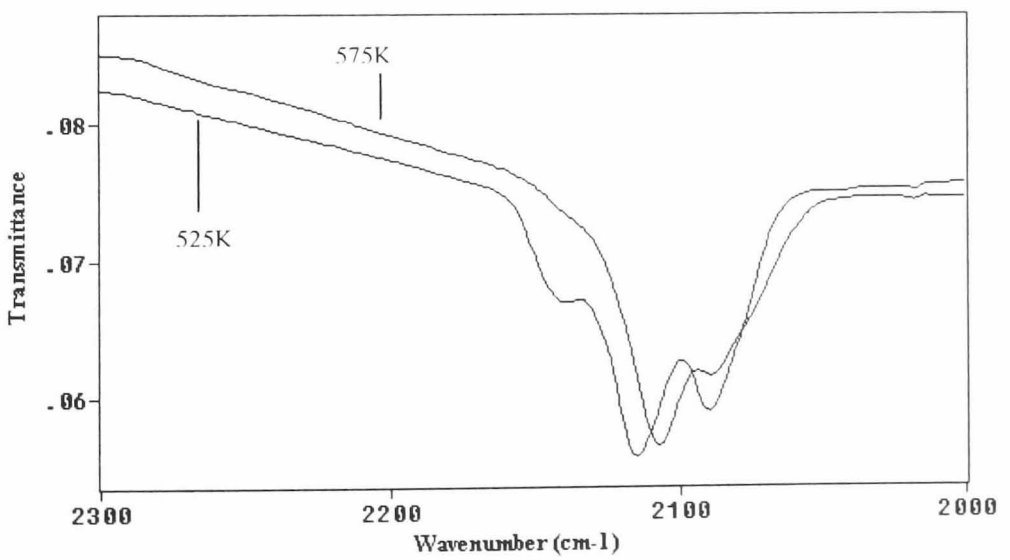

FIGURE 4- 27 Triple peaks at 425K and 575K (desorption of –SiH_3 at 575K)

Figure 4-27 shows an overlaid FTIR spectra of porous silicon samples heated to 525K and 575K. As the peak due to -SiH_3 (2140cm-1) disappears at 575K, the peak due to –SiH_2 at 2110cm^{-1} shifts towards lower wave numbers. At 525K, -SiH_2 absorption appears at 2112cm^{-1} and are shifted to 2104cm^{-1} at 575K when all the SiH_3 groups have desorbed. This could be related to the environment of the hydrogen in the structure of porous silicon. It is necessary to mention here that the peak temperature observed for the desorption of silane, SiH_4 with TPD analysis was found to be 575K ±5K (Figures 4-8 to 4-10).

When porous silicon samples are heated at higher temperatures (600K, 625K, 650K, and 700K) there is a gradual decrease in the intensity of the peaks at 2107 and 2090 cm^{-1}. It should be emphasised that there is a steeper decrease in the intensity of the Si-H peak at 2090 cm^{-1} compared with that of SiH_2. Figure 4-28 shows the FTIR spectra of porous silicon samples heated to the temperatures mentioned above. The FTIR spectrum at 650K shows that most of the Si-H species are desorbed at this temperature. This is supported by the TPD desorption spectra for hydrogen(Figure 4-5).

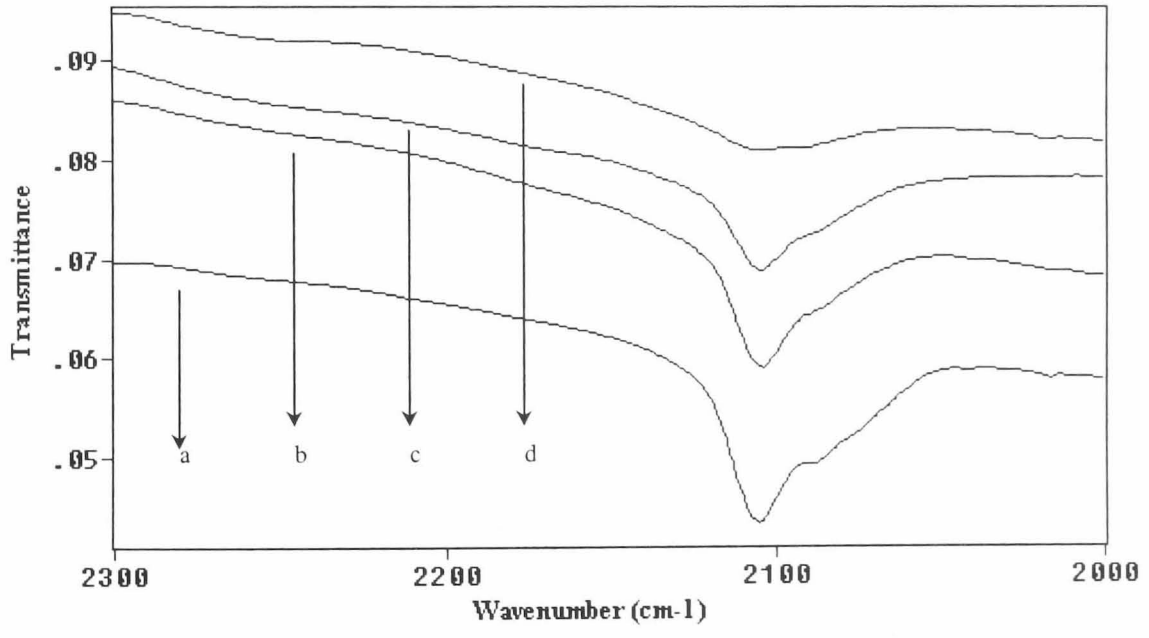

FIGURE 4- 28 Effects of heating on the triple peaks in the 2100 cm^{-1} region

(shows gradual disappearance of SiH_2 and SiH groups- a-d are 600, 625, 650 and 700K respectively

4.4.3 Doublet at 669 cm^{-1} and 629 cm^{-1}

Figure 4-29 shows the doublet at 667 and 627 cm^{-1} for as-anodised porous silicon.

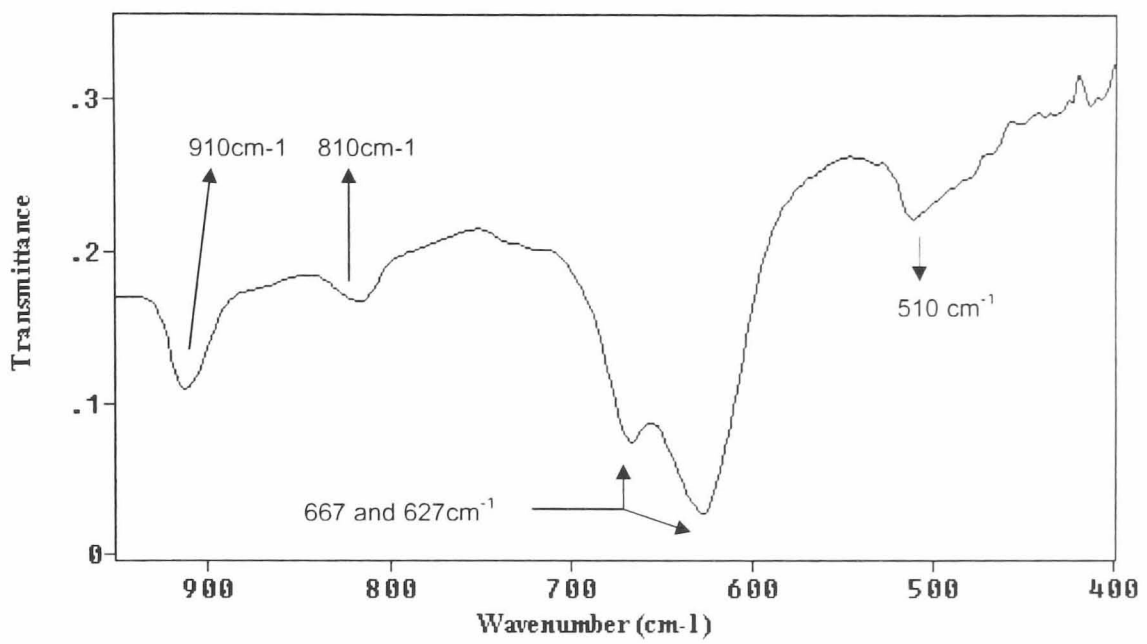

FIGURE 4- 29 FTIR spectrum showing the double peak from as-anodised PS

The peak at 667 cm^{-1} was found to disappear at 575K, the same temperature as that noted for the disappearance of the $-SiH_3$ group (Figure 4-30). A very small sharp peak was observed at 667 cm^{-1} with the PS sample heated to 575K. This peak is comparable to a peak at the same wave number for a FTIR spectrum obtained with c-Si as in Figure 4-30

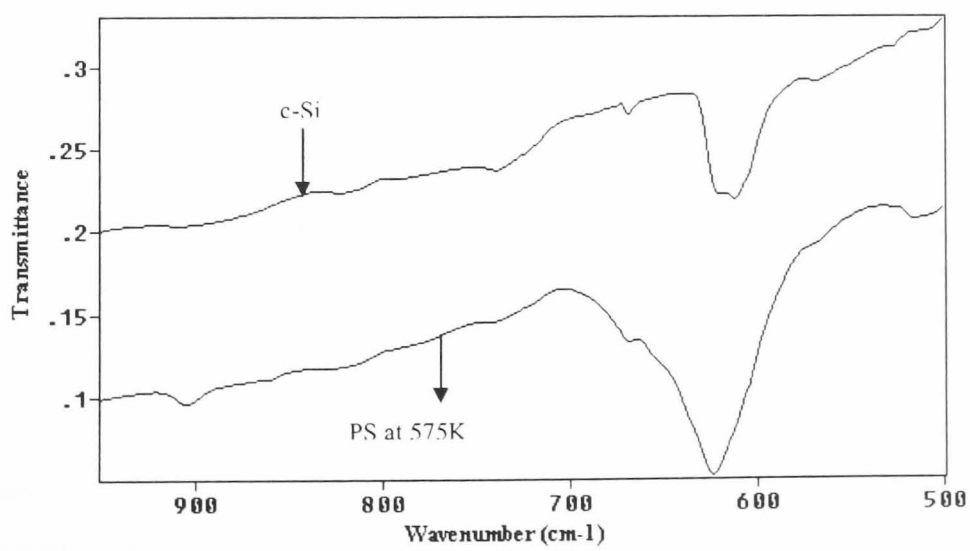

FIGURE 4- 30 Comparison of FTIR spectra of c-Si and PS heated to 575K (700 cm^{-1} to 500 cm^{-1} region)

When the porous silicon samples are heated to 600K, 625K, 650K, and 700K the intensity of the singlet at 629cm^{-1} is found to decrease. This finding corresponds to a loss of Si-H bonds (Figure 4-32). From these evaluations the peak at 669 cm^{-1} is assigned to –SiH_3 and the peak at 629 cm^{-1} to the –SiH vibrations.

The FTIR spectrum of porous silicon samples heated to 875K resembles the spectrum of single crystal Si except that the PS shows the presence of Si-O bonds in the region of 1100cm^{-1}. Figures 4-35 and 4-36 illustrate the similarities except for the presence of Si-O vibrations. The double peak observed at 669/629 cm^{-1} disappears with heating to above 875K and another peak with lower intensity appears at 610 cm^{-1} . This characteristic peak is observed with FTIR spectrum of c-Si as well and is due to the vibration of silicon lattice and is referred to phonon-phonon vibration (Krishnan et.al. 1990). This band is assigned to a combination of TO (transverse optical phonon) and TA (transverse acoustic phonon)and is commonly referred to as the "2 phonon bands". This results in a small absorption coefficient of about 10cm^{-1} (Pajot 1977) compared to the coefficient at 628 cm^{-1} peak observed for PS which is ~2500 cm^{-1}

4.4.4 Peak in the region of 1100 cm^{-1}

No visible peak was observed with as anodised-porous silicon and porous silicon heated to 575K. A gradual increase in the number of Si-O oscillators in the region of 1100 cm^{-1} was observed with further heating. Figures 4-33 and 4-34 show overlaid spectra of porous silicon heated to 550K, 575K and 650K, 675K and 700K in the region of 1100 cm^{-1} respectively. The observed peak is broad and has a shoulder. This type of peak is characteristic of SiO_2 grown on a Si wafer in steam ambient.

This broad peak was assigned to the Si-O-Si asymmetric stretch vibrational mode (Pliskin 1977). The broadness of the peak is due to multiple environments of the Si-O oscillators. The appearance and the increase in the intensity of this peak is interpreted in terms of the oxidation of the Si atoms by the moisture and \ or oxygen found in the pore cavities. It may also be possible that the "free" dangling bonds of the Si atoms from the pore walls, after the desorption process, are free to bond with available oxygen.

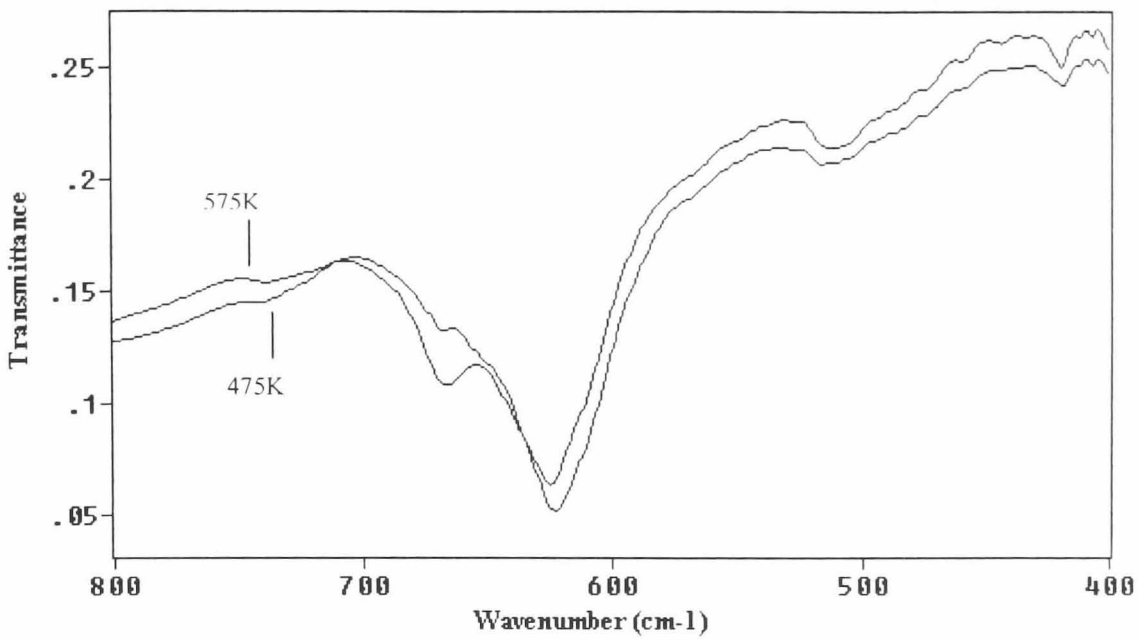

FIGURE 4- 31 Effects of heating on the double peaks at 668 cm^{-1} and 628 cm^{-1} (425K and 575K)

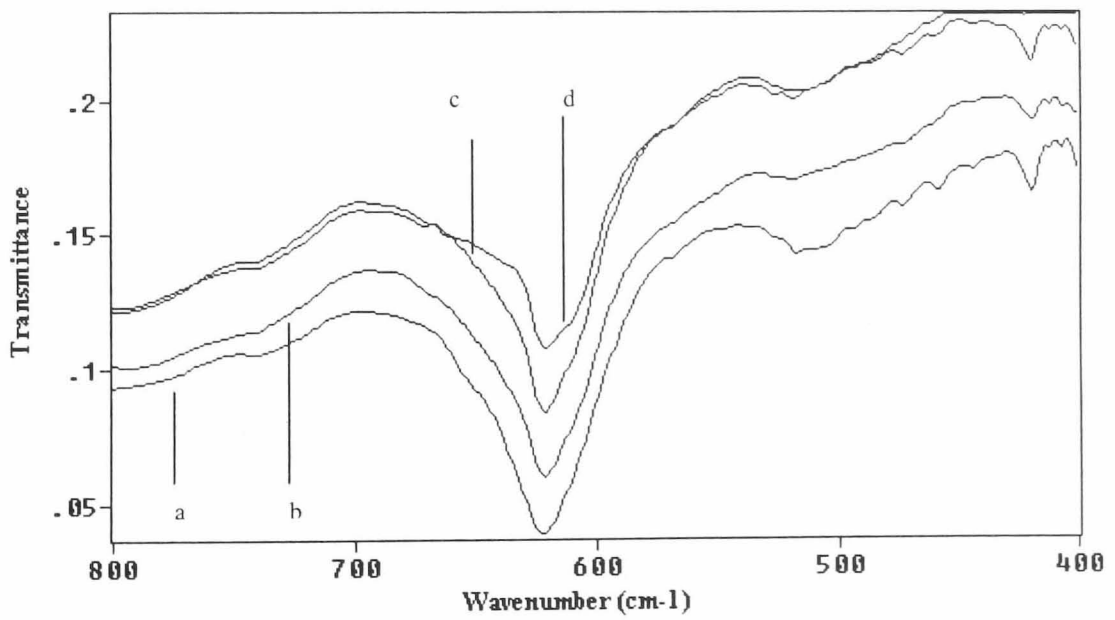

FIGURE 4- 32 The gradual loss of the double peaks (668 cm^{-1}/628 cm^{-1}) with temperature (FTIR Spectra a-d are from PS heated to 600, 625, 650 and 700K respectively)

4.4.5 Peak at 910 cm^{-1} and at 822 cm^{-1}

It is very difficult to assign these peaks to any specific oscillators as Si-H_x as well as Si-F_x vibrate in this region (Borghesi 1993). The peak at 910cm^{-1} is interpreted as the asymmetric bending vibrations of the -SiH_2 group and the peak at 810 cm^{-1} is probably due to Si-F_x groups. This is based on the findings from the investigations carried out by the author on the ageing process of porous silicon and will be discussed in Chapter 5.

4.4.6 Comparison of "High" Temperature Porous Silicon and the blank c-Silicon

Figures 4-35 and 4-36 show FTIR spectra of as anodised PS, heated to 875K and a blank c-Si . Figure 4-35 shows that the triple peaks at ~2100 cm^{-1} and the peak at 909cm^{-1} disappear at higher temperatures and a unresolved double peak at 1135cm^{-1} and 1054cm^{-1} develop in the Si-O asymmetric vibrational region. Figure 4-36 shows that porous silicon heated to 875K resembles the c-Si except in the 1100cm^{-1} region. The double peak at 667/628 cm^{-1} (due to Si-H_x) observed in porous silicon was replaced with a lower intensity not-so defined double peak at 620/613 cm^{-1} which is similar to C-Si. This is interpretes as Si-Si phonon vibration.

TABLE 4- 4 Summary of FTIR Observations with Heating

Wave numbers (cm^{-1})	Assignments	Effects on Heating
2140	H_2Si-H Asymm.stretching	Stable up to 575K
2110	HSiSi-H Asymm.stretching	Starts to decrease with Si-H and disappears at 700K
2090	Si_2Si-H Asymm.stretching	Stable up to 625-650K
1110-1050	Si-O-Si Stretch	Gradual increase with peak intensity
910	Si-F_x or Si-H bending	Controversy in the literature
818	Si-F_x	Difficult to evaluate, due to Si-O-Si overlap
667	H_2Si-H wagging mode	Disappears at 575K
628	HSiSi-H bending mode	Disappears at ~ 700K
620 \ 613	Si-Si phonon vibration	Appears at higher temperature very similar to c-Si

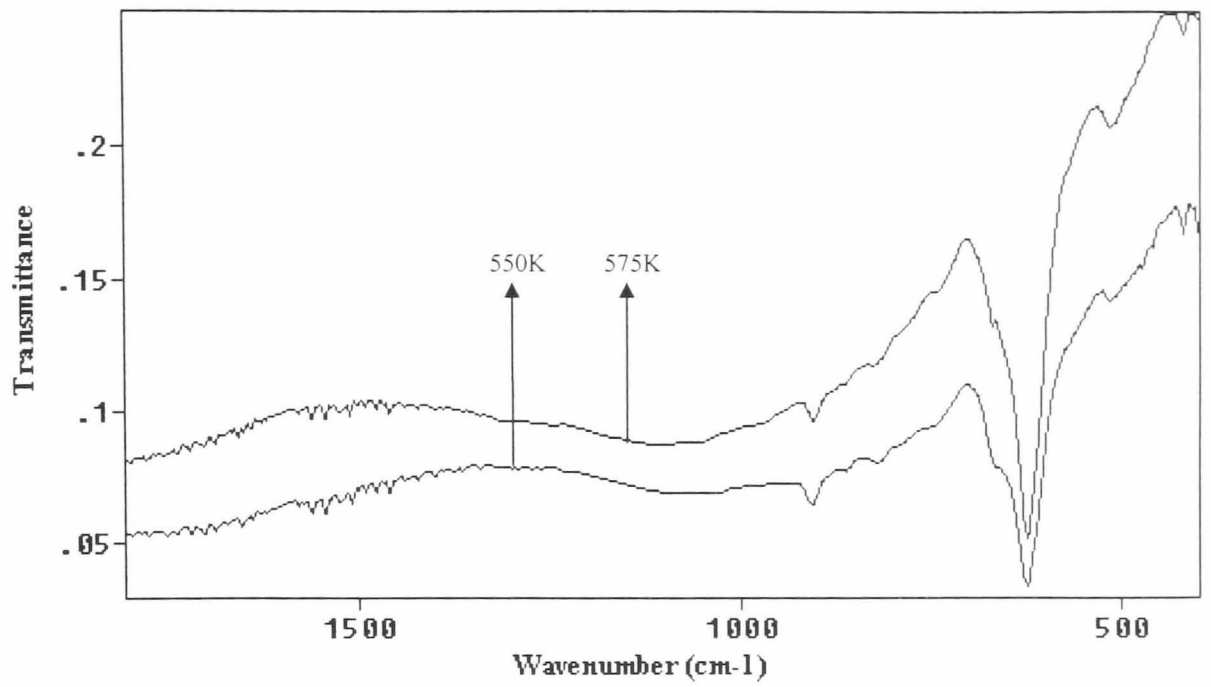

FIGURE 4- 33 FTIR spectra showing lower level of oxidation of PS at 550K and 575K

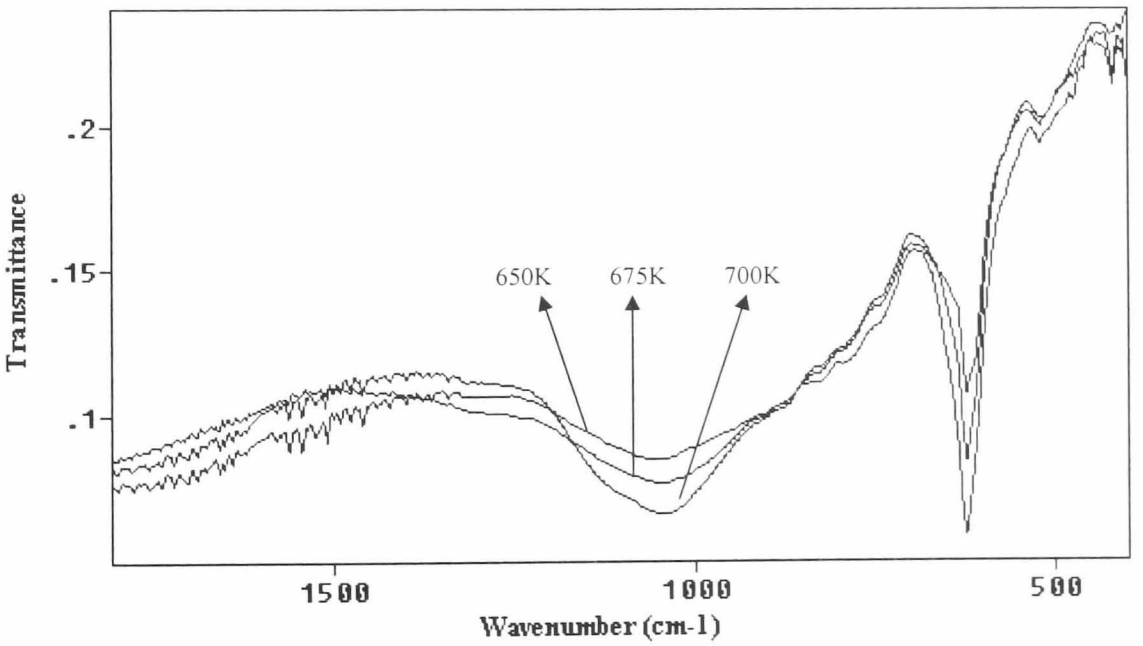

FIGURE 4- 34 Overlaid FTIR spectra showing gradual oxidation of PS with temperature

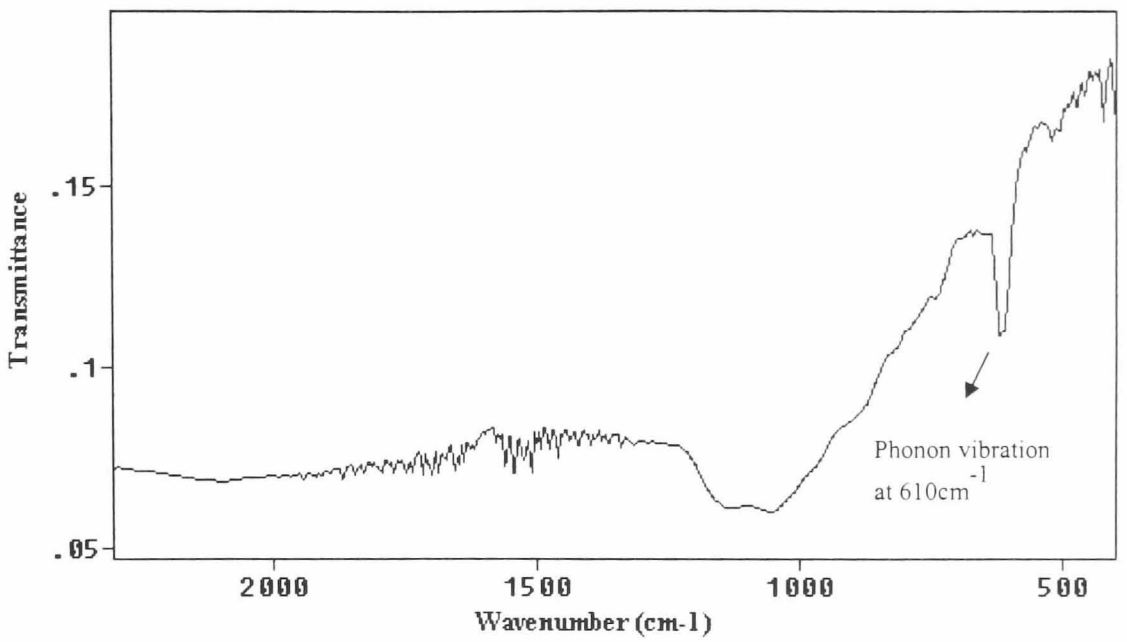

FIGURE 4- 35 FTIR spectrum of PS heated to 875K

(Only Si-O exists; other peaks disappeared apart from phonon vibration at ~610 cm^{-1})

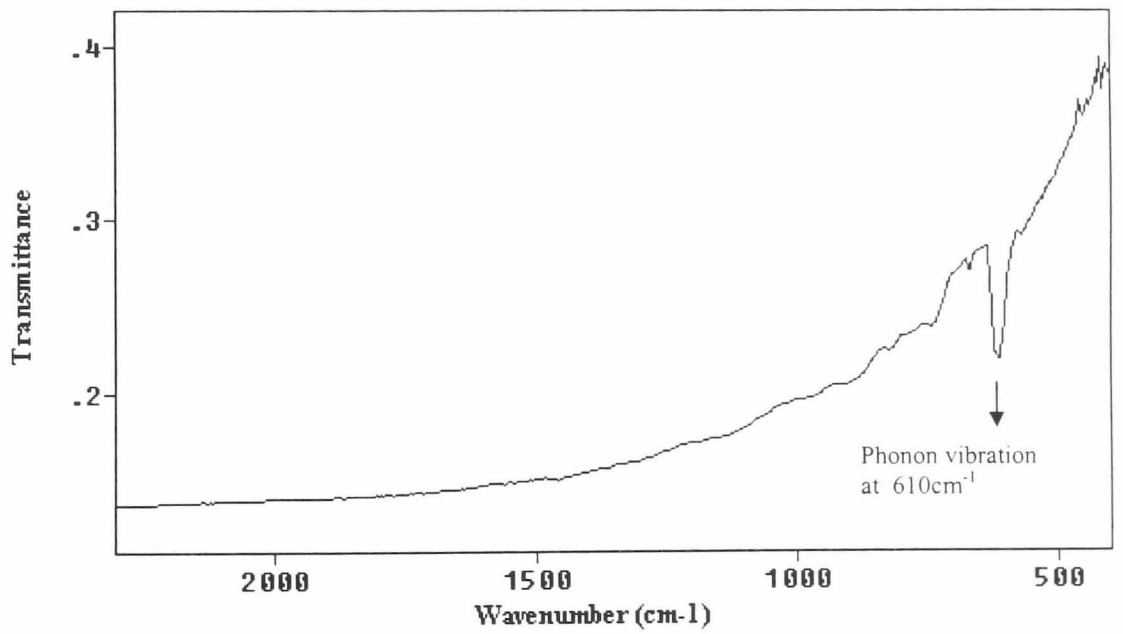

FIGURE 4- 36 FTIR spectrum of a c-Si wafer, 20-50 Ω cm, FZ (note the peak at~610 cm^{-1})

4.5 Ageing Process with Porous Silicon

These investigations were carried out with porous silicon samples prepared in the same way as for TPD and FTIR analyses and stored in a white box. The spectra were obtained every day for 19 days (except for weekends) and random measurements were taken up to 240 days (8 months). For clarification, the FTIR spectrum is divided into two regions of 4000cm^{-1}–2000 cm^{-1} and 2000cm^{-1}-400cm^{-1}.

4.5.1 1 – 19 Days-old Porous Silicon Samples

The porous silicon samples kept for 1 to 10 days show no difference in the triplet assigned to Si-Hx stretching modes at 2117, 2109 and 2090 cm^{-1}. Figure 4-37 shows this effect. A 10 days old porous silicon sample is beginning to show an extra set of small broad peaks at 2202cm^{-1} and 2259cm^{-1}. These peaks were found to increase with the ageing period. Figure 4-37 shows as-anodised, one day and 10 days old porous silicon samples in the region 2300-2000 cm^{-1}.

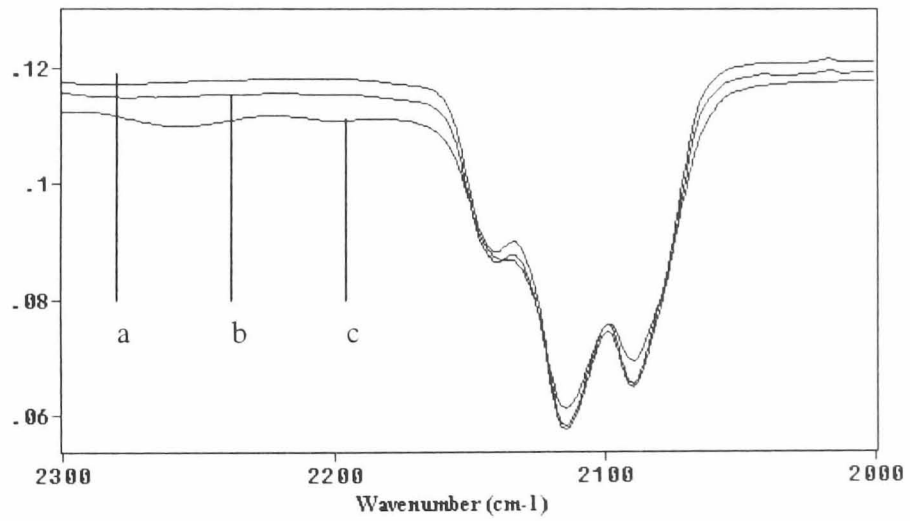

FIGURE 4- 37 FTIR of the triple peaks of as-anodised, one day and 10 days-old PS

(Spectra a, b and c represent as-anodised, 1 day and 10 days old samples respectively)

Slow oxidation was observed from day 1. The process is associated with development of a broad peak with a shoulder at ~ 1100cm^{-1}, typical of wet oxide grown on silicon wafer. Figure 4-38 shows overlaid infrared spectra of as-anodised, 8 and 19 days-old samples. It should be noted that the peak at 818cm^{-1} decreased in intensity as the

moisture increased with time. This is interpreted as hydrolysis of Si-F bonds by absorbing moisture. Also a peak at 878cm^{-1} started to appear and is quite prominent with the 19 day-old sample. There is no change observed with the doublet at 669 and 626cm^{-1}. The triplet in the 2100 cm^{-1} region shows (Figure 4-39) slow decrease in the sharpness of the 2140 cm^{-1} peak assigned to $-SiH_3$ group in the 19 day-old sample compared to as-anodised porous silicon

4.5.2 19 to 59 day-old Porous Silicon Samples

These samples developed some interesting features during this period of ageing. It was observed that the intensity of the peak at 2255cm^{-1}, first seen with a 10 day-old sample, increased with time. This is interpreted as the vibrational frequency of Si-H bonds with back bonded oxygen (O). Also, most of the $-SiH_x$ group around 2100 cm^{-1} disappeared and a small shoulder was seen on the triplet at 2140cm^{-1} (Figure 4-40). In addition to these developments, a new set of triplets was observed at 2957, 2924 and 2857cm^{-1}. They are assigned to C-H modes of vibrations and are possibly originated from organic vapour contamination.

Figure 4-41 shows that the peak due to Si-O stretching vibrations is well developed and is very broad. It extends from 1208 – 1053cm^{-1}. The peak at 909 cm^{-1} is unchanged and an increase in peak intensity at 878cm^{-1} is observed. The doublet at 669cm^{-1}/629cm^{-1} is similar to the doublet observed with as-anodised porous silicon. Another well-developed peak was observed at 463 cm^{-1} which was assigned to the cyclic SiO_4 group (Beckman 1965)

4.5.3 3 to 8 Months Old Porous Silicon Samples

It was observed that these samples showed increases in the features noted above for 19 - 59 days old samples. Furthermore, carbon-based contamination was observed in the 1500cm^{-1} region (Figure 4-42). One peak of the doublet at 668 cm^{-1} has disappeared and a small, sharp peak replaces it instead. . This is very similar to the Si-Si phonon vibration observed with c-Si (Figure 4-37). The intensity and the broadness of the peak assigned to Si-O stretching vibration increased significantly. This peak occurs in the range 1208-1053 cm^{-1}. The intensity of the peak at 878 cm^{-1} was found to increase with time.

Many more singlets, 967, 935, 862, 741 and 455cm^{-1} appeared possibly as a result of back-bonded oxidation of silicon. In the region 4000 – 2000 cm^{-1}, a very broad peak developed in the region of 3600cm^{-1} (Figure 4-43). This is assigned to SiO-H stretching mode of vibration (Pliskin 1977). Another set of extra peaks at 2365 and 2344cm^{-1} were observed (Fogure 4-44).

Only a single peak at 2116cm^{-1} was observed instead of the Si-H_x triplet at 2100cm^{-1} region (Figure 4-40)

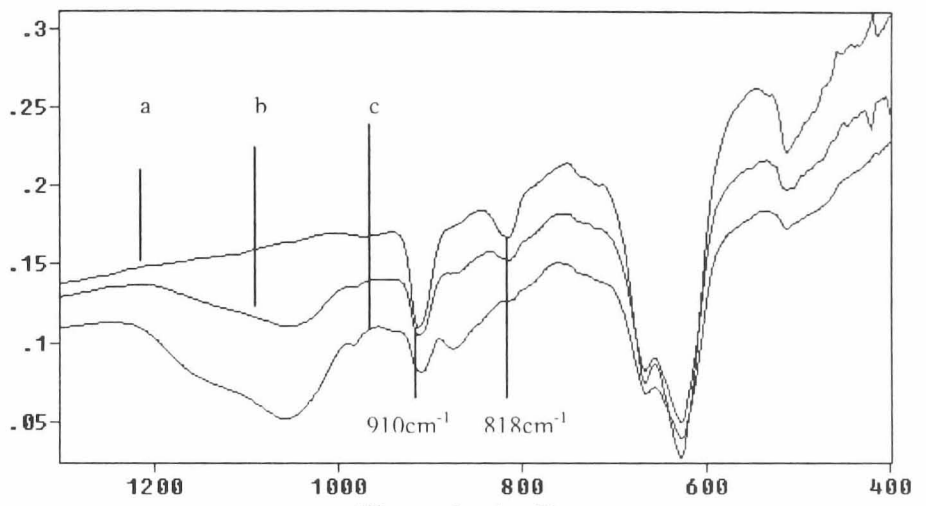

FIGURE 4- 38 Overlaid FTIR spectra of as-anodised, 8 and19 days-old PS samples

(Spectra a, b and c represent 0, 8 and 19 days-old PS respectively. Note the changes at 910 cm-1)

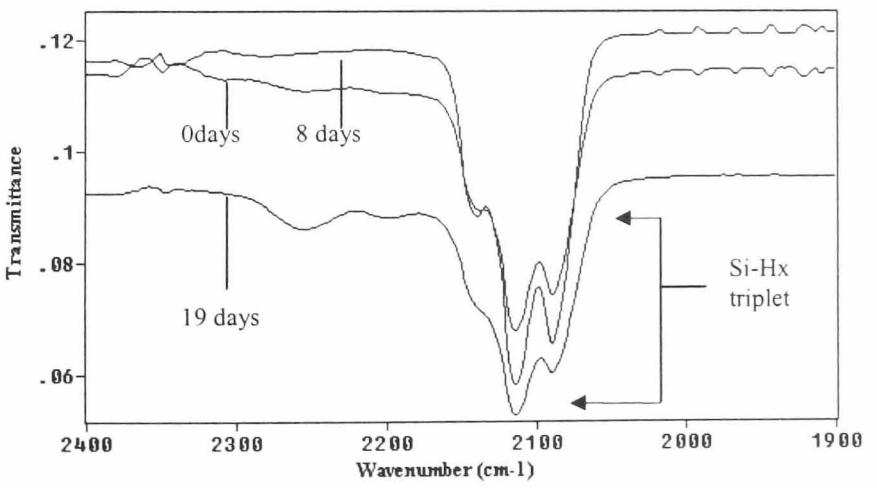

FIGURE 4- 39 Appearance of extra peaks at 2257 and 2201 cm^{-1} with 19 days-old PS

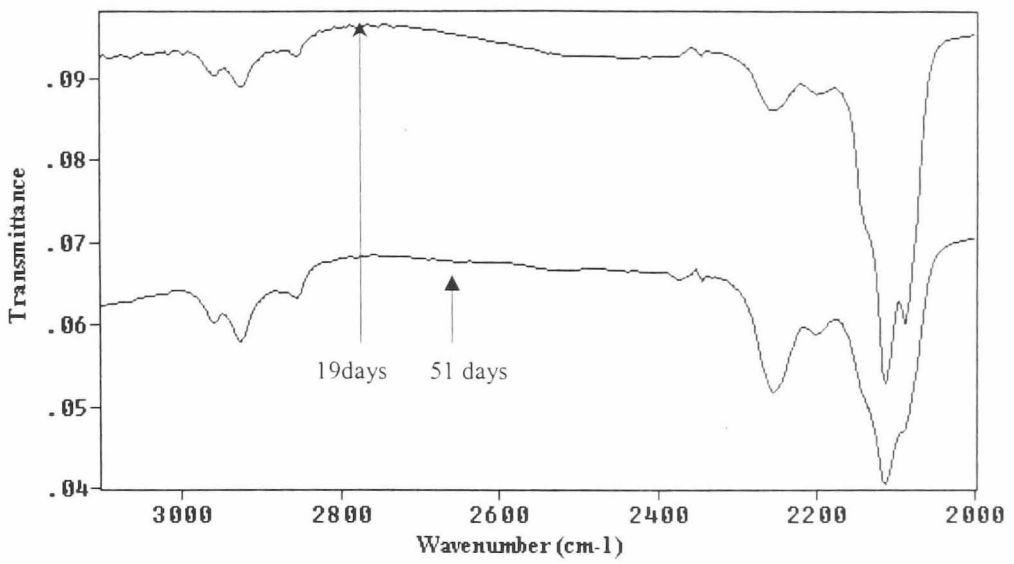

FIGURE 4- 40 Overlaid FTIR spectra of 19 and 51 days-old PS (3500-2000 cm^{-1} region)

(Note the development of a triplet at 2900cm^{-1})

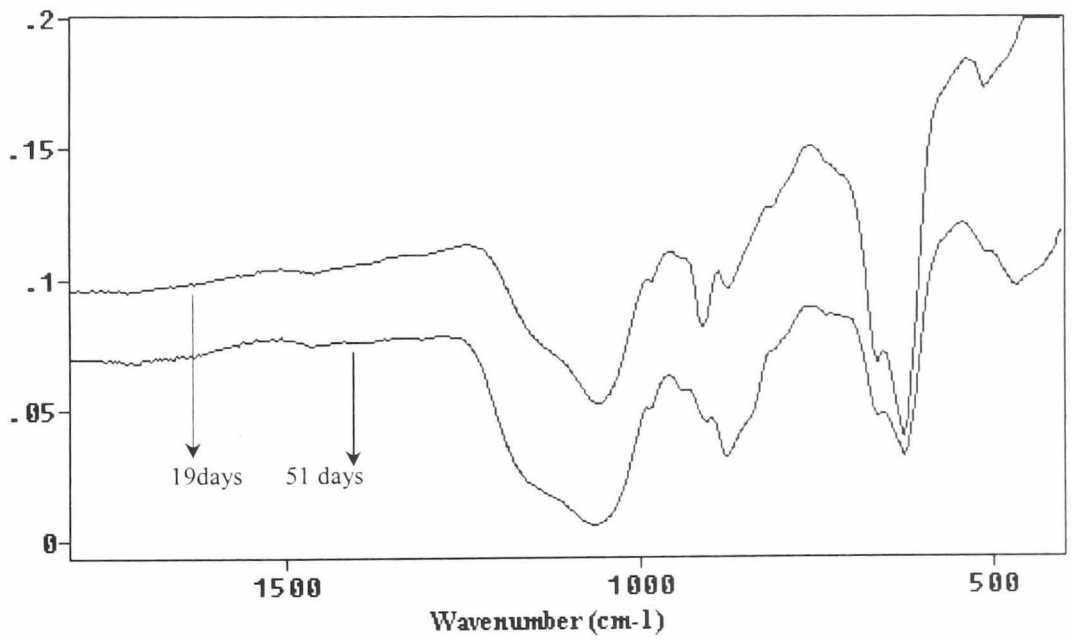

FIGURE 4- 41 Overlaid FTIR spectra of 19 and 51 days-old PS (2000-400 cm^{-1} region)

(Note the developments at 875 $cm^{-1}$and 455 cm^{-1})

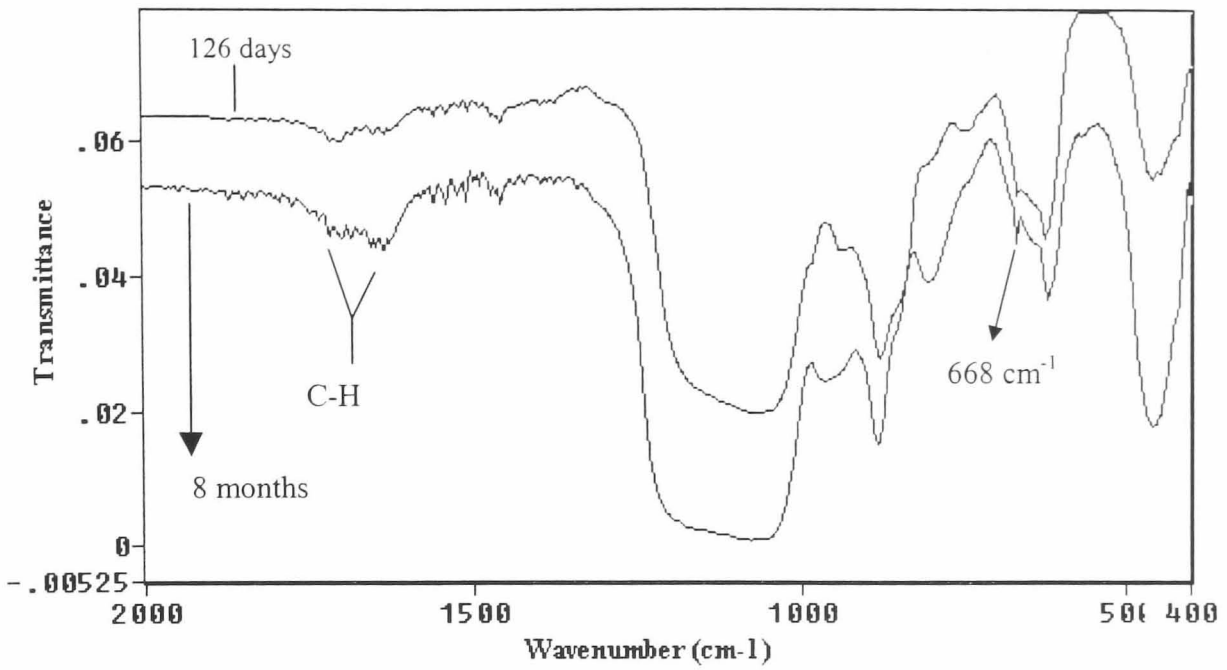

FIGURE 4- 42 FTIR spectra showing C contamination and the removal of 668 cm^{-1} peak

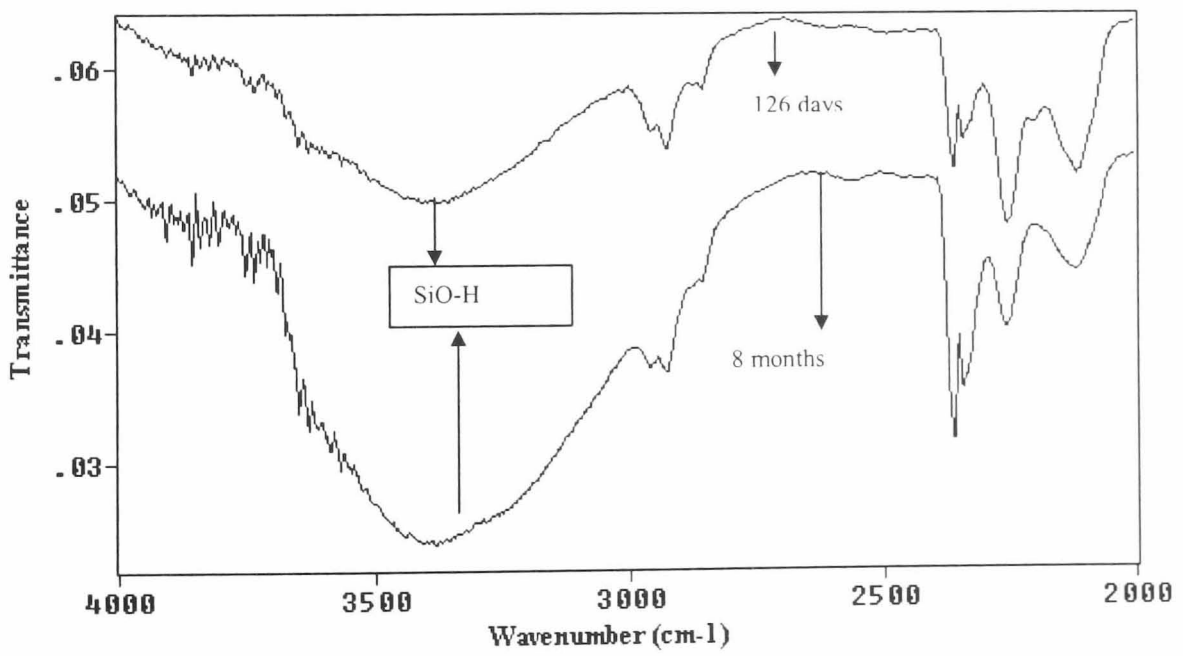

FIGURE 4- 43 Development of SiO-H groups and 2365 cm^{-1}/2344 cm^{-1} doublet (126 days and 8 months –old PS)

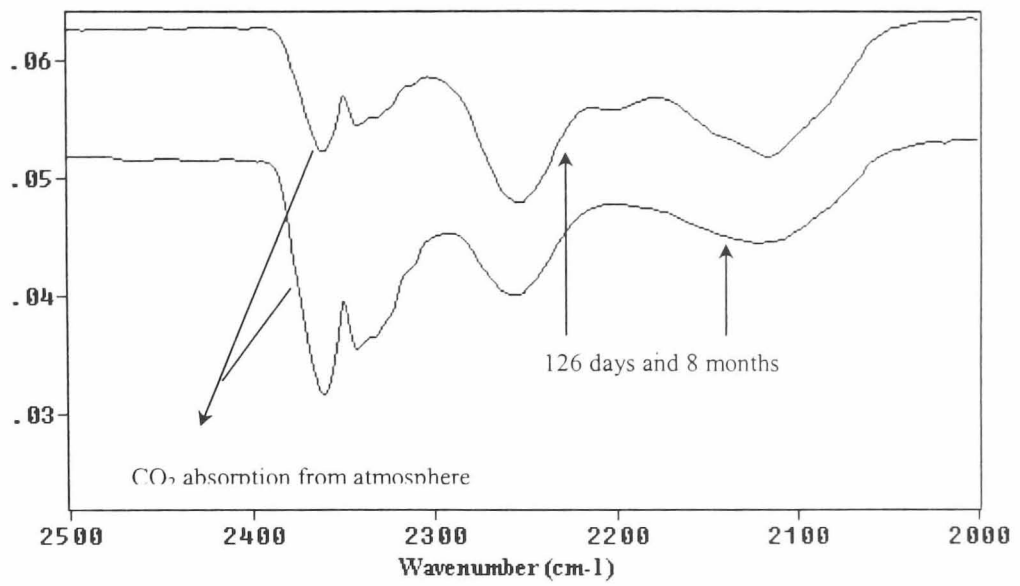

FIGURE 4- 44 Double peaks at 2365 cm^{-1}/2344 cm^{-1} due to CO_2 absorption

4.6 Summary

1. The analyses were carried out with the same PS samples from 0 days (as-anodised PS) to 8 months old.
2. The summary of the observations is presented in Table 5-10 in Chapter 5 with the details of the assignments and the ageing process.

Chapter 5 Discussion

Since the early work of Uhlir (1956 333-47) and later by Canham (1990) on the photoluminescence (PL) properties, the interest in PS has grown exponentially. Before 1990 there were less than 200 papers published on PS and by year 2001, it is projected to be greater than 2000 (Cullis et.al. 1997). PS is generally prepared by the electrochemical etching of c-Si in HF-based electrolytes. "Stain-etched" PS films also have been produced and studied for over thirty years. The electrolyte in this case consists of HF, HNO_3 and H_2O. The preferred method is the first method mentioned as it produces reproducible, uniform PS layers with variable thickness and porosities.

The properties of PS are viewed on the basis that it is a porous material and that it is produced from c-Si wafers for microelectronic purposes. The properties of this material can be roughly summarised as:

i. Porosity - pore size, volume, surface area, pore size distribution etc.
ii. Structure - crystallinity, pore shapes with respect to doping levels of c-Si etc.
iii. Mechanical properties such as strain, microhardness
iv. Thermal properties - thermal conductivity, structural effects during heating
v. Chemical properties - chemical composition of porous walls
vi. Stability includes storage and drying of porous layers
vii. Applications. This covers very many areas such as luminescent and optoelectronic properties, sensors, micromachined devices, solar cells and many more.

It is important to mention here that there are many more areas than mentioned above being researched on PS. PS can be produced under many variable conditions and its properties are very much dependent on these conditions. The dependency of pore distribution, size and porosity on the dopant type and concentration of PS makes it difficult to establish the chemical nature of the pore walls. The details are reviewed in Chapter 2

This research work was based on PS samples that were produced from three types of commonly used electrolytes, to investigate the chemical nature of pore walls of PS. They are:

i. 40% HF (Electrolyte A)

ii. 40% HF + C_2H_5OH (Electrolyte B)

iii. 40% HF + Chemical etching in the same HF medium (Electrolyte C)

The experimental conditions for the preparation, drying and storing of PS were given in detail in Chapter 4.

5.1 The General Layout of Chapter 5

The assignment of wavenumbers for the FTIR spectrum of PS is very important in the discussion of possible mechanisms for the desorption of various gaseous species. There is a lot of controversy in the assignment of these FTIR peaks to PS. This will be discussed in section 5.2

Five kinds of gaseous species and their fragmentation products were identified during TPD analyses. They were:

1. Silane and Si-H species species ($Si-H_x$)
2. Hydrogen (H_2)
3. Fluorosilyl species ($Si-F_x$)
4. Fluorohydride species (F_xH_y)
5. F^+ species

Attempts were made to explain the possible origins of these species and their desorption mechanisms from the spectra obtained from TPD and FTIR analyses. The origin and the mechanism of desorption of each species is discussed under separate headings.

5.2 Assignment of FTIR peaks in as-anodised PS

It is very important to establish the environment of hydrogen in PS as it is the dominant adsorbed species on the pore walls. FTIR spectroscopy is capable of analysing the bonding nature of the adsorbed species on Si and is used in the investigation of the nature of pore walls. A triple peak was observed (Figure 4-25) in the region of 2140-2090cm^{-1}. The assignment of these peaks to -Si-H, $-Si-H_2$ and $-SiH_3$ species still has some ambiguities. Gupta et al (1988) made a detailed analysis using a thermal desorption technique with an *in-situ* FTIR arrangement. He observed a double peak and

assigned 2110 and 2087 cm^{-1} to the SiH_2 and SiH groups. A small shoulder was also observed at 2140 cm^{-1} in the silicon hydride region. It was suggested that this shoulder might be due to the substitiuent effect of oxygen atoms. Some other research groups (Ogata et al 1995, Kato et al. 1989, Harper et al 1996, Borghesi et al. 1993) have observed the triplets and have assigned vibrations of the stretching modes 2090, 2110 and 2140 cm^{-1} to -SiH, $-SiH_2$ and $-SiH_3$ respectively. A few other groups (Anderson et al 1993, Tsai et al 1991) refer to Gupta group's publications in assigning the silicon hydride vibrations.

One of the underlying problems in the FTIR assignments is the way the PS had been anodised. It has been shown (Sasaki et al 1994) that the concentration of HF used in the anodisation process affects the vibrational spectra. It was observed that the relative amount of $-SiH_2$ to -SiH increased with a decrease of HF concentration. The presentation of results must include reference to the experimental conditions of preparation and storage of PS. It is important to mention here that some of the results were obtained from "free standing" films, which are produced from an electropolishing process.

The assignment of the triple peaks were carried out by the authorof this work on the basis of Electronegativities of the attached groups to Si (in this case H atoms). Electronegativity is a measure of the relative tendency of an atom to attract a bonding pair of electrons. The assigned values to the elements are on an arbitrary scale from 0 to 4. The electronegativities of H, Si and F atoms are 2.1, 1.8 and 4.0 respectively (Stark et al. 1991). The study of vibrational frequencies of Si-H groups (SiH, SiH_2, and SiH_3,) in substituted silane molecules (Lucovsky 1979) displayed shifts in frequencies with respect to electronegativities. For example, the following frequency shifts were observed with fluorine substituted silanes.

$SiHF_3$	2314 cm-1
SiH_2F_2	2245 cm-1
SiH_3F	2206 cm-1

Since fluorine is considerably more electronegative than silicon or hydrogen, the electrons of silicon atoms are strongly attracted to the fluorine atoms resulting in a highly polarised molecule. This effect increases the attractive interaction between H and Si atoms decreasing their separation and increasing the vibrational frequency. Decreasing the number of F atoms from 3 to 2 or 1 reduces this effect and hence results in decrease of the Si-H frequency.

This frequency shift has been observed with a silicon atom substituted with H atoms as the H atom is more electronegative (2.1) than Si atom (1.8). In porous silicon the Si-H group has 3 neighbouring Si atoms and is represented by (1), the -SiH_2 group will have two neighbouring Si atoms and the -SiH_3 group will have 1 neighbouring atom as shown in the diagram below.

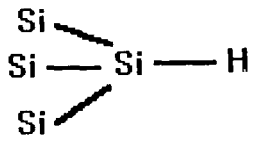

Si_3Si-H
(1)

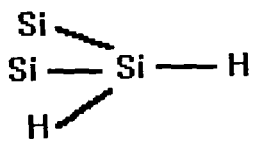

Si_2HSi-H
(2)

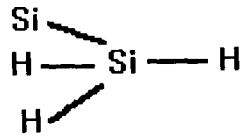

SiH_2Si-H
(3)

As the vibrational frequency increases with increase in electronegativity, it is reasonable to say that the assignment for the triple peak observed will be as follows:

-SiH	2090 cm^{-1}
-SiH_2	2110 cm^{-1}
-SiH_3	2140 cm^{-1}

The Si-H vibrational shifts for F substituted silanes are greater than for H substituted molecules. This is due to the very high electronenegativity value for F (Stark et al., 1991)

5.3 Assignment of peaks in the region 1800-400 cm^{-1} (as-anodised PS)

It is quite a difficult task to assign peaks in this region for PS samples as Si-H and Si-F vibrations overlap below 900 cm^{-1}. The assignment of the peaks in this region was based on the TPD findings. The following table gives the wave numbers assigned to FTIR peaks observed with as-anodised PS. Table 4-4 gives the details of the heating effects relating to the assignment of the wave numbers

Wave Numbers (cm^{-1})	Assignments
910	Si-H scissors
818	Si-F_x Symm. stretch
667	H_2Si-H bending
628	Si-H_3 wagging
515	Si-Si TO phonon vibration (due to O and F)
418	Si-O-Si rocking

5.4 Silane Formation

Thermal desorption techniques were used by many groups to observe the gases/adsorbates evolved from PS. Some observed silane evolution but the mechanism of it was not explained (Yoshioka. 1969; Williams et al. 1983). As recently as 1994, the Zoubir group reported not detecting SiH_4 from TDS (thermal desorption spectroscopy) experiments. Martin et al. reported to have observed H_2 and SiH_x when a PS sample prepared from Si(111) n type c-Si was heated (2000). TDS measurements were done in a quartz tube evacuated by a turbomolecular pump to a base pressure of 10^{-7} mbar. The sample was heated at a constant rate of 10°C $min^{-1}$and the evolution of H_2 and SiH_x species was monitored with a mass spectrometer.

Silane formation from silicon surfaces in contact with water was reported by the Lampert group in 1986. They observed monosilane formed when a freshly cleaved, etched or polished Si surface was exposed to water vapour. Silane was identified from its IR spectrum as well as from the darkening effect on a photographic plate. The mechanism was not known but it was suggested that adsorbed H_2O is able to cleave Si-Si bonds at the adsorption sites, resulting in Si-OH and SiH groups. Canham et al (1994) used chemography technique to show the presence of silane in PS exposed to 100% relative humidity at room temperature. They have shown that the microporous PS sample kept in the air for up to 2 years retained its ability to darken the photographic film. Also, it was shown that any trapped aq.HF was not responsible for the darkening effect. A plausible mechanism was proposed. It was suggested that silane evolution was primarily due to the hydrolysis of trihydride groups formed on the surface of the pore walls.

5.4.1 Observation of Silane with TPD and FTIR Analyses

It was observed that silane was liberated during the heating of PS samples along with other gases. The Table 5-1 below gives the fragmentation pattern of silane produced in a Mass Spectrometer with ionisation energy of 70eV (Dudly et.al. 1971)

TABLE 5- 1 Fragmentation pattern for silane

m/z	Ions	Relative Abundance
32	SiH_4^+	7%
31	SiH_3^+	78%
30	SiH_2^+	100%
29	SiH^+	29%
28	Si^+	27%

Figures 4-8, 4-9 and 4-10 show TPD desorption spectra of silane and its fragmentation products (SiH_4^+, SiH_3^+, SiH_2^+, SiH^+ and Si^+) with m/z values of 32, 31, 30, 29 and 28 respectively. The peak temperature for the silane evolution was found to be 570K ±10K. It should be noted that m/z 28 does not show a similar desorption pattern to other fragmentation products. This is most likely due to CO and/or N_2, which share the same m/z value of 28 for their molecular ions, in the pores of the PS.

The spectrum of as-anodised PS (Figure 4.25) shows a triple peak at 2140 cm^{-1}, 2115 cm^{-1} and 2091 cm^{-1}. These wave numbers were assigned to $-H_2Si-H$, -HSi-H and -Si-H respectively (Ogata et al. 1995, Janz et al. 1961). The disappearance of the peak at 2140cm^{-1} was observed when the PS sample was heated to 570K ± 10K (Figure 4-27). This means that at this temperature Si-Si bonds were broken in $\equiv Si\text{-}SiH_3$ groups on the pore walls of PS. The disappearance of the silyl groups ($-SiH_3$) coincides with the silane formation observed with the TPD technique (Figure 4-8). Silane evolution was observed with PS prepared from all three types of electrolytes. This indicates that the alcohol component of the electrolyte did not participate in the silane formation process.

5.4.2 The Proposed Mechanism for Silane Formation

The HF based electrolyte forms a junction with the crystalline silicon during the anodisation process, and the pores are in touch with the aqueous electrolyte. Thus the pore walls are covered with physisorbed moisture as well as the silicon dangling bonds are covered with mainly hydrogen and fluorine related species, as indicated from the

TPD work. The existance of trihydride terminated PS wall was shown by STM technique (Morita et al. 1991)

The proposed mechanism is as follows:

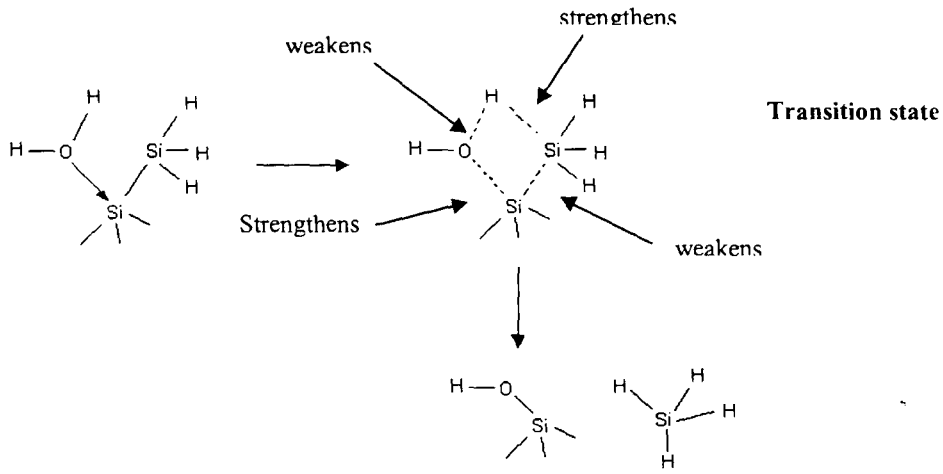

$$\equiv Si\text{-}SiH_3 + H_2O \rightarrow SiH_4 + \equiv Si\text{-}OH$$

The mechanism of silane formation is explained by a nucleophilic second order (S_N2) reaction mechnism (Sommer 1964). The oxygen on the water molecule has a lone pair of electrons and it acts as a nucleophilic ("hole-loving") center. . The bond between Si and the SiH_3 group ($Si_3Si\text{-}SiH_3$) weakens, as there is some polarisation between the two Si atoms. This causes O to form a strong bond with $SiSiH_3$ ($O\text{-}SiSi_3$). The bond between HO-H weakenens and the H atom from the water molecule forms a strong bond with SiH_3 as shown in the diagram. This type of reaction occurs by a four-centre process as shown by a transition state. The bond between $Si_3Si\text{-}SiH_3$ breaks and the products,≡Si-OH (silanol group) and silane are formed.

5.5 Hydrogen Evolution

During the anodisation of silicon, hydrogen is produced. Dissolution of silicon to produce porous silicon has attracted lots of research work to understand the mechanism of forming PS. There is an excellent review on the subject available (Smith and Collins 1992). Also, it was reviewed in Chapter 2 of this work. The hydrogen formed during anodisation as atoms with one electron. These form hydrogen molecules with other hydrogen atoms and are liberated as a gas.

$$H^{\bullet} + H^{\bullet} \rightarrow H_2 \uparrow$$

Atomic hydrogen is a very reactive species and it forms bonds with the dangling bonds of freshly etched silicon. The pore walls of PS are covered mainly with hydrogen to give Si-H, Si-H_2 and Si-H_3 groups and some of the surface Si atoms are attached to fluorine based species found in the electrolyte.

Desorption of hydrogen was investigated by using TPD and *in-situ* FTIR Spectroscopy (Gupta, 1988). An isothermal annealing method was used to desorb H_2 from mono- and di- hydrides. The double peak at 2102 and 2087 cm^{-1} were assigned to Si-H and Si-H_2 stretching modes (in reverse order to the present work) respectively. FTIR peaks at 2110 cm^{-1} (-SiH) and 910 cm^{-1} (-SiH_2) were used to evaluate desorption kinetics. Second order kinetics were predicted for both hydrides. TPD and stress measurements were used by Diawara et al. (1994) to compare H_2 effusion with the film stress. The as-anodised PS films are found to be under compression (Young et al. 1985), and so the changes in stress and the hydrogen effusion were measured during thermal annealing. Second order kinetic processes for both stress and hydrogen effusion were predicted. The Zoubir group (1994) applied TDS (Thermal Desorption Spectroscopy) and FTIR. They observed effusion curves for H_2 desorption at 400°C (673K) and 500°C (763K) and assigned them to di- and mono-hydrides. Also, Si-F_x (x=1,2,3) species and Si-H_y (y=1,2,3) were observed when a quadrupole mass spectrometer was used as a detector. No silane (SiH_4) was observed. It is important to emphasise that the triple peaks observed in the Si-H vibration region at 2090, 2110 and 2140 cm^{-1} were assigned to -SiH, =SiH_2 and -SiH_3 groups respectively. This contradicts Gupta's assignments. The difficulty of using these references to previous work on thermal desorptions is that, as was mentioned earlier, the PS samples were prepared using different methods and conditions. The surface chemistry of these PS films depends on the way they are produced. The Table 5-2 shows some of the key papers published on the thermal desorption from porous silicon.

TABLE 5- 2 Summary of the properties of PS prepared using different conditions

PS details	Electrolyte	Anodising Conditions	Kinetic Data	Heating Rate	Other Information	Reference
P type, Si(100) 1-10 Ω cm Al on the back of Si	50% HF:C_2H_5OH 1:1	25 mA cm^{-2} 5 minutes	2^{nd} order for Stress and H_2 effusion	20°C Min^{-1}	420°C and 525°C (693K and 798K)	Diawara et al; 1994?
P+ type, Si(100) 0.005 Ω cm Al on the back of Si	50% HF:C_2H_5OH 1:1	25 mA cm^{-2} 5 minutes	2^{nd} order for Stress and H_2 effusion	20°C Min^{-1}	390°C and 500°C (663K and 773K)	Diawara et al; 1994?
P type Si(100), CZ 0.464 Ω cm Ta on back of Si	33% HF: C_2H_5OH	200 mA cm^{-2} 5 seconds	2^{nd} order for H_2 desorption (mono & di- hydrides) E_a $4.7x10^{-2}$ and $1.7x10^2$ kcal mol^{-1}	8K S^{-1} (480K Min^{-1})	Only simulated TPD curve; peak area 3:1 ratio?	Gupta et al., 1988
P-type, Si100) No resistivity details	50% HF:C_2H_5OH 1:1	10-100 mA cm^{-2} No anodisation time	None	1K Min^{-1}	340°C and 450°C (413K and 723K), ref-Gupta for FTIR peaks	Petrova-Koch et al., 1991??
P^+ type Si(100) 0.015-0.25 Ω cm	40% HF:C_2H_5OH 1:1	75 mA cm^{-2} 30 minutes	None	20°C Min^{-1}	DSC technique only 375°C (648K)	Salonan et al., 1999
N+-type Si(100) 0.35-0.95 Ω cm	40% HF:C_2H_5OH 1:1	75 mA cm^{-2} 30 minutes	None	20°C Min^{-1}	DSC technique 375°C and 490°C (648K and 763K)	Salonan et al., 1999
Si (111), N- & P-type 0.005-100 Ω cm	HF/HNO3 gaseous (Stain etched)	None	E_a 16-17 kcal mol^{-1}	Not given	125°C and 300°C (398K and 573K)	Yoshikova, 1969
P-type, Si(111) 87-112 Ω cm	3g.NaNO3 in 100 cm3 49% HF (chemical etch)	10 minutes in daylight!	E_a 46 kcal $mol^{-1}$and 57.8 kcal mol^{-1}	15°C Min^{-1}	400°C and 500°C (673K and 700K)	Hadj Zoubir, 1994, 1995

5.5.1 Proposed Mechanism for H_2 formation

Despite many experimental and theoretical works carried on hydrogen adsorption and desorption on c-Si, the mechanism still remains controversial. Several desorption models have been proposed but none are conclusive. For semiconductors such as Si, the atoms are covalently bonded i.e the valence electrons from neighbouring Si atoms are shared. The surface Si atoms find it hard to compensate for the loss of nearest neighbours. The dangling bonds created at the surface cannot be easily satisfied except through some form of rearrangement or reconstruction (Somorjai 1994). The reconstruction results in a (2x1) surface when alternative rows of surface atoms move towards each other to form "unoccupied" dimers (>Si = Si<). The diagram below shows a schematic diagram of 1x1 and a reconstructed Si (100) surface

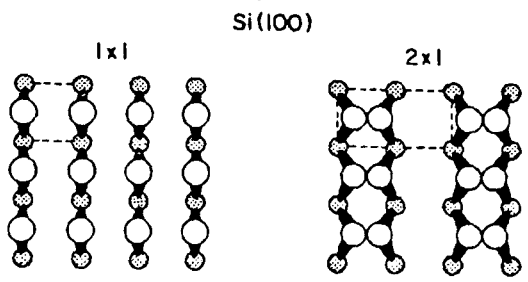

Sakurai and Hagstrum (1976) reported that atomic hydrogen chemisorption on the reconstructed clean Si(100)2x1 surface would produce either the monohydride Si(100)2x1:H structure or the dihydride Si(100)1x1 structure depending on the experimental conditions. D'Evelyn et al. (1992) proposed a theoretical model that predicted the weak Si-Si π-bond favours the pairing and desorption of H_2 by a "concerted" mechanism. This applies to a Si(100)-2x1 Si surface at low coverage which gives a doubly occupied dimer or monohydride. Laser-induced thermal desorption (LITD) and TPD experiments by Sinnaiah et.al. (1990) found that H_2 desorption from monohydride follows first order kinetics with E_a of 45 kcal mol^{-1} for the coverage up to one monolayer. A concerted mechanism with a hydrogen in a excited state (H*) was proposed. A similar method was used by Wise et al. (1991) to study monohydrides on Si(111)7x7 and Si(100)2x1 surfaces. First order kinetics were observed for both with E_a values 62 and 58 kcal mol^{-1} respectively. He concluded that the kinetic parameters are consistent with a desorption mechanism in which hydrogen surface mobility allows two H atoms to migrate to adjacent sites. The migrated H atoms recombine and H_2

molecules can desorb. A recombinative desorption mechanism for monohydride desorption from Si (100) 2x1 and Si (111) 7x7 surfaces was proposed by Shane et al.(1992). They concluded that the desorption from monohydrides for both surfaces goes through a dihydride-like intermediate phase.

For Si(100):

$H\text{-}Si\text{-}Si\text{-}H \leftrightarrow Si\text{-}SiH_2$ ⋯⋯▶ 1a

$Si\text{-}SiH_2 \rightarrow Si\text{-}Si + H_2$ ——▶ 1b

For Si(111):

$Si\text{-}H + Si\text{-}H \rightarrow Si + SiH_2$ ——▶ 2a

$SiH_2 \rightarrow Si + H_2$ ——▶ 2b

In the above model, desorption from dihydride occurs through the combination of two hydrogens from the same Si atom. A different desorption mechanism, in which H atoms in adjacent dihydride units (Si(100) 1x1:H) recombine, has received more support in the literature (Ciaci et al. 1984, Zheng et al. 1992, Cheng et. al. 1991). Many more papers are available on the desorption of H_2 from c-Si surfaces, but they are not highly relevant to this work as porous silicon exhibits multi crystalline planes.

Application of these data to PS is not possible as PS does not have defined crystal planes like c-Si. The results obtained from PS cannot be analysed in terms of any particular crystal plane as the pore surfaces are not unidirectional but are isotropic. The microstructure of pores has been extensively studied (Beale et al. 1985, Smith et al. 1988). The structure of the pores was shown to be dependent on the electochemical parameters, dopant type and density and the type of electrolyte (Canham, 1997, Herino, 1997, Cullis 1997). With p^- type (20-50 Ω cm), the main direction of pore growth is found to be in the (110) plane from TEM studies (Young et al 1985). Even though the silicon in porous silicon retains some crystallinity, the Si nanocrystals of the pore walls are randomly oriented. One thing is certain and that is the pore walls of PS exhibit surfaces with "multi-crystalline planes".

FZ silicon is used in this work and the PS produced from this type of Si produces microporous material. The pore structure consists of a random array of fine holes which run continuously to the surface and give a "fur-like" appearance.

Figures 4-5, 4-6 and 4-7 are the TPD spectra for H_2 desorption from PS samples prepared from Electrolytes A, B, and C respectively. All of them show two "humps" in the region of 600-730K which are believed to have arisen from two types of hydrogen environments. A very small "blip" was observed with m/z 29 at a lower temperature (~ 525K), the origin of which is not understood. The averaged peak temperature values for H_2 desorption were taken from 3 samples and are given in Table 5-3 below. The accuracy of the peak tempeature values is ± 5K

TABLE 5- 3 Peak temperatures observed with H_2 desorption spectra

Electrolyte	**Peak Temperature 1 (β_1) ± 5K**	**Peak Temperature 2(β_2) ± 5K**
A	620	720
B	625	725
C	610	700

The lower temperature peak β_1 and the high temperature peak β_2 are generally identified as H_2 desorbing from dihydride and monohydride species respectively (Zheng et al. 1992; Flowers et al. 1993, Cheng et al. 1991). But this work found that β_1 is due to -SiH and β_2 is from $-SiH_2$. In other words hydrogen from -SiH desorbs at lower temperature than from $-SiH_2$ species. This was confirmed by correlating TPD spectra for H_2 desorption and the results from FTIR spectra obtained using heated PS samples with 25K intervals. Figure 5-1 shows overlaid FTIR spectra of PS heated from 325K to 625K in the 2100 cm^{-1} region.

The following observations are to be noted:

1. The $-SiH_3$ peak (2140 cm^{-1}) disappears at ~575K.
2. The peak for $-SiH_2$ (2110 cm^{-1}) shifts to 2102 cm^{-1} with the disappearence of $-SiH_3$ species.
3. There is a gradual decrease in intensities of $-SiH_2$ and -SiH peaks with increase in temperature and the peak due to -SiH disappears before $-SiH_2$
4. The peak due to -SiH (2108 cm^{-1}) disappears around 625-650K

5. More desorption occurs till the temperature reaches about 700K. Disappearence of -SiH_2 peak.-see Figure 4-28

To summarise the sequence of the desorbing order for Si-H_x species is as follows:

$-SiH_3$ > $-SiH$ > $-SiH_2$

The TPD spectra for all three electrolytes (Electrolytes A, B, C) are found to be similar indicating that the pore surfaces of all three types of PS are similar with respect to Si-H_x species. The two "humps" of the TPD spectra (Figures 4-5, 4-6 and 4-7) are not completely resolved into two peaks. In other wards maximum desorption occurs at the peak temperatures but the desorption from SiH_2 (β_1 peak) starts before the desorption from SiH (β_2) decreases to a minimum level. This results in a partial overlap between the β_1 and β_2 peaks.. This can be explained by the FTIR spectra. Figure 5-1 shows overlaid FTIR spectra of PS samples heated to 325K, 500K and 625K in the vacuum. The peak at 2140 cm^{-1} due to $-SiH_3$ nearly disappears at 500K (total disappearence observed at ~570K) During this time the peak at 2110 cm^{-1} (due to $-SiH_2$) shifts to 2102 cm^{-1} without any loss of its intensity. Gradual loss of both peaks at 2102cm^{-1} and 2090 cm^{-1} occurs during further heating.

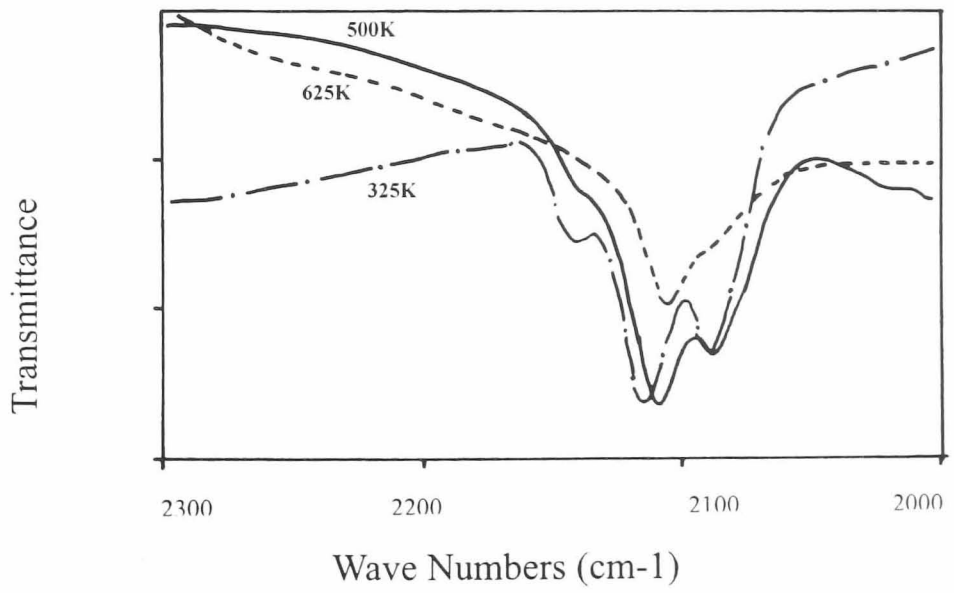

FIGURE 5- 1 Overlaid FTIR spectra of triple peaks (Si-H_X) at 325K,500K and 625K

Ratio of The Area Under the H_2 Desorption Spectra

The areas under the peaks were calculated for the H_2 desorption spectra obtained from PS prepared from all three electrolytes. The Table 5-4 in the next page gives the details.

TABLE 5- 4 $\beta_2 : \beta_1$ ratio of peak areas of H_2 desorption spectra (all three electrolytes)

Electrolyte	Peak1 (β_2)-Area	Peak 2 (β_1) –Area	***Ratio ($\beta_2 : \beta_1$)
A	11.8	14.2	1 : 1.20
B	7.8	8.45	1 :1.08
C	6.2	5.2	1 :0.84

****$\beta_2 : \beta_1$ ratio represents $\underline{SiH : SiH_2}$ ratio*

PS anodised in Electrolyte C has gone through a chemical etching in 40% HF for 4 hours. PS samples from Electrolytes A and B show about a 1:1 ratio for the amount of H_2 desorbed from SiH_2 and SiH species. Table 5-5 shows the peak ratios obtained by some other researchers

TABLE 5- 5 $\beta_2 : \beta_1$ ratio of peak areas of H_2 desorption spectra –literature values

Sample type	Anodising conditions	*Ratio ($\beta_2 : \beta_1$)	References
P type Si(100), CZ 0.464 Ω cm Ta on back of Si	33% HF: C_2H_5OH 200 mA cm^{-2} 5 seconds	1:3	Gupta et. Al., 1988
P-type, Si100) No resistivity details	50% HF:C_2H_5OH, 1:1 10-100 mA cm^{-2} No anodisation time	1 : 1	Petrova-Koch et al., 1991
P-type, Si(111) & Si(100) 87-112 Ω cm	3g.$NaNO_3$ in 100 cm^3 49% HF (chemical etch) 10 minutes in daylight!	1 :0.71	Zoubir et al., 1995
n-type, Si(111) 16-24Ω cm	HF:H_2O, 1:4. 15 $mAcm^{-2}$ illuminated (30$mWcm^{-2}$)	1: 66	Martin et al,personal communication 1998

** $\beta_2 : \beta_1$ ratio represents $\underline{SiH_2 : SiH}$*

Since the pore growth in P^- high resistive (20-50 Ω cm) wafer is not directional, the pore surface can be considered as rough and multi-faceted. These surfaces cannot be defined as either Si(110), Si(100) or Si(111). The reconstructed Si surfaces that are referred in the literature for c-Si, for example, Si(100) 2x1 which is monohydride covered surface or Si(100) 1x1 dihydride covered or Si(100) 3x1 which is a surface with mono- and di- hydride covered in alternating positions, cannot be applied fully to interpret the H_2 desorption mechanism for PS. Nevertheless, the results obtained for PS

reflect the nature of bonding in all pore surface Si atoms with different configurations and to a lesser extent to the crystallographic orientations.

The evidence for the existence of -SiH_3, -SiH_2 and -SiH groups on the pore surfaces comes from the FTIR spectrum with a triple peak in the Si-Hx vibration region. Some papers reported a double peak produced by only -SiH and -SiH_2 was observed in the Si-H_x region (Anderson et al.1993, Hory et al. 1995; Sasaki et.al 1994; Gupta et al. 1988). Others observed a triple peak in the 2100 cm^{-1} region, corresponding to all three Si-H_x species (Ogata et.al 1995, Chabal 1985, Zoubir 1995). The reasons for this can be different infrared instruments used or perhaps different concentrations of HF in the electrolyte used for the anodisation of PS (Sasaki and Kitahara 1994). Sasaki and Kitahara reported that the ratio SiH_2 : SiH increases with the decrease in HF concentration. Also, fluorine and oxygen are found on PS anodised for a long period. Some of the possible structures for Si-H_x on a pore surface are given on this and the next page.

5.5.2 Possible Si-H Features on Pore Surface

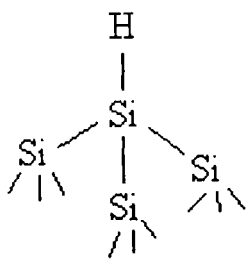

I

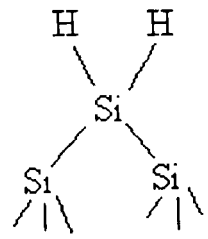

II

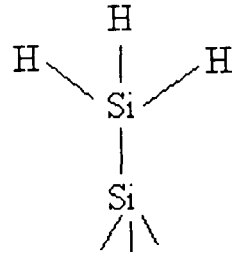

III

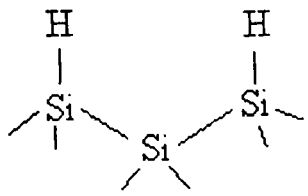

IV

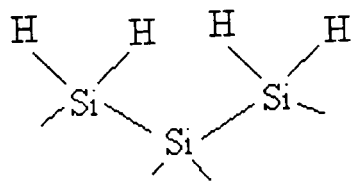

V

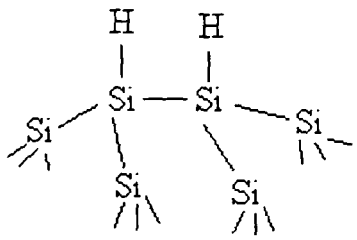

VI

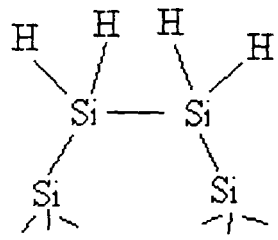

VII

5.5.3 Some Possible H_2 Desorption Processes

1. 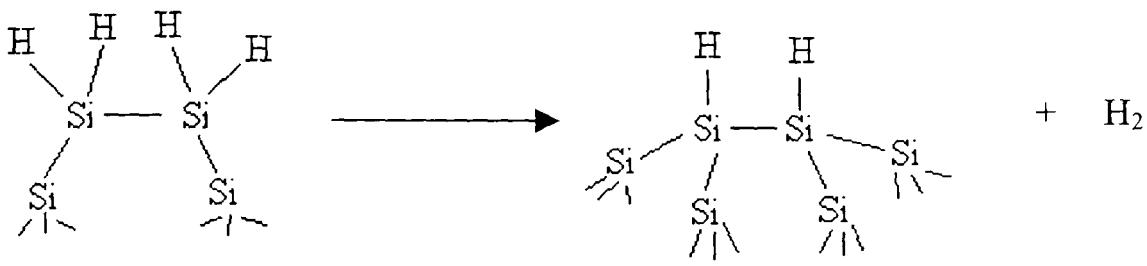

2. 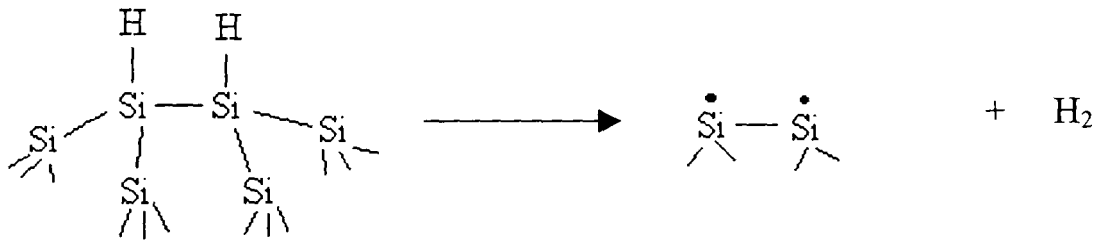

3. 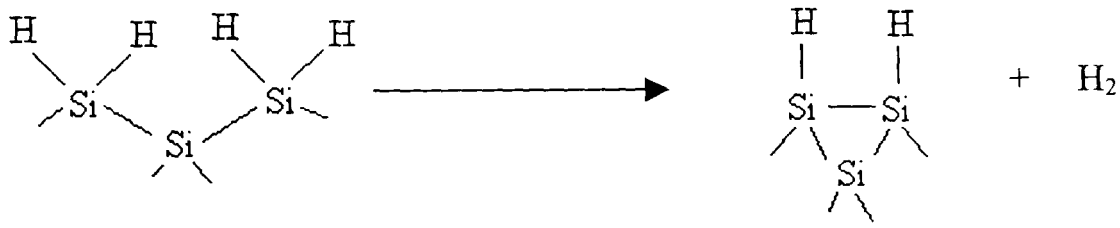

4. 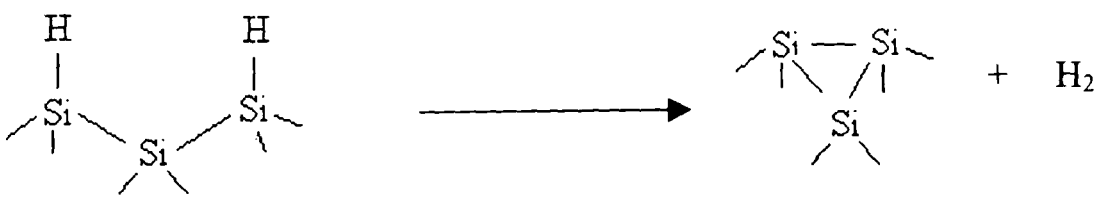

5. 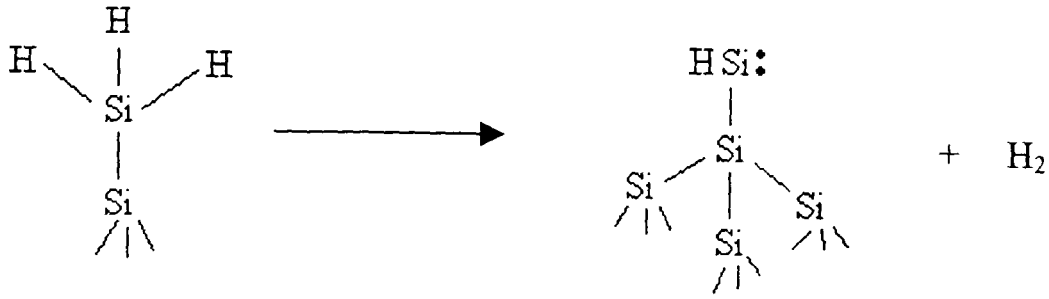

6. 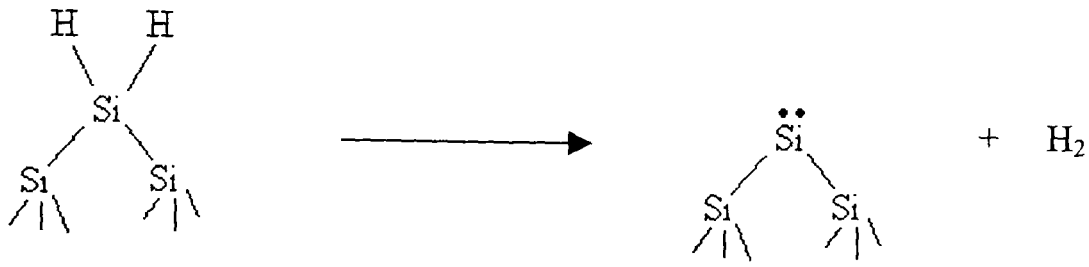

7. 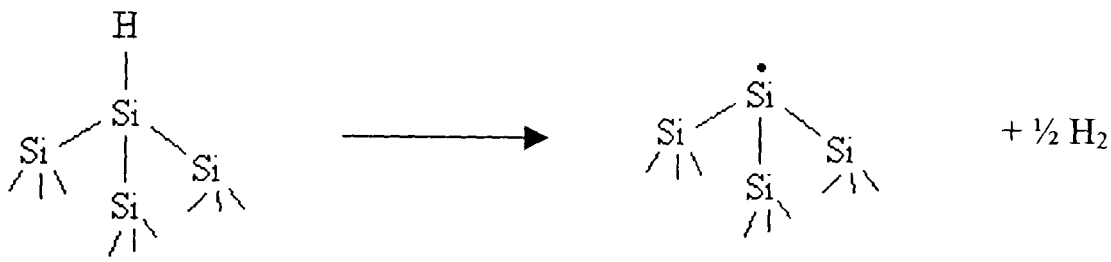

5.6 Possible Desorption Processes

Schematics of possible structures were given in figures I to IV for Si-H and Si-H_2 groups. The pores are multi-directional (isotropic) and there is no single crystal plane or just one type of reconstructed surface such as Si(100) 2x1. Therefore many types of planes with higher numbers for Miller Indices are possible. It is important to mention here that more than the seven structures shown may be possible with PS. Various H_2 desorption processes are possible with these structures and seven of them are illustrated above.

5.7 Fluoro-silyl Species ($Si-F_x$)

Even though the porous silicon surface is more or less covered with $Si-H_x$ species there is much evidence to suggest that $Si-F_x$ species are also present on the surface. There are two aspects of adsorption to be considered when the pore surface of PS is investigated

1. Effects of dipping c-Si in HF - dissociation products of HF in water or ethanol are found.
2. The products that are formed during anodic dissolution.

Extensive studies of the surface of HF-dipped c-Si have been published as this step is used to remove native SiO_2 before any processing steps to produce devices. Chabal et al. (1989) investigated HF-dipped Si surfaces with Attenuated Total Reflection spectroscopy (ATR) and reported that the HF treated surface is inhomogeneous and that $Si-H_x$ (x=1,2,3) species are present. Grunder et al. (1991) using HREELS and XPS found mainly Si-Hx and small amounts of fluorine and oxygen. It was also found that the amount of Si-F is dependent on the concentration of HF. With a Si(100) surface dependence was found to be logarithimic. Also, it was reported that the surface coverage of Si-F increased by two fold with longer immersion times in 50% HF and then levels off. This was interpreted in terms of an equilibrium between the fluoridating reaction and the dissolution of fluorinating species.

The exact species participating in the anodisation process have been investigated. Venkadeswara Rao et. al. (1991) investigated the HF/Si interface using Fourier Transform Electromodulated Infrared Spectroscopy (FTEMIRS) *in-situ* and FTIR methods. A broad spectrum was observed in the 2100cm^{-1} region with the FTEMIRS method whereas the FTIR spectrum of PS removed from the electrolyte showed the characteristic three peaks for the $Si-H_x$. An attempt was made to detect the intermediate species in the anodic dissolution process and it was concluded that if these species exist at all, their life time is shorter than 0.3ms.

5.8 Desorption of $Si-F_x$ and H_x-F_y species

Desorption of fluorine related species were investigated by TPD spectroscopy. FTIR spectroscopy was not very useful in this study as the intensities of Si-F bonds are found

to be much lower than Si-H bonds. Also, in the fingerprint region (1400-400 cm-1), the Si-H and Si-F vibrations overlap each other and it is hard to assign those of SiF_x.

The desorption spectrum for m/z 85 (SiF_3^+) shows three distinctive peaks with the porous silicon prepared from electrolyte A (Figure 4-11). This indicates that SiF_3^+ species originated from three different sites within the porous silicon. The porous silicon prepared from alcoholic electrolyte (Electrolyte B) shows a broad single peak and a larger well defined peak at higher temperature (Figure 4-12). The porous silicon prepared from Electrolyte C (Figure 4-13) shows three peaks but the first and second peaks are not well resolved and the second peak is larger than the third high temperature peak. The peak temperatures of the Si-F_x series from all three electrolytes are given in Table 5-6

TABLE 5- 6 Peak Temperatures for SiF_x Species

Electrolyte	Peak T_1 [K]	Peak T_2 [K[	Peak T_3 [K]
A	420	590-630	970
B	No Peak	625-650	850
C	450-500	600	890

5.8.1 Fragmentation products of SiF_4

The main Si-F_x species observed with TPD are observed together with fragmentation products of Si-F_4. Table 5-7 shows the abundance of SiF_4 fragments observed with mass spectroscopy.

TABLE 5- 7 Fragmentation Pattern of SiF_4

m/z	Ions	Abundance (Gmelin)	Abundance(Dudley et.al)
19	F^+	1.09%	1.2%
47	$^{28}SiF^+$	3.7%	3.2%
48	$^{29}SiF^+$	0.21%	-
49	$^{30}SiF^+$	0.12%	-
66	$^{28}SiF_2^+$	0.77%	1.0%
33	$^{28}SiF_2^{++}$	2.83%	2.4%
85	$^{28}SiF_3^+$	100%	100%
86	$^{29}SiF_2^+$	5.24%	-
87	$^{30}SiF_2^+$	3.40%	-
104	$^{28}SiF_4^+$	2.52%	1.7%

The ratios of the fragmentation products of SiF_4 from the literature are as follows:

SiF_4^+	:	SiF_3^+	:	SiF_2^{++}	:	SiF_2^+	:	SiF^+	:	F^+
2	:	100	:	3	:	1	:	4	:	1

The measured partial pressure(PP) of SiF_3^+ is about $4E^{-9}$ and the expected corresponding PP of F^+ would be about $4E^{-11}$. In fact the measured PP of F^+ is found to be $3.5E^{-10}$, i.e. about 10 times higher than the expected value. Figures 5-3 and 5-4 show a combined spectra of SiF_2^{++}, SiF_2^+, SiF^+ and F^+ species. The appearence temperature and PP of F^+ species are definitely different from the Si-F_x species. This means that most of the F^+ species are not coming from SiF_4 but from another source such as HF electrolyte.

The Table 5-8 below gives the partial pessures of the peaks observed with SiF_x species and all the fluorine based species observed with the desorption of PS. From the table it can be seen that the PP of SiF_2^{++} and SiF^+ from the literature do not follow what was observed with the desorption products from PS.

5.8.2 TPD spectra of fluorinated hydrides

Four distinct hydrofluoride species were observed with the TPD investigation. They were: HF^+, $H_2F_2^+$, $(H_3O)F^+/F_2^+$ and HF_2^+ at m/z values of 20, 40, 38 and 39 respectively. Also, F^+ at m/z value 19 was found to desorb from PS when it is heated. Tables 5-8 and 5-9 give the details of their peak temperatures and partial pressures.

5.8.3 Properties of aqueous HF

Unlike the other hydrohalic acids (HX), which are extremely strong, HF is very weak in aqueous solutions. On dilution it was found that the dissociation constant decreases. In water, it ionises to give,

$$H_2O + HF \leftrightarrow [H_3O^+F^-] \leftrightarrow H_3O^+{}_{(aq)} + F^-{}_{(aq)}$$

$$K_a = [H_3O^+]\,[F^-] / [HF]\,[H_2O]$$

$$K_a = 1.1 \times 10^{-3} \text{ or } pK_a = 2.98 \quad (pK_a = -\log K_a)$$

This indicates rather small free hydrogen ion concentration as a result of the strongly bonded, undissociated ion-pair $[H_3O^+F^-]$ being favoured in solution.

The F^- ions in the solution form hydrogen bonds with the undissociated HF molecules.

$$F^- + HF \rightarrow [F\text{—}H\text{----}F]^-$$

Hydrogen bonding in this ion is exceptional in that it is stronger than normal and the H atom is symmetrically situated between the two fluorines. For this reaction,

$$K_{a2} = [F\text{—}H\text{----}F]^- / [F^-]\,[HF]$$
$$= 2.6 \times 10^{-1} \text{ ; or } pK_{a2} = 0.58$$

This indicates that an appreciable number of fluoride ions in the solution are coordinated by HF to give HF_2^- rather than by H_3O^+ despite the larger concentration of water molecules (Greenwood and Earnshaw 1990).

To summarise, the aqueous solution of HF contains $[HF_2^-]$, HF, $[H_3O^+F^-]$ and associated HF molecules such as $(HF)_2$.

The Si-F_x species show some differences. Table 5-9 shows the peak temperatures for the SiF_3^+ peaks. There were three peaks for SiF_3^+ (Figure 4-11), of which one is at higher temperature (970K) with electrolyte A whereas with electrolyte B only two peaks with one at higher temperature (850K) appear (Figure 4-12). In these two cases the higher temperature peak is at least 10 times bigger than the lower temperature peaks. Electrolyte C which is same as Electrolyte A but undergone chemical etching for 4 hours. The lower temperature peaks are not well resolved but their partial pressures are comparable to the third higher temperature peaks (Figure 4-13).

5.8.4 Proposed Mechanism For Lower Temperature Si-F_x Peaks

Two different mechanisms are proposed to account for these observations. The porous structures can be compared to zeolite structures. Zeolites have aluminosilicates framework, which are characterised by the presence of channels that consist of a 3-D maze of interconnecting tunnels. Besides its function as a molecular sieve, it behaves as an ion exchanger (Shriver et al. 1999). The lower temperature Si-F_x peaks were explained by this mechanism

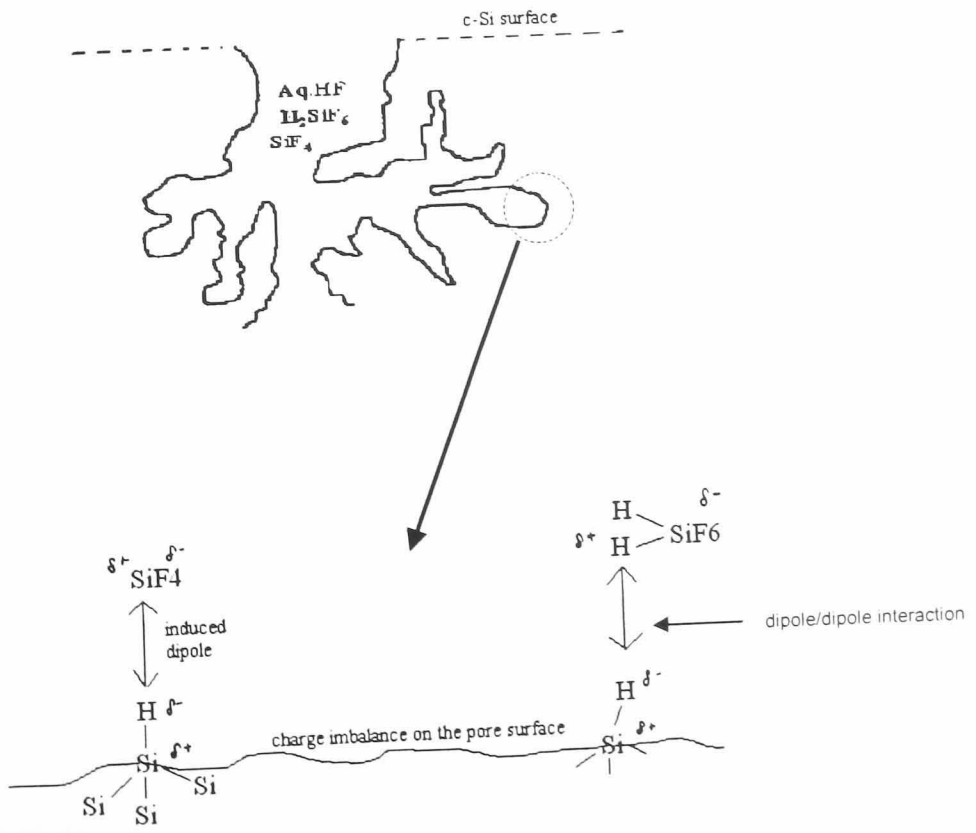

FIGURE 5- 2 Electrostatic attraction between pore walls and electrolyte

Microporous material is classified as having pore diameters less than 2 nm by IUPAC classification of pore size. The pores can have many little buds branching out isotropically in many directions in P^- substrates. These little buds can be as small as 0.4- 0.5 nm. All of these pores will have all the species mentioned earlier. A schematic of a pore is illustrated in Figure 5-2. The Si atoms on the surface of the pores are not neutral. The dangling bonds are covered with H atoms formed from the electrolysis process as well as F species from the electrolyte. Water, the medium for the electrolyte is also dissociatively adsorbed as H and OH on to the Si surface. In other words the surface of silicon contains charges as shown in Figure 5-2. There is electrostatic attraction between these Si atoms and molecules such as H_2SiF_6, SiF_2 and SiF_4. They are held by weak electrostatic and/or van der Waals forces. During heating, at lower temperatures these species were released and their fragmented products were obtained. It is important to mention here that the observed ratio of the fragmented products did not follow the literature values. The partial pressures of SiF_2^{++}, SiF_2^{+} and SiF^{+} were found to be higher than the SiF_3^{+} peak which is the base peak for SiF_4 fragmentated products (Table 5-7). This means that Si-F and Si-F_2 must have been present as separate entities.

5.8.5 Proposed Mechanism For High Temperature Peak

It should be noted that SiF_2^{++}, SiF_2^{+} and SiF^{+} were not detected together with the high temperature SiF_3^{+} peak observed with TPD spectra. This suggests that the SiF_3^{+} species observed at high temperature has different origin/environment to that observed at lower temperature

It is proposed that F atoms can bond to Si to give Si-F_y (y=1,2,3) similar to Si-H_x species. Migration of F atoms at high temperatures was studied using SIMS and TPD techniques by the Jeng group (1992). They reported that migration of the F atoms occurred above 550°C (823K) and indicated that it is a strongly temperature-dependent thermallyactivated process. The higher temperature peak can be explained in terms of a diffusion mechanism. This means that a Si-Si bond breakage occurs during the release of SiF_3^{+}. This is supported by the bond dissociation energies reported in the literature (Kato et.al. 1988). Si-F (129.3 kcal mol^{-1}) > Si-Si (42.2 kcal mol^{-1}).

.

TABLE 5- 8 Partial pressures of F-based species observed with PS from Electrolytes A, B and C (at their peak temperatures)

Electrolyte	SiF_3^+ Partial pressure(mbar)			HF_2^+ Partial pressure(mbar)		HF^+ Partial pressure(mbar)			$H_2F_2^+$ Partial pressure(mbar)			F^+ Partial pressure(mbar)			$(H_3O)F^+/F_2^+$ Partial pressure(mbar)	
A	4.1 $x10^{-10}$	1.0 $x10^{-10}$	1.5 $x10^{-9}$	3.2 $x10^{-10}$	2.8 $x10^{-10}$	6.0 $x10^{-11}$	6.0 $x10^{-11}$	6.0 $x10^{-11}$	6.0 $x10^{-11}$	4.0 $x10^{-11}$	7.0 $x10^{-11}$	1.3 $x10^{-11}$	3.0 $x10^{-11}$	3.6 $x10^{-11}$	in the 10^{-11} level not very distinctive	
B	None	1.0 $x10^{-10}$	1.4 $x10^{-9}$	4.0 $x10^{-9}$	6.0 $x10^{-9}$	1.2 $x10^{-10}$	1.2 $x10^{-10}$	None	None	2.0 $x10^{-10}$	6.0 $x10^{-10}$	2.8 $x10^{-10}$	3.0 $x10^{-10}$	1.2 $x10^{-10}$	v.low; $\sim10^{-12}$ level	
C	6.0 $x10^{-10}$	1.2 $x10^{-9}$	8.0 $x10^{-10}$	5.0 $x10^{-9}$	6.2 $x10^{-9}$	None	1.0 $x10^{-10}$	4.0 $x10^{-10}$	1.2 $x10^{-9}$	1.0 $x10^{-9}$	None	1.0 $x10^{-10}$	1.5x10^{-10}	1.2 x10-9	1.0 $x10^{-9}$	1.0 $x10^{-9}$

**** The peak temperatures of fluorosilyl- and fluorohydrides are given in Table 5-9.

TABLE 5- 9 Peak temperatures observed with F-based species (PS from Electrolytes A, B and C)

Electrolyte	380-410 (K)	450-500(K)	530-550 (K)	600-640 (K)	650-700 (K)	790 (K)	850-970 (K)
	SiF_3^+			SiF_3^+			SiF_3^+
	F^+			F^+	F^+		
	HF^+		HF^+	HF^+			
A	$H_2F_2^+$		$H_2F_2^+$	$H_2F_2^+$			
	$(H_3O)F^+$		$(H_3O)F^+$	$(H_3O)F^+$			
	HF_2^+			HF_2^+			
				SiF_3^+			SiF_3^+
	F^+		F^+	F^+		F^+	
			HF^+	HF^+			
B			$H_2F_2^+$	$H_2F_2^+$			
				$H_3O)F^+$			
				$H_2F_2^+$			
		SiF_3^+		SiF_3^+			SiF_3^+
	F^+	F^+		F^+	F^+		
		HF^+		HF^+			
C		$H_2F_2^+$		$H_2F_2^+$			
		$(H_3O)F^+$		$(H_3O)F^+$			
		HF_2^+		HF_2^+			

The m/z values for F^+,HF^+, $(H_30)F^+/F_2^+$, HF_2^+ $H_2F_2^+$ are 19, 20, 38, 39 and 39 respectively.

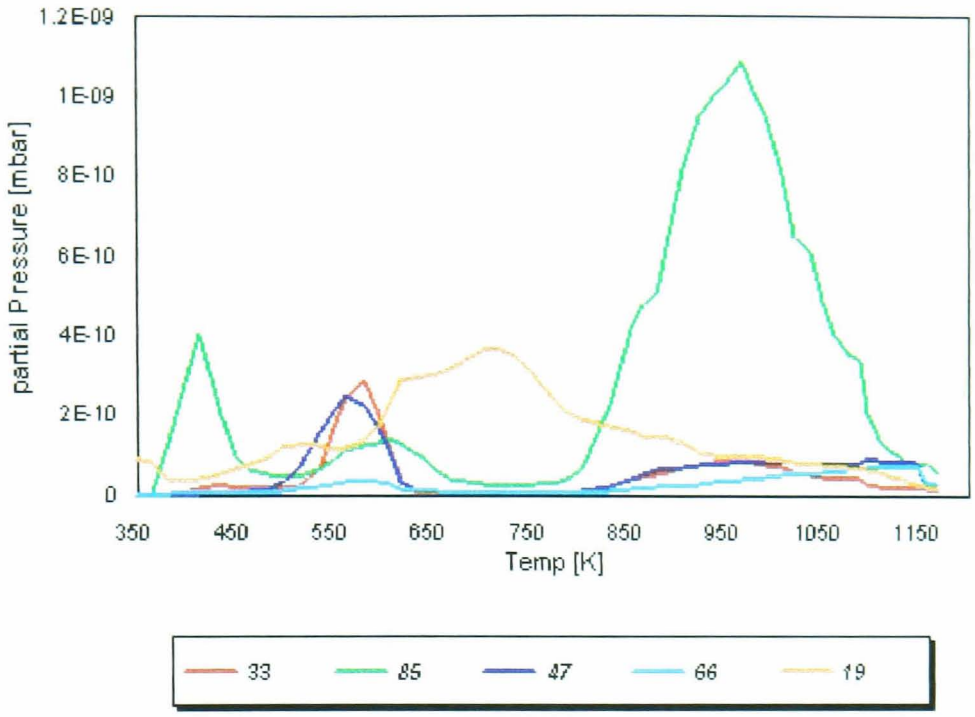

(33- SiF_2^{++}, 47- SiF^+, 66- SiF_2^+, 85- SiF_3^+, 19- F^+)

FIGURE 5- 3 Comparison of the TPD spectra of F-based species from PS (Electrolyte A)

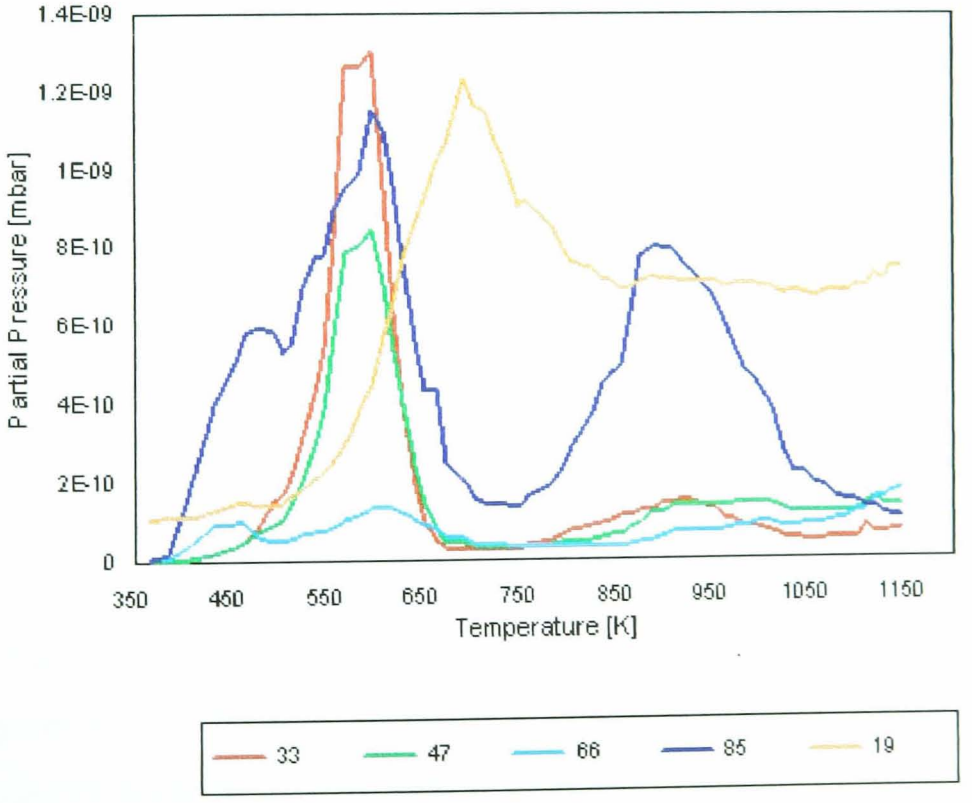

(33- SiF_2^{++}, 47- SiF^+, 66- SiF_2^+, 85- SiF_3^+, 19- F^+)

FIGURE 5- 4 Comparison of the TPD spectra of F-based species from PS (Electrolyte C)

5.8.6 Mechanism for Fluorine Evolution.

From the literature (Gmelin Handbook 1993) one of the possible fragmentation products of SiF_4 is F^+ and the relative abundance of it should be 100 times smaller than the base peak SiF_3^+. Figures 5-3 and 5-4 show that it is not so. It is proposed that origin of F^+ observed in the TPD spectra (Figures 5-3 and 5-4) are from different environments as the peak temperatures and the respective partial pressures were found to be different. The lower temperature appearance of F^+ (380-410 K) could come from the electrolyte and the higher temperature peaks, in the range of 650-790K, could possibly be the result of Si-F bond breakage.

It is difficult to propose a mechanism for the desorption of F^+. Further work is needed to study the origin of F^+ species. One possible way suggested is to produce PS from an electrolyte with F isotopically-substituted HF and analyse the F^+ ions emitted. It is discussed in Chapter 6 under the heading "Proposed Future Work"

5.9 Ageing Process with porous silicon

The investigation into the ageing process was carried out with PS prepared from 40% HF electrolyte. The changes were observed during the period from day 1 to 8 months. Table 5-10 summarises the observations from FTIR spectra, assignments of the peaks and the references used for their interpretations.

5.9.1 Region 4000-2000 cm^{-1}

The characteristic triple peak for $Si-H_x$ at~2100 cm^{-1} broadens with storage time and the peak at 2140 cm^{-1} ($-SiH_3$ group) gradually disappears (Figure 4-40). This supports the proposed mechanism, involving hydrolysis of $-SiH_3$ species, to produce silane (Canham 1994, Lampert et al. 1986, William et.al 1983). The appearance of two extra peaks at 2257 and 2201 cm^{-1} and the increase in the intensity of peak at 2257 cm^{-1} with time (Figures 4-39, 4-40) suggests that more than one oxygen atom per one Si atom is back-bonded to $Si-H_x$ during the oxidation process. When one O atom forms a bond with a Si-H configuration, the two Si-Si backbonds that remain are considered to be less stable than Si-Si bonds in bulk Si. This is due to the difference in bond length between Si-O-Si and this effect was due to more electronegative O atom. The higher electronegativity of the oxygen atom modifies the electron density around Si atom. This causes the infrared vibrations to be shifted to higher wave numbers (Kato et. al. 1988).

Another triple set of peaks at 2957, 2920 and 2857 cm^{-1} was observed to develop with time. These are interpreted as carbon based, Si-CH_3 species. C-based contamination is not avoidable in the laboratory environment where volatile organic reagents are kept. The "sponge-like" PS structure with very large surface area is very efficient in absorbing these vapours. The development of small peaks at 1463 and 1515 cm^{-1} are also interpreted as Si-CH_3 vibrations (Borghesi et al.1993; Lucovski 1979). Two more peaks at 2365, 2344 cm^{-1} were found to develop with time (Figure 4-44) and are interpreted as CO_2 adsorption (Borghesi et. al.1993). Not surprisingly, moisture adsorption was very prominent. Gradual development of a broad peak in the region at 3400 cm^{-1} region was observed (Pliskin, 1977). This was interpreted as SiO-H vibrations. The broadness has been reported to have arisen from hydrogen bonding between the OH groups.

5.9.2 The Region 2000-400 cm^{-1}

It is very difficult to assign peaks in this region as Si-F_x and Si-H_x IR vibrations occur in this region. The peak at 910 cm^{-1} was assigned to a SiH_2 vibration in the literature (Ogata et al. 1995). It was observed from Figure 4-38 that there is a decrease in the intensity up to 8 days old sample and the intensity of this peak stayed constant after that. It is thought that this peak comes from a combined vibration of Si-F_x and Si-H_x groups. The decrease in intensity was interpreted as loss of Si-F_x oscillators as these species are known to hydrolyse with moisture (Kato et al.1988, Grundner 1991). This decrease in intensity was found to be similar to the peak at 818 cm^{-1} (Figure 4-38) which also was interpreted as due to Si-F_x vibrations.

A new peak at 878 cm^{-1} was observed to develop with time and was found to shift to 883 cm^{-1} (Figure 4-41). This was interpreted as the overtones of Si-O-Si vibrations. The shift was interpreted as further bonding of more electronegative oxygen atoms. The intensity of the peak at 455 cm^{-1} was also found to increase quite considerably with time. This peak was assigned to cyclic SiO_4 units (Beckman 1965).

Remarkable change with the double peak at 668/626 cm^{-1} was observed with time. The peak at 668 cm^{-1} completely disappeared after about 3 months (Figure 4-42). Only a single characteristic peak of Si-Si phonon vibrations was observed. It is suggested that

this could be due to the disappearance of a $-SiH_3$ peak. This work assigned, from the evidence of heating experiments, the peak at 668 cm^{-1} as arising from the SiH_3 group.

TABLE 5- 10 FTIR peak assignments for "ageing" PS from electrolyte A

WaveNum..	Assignments	Ageing details	References
3458	SiO-H asymm.stretch	Starts to show after 29 days as a single peak; by 124 days double peak ; a broad single peak at ~3400cm^{-1} after this time	Pliskin W.A.1977
3299	H-OH-(Moisture)		
2957	Due to C-H_3 asymm.	Distinct triplet; siginficant with time	Borghesi, A. et. al. 1993 Feng, Z. C. et. al., 1994
2920	Due to C-H_3 symm.		
2857	Due to C-H_2 symm.		
2365	CO_2 absorption		Borghasi.A et.al. 1993
2344	CO_2 absorption		
2257	O_2Si-H stretch	~10days and increase in intensity with oxide growth	Ogata, Y.et. al. 1995 Kato, Y. et. al. 1988
2201	OSi-H	Appears but stays without any change up to 8 months	
2140	H_2Si-H stretch	This peak gradually getting shallower ~29days	Ogata, Y.et. al. 1995 Beckman, K.H. 1965
2116	HSi-H stretch	Stable peak but shows decrease in intensity by 8 months. The triplet region was observed to be wider with ageing	
2110	SiSi-H stretch	Peak gradually getting shallower by ~54 days (~3 months)	
1463	Si-CH_3 ssymm. stretch	Both peaks appear with samples kept for 4 months over. Definite time period cannot be defined	Borghesi, A. et. al. 1993 Lucovsky, 1979
1515	Si-CH_2 asymm. stretch		
1208-1058	Si-O-Si asymm.Stretch	Peak at 1045cm^{-1} was observed in the beginning, it intensifies with time and covers larger region with time	Pliskin, W.A., 1977
963	Si-O weak vibration	Very small increase was observed with 8 months old sample	Borghesi, A. et. al., 1993
910	Si-H_x bending or/and Si-F_x stretch	Gradual decrease till 19days constant after that.	Author's interpretation
878→883	O-Si stretch & H-OSi bend	Was not observed in the beginning; appeared ~8days and peak intensity increased considerably with time	Author's interpretation
818	Si-Fx symmetric vibration	Disappeared by 14days; possible hydrolysis by moisture	Author's interpretation
802	Si-O bending	Very weak overtone; seen in 8 months old sample	Borghesi, A. et al. 1993
668	H_2Si-H Bending	Disappeared by 119 days; a sharp small peak remained. Si-Si Phonon vibration	Ogata et al. 1995 J.R.Ferraro et al. 1989
626	Si-H wagging	Observed up to 8 months but decreases slightly in peak intensity	Ogata et al 1995
455	Si-O Rocking	Appeared ~29days; very intense peak grows with ageing; due to cyclic SiO4 units	Beckman, K.H. 1965

Chapter 6 Conclusions

This work was undertaken to explore the nature of adsorbed chemical species on the pore surface during the formation of porous silicon and its storage procedures. The conclusions of this work would shed some light onto some previously unexplained behaviour of applications using porous silicon as the starting material.

6.1 Summary of This Work

a) The PS used in this work was produced from p^- (50-100 Ω cm) FZ silicon wafers. These wafers were back implanted with $1x10^{15}$ boron cm^{-2} at 40 KeV and were annealed under N_2 with 1% O_2 at 1050°C for 30 minutes. FZ wafers have less oxygen content than CZ wafers and are better for FTIR work. The FTIR spectrum of a blank CZ wafer shows a sharp peak at 1107 cm^{-1}, and is due to Si-O vibrations.

b) Three most commonly used electrolytes were chosen to prepare porous silicon

i. Aquous 40% HF (Electrolyte A)

ii. "20% ethanoic HF" – 1:1 ratio of C_2H_5OH and 40% HF (Electrolyte B)

iii. Aquous 40% HF followed by 4 hours of chemical etching (Electrolyte C)

All PS samples were anodised for 2 minutes with current density 2mA cm^{-2} and spin dried with no rinse in deionised water.

c) The TPD system and the Heating Unit were developed in the Middlesex University Microelectronics centre. The development and characterisation of the system are as important as the results obtained from them for this work. Even though the vacuum system can be purchased it was decided to build on site due to the economic factors. The heating unit was designed and built for this work as no commercially available system is suited for this purpose. It was discussed in Chapter 3

d) The storage facilities were investigated with a blue wafer box , a white wafer box with a screwtop, a vacuum desiccator (air was displaced by Ar and it was evacuated to 10^{-4} torr pressure) and a white wafer box kept in the vacuum desiccator. All were tested upto 240 days (~ 8 months). The chosen method was to place the as-anodised wafer in a white wafer box and keep it in the vacuum desiccattor.

e) TPD analyses were carried out by heating the samples linearly at a heating rate 1.5 Ks^{-1}. The starting base pressure of the TPD vacuum chamber was ~ $\leq 10^{-8}$ mbar

6.2 Conclusions from the Results

a) The gaseous species in the vacuum chamber with and without PS were scanned through the range 1-100 amu using the analogue mode facility available with the quadrupole mass spectrometer. Increase in base pressure with the PS sample indicates that gaseous species were given out during the pumping process. Apart from the components of air (O^+, N_2^+ or/and CO^+, O_2^+ and CO_2^+) the most significant increase was found to be F species. There was no increase in the H_2^+, while the possible origin of F^+ may be from HF_2^- ions found in HF based electrolytes.

b) The main species and their fragmentation products were identified when the PS was heated in the TPD vacuum chamber using the analogue mode facility of the QMS. They were hydrogen, silane and its fragmentation products, Si-F_x species and H_x-F_y species. The PS samples prepared from Electrolytes A, B and C were compared. These results were complemented by FTIR results. These results were obtained with PS samples heated to different temperatures with 50K intervals.

c) Hydrogen evolution from PS

The TPD spectra of PS obtained from all three electrolytes show two "humps" which have arisen from two types of detectable hydrogen environments. The temperature difference between the two peaks were similar (~ 100K). This suggests that there is no difference in the way hydrogen desorption occurs in the PS prepared from the three electrolytes.

The evidence from the FTIR work compared with the TPD peak temperatures of the H_2 desorption spectra suggest that the lower temperature TPD peak corresponds to hydrogen from Si-H. The sequence of the desorbing order for Si-Hx is as follows:

$$-SiH_3 > -SiH > SiH_2$$

It is important to mention here that many theoretical and experimental studies have been published on the desorption of hydrogen from c-Si with specific crystal planes and the mechanism of the desorption processes from these specific surfaces still remain controversial. None of the studies so far is conclusive. It is practically impossible to apply these data to PS as the pores have "multi-crystal planes". The pore structures are dependent on many experimental factors such as the resistivity of c-Si, anodising conditions as well as the nature of the electrolytes. These dependencies were reviewed indetail in Chapter 2. P^- c-Si used in this work is known to produce isotropic micro-pores (multidirectional pore growth)

Schematics of possible Si-H features on the pore surfaces and the suggested desorption processes were given in Chapter 5 for Discussions. They are mainly based on Si-H and $Si-H_2$ structures.

d) Silane and its fragmentation products

Silane and its fragmentation products (SiH_4^+, SiH_3^+, SiH_2^+,SiH^+ and Si^+)were observed at 575K. This was complemented by the disappearence of the FTIR peak at 2140 cm^{-1} (570K ±10K), due to $-H_2Si-H$ group. This peak is a part of a triple peak assigned to $Si-H_x$ vibration observed in the FTIR spectrum of as-anodised PS

The proposed mechanism is as follows:

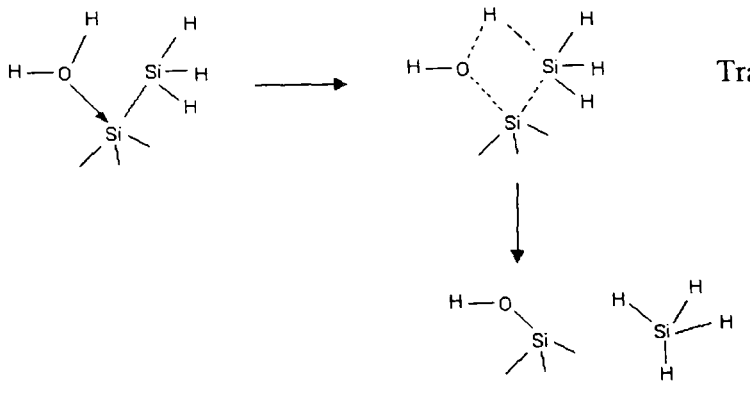

$$\equiv Si\text{-}SiH_3 + H_2O \rightarrow SiH_4 + \equiv Si\text{-}OH$$

The nucleophilic –OH group of water, H-OH, attaches itself to a Si atom of the pore wall surface. The H from the H-OH then attaches itself to Si of the $-SiH_3$ group and silane is released.

e) Fluorosilyl Species ($Si\text{-}F_x$)

Desorption of fluorine related species was investigated by TPD method as FTIR spectroscopy was not very useful. This is because Si-F bonds produce vibrations of lower intensty than those from Si-H bond vibrations. Unlike hydrogen and silane desorption, $Si\text{-}F_x$ desorption was found to be sensitive to the nature of the electrolyte. Three distinct peaks were observed at 420K, 590-630K and 970K with PS produced from Electrolyte A. With Electrolyte B only two peaks at 625-650K and 850K were observed. A PS sample produced from Electrolyte C was similar to PS produced from Electrolyte A except that the high tempeature peak was at a lower temperature of 890K.

The lower temperature peaks were explained in terms of zeolite structures which are characterised by the presence of interconnectiong channels. The molcules/ions that are present in electrolytes, such as H_2SiF_6, SiF_4 and SiF_2 (presence of this species is controversial at present), are held by van der Waals forces and/or electrostatic forces and are desorbed at lower temperatures.

The partial pressures of SiF_2^{++}, SiF_2^{+} and SiF^{+} were found to be higher than that from SiF_3^{+}. This means that these species are not only produced from SiF_4 and they must have been present in the HF based electrolytes as separate entities. These species were not detected together with the higher temperature SiF_3^{+} peak.

The higher temperature TPD peak of SiF_3^{+} was interpreted as the result of migration of F atoms followed by a $Si\text{-}SiF_3$ bond breakage. This is supported by the dissociation enegies found in the literature for Si-F and Si-Si which are 129.3 kcal mol^{-1} and 42.2 kcal mol^{-1} respectively.

The measured partial pressures of these species were compared to the partial pressures of the fragmentation products of SiF_4 from the literature. The ratios of the partial pressures of these fragmentation products were similar to those of literature values except for the F^{+} species. It should be 100 times smaller than the base peak SiF_3^{+}but it is found to be 10 times higher. This means that F^{+} must have more than one origin. It is suggested that it could come from the electrolyte at lower temperature and from Si-F at higher temperature.

f) Fluorohydride species (H_x-F_y)

Four distinct hydrofluoride species were observed with the TPD investigation. They were, HF^+, $H_2F_2^+$, $(H_3O)F^+/F_2^+$ and HF_2^+ at m/z values of 20, 40, 38 and 39 respectively. Aqueous HF contains $[HF_2^-]$, HF, $[(H_3O)^+F^-]$ and associated HF molecules such as $(HF)_2$ and were interpreted as the origin of the desorbed species

g) Ageing Process

This investigation was carried out from day 1 to 8 months period. Table 5-10 summarises the changes observed with PS sample. $-CH_3$ and $-CH_2$ related vibrations were observed with ~4 months old sample. Si-F_x related vibrations at 818 cm^{-1} gradually disappeared after 14 days. This was interpreted as the hydrolysis of the Si-F group.

Moisture oxidation was observed from the beginning at 1045 cm^{-1}; this intensified and broadened with time to 1208-1058 cm^{-1}. Also, a broad peak due to SiO-H (silanol) started to develop with a 29 days old sample. The effect of moisture was observed with the characteristic triple peak assigned to Si-H_x group. Two extra peaks at 2257 and 2201 cm^{-1} due to O_2Si-H and OSi-H started to develop with a 10 days old sample.

h) The best way to store PS samples is in screw-top white boxes and store the boxes in vacuum desiccator flushed with dry argon gas. This way most of the air components are removed and minimum chance to adsorb/absorb any "foreign species".

6.3 Proposed Future Work

The future work needs to be concentrated in three main areas

1) The modification of the TPD system
2) Measurement of Temperature
3) The anodisation procedure
4) using isotopic reagents

6.3.1 The Modification of TPD System

The system in Figure 3-1 has only one vacuum chamber and it is unavoidable that breaking the vacuum to the environment occurs every time a sample is placed in the chamber. Once the sample is placed into the vacuum chamber, it takes about an hour to pump the system to ~10^{-6} mbar pressure. A load-lock system with two chambers commonly used to achieve ultra-high vacuum would be ideal for this type of work. This means that the second chamber can be used to transfer the sample and transported to the high vacuum chamber without breaking the vacuum. Porous silicon has a very high surface area and exposure to air must be kept to a minimum.

The heating experiments with FTIR were carried out by heating the sample to a known temperature and then taking it out from the vacuum chamber to do the FTIR scanning. This was repeated with a fresh sample from a single PS wafer for each temperature. The results obtained by this method of scanning can be interpreted qualitatively. The TPD system can be improved by having a FTIR and XPS spectroscopic systems in situ so that changes on the surface of the PS during heating can be monitered. This means that from a single PS sample all the changes during heating can be investigated. This allows desorbing kinetics of various species to be investigated.

6.3.2 Anodisation Process

The present investigation was carried out using p^- high resistive wafers in HF-based electrolytes for 2 minutes. The origin of hydrogen is not well understood. Is it from the aqueous media or is HF responsible for the hydrogen liberation. Many papers have been published on the mechanism of pore formation. One possiblility is the use of isotopic HF where $^1H^{19}F$ (nomal HF) can be replaced with $^2H^{19}F$, which is an isotopic HF. There is a difference of 1 amu (atomic mass unit) difference in the atomic weight of hydrogen and isotopic hydrogen; these species can be analysed with QMS as the detector in the TPD system. This will help to identify H_xF_y species as well. For example, $(H_3O)F^+$ species can be distinguished from F_2^+ species where they both normally have amu value of 38. If the mechanism proposed in the literature for the formation of $(H_3O)F^+$ is as follows then this species with $^2H^{19}F$ will give a amu value of 39.

$H_2O + {}^1H^{19}F \rightarrow [H_3OF]$ $[H_3OF]$ has amu 38

$H_2O + {}^2H^{19}F \rightarrow [{}^1H_2{}^2HOF]$ $[{}^1H_2{}^2HOF]$ has amu 39

The above is an example to show isotopic experimental technique is very useful in understanding mechanistic aspecte of reaction processes.

This work has shed some light on the processes that go on at the pore surfaces from the time of anodisation to the time of device fabrications. Also, this work hopes to increase the awareness of the importance of careful interpretation of the material properties of porous silicon.

Chapter 7 References

Anderson, R.C., Muller, R.S. and Tobias, C.W, "Chemical Surface Modification of Porous Silicon", *J. Electrochem. Soc.*, 140, 1993, 1393 - 96

Ibid, "Investigation of Porous Silicon Sensing for Vapour Sensing", *J. Electrochem. Soc.*, A21 - A23, 1990, 835 - 39

Atkins, P.W., *Physical Chemistry,* Oxford University Press, 1990

Barla, K., Bomchil, G., Pfister, J.C. and Freund, A., "Determination of Lattice Parameter and Elastic properties of Porous Silicon by X- ray diffraction", *J. Cryst. Growth*, 68, 1984, 727-32

Barla, K., Bomchil, G., Herino, R., Monroy, A. and Gris, Y., "Characteristics of SOI CMOS Circuits Made in $N/N^{+}/N$ oxidised Porous Silicon Structures", *Elect. Lett.* 22, 1986, 1291 - 93

Barrao, C., Faglia, G., Comini, E., Sberveglieri, G., Taroni, A., La Ferrara, V., Quercia, L.and Di Francia, G., "A Novel Porous Silicon Sensor for Detection of sub-ppm NO_2 Concentrations", *Sensors and Actutors B-Chemical,* 77, 2001, 62-66

Barret, S., Gaspard, F., Herino, R. Ligeon, M. and Ronga. I., "Porous Silicon As a Material in Microsensor Technology", *Sensors and Actutors*, A33, 1992, 19-24

Beale, M.I.J., Benjamin, J.D., Uren, J.D., Chew, N.G. and Cullis, A.G., "An Experimental and Theoretical Study of the Formation and Microstructure of Porous Silicon", *J. of Cryst.Growth* , 73, 1985, 622 - 36

Beale, M.I.J., Chew, N.G., Cullis, A.G., Garson, D.B. Hardeman, R.W., Robins, D.J. and Young, I.M., "A Study of Silicon MBE on Porous Silicon Substrates", *J. Vac. Sci. Technol.*, B3, 1985, 732 - 35

Beale, M.I.J., Chew, N.G., Uren, M.J., Cullis, A.G. and Benjamin,J.D., "Microstructure and Formation Mechanism of Porous Silicon", *Appl. Phys. Lett.* 46, 1985, 86-88

Beale, M.I.J., Cox, T.I., Canham, L.T. and Brumhead, D., "The Depth Dependence of Photoluminescence and Electrolytic Electroluminescence in Porous Silicon Films", *Mat. Res.Soc.Symp. Proc.*, 283, 1993, 377-82

Beckmann, K.H., "Investigation of the Chemical Properties of Stain Films on Silicon by Means of IR Spectroscopy", *Surf. Sci.* 3, 1965, 314 - 32

Bengtsson, M., Ekstrom, S., Marko-Varga, G.and Laurell, T., "Improved Performance in Silicon Enzyme Micreoreactors Obtained by Homogeneous Porous Silicon Carrier Matrix", *Talanta*, 56(2), 2002, 341-353

Benjamin, J.D., Keen, J.M., Cullis, A.G., Innes, I. And Chew, N.G., "Large Area Uniform Silicon-on-Insulator Using a Buried Layer of Oxidised Porous Silicon", Appl.Phys.Lett., 49,1986,716-18

Bi-Cai, Pan., PhD Thesis, Univ. of Sci. and Technol. of China, 1993 (cited in Li. Quing-Shan, 1995)

Billat, S. , Bsiesy, A., Gaspard, F., Herino, R., Ligeon, M., Muller, P. , Romeslain, R. and Vial, J.C., "Electroluminescent Properties of Porous Silicon Films under Electrochemical Oxidation", *Mat.Res.Soc.Symp.Proc.*, 256, 1992, 215 -18

Bomchil, G., Halimaoui, A. and Herino, R., Porous Silicon: The Material and its Applications to SOI Technologies", *Microelect. Eng.*, 8, 1988, 293 - 310

Ibid, "Porous Silicon: The Material and its Applications in Silicon-on-Insulator Technologies", *Appl. Surf. Sci.*, 41/42, 1989, 604 - 13

Bondarenko, V.P. and Dorofeev, A.M., "Why Porous Silicon for SOI", *Physical and Technical Problems of SOI Strucures and Devices*, (eds. Colinge, J.P. , Lysemko, V.S. and Nazarov, A.I.N.), Kluwer Academic Publishers, 1995, 15 - 26

Bondarenko, V.P. Bogatirev, Y.V., Dolgyi, L.N., Dorofeev, A.M., Panfilenko, A.K. Shvedov, S.V., Troyanova, G.N., Vorozov, N.N. and Yakovtceva, V.A., "1.2μm CMOS/SOI on Porous Silicon, *Ibid*, 275 - 80

Borghesi, A, Sasslla, A., Pivac, B., Pavesi,L., "Characterisation of Porous Silicon in Homogeneities by High Spatial Resolution Infrared Spectroscopy", *Solid State Comm.*, 87(1), 1993, 1-4

Brandt, M.S., Fuchs, H.D., Stutzmann, M., Weber, J. and Cardona, M, "The Origin of Visible Luminescence from Porous Silicon: A New Interpretation", *Solid State Comm.*, 81, 1992, 307 - 12

Bsiesy, A., Nicolau, A., Ermolieff, A., Muller, F. and Gaspard, F., "Electroluminescence from n+ -type Porous Silicon Contacted with Layer-by-layer Deposited Polyaniline", *Thin Solid Films,* 255, 1995, 43-48

Burkhardt, P.J.and Poponisk, M.R., "Porous Silicon Dioxide Moisture Sensor and Method for Manufacturing of a Moisture Sensor", *United State Patent.* 4,057,827, 1977

Canham, L.T., "Silicon Quantum Wire Array fabrication by Electrochemical and Chemical Dissolution of Wafers", *Appl. Phys. Lett.*, 57, 1990, 1046 - 48

Canham, L.T., Houlton, M.R., Leong, W.Y., Pi ckering, C. and Keen, J.M., "Atmospheric Impregnation of Porous Silicon at Room Temperature", *J. Appl. Phys.* 70, 1991, 422 -431

Canham, L.t., Leong, W.Y., Beale, M.I.J., Cox, T.I. and Taylor, L., "Efficient Visible Electroluminescence from Highly Porous Silicon Under Cathodic Bias", *Appl. Phys. Lett.*, 61, 1992, 2563-65

Canham, L.T., Saunders, S.J., Healey, P.B., Keen,A.M. and Cox, T.I., "Rapid Chemography of Porous Silicon Undergoing Hydrolysis", *Adv.Mater.*, 1994, 6(11), 865-68

Canham, L.T, Reeves, C.L., Wallis, D.J., Newey, J.P., Houlton, Sapsford, G.J., Godfrey, R.E., Loni, L., Simons, A.J., Cox, T.I. and Ward, C.L. "Silicon as an active Biomaterial", *Mat.Res.Soc.Symp.Proc.*, 452, 1997, 579-589

Canham, L.T., "Pore Type, Shape, Size, Volume, and Surface Area in Porous Silicon", *Properties of Porous Silicon*, (ed. Leigh Canham, DERA, Malvern), UK., published by INSPEC, IEE, 1998, 183-88

Canham, L.T. and Aston, R., "Will a Chip Everyday Keep the Doctor Away?" *Physics World,* July 2001, 27-31

Chabal, Y.J. and Raghavachari, K.,"Surface Infrared Study of Si(100)-(2x1)H, *Phys.Rev.Lett.*,53(3), 1984, 282-85

Chabal, Y.J., "Infrared Study of the Chemisorption of Hydrorogen and Water on Vicinal (100) 2 x 1 Surface", *J. Vac. Sci. Technol.*, A3, 1985, 1448 - 51

Chabal, Y.J., Higashi, G.S., Raghavachari, K. and Burrows, V.A., "Infrared Spectroscopy of Si (111) and Si (100) Surfaces After HF Treatment: Hydrogen Termination and Surface Morphology", *J. Vac. Sci. Technol.*, A7, 1989, 2104 - 09

Chan, S., Li, Y., Rothberg, L.J., Miller, B.L.and Fauchet, P.M., "Nanoscale Silicon Microcavities for Biosensing", *Materials Science & Engineering C-Biomedic and Supramolecular Systems,* 15(1-2), 2001, 277-82

Cheng, C.C. and Yates,Jr., J.T., "H-induced Surface Restrucuring on Si(100): Formation of Higher Hydrides", *Physics Review B*, 43(5), 1991, 4041-45

Ciraci, S. And Batra, Inder P., "Theory of Transition from the Dihydride to the Monohydride Phase on the Si(100) Surface", *Surf. Science*, 178, 1986, 80-89

Comello, V., "Ultrahigh Vacuum CVD's "Secret Reviewed", *Semicond. Intnl.*, Dec.1990, 18

Cottrell, T.R., Benziger, J.B., Yee, J.C., Chun, J.K.M. and Bocarsly, A.B., "Organic-Inorganic Junctions Formed on Porous Silicon: Isolation of a Surface Configuration Primary to the Luminescence Mechanism", *Mat.Res.Soc.Symp. Proc.*, 283, 1993, 411-16

Cullis, A.G. and Canham, L.T., "Visible Light Emission due to Quantum Size effects in Highly Porous Crystalline Silicon", *Nature,* 1991, 335-38

Cullis, A.G., " Structure and Crystallinity of Porous Silicon", *Properties of Porous Silicon*, (ed. Leigh Canham, DERA, Malvern), UK., published by INSPEC, IEE, 1998, 99-105

Cullis, A.G., Canham, L.T. and Calcott, P.D.J., "The Structural and Luminescence Properties of Porous Silicon", *J.Appl.Phys.*, 82, 1997, 909-55

Csepregi, L., Kennedy, E.F., Gallegher, T.J., Mayer, J. W. and Sigmon, T. W., "Reordering of amorphous Si: Implanted with ^{31}P, ^{75}As, ^{19}B Ions", *J. Applied Phys.*, 48, 1984, 4234-4240

D'Avitaya, F.A., Barla, K., Herino, R.and Bomchil, G., "Improvement of Silicon Epitaxy on Porous Silicon Substrates", *1st International Symposium on MBE*, Toronto, Canada, 1985, Abs. no. 144

D'Evelyn, M.P., Yang, Y.L. and Sutcu, L.F., "π-bonded Dimers, Preferential Pairing, and First-order Desorption Kinetics of hydrogen on Si(100)-(2x1)", *J. Chem. Phys.*, 96(1), 1992, 852-55

de Jong, A.M.,and Niemantsverdriet, J.W., "Thermal Desorption Analysis: Comparative Test of Ten Commonly Applied Procedures" *Surf. Science*, 233, 1990, 355-65

Diawara,, J.F., Yelon A.C., Petrova-Koch, V. And Nikolov,A., "Temperature Dependence of Stresses and H Desorption in Porous Silicon", *Mat.Res.Soc.Symp.Proc.*, 358, 1995, 555-58

Dolino, G. and Bellet, D., "Variations in the Lattice Parameter of Porous Silicon Produced by Wetting and Vapour Adsorption", *Thin Solid Films*, 255, 1995, 132 - 34

Drost, A., Steiner, P., Moser, H. and Lang,W. "Thermal Conductivity of Porous Silicon", *Sensors and Materials*, 7, 1995, 111 – 20

Dudly, F.B., "Negative Ion Mass Spectra of Various Fluorine containing Molecules", *Organic Mass Spectrometry*, 5, 1971, 953-57

Dubin, V.M., "Formation Mechanismof Porous Siicon Layers Obtained by Anodisation of Monocrystalline n - type Silicon in HF Solution", *Surf. Science*, 274, 1992, 82 92

Earwaker, L.G., Farr, J.P.G., Alexander, I., Sturland, I. and Keen, J.M., "Determination of Fluorine Distribution in Porous Silicon Using Nuclear Reaction, XPS and Auger Analysis", *Nucl. Inst. Meth. in Phys. Res.*, 218, 1983, 481 - 84

Earwaker, L.G., Farr, J.P.G., Grzeszezyk, P.E. and Sturland, I., "Analysis of PS", *Ibid*, B9, 1985, 317 -20

Ehara, K., Unno, H. and Muramoto, S., "1.5μm FIPOS/CMOS VLSI Process with Low Wafer Warpage and Silicon Deposit - Defect - Free", *Electrochem. Soc.* Ext. Abs, 85, 1985, 457

Falconar, J.L. and Schwarz, J.A., "Temperature- Programmed Desorption and Reaction: Applications to Supported Catalysts" *Catal. Rev. Sci. Eng.*, 25, 1983, 141 - 227

Feng, Z.C., Wee, A.T.S. and Tan, K.L., "Surface and Optical Analysis of Porous Silicon Membranes", *J.Phys. D: Appl. Phys.*, 27, 1994, 1968 - 75

Ferraro, J.R., Krishnan, K., *Practical Fourier Transform Infrared Spectroscopy*, Academic Press, London, 1990

Fischer, R., *Topics in Applied Physics: Amorphous Semiconductors*, eds. Brodsky, M.H., Springer-Verlag N.Y., 1979,159

Flowers, C.F., Jonathan, N.B.H., Liu, Y. And Morris,A., "temperature Programmed Desorption of Molecular Hydrogen from a Si(100)-2x1 Surface : Theory and Experiment", *J.Chem.Phys.*,99(9), 1993, 7038-48.

Futagi, T., Matsumoto, T., Ohita, Y. and Mura, H.M., "Visible Electroluminescence from PN Junction type μc-SiC/Porous Si/c-Si Structures", *Mat. Res. Soc. Symp. Proc.* 283, 1993, 389-95

Gmelin Handbook of Inorganic and Organometallic Chemistry, 8th Edition,B7, eds Pietach, E.H.C., Kotowshi, A. and Goehring, M.B., Springer-Verlag, 1992

Gonchond, J.P., Halimaoui, J.P. and Gura, K.O., "High Resolution SEM Study of Porous Silicon", *Microscopy of Semiconducting Materials*, V117 (eds. Cullis, A.G. and Long, N.J.), 1991, 235 -38

Goodes, S.R., Jenkins, T.E., Beales, M.J., Benjamin, J.D. and Pickering, C., "The Characterisation of Porous Silicon by Raman Spectroscopy", *Semicond. Sci. Technol.*, 3, 1988, 483 - 87

Graf, D., Grundner, M. and Schultz, R., "Reaction of water with HF Treated Si (111) and (100) Surfaces", *J. Vac. Sci. Technol.*, A7, 1989, 808 -13

Greenwood, N.N., and Earnshaw, A., *Chemistry of the Elements*, Pergammon Press, Oxford, 1990

Gregg, S.J. and Sing, K.S.W., *Adsorption, Surface Area and Porosity,* Academic Press, London 1982

Gregora, I., Champagnon, B. and Halimaoui, A., "Raman Investigation of Light Emitting Silicon Layers: Estimate of Characteristic Crystallite Dimensions", *J.Appl. Phys.*, 75(6) 1994, 3034-39

Grosman, A., Ortega, C., Siejka, J. and Chamarro, M., "A Quantitative Study of Impurities in Photoluminescent and Non-photoluminescent Porous Silicon layers", *J. of Appl. Phys.*, 74, 1993, 1992-96

Grundner, M. and Schultz, R., " Deposition and Growth Limits of Microelectronics", *AIP Conference Proceedings*, No.167, American Institute of Physics, N.Y., 1988, 329 - 32

Grundner, M., Graf, D. Hahn, P.O. and Schrigg, A., "Wet Chemical Treatment of Silicon Surfaces: Chemical Composition and Morphology", *Solid St. Technol.*, Feb. 1991, 69-71

Gupta, P., Colvin, V.L., Brand, J.L. and George, S.M., " Desorption Kinetics of Hydrogen from Silicon Surfaces Using Transmission FTIR", *AIP Conference Proceedings*, No. 167, American Institute of Physics, 1988, 52 -59

Gupta, P., Colvin, V.L. and George, S.M., "Hydrogen Desorption Kinetics from Monohydride and Dihydride Species on Silicon Surfaces", *Physics Review B*, 37, 1988, 8234-43

Halimaoui, A., Oules, C., Bomchil, G, Bsiesy, A., Gaspard, F., Herino, R., Ligeon, M. and Muller,F. "Electroluminescence in the Visible Range During Anodic Oxidation of Porous Silicon Films", *Appl. Phys. Lett.*.59,1991, 304-06

Hammers, R.J., Avouris,Ph. And Bozso, F., "A Scanning Tunneling Microscopy Study of the reaction of Si(001)-(2x1) with Ammonia", *J.Vac.Sci.Technol.*, A6(2), 1988, 508-11

Harderman, R.W., Beale, M.I.J., Gasson, D.B., Keen, J.M. Pickering, C. and Robbins, D.J., "Porous Silicon Films: Preparation and Examination with Surface and optical Methods", *Surf. Science*, 152/153, 1985, 1051 - 62

Harper, J. and Sailor, M.J., "Detection of Nitric Oxide and Nitrogen Dioxide with Photoluminescent Porous Silicon", *Analytical Chemistry*, 68(21), 1996, 3713 17

Herino, R., Perio, A., Barla, K. and Bomchil, G., "Microstructure of Porous Silicon and Its Evolution with Temperatures", *Mat. Lett.*, 2, 1984, 519 - 23

Herino, R., Bomchil, G., Barla, K., Bertrand, C. and Ginoux, J.L., " Porosity and Pore Size Distributions of Porous Silicon layers", *J. Electrochem. Soc.*, 134, 1987, 1994-00

Herino, R., "Pore Size distribution in Porous Silicon", *Properties of Porous Silicon*, (ed. Leigh Canham, DERA, Malvern), UK., published by INSPEC, IEE, 1998, 89-96

Hirose, M., Yasaka, T., Takakura, M. and Miyazaki, S., "Initial Oxidation of Chemically Cleaned Silicon Surfaces", *Solid St. Technol.*, December 1991, 43 -48

Holmstrom, R.P. and Chin, J.Y., "Complete Dielectric Isolation by Highly Selective and Self Stopping Formation of Oxidised Porous Silicon", *Appl. Phys. Lett.*, 42, 1983, 386 - 88

Hory, M.A., Herino, R., Ligeon,M., Muller, F., gaspard, F., Mihalcescu, I. And Vial, J.C., "Fourier transform IR Monitoring of Porous Silicon Passivation During Post-treatments such as anodic oxidation and Contact with Organic Solvents", *Thin Solid films*, 255, 1995, 200-203

Imai, K. and Yoriume, Y., "Application of IPOS Technique to MOS IC's", *Jap.J.of Appl. Phys.*, 18, 1979, 281 - 85

Imai, K. "A New Dielectric Isolation Method Using Porous Silicon", *Solid St. Electron.*, 24, 1981, 159 - 64

Imai, K. and Unno, H., " FIPOS (Full Isolation by Porous Oxidised Silicon) Technolocy and Its Application to LSI's", *IEEE Trans. Elect. Devices*, ED - 31, 1984, 297 - 302

Ito, T., Kato, Y. and Hiraki, A., "Hydrogen Bonding on to Microcrystalline Surfaces within Anodised Porous Silicon Crystals Studied by IR Spectroscopy", *The Structure of Surfaces II,* (eds. van der Veen, J.F. and Van Hove, M.A.), Springer, 1988, 378 - 83

Ito, T., Yamana, A., Hiraki, A. and Satou, M., " Silicidation of Porous Silicon and its Application for the Fabrication of a Buried Metal Layer", *Appl. Surf. Sci.*, 41, 1989, 301 - 05

Ito, T. and Hiraki, A., "Ageing Phenomena of Light Emitting Porous Silicon", *J. of Luminescence*, 57, 1993, 331- 39

Iyer, S.S. and Xie,Y.H., "Light Emission from Silicon", *Science,* 260, 1993, 40-46

Janz, G.J. and Mikawa, "Silanes: Vibrational Assignments and Frequency Correlations", 34(10), 1485-05

Jardin, C., Gruzza, B., Vazsonyi, F. and Gergely, G., "Interdisciplinary Surface Study on Porous Silicon (p-Si) - II . Cathodoluminescence(CL), Auger (AES), Electron Energy Loss (EELS) and Raman Spectroscopy of Different pSi Samples", *Vacuum* , 46, 1995, 497 - 99

Jeng, S.P., Ma, T.P., Canteri, R., Anderi, M.and Rubloff, G.W., Anomalous Diffusion of Fluorine in Silicon", *Appl.Phys.Lett.*, 61(11), 1992, 1310-12

Jin, J.Y., Min, N.K., Kang, C.G., Park, S.H., Hong, S.I., "Characteristic of Urea Sensor Based on Platinum Deposited Porous Silicon", *J.of the Korean Physical Society*", 39, 2001, S67-S69

Jung, K.H., Sihih, S., Hisieh, T.Y., Campbell, J.C., Kwong, D.L., George,T., Lin, T.L., Liu, H.Y., Zavada, J. and Novak, S. "Structure and Composition of Luminescent Laterally Anodised Porous Si", *Mat. Res. Soc. Symp. Proc.* 256, 1992, 31-34

Kalkhoran, N.M., Namavar, F. and Maruska, H.P., *Ibid,* 256, 1992, 89-94

Kato, Y., Ito, T. and Hiraki, A., "Initial Oxidation Process of Anodised Porous Silicon with Hydrogen Atoms Chemisorbed on the Inner Surface", *Jap. J. of Appl. Phys.*, 27, 1988, L1406 - L1409

Ibid, "Low Temperature Oxidation of Crystalline Porous Silicon", *Appl. Surf. Science*, 41/42, 1989, 614 -18

King, D.A., "Thermal Desorption From Metal Surfaces: A Review" *Surf.Science*. 47, 1975, 384-402

Klumpp, A., Schaber, U., Kühl, K and Sandmaier, H., "Amorphous Silicon Carbide and its Application in Silicon Micromachining", *Sensors and Actuators*, A41 -42, 1994, 310 - 16

Koch, F., Petrova-Koch, V., Muschik, A. Nikolov, A. and Gavrilenko, V., "Some Perspectives on the Luminescence Mechanism via Surface-Confined States of Porous Si" *Mat. Res. Soc. Symp. Proc.*, 283, 1993, 197-202

Koshida, N. and Koyama, H., "Visible Electro- and Photoluminescence from Porous Silicon and Its Related Optoelectronic Properties", *Mat. Res. Soc. Symp. Proc.*, 256, 1992, 219 - 22

Ibid, "Efficient Visible Electroluminescence from Porous Silicon", *Appl. Phys. Lett.*, 60, 1992, 347-49

Koshida, N., Koyama, H., Ozaki, T., Araki, M., Oguro, T. and Mizuno,H., "Optoelectronic Effects in Porous Silicon Related to the Visible Luminescence Mechanism", *Mat. Res. Soc. Symp. Proc.* 358, 1995,695-700

Kozlowski, F and Lang, W., "Spatially resolved Raman Measurements on Electroluminescent Porous n-Silicon", *J.Appl.Phys.*, 72(11), 1992, 5401-5408

Kozlowski, F., Steiner, P. and Lang, W., "Micro Raman Investigations and a Structure Model for Electroluminescent Porous n-Silicon", *Porous Silicon* (eds. Feng, Z.C and Tsu, R.), World Scientific, Singapore, 1994, 149-171

Kozlowski, F., Steiner, P., Lang, W. and Sandmaier, H., "Light emitting diodes in Porous Silicon", *Sensors and Actuators A*, 43, 1994, 153-56

Krishnan, K., Stout, P.J., Watanabe,M., "Characterisation of Semiconductor Silicon Using Fourier Transform Infrared Spectrometry, *Practical Fourier Transform Infrared Spectroscopy*, eds. Ferraro, J.R., Krishnan, K., 1990. 285-349

Kux, A., Müller, F. and Koch, F., "Luminescence Activation of Porous Silicon by Post-Anodisation Treatment", *Mat. Res. Soc. Symp. Proc.*, 283, 1993, 311-315

Labunov, V., Bonderenko, V., Glinenko, L., Dorofeev, A . and Tabulina, L., "Heat Treatment Effect on Porous Silicon", *Thin Solid Films*, 137, 1986, 123 - 34

Labunov, V.A., Bondarenko, V.P., Borisenko, V.E. and Dorofeev, A.M., "High-Temperature Treatment of Porous Silicon", *Phys. Stat. Sol.*, 102, 1987, 193- 98

Lampert, I., Fuβstetter, H. and Jacob, M. "Evidence for SiH_4 Formation during the Reaction of water with a Silicon Surface", *J.of Electrochem.soc.*, 1986, 1472-74

Lang, W., Kühl, K. and Obermeier, E., "A Thin- Film Bolometer for Radiation Thermometry at Ambient Temperature", *Sensors and Actuators,* A21 -23, 1990, 473-77

Lang, W., Steiner, P. Kozlowski, F., "Porous Silicon Electroluminescent Devices", *J. of Luminescence,* 57, 1993, 341-49

Lang, W., Steiner, P., Richter, A., Marusczyk, K., Weimann, G. and Sandmaier, H., "Application of Porous Silicon as a Sacrificial Layer", *Sensors and Actuators* A43, 1994, 239 -42

Lang, W., Steiner, P. and Sandmaier, H., " Porous Silicon: A Novel Material for Microsystems", *Sensors and Actuators*, A51, 1995, 31 - 36

Lang, W., Steiner, P., Schaber, U. and Richter, A., "A Thin Film Bolometer Using Porous Silicon Technology", *Ibid*, A43, 1994, 185 - 87

Lehmann, V.,and Göscle, U., "Porous Silicon Formation: A Quantum Wire Effect", *Appl. Phys. Lett.*, 58, 1991, 856 – 58

Lévy - Clément, C., Lagoubi, A., Newmann-Spallanet, M., Rodot, M. and Tenne, R., "Efficiency and Stability Enhancement of n-Si Photoelectrodes in Aqueous Solution", *J.Electrochem. Soc.*, 138, 1991, L69 –70

Li, Quig-Shan and Fang Rong-chuan, "Formation and Optical Properties of Porous Silicon", *Porous Silicon,* (eds. Feng, Z.C and Tsu, R.) World Scientific, Singapore, 1995, 235-57

Lin, T.L. and Wang, K.L., "New Silicon - on - Insulator Technology Using a Two-step Oxidation Technique", *Appli. Phys. Lett.*, 49, 1986, 1104 - 06

Loni, A., Simons, A.J., Cox, T.I., Calcott, P.D.J. and Canham, L.T., "Electroluminescent Porous Silicon Device with an External Quantum Efficiency Greater than 0.1% Under CW Operation" *IEEE Elect. Lett.*, 31, 1995, 1288-89

Lucovski, G., "Relation of Si-H Vibrational Frequencies to Surface Bonding Geometry", *J. Vac. Sci. Technol.*, 18(5), 1979, 1225-28

Martin, P., *Personal Communication*, 1998

Martin, P., Fernandez, J.F. and Sanchez, C.R., "TDS Applied to Investigate the Hydrogen and Silane Desorption from Porous Silicon", *Physica Status Solidi A-Applied Research*", 182(1), 2000, 255-60

Maruska, H.P.,Namavar, F and Kalkhoran, N.M., "Theory of Porous Silicon Injection Electroluminescence", *Mat. Res. Soc. Symp. Proc.*, 283, 1993, 383-88

Memming, R. and Schmandt, G., "Anodic Dissolution of Silicon in HF Acid Solutions", *Surf. Science,* 4, 1966, 109 - 24

Memming, R., *Comprehensive Treatise on Electrochemistry* (eds. Convey, B.E., Bockris, J.O'M., Yeager, E., Khan, S.U.M..and White, R.E.), 7, Plenum, N.Y., 1983

Mimura, H., Futagi, T., Matsumoto, T., Ohta, Y., Kitamura, K. and Kanemitsu, "Electroluminescence from μc-SiC/Porous Si PN Junctions", *Mat.Res.Soc.Symp.Proc.*, 298, 1993, 385-90

Min, N.K., Kang, C.G., Jin, J.H., Ko, J.Y.and Kim, S.K., "Porous Silicon-based UV Detector", *J. of the Korean Physical Society*, 39, 2001, S63-S66

Misra, S.C.K.and Angelucci, R., "Polyaniline Thin Film Porous Silicon Sensors for the Detection of Microorganisms", *Indian Journal of Pure & Applied Physics*, 39,(11), 2001, 726-30

Morita, Y., Miki, K., Tokumoto, H., "Direct Observation of SiH_3 on a 1% HF-treated Si(111) Surface by Scanning Tunnelling Microscopy", *Appl.Phys.Lett.* 59(11), 1991, 1347-49

Muller, G.andBrendel, R., "Simulated Annealing of Porous Silicon", *Physica Status Solidi A-Applied Research*, 182(1), 2000, 313-18

Münder, H., Berger, M.G., Fronhoff, S., Lüth, H., Rossow, U., Frotscher, U. and Richer, W., "Degradation of Porous Silicon Layers Caused by the Thermal Treatment", *Mat. Res. Symp. Proc*, 283, 1993, 281-87

Nesbit, L.A., "Advances in Oxidised Porous Silicon for SOI", *Tech. Digest IEDM*, 1984, 800 - 04

Oates, A.S., and Kin, W., "Infrared Measurements of Interstitial Oxygen in Heavily Doped Silicon", *J. of Crys.Growth*, 89, 1988, 119-123

Ogata, Y., Niki, H., Sakka, T. and Iwasaki, M., "Hydrogen in Porous Silicon: Vibrational Analysis of SiH_x Species", *J. Electrochem. Soc.*, 142, 1995, 195 - 201

Oules, C., Halimaoui, A., Regalini, J.L., Herino, R., Perio, A., Bensahel and Bomchil, G., " Epitaxial Silicon Growth on Porous Silicon by Reduced Pressure, Low Temperature Chemical Vapour Deposition", *Mat. Sci. and Eng.*, B4, 1989, 435 -39

Oules, C., Halimaoui, J.L., Regolini, J.L., Perio, A. nd Bomchil, G., "Silicon on Insulator Structures Obtained by Epitaxial Growth of Silicon over Porous Silicon", *J. Electrochem. Soc.*, 139(12), 1992, 3595-99

Pajot,B., "Defects in Semiconductors", *Analysis*, 5, 1977, 293-95

Park, R.L., and Lagally, M.G., (eds.), *Solid state Physics : Surface,Methods of Experimental Physics,* vol.22, Academic Press., New York, 1985

Pascual, A., Fernandez, J.F., Sanchez, C.R., Manotas, S and Agullo-Rueda, F., "Structural Characterisation of p-yype Porous Silicon and Their Relation to the Nucleation and Growth of Pores", *J. of Porous Materials*, 9, 2002, 57-66.

Pavesi, L., Mazzoleni, C., Tredicucci, A. and Pelligrinni, V., "Controlled Photon Emission in Porous Silicon Microcavities" *Appl. Phys. Lett.*, 67, 1995, 3280-82

Pavesi, L., "Porous Silicon: A Route Towards a Si-Based Photonics" *Microelect.J.*, 27, 1996, 437-48

Petrova-Koch, V., Muschik,T., Kux, A., Meyer, B.K. and Koch, F., "Rapid-Thermal-Oxidised Porous Si-The Superior Photoluminescent Silicon" *Appl. Phys. Lett.*, 61, 1992, 943-45

Petrova-Koch, V., Kux,A., Muller, F., Muchik, T., Koch, F.and Lehmann,V.,"Composition and Morphology of Luminescent Porous Si", *Mat.Res.Soc.Symp.Proc.,* 256, 1992, 41-46

Pickering, C., Beale, M.I.J., Robbins, D.J., Pearson, P.J.,and Greef. R., "Optical Studies of the structure of PS Films formed in p-type Degenerate and Non-degenerate Silicon", *J. Phys. C: Solid State Phys.*, 17, 1984, 6535 - 52

Pietsch, G.J., Köhler, U. and Henzler, M., "Chemistry of Silicon Surfaces After Wet Chemical Preparation: A Thermodesorption Spectroscopy Study", *J. Vac. Sci. Technol.*, B12, 1994, 78- 87

Pliskin,W.A., "Comparison of Properties of Dielectric Films Deposited by Various Methods", *J.of Vac.Sci.Technol.*, 14(5), 1977, 1064-1081

Potzinger, P. and Lampe, F.W., "The Electron Impact Study of Ionisation and Dissociation of Monosilane and Disilane", *The J. of Phys.Chemistry*, 73(11), 1969, 3912-17

Prasad, A., Balakrishnan, S., Jain, S.K.and Jain, G.C., "Porous Silicon Oxide Anti-Reflection Coating for Solar Cells", *J. Electrochem Soc.*, 129, 1982, 596 - 99

Prokes, S.M., Glembocki, O.J., Bermudez, V.M.and Kaplan, R., "SiHx Excitation: An Alternative Mechanism for Porous Si Photoluminescence", *Phys. Rev. B*, 45, 13788-91

Prokes, S.M., "The Relationship of Structures and Surfaces to Light Emission Properties in Porous Silicon", *Porous Silicon,* (eds. Feng,Z.C. and Tsu, R.), World Scientific, Singapore, 1994, 275-300

Prutton, M., *Surface Physics*, Oxford Physics Series, Clarendon Press, Oxford, 1975

Rao, A.V., Ozanam, F. and Chazalviel, J.N. "In situ Fourier-Transform electro-modulated IR Study of Porous Silicon Formation: Evidence for Solvent effects on the Vibrational Linewidths", *J of Electrochem. Soc..*, 138(1), 1991, 153-59

Rao, A.V., Ozanam, F. and Chazalviel, J.N., "In-situ Infrared Study of the Silicon sueface in HF Electrolyte", *J.of Electron spectroscopy and Related Phenomena*, 54/55, 1990, 1215-18

Read, A.J., Needs, R.J., Nash, K.J., Canham, L.T.,Calcott, P.D.J. and Qteish, A., "First Principle Calculations of the Electronic Properties of Silicon Quantum Wires", *Phys Rev. Lett.*, 69, 1992, 1232-35

Redhead, P.A., "Thermal Desorption of Gases" *Vacuum,* 12, 1962, 203-11

Richter, A., Steiner, P, Kozlowski, F and Lang,W., "Current Induced Light Emission from a Porous Silicon Device", *IEEE Elect.Dev. Lett.*, 12, 1991, 691-92

Rittersma, Z.M., "Recent Achievements in Miniaturised Humidity Sensors-A Review of Transduction Techniques", *Sensors and Acutators A-Physical*, 96, 2002, 196-210.

Sabet-Dariani, R., Haneman, D., Hoffman, A. and Cohen, D.D., "Composition of Porous Silicon", *J. Appl. Phys.*, 73, 1993, 2321 - 25

Sabet-Dariani, R. and Haneman, D., "Heat-Treatment Effects on Porous Silicon", *Ibid*, 76, 1994, 1346 - 48

Sakurai, T. And Hagstrum, H.D, "Interplay of the Monohydride Phase and a Newly Discovered Dihydride Phase in Chemisorption of H on Si(100)2x1, Physics Review B, 14(4), 1976, 1593-98

Salonen, J., Lehto, V.P. and Laine, E., "Thermal Oxidation of Free-standing Porous Silicon films", *Appl.Phys.Lett.*, 70(5), 1997,637-39

Salonen, J, *Private Communications*, 1999

Sasaki, Y. and Kitahara, M., "Structure and Formation on Porous Silicon layers as Studied by Infrared Absorption and Raman Scattering", *J.Appl.Phys.*, 76(7), 1994, 4344 - 50

Seals, L., Gole, J.L., Tse, L.A., Hesketh,P.J., "Rapid, reversible, Sensible Porous silicon gas sensor", *J. of Appl.Phys.*, 91(4), 2002, 2519-23
Searson, P.C. and Zhang,X.G., "The Anodic Dissolution of Silicon in HF Solution", *J.Electrochem.Soc.*,137, 1990, 2539 - 46

Shane, S.F., Kolanski, K.W. and Zare, R.N., "Recombinative Desorption of H_2 on Si(100)-(2x1) and Si(111)-7x7: Comparison of Internal State Distributions", *J. Chem. Phys.*, 97(2) ,1992, 1520-30

Shane, S.F., Kolanski, K.W. and Zare, R.N., "Internal-state Distributions of H2 Desorbed from Mono- and dihydride Species on Si(100)", *J. Chem. Phys.*, 97(5) ,1992, 3704-09

Shriver, D.F. and Atkins, P.W., *Inorganic chamistry*, Oxford University Press, Oxford, 1999

Sinniah, K., Sherman,M.G., Lewis, L.B., Weinberg, W.H., Yates Jr. J.T. and Janda, K.C., "Hydrogen Desorption from monohydride Phase on Si(100)", *J.Chem.Phys.*, 92(9), 1990, 5700-11

Smestad, G., Kunst, M. and Vial, C. "Photovoltaic Response in Electrochemically Prepared Photoluminescent Porous Silicon", *Solar Energy Materials and Solar Cells*, 26, 1992, 277-83

Smith, R.L., Chuang, S.F. and Collins, S.D., "A Theoretical Model of the Formation Morphologies of Porous Silicon", *J. of Elect. Materials*, 17, 1988, 533-41

Smith, R.L. Chuang, S.F. and Collins, S.D., "Porous SiliconMorphologies and Formation Mechanism", *Sensors and Actuaors*, A21-23, 1990, 825-29

Smith, R.L, and Collins, S.D., "Porous Silicon Formation Mechanism", *J.Appl.Phys.*, 71(8), 1992, R1-R22

Sommer, L.H., "*Stereochemistry, Mechanism and Silicon*", McGraw Hill, New York, 1964

Somorjai, G.A. *Introduction to Surface Chemistry and Catalysis*, Wiley -Interscience, New York, 1994

Stark, J.G. and Wallace, H.G, "*Chemistry data Book*", 2nd Edition, John Murray (Publishers) Ltd. London, 1991, 24

Steiner, P., Richter, A. and Lang, W. "Using Porous Silicon as a Sacrificial Layer", *J. Micromech. and Microeng.*, 3, 1993, 32 - 36

Steiner, P.and Lang, W., "Micromachining Applications of Porous Silicon", *Thin Solid Films*, 255, 1995, 52 -58

Stulen, R.H., "Recent Developments in Angle-Resolved Electron-Stimulated Desorption of Ions from surfaces" *Prog. Surf. Science* ,32, 1989, 1-38

Sugiyama, H. and Nittono, O., "Characterisation of Porous Silicon Layers by Means of X-ray Double - Crystal Diffractometry", *ISIJ International*, 29, 1989, 223 - 28

Ibid, "Annealing Effects on Lattice Distortion in Anodised Porous Silicon Layers", *Jap. J. of Appl. Phys.*, 28, 1989, L2013-16

Ibid, "Microstructure and Lattice Distortion of Anodised Porous Silicon Layers", *J. of Cryst. Growth*, 103, 1990, 156-63

Takai, H. and Itoh, T., " Isolation of Silicon Film Growth on Porous Silicon Layers", *J. Elect. Materials* , 12, 1983, 973 - 82

Theunissen, M.J.J., "Etch Channel Formation during Anodic Dissolution of N- type Silicon in Aqueous Hydrofluoric Acid", *J. Electrochem. Soc.*, 119, 1972, 351-60

Thiel, P.A., Williams, E.D., Yates Jr., J.T. and Weinberg, W.H., "The Chemisorption of CO on Rh(111)", *Surf. Science,* 84, 1979, 54-64

Thomas, N.J., Davis, J.R., Keen, J.M., Castledine, J.G., Brumhead, D., Goul ding, N., Alderman, J., Farr, J.P.G., Earwaker, L.G., L'Ecuyer, J., Sturland, I.M. and Cole, J. M., "High Performance Thin-Film Silicon-on-Insulator CMOS Transisters in Porous Anodised Silicon", *IEEE Elect. Dev. Lett.*, 10, 1989, 129 - 31

Tinsley-Bown, A.M., Canham, L.T., Hollings, M., Anderson, M.H., Reeves, C.L., Cox, T.I., Nicklin, s., Squirrell, D.J., Perkins, E., HutchinsonA., Sailor,M.J.and Wun, A., "Tuning the Pore size and Surface Chemistry of Porous silicon for Immunoassays", *Physica Status Solidi A-Applied Research*, 182(1), 2001, 547-53

Tsai, C., Li, K.H., Sarathi, J. and Campell, J.C., Hance, H and White, J.M., "Thermal Treatment Studies of the Photoluminescence Intensity of Porous Silicon", *Appl. Phys. Lett.*, 59, 1991, 2814 - 16

Tsai, C., Li, K.H. and Campbell, J.C., "Rapid Thermal Oxidised Porous Silicon Photodetectors" *IEEE Elect. Lett.*, 29, 1993, 134-35

Tsao,S.S., "Porous Silicon Technologies for SOI Structures", *IEEE Circuits and Devices Magazine*, 1987, 3-7

Tsuo, Y.S., Heben, M.J., Wu, X., Xiao, Y., Moore, C.A., Verlinden, P. and Deb, S.K., "Photovoltaic Device Applications of Porous Silicon", *Mat.Res.Soc.Symp.Proc.*, 283, 1994, 405 - 10

Tsuo, Y.S., Xiao, Y. and Moore, C.A., "Device Applications of Porous and Nanostructured Silicon", *Porous Silicon* (eds. Feng, Z.C. and Tsu, R.), World Scientific, Singapore, 1994, 347 -62

Uhlir Jr., A., "Electrolytic Shaping of Germanium and Silicon", *The Bell Syst. Tech. J.*, 1956, 333 - 47

Unal, B., Parbukov, A.N.and Bayliss, S.C., "Photovoltaic Properties of a Novel Stain Etched Porous Silicon and Its application in Photosensitive devices", *Optical Materials*, 17(1-2), 2001, 79-82

Unigami, T. and Seki, M., "Structural Porous Silicon Layer and Heat-Treatment Effect" *J. Electrochem.Soc.*, 125, 1978, 1339 -44

Unigami, T., "Oxidation of Porous Silicon and Properties of its Oxide Film", *Jap. J. Appl. Phys.*, 19, 1980, 231 - 41

Ibid, "Formation Mechanism of Porous Silicon by Anodisation in HF Solution", *J.Electrochem.Soc.* , 127, 1980, 476 - 83

Vial, J.C., Bsiesy, A., Fishman, G., Gaspard, F., Herino, R., Ligeon, M., Muller, F., Romestain, R. and Macfarlane, R.M., "Radiative and Non-Radiative Processes for the Lighr Emission from Porous Silicon", *Mat.Res.Soc.Symp.Proc.*, 283, 1993, 241-47

Watanabe,S., Nakayama, N.and Ito, T., "Homogeneous Hydrogen-terminated Si(111) Surface Formed Using Aqoeous HF Solution and Water", *Appl.Phys.Lett.*, 59(12), 1991,, 1458-60

Williams, M.,Ezis, A., "Slip Casting of Silicon Shapes and their Nitriding", *Ceramic Bulletin* 62(5), 1983, 607-10

Wise, M.L., Koehler, B.G., Gupta,P., Coon,P.A. and George, S.M., "Comparison of Hydrogen Desorption Kinetics from Si(111)7x7 ans Si(100)2x1", *Surf. Science*, 258, 1991,, 166-76

Woodruff, D.P., and Delchar, T.A., *Modern Techniques of Surface Science*, Cambridge Solid State Science Series. Cambridge University Press. New York 1986

Xie, Y.H., Wilson, W.L., Ross, F.M., Mucha, J.A., Fitzgerald, E.A. and Macaulay, J.M. "Luminescence and Structural Study of Porous Silicon Films", *J. Appl. Phys.*, 71(5), 1992, 2403-07

Yamana, M., Kashiwazaki, N., Kinoshita, A., Nakano, T., Yamamoto, M. and Walton, C., "Porous Silicon Oxide Layer Formation by the Electrochemical Treatment of a Porous Silicon layer", *J. Electrochem. Soc.* , 137, 1990, 2925 -27

Yang, W.S., Jona, F. and Marcus, P.M., "Atomic Structure of Si (001) 2x1", *Phys. Rev.* B28, 1983, 2049-59

Yon, J.J., Barla, K., Herino, R. and Bomchil, G., "The Kinetics and Mechanism of Oxide Layer Formation from Porous Silicon Formed on p-Silicon Substrate", *J. Appl. Phys.*,62, 1987, 1042 -48

Yoshioka, S., "Investigation of the Chemical Properties of Stain Films on Silicon by means of Infrared Spectroscopy and Omegatron Mass analysis", *Philips Res.Repts.*, 24, 1969, 299-321

Young, I.M., Beale, M.I.J. and Benjamin, J.D., "X-ray Double Crystal Diffraction Study of Porous Silicon", *Appl. Phys. Lett.*, 46, 1985, 1133 -35

Young, D.M and Cromwell, A.D.,*Physical Adsorption of Gases* , Butterworths, London 1962

Yu, L.Z. and Wie, C.R., "Fabrication of MSM Photoconductor on Porous Silicon Using Micromachined Silicon Mask", *IEEE Elect. Lett.*, 28, 1992,911-13

Zhang, Shu-Lin, Wang, X., Ho, K.S., Li, J., Diao, P. and Cai, S., "Raman Spectra in a Broad Frequency Region of p- type Porous Silicon", *J. Appl. Phys.*, 76, 1994, 3016 -19

Zhang, X.G., Collins, S.D. and Smith, R.L., "Porous Silicon Formation and Electropolishing of Silicon by Anodic Polarisation in HF Solution", *J. Electrochem. Soc.*, 136, 1989, 1561 - 65

Zhao, G., Huang, Y. and Bao, M., "SOI Structure Pressure Transducer Formed by Oxidised Porous Silicon", *Sensors and Actuators*, A21 -A23, 1990, 840 -43

Zheng, J.P., Jiao, K.L., Shen, W.P., Anderson, W.A. and Kwok, H.S., "Highly Sensitive Photodetector Using Porous Silicon", *Appl.Phys.Lett.*, 61, 1992, 459-61

Zheng, X.M. and Smith, P.V., "Hydrogen Chemisorption on the Si(100) Surface", *Surf. Science*, 279, 1992, 127-36

Zhu, W.Y., Gao, Y.X., Zhang, L.Z., Mao, J.C., Zhang, B.R., Duan, J.D., and Qin, G.G. "Time Evolution of the Localised Vibrational Mode Infrared Absorption of Porous silicon in Air", *Super Lattices and Microstructures*, 12(3), 1992, 409-12

Zorinsky, E.J., Spratt, D.B. and Vurkus, R.L., "The "Islands" Method - A Manufacturable Porous Silicon SOI Technology", *IDEM Tech. Digest Papers*, 1986, 431 -34

Ibid, "The "Islands" Method: a VLSI Compatible SOI Technology", *IEEE SOS-SOI Workshop*, Captive Island, USA, 1986, 13-16

Zoubir, N.H., Vergnat, M., Delatour, T., Burneau, A. and de Donato,Ph., "Interpretation of the Luminescence Quenching in Chemically etched Porous Silicon by the Desorption of SiH_3 Species", *Appl.Phys.Lett.*, 65(1), 1994, 82-84

Zoubir, N.H. and Vergnat, M., "Thermal Desorption Spectroscopy Study of Chemically Etched Porous Silicon", *Appl. Surf.Science*, 89, 1995, 35-38

Appendix 1 Calculation of Thickness and Porosity of PS

The adapted method was described by Herino grouup, 1987. The Si wafer was weighed before and after anodisation. The PS layer was dissolved in 1M (molar) NaOH solution, rinsed in DI water and spin-dried. The wafer was weighed after this process. The following method was used for the calculation of the thickness etc.

The weight of the wafer before anodisation $= m_1$ g.

The weight of Si after anodisation $= m_2$ g.

The weight after NaOH strip $= m_3$ g.

The weight loss after the anodisation $= (m_1 - m_2)$ g.

The weight loss after the NaOH strip $= (m_2 - m_3)$ g.

Total loss of Si $= (m_1 - m_2) + (m_2 - m_3)$ g.

$= (m_1 - m_3)$ g.

Total volume of pores in PS layer (cm^3) = total Si loss / density of Si

$= (m_1 - m_3) / 2.33$

Thickness of porous layer = volume of Si / surface area of Si

$= (m_1 - m_3) / 2.33 \times 1/\pi r^2$

where, r is the radius of the anodised area.

$$\% \text{ porosity} = \frac{\text{loss of Si after anodisation}}{\text{total wt loss of Si}} \times 100$$

$$= (m_1 - m_2) / (m_1 - m_3) \times 100$$

Appendix 2 Gas - Solid Interactions

Introduction

When two immiscible phases are brought into contact, it is found that the concentration of one phase is greater at the interface than in its bulk. This phenomenon for accumulation to take place at the interface is called adsorption. The interfaces can exist between immiscible liquid- liquid, liquid-gas, solid-gas, solid-liquid and also between two immiscible liquids. This section deals only with the gas-solid interface as it is relevant to PS.

Structure of surface

Inspection of any crystal surface reveals large regions where atoms in parallel planes are separated by *ledges* (~10^4 Å high). This is due to a small mismatch of atomic planes called *dislocation*. Dislocation is a one-dimensional defect and exists in parallel planes. These parallel planes are called *terraces*. Most semiconductor materials show dislocation densities of the order of 10^4-10^6 cm^{-2} which are much lower than metals or ionic crystals which show 10^6-$10^8 cm^{-2}$ defects, because of their different bonding properties. The average surface concentration of atoms can be taken as of the order of 10^{15} cm^{-2} (Somorjai 1994). Thus each terrace may contain roughly $10^{15}/10^6 = 10^9$ atoms in a low dislocation density surface for a semiconductor.

During adsorption of atoms or molecules by substrate atoms (formation of chemical bonds), the surface atoms relocate along the surface to optimise the strength of adsorbate-substrate bonds. Adsorbate induced restructuring of the surface is found in many chemisorption situations. This is called reconstruction and leads to the formation of new and unexpected surface structure. The surface is therefore heterogeneous on the atomic scale and exhibits restructuring responding to its changing local environment.

On a macroscopic scale, a surface may be represented diagrammatically as a plane, the potential energy of which fluctuates from point to point. If the energy fluctuation is the same between any pair of sites and all the sites have the same energy, the surface is said to be homogeneous. If the fluctuation is irregular and the sites have different energies, the surface is heterogeneous. The nature of the surfaces is vital in understanding the mechanism of the processes that occur on the surface.

The adsorption - desorption processes

Adsorption is of practical significance in a wide variety of problems and processes. It is the first stage in the formation of an oriented overgrowth - epitaxial growth of thin films. The gas molecule or atom that is adsorbed on the solid surface is called an *adsorbate* and the solid surface is called *substrate* or *adsorbent.*

The adsorption process is generally exothermic, that is, it involves the evolution of heat. The general thermodynamic requirement for a reaction to proceed is that the free energy change (ΔG) for the reaction must be negative. The ΔG for the adsorption reaction can be written as :

$\Delta G = \Delta H - T\Delta S$

where ΔH is the enthalpy of adsorption and ΔS is the entropy change for the reaction

The translational freedom[1] of the adsorbate is reduced when it is adsorbed on to a substrate surface, ie, it loses one degree of freedom and there will be a decrease in entropy($-\Delta S$). Therefore, it can be seen from the above equation that the ΔH must be negative, ie, it is exothermic. Exceptions may occur if the dissociation of the adsorbate molecules produces highly mobile species on the surface of the substrate. The adsorption process is roughly divided into two categories:

1. Physisorption
2. Chemisorption

Physisorption

In physisorption, the adsorbate-adsorbate interactions are usually comparable in strength to the adsorbate-substrate interaction, all of which are dominated by van der Waals forces. The van der Waals type of bond involves no charge transfer from the substrate to the adsorbate or vice versa. This type of interaction can happen through dispersion or London force or/and dipolar interaction. Since this type of adsorption involves forces of physical attraction, it can be compared with those causing the liquefaction of gases. This is a long range but weak interaction and the energy released when a particle is physisorbed is of the same order of magnitude as the enthalpy of condensation. The values are of the order of 4-5kcals $mole^{-1}$. This is insufficient to break a bond so a

[1] There are three types of motion shown by molecules; translational, rotational and vibrational

physisorbed molecule retains its identity. The process of physisorption is nonspecific and any gas will adsorb on any solid under suitable circumstances.

Once the gas atom is adsorbed, the value of $\Delta H_{ads}/RT$ which is the ratio of the average bond energy, ΔH_{ads}, and the average thermal energy, RT, determines the residence time τ of the gas atom on the surface (Redhead 1962, 203-11).

$$\tau = \tau_0 . \exp(\Delta H_{ads}/RT)$$

where τ_0 is related to the period of a single atom vibration and is in the order of 10^{-13}s. For a weakly physisorbed condition, the residence time is of the order of magnitude of τ_0. In view of all the considerations discussed, physisorption is expected to occur only at relatively low temperatures.

Chemisorption

Chemisorption is the kind of adsorption process where chemical bonds (usually covalent) form between the surface atom and the adsorbate molecule. The adsorbate molecules tend to favour sites that maximise the co-ordination number with the substrate

Co-ordination number is the number of atoms immediately surrounding any selected atom.

Specificity and enthalpy of adsorption

In chemisorption, a high specificity is observed when the chemical bonds of adsorbate - substrate are formed. Gas-substrate interactions vary for different materials and also for different crystal planes of the same material. A gas molecule goes through a process of dissociation at the surface before it forms a surface bond with the dangling bonds of the surface atoms.

Physisorption is normally fast but it can be slow if adsorption is taking place in a porous medium. If the substrate is porous or possesses capillaries of a few angstroms in diameter, penetration of adsorbate atoms or molecules to the surface of the pore walls of the substrate may be an extremely slow process. This penetration may result in chemisorption but it may also be physical adsorption. Therefore, a slow rate of adsorption is by no means certain to be chemisorption.

It is very difficult to define the types of adsorption process as many factors influence these processes. Chemisorption ceases when the adsorbate atoms or molecule can no longer make direct contact with the surface atoms and is therefore a single layer process. With physical adsorption, no such limitation applies and under suitable conditions of temperature and pressure, physically adsorbed layers many molecules thick can be obtained. Therefore, if the extent of the adsorption is known to exceed a monolayer, it is certain that the second and higher layers at least are physically adsorbed.

Reconstruction of surfaces

This phenomenon is observed when a surface assumes an atomic structure that differs fundamentally from the observed bulk structure terminated abruptly on the surface. For semiconductor surfaces (Si, Ge, GaAs), which are covalently bonded, the surface atoms find it difficult to compensate for the loss of nearest neighbours. The dangling bonds that exist on the substrate surface cannot easily be satisfied except through rearrangement of these atoms. Therefore, most semiconductors reconstruct and major rebonding of the surface atoms occurs to relieve the forces of stress on the surface. This is called reconstruction. The associated perturbation propagates several atomic layers into the surface until the bulk lattice is recovered. Figure 23 is an schematic of a (2x1)

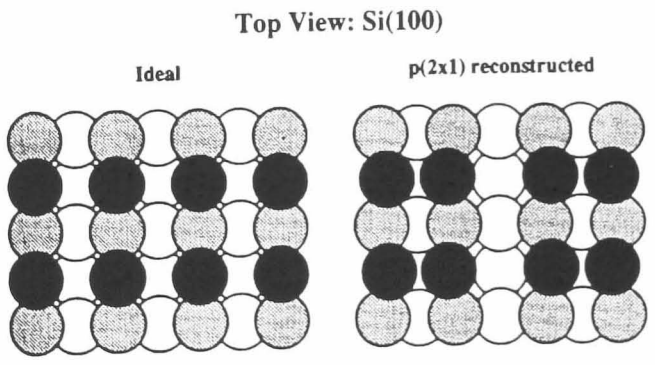

reconstructed Si (100) face and the ideal face as obtained by LEED surface technique. The outermost plane consists of buckled dimers and relaxation extends to three atomic layers in the bulk (Yang et al 1983).

Chemisorption often induces rearrangement of the substrate atom around the adsorption site. The formation of a strong adsorbate-substrate bond which is an exothermic process in the case of chemisorption provides the required energy for the restructuring.

Restructuring occurs in order to maximise the bonding and stability of the chemisorbed complex.

Sticking probability

The rate at which a surface is covered by adsorbate depends on the substrate's ability to dissipate the energy of an incoming particle as thermal motion when it collides with the surface. The proportion of collisions with the surface that successfully lead to adsorption is called the *sticking probability*, S. The sticking probability is defined as the ratio of the rate of capture of a molecule in the chemisorbed state to the rate of collision of the gaseous molecule with the surface. Sticking probabilities are rarely equal to unity and the following factors may be responsible for it:

Activation energy

If the chemisorption process goes through an activated process, then only the molecules with the necessary activation energy, E_a can be adsorbed.

The condition for an atom or molecule to chemisorb is that it must lose a certain amount of energy exceeding its original thermal energy during collision. This means that inelastic collision with sufficient energy transfer lead to chemical bond formation. However, this factor is important in a physisorption process as well. The physisorbed state is the precursor state through which chemisorption is believed to occur.

Collision with the occupied site

The molecule can be adsorbed into a weakly held second layer and migrate over the covered surface to the vacant site. It is possible that some such molecules can desorb before finding a vacant site, particularly at higher coverages. The process in which all molecules find a site will give a value of S independent of coverage. Conversely, weak physisorption produces dependency of S on the surface coverage. The S values decrease as the coverage increases.

Appendix 3 Desorption Spectroscopy

Introduction

The desorption of a molecule or atom is always activated as the adsorbed molecule or atom has to be raised from its adsorption potential well. The nature of the desorption process has fundamental implications in understanding the nature of elementary chemical processes on the surfaces and the specification of the bonding mechanism.

Desorption spectroscopy is based on supplying sufficient energy to the adsorbed species to desorb and characterise the desorbed species by some method. The heating of the substrate can be achieved by a laser, an electron beam, or by a resistive heater. Common desorption spectroscopy methods are:

a) Electron stimulated desorption(ESD)
b) Photon stimulated desorption(PSD)
c) Thermal desorption spectroscopy(TDS) or Temperature programmed desorption spectroscopy(TPD)

In all these methods the adsorbate-substrate system is heated and the desorbed molecules are detected *in situ* by a quadrupole mass spectrometer alone or with other surface analytical techniques. These techniques include low energy electron diffraction (LEED) and Fourier transform infrared spectroscopy (FTIR) and are used for the study of the substrate surface during the desorption processes. Only Temperature Programmed Desorption Spectroscopy is dealt in this section as it is relevant to this work.

Temperature Programmed Desorption Spectroscopy(TPD)

TPD is one of the most frequently used techniques in surface science. When an adsorbed layer on a substrate is heated resistively, the surface species desorb. The surface residence time (τ) of adsorbate molecules depends exponentially on temperature. This can be expressed by an Arrhenius type equation.

$$\tau = \tau_0 . \exp (E/RT) \qquad (1)$$

where τ_0 is residence time for a single atom in the potential well.
Maximum desorption occurs at a given temperature, T_p, characteristic of a particular adsorbate - substrate interaction.

Thermal desorption analysis can be carried out in two ways:

a) *Flash desorption,* in which the sample is heated rapidly, typically in seconds and all the gases are removed indiscriminately. The increase in partial pressure due to the desorption of gas is measured as a function of time with a sensitive mass spectrometer. The desorption rate should be higher than the pumping rate of the experimental vacuum system.

b) *TPD method* in which the heating is gradual and the desorption spectrum is more energy resolved. The desorption peak of the particular binding state appears as a peak rather than a plateau as in the case of flash desorption (Woodruff 1986).

Treatment of Experimental Desorption Data

A number of mathematical techniques are available in the literature to analyse and extract information from TPD spectra. Reviews are presented in references Park et al 1985, Woodruff et al 1986, de Jong et al 1990, King 1975 and Falconar et al 1983.

At least ten different procedures have been proposed in the literature for the evaluation of desorption parameters from TPD spectra (de Jong et al 1990, Falconar et al 1983). Most of the analytical techniques make some assumptions and the applications vary depending on the particular nature of the adsorbate-substrate system under consideration. An adsorption spectrum corresponds to a plot of desorption rate versus temperature or time. Most of the techniques use one or two data points from the spectrum, usually parameters such as peak temperature, peak height, half width or slope at the inflection points (Falconer et. al. 1983).

Six such methods were reviewed by the Falconer group but only Redhead's method (Redhead 1962) will be discussed in detail as it is the most appropriate method for the present work related to porous silicon.
The techniques discussed by Falconer group are :

- Heating rate variation
- Desorption rate isotherms
- Peak width analysis(CAW method)
- Skewness parameter analysis
- Shape index analysis
- Redhead's method

Redhead's Method

The rate of thermal desorption is usually described in terms of an Arrhenius expression which is given below:

$$- d\theta/dt = \nu\theta^x \exp(- E_d/RT) \qquad (2)$$

where θ is the surface coverage, x is the order of the desorption reaction (x = 0, 1 or 2), ν is the frequency factor and E_d is the energy for the desorption process. ν,the frequency factor is related to the number of collisions and to the fraction of collisions that have the correct geometry. The derivation of applicable relations between maximum peak temperature, T_p, the frequency factor, ν and the desorption energy E_d were carried out by Redhead (1962).

When a substrate - adsorbate is heated linearly from T_0 to T for time, t,

$T= T_0 + \beta t$

where β is the linear heating rate

$dT/dt = \beta$

$d\theta/dt = d\theta/ dT \,.\, dT/dt = \beta\, d\theta/dT$

substituting in eqn. (3),

$- d\theta/dT = \nu\, \theta^x/\beta \,.\, \exp(- E_d/RT)$

It was shown (Glasser 1985) that, for the fast pumping where the rate of pumping is much greater than the rate of evolution of gas, the amount of gas desorbed is directly proportional to the time or temperature. The shape of the peak depends on the order of the kinetics. A symmetrical curve about the peak temperature is observed for a second order reaction but not for the first order (Woodruff 1986).

Maximum desorption occurs at the peak position of the TPD curve, when

$d^2\theta/dT^2 = 0$

When equation (3) is differentiated with respect to temperature,

$- d^2\theta/dT^2 = \nu/\beta \{ x \theta^{x-1} . d\theta/dT \exp(-E_d/RT) + \theta^x E_d/RT^2 \exp (- E_d/RT) \} = 0$

The temperature at the peak pressure is the peak temperature T_p, and the following equation can be derived from the above equation:

$E_d/RT^2_p = \nu x \theta^{x-1}/ \beta . \exp(-E_d/RT_p)$ (3)

For the first order reaction, where $x = 1$,

$E_1/RT^2_p = \nu_1 / \beta. \exp(-E_1/RT_p)$ (4)

It can be seen that T_p is independent of initial coverage for the first order kinetics. This means that the series of desorption peaks at increasing coverage has the same T_p and the same full peak width at half maximum (FWHM).

When $x = 2$,

$E_2/RT^2_p = 2 \nu_2\theta_p / \beta. \exp(-E_2/RT_p)$ (5)

where θ_p is the coverage at T_p. There is a shift in peak temperature with coverage seen with second order desorption. Generally, a second order desorption curve is symmetrical about the peak temperature so that θ_p the surface coverage at T_p is just $\theta_o / 2$ where θ_o is the initial coverage.

$E_2/RT^2_p = \nu_2\theta_0 / \beta. \exp(-E_2/RT)$ (6)

So, for increasing coverages a series of desorption peaks whose maxima shift to lower peak temperatures is indicative of second order desorption kinetics.

There are some exceptional cases of first order desorption where the activation energy decreases as the coverage increases. When this happens, the peak also shifts to lower temperature at higher coverage. E_d values and ν values can be extracted from equation (4) for first and second order desorptions.

Evaluation of E_d

If a value of ν is assumed and a value for T_p is obtained experimentally, then E_d can be calculated from a single TPD curve using Redhead's method. A value of 10^{13} s^{-1} is commonly used for the frequency factor ν. The justification for this value arises from the assumption that the vibration of the surface bond is a prerequisite for a first order desorption process and the vibration frequency for a single bond is about 10^{13} s^{-1}. For

most desorption processes, the relationship between E_d and T_p is very nearly linear and approximated by Redhead (1962) as follows:

$$E_d = RT_p [(\ln \nu T_p/\beta) - 3.46] \qquad (7)$$

Deviations from equation (6) from the analytically correct expressions are within 1.5% provided that ν/β falls between 10^8 and 10^{13} K^{-1}. This equation is valid only for the first order desorption.

For a second order desorption, T_p depends on the surface coverage; θ_0 may be found from the area under the TPD curve and a plot of $\ln\theta_0 T_p^2$ as a function of $1/T_p$ will give a straight line with a slope E_d/R. However, it should be pointed out here that there are exceptional first order desorption processes with E_d dependent on coverage which is not the case in most first order processes. The second order desorption processes and the exceptional first order cases can be distinguished by a plot of $\ln\theta_0 T_p^2$ vs $1/T_p$ where the second order process with fixed E_d will give a straight line.

Determination of ν

If E_d is determined by another method, the value of ν can be calculated from the following equation which is derived from equation (4)

$$\nu_x = (E_d\beta / RT_p^2\theta_0^{x-1}) \exp(E_d/RT_p)$$

where order of reaction, x is 1 or 2. This is applicable to first and second order kinetics.

MISSING

PRINT

Presentations and Publications

1. Presentations to the collaborators' meetings 1991-1995 . The collaborators were:

   DERA, Malvern
   Imperial College
   Liverpool University
   Birmingham University
   Queen Mary and Westfield College

2. Presentation at the PSST-98 Conference at Mallorca, 1998 on "An investigation into Silane Evolution from Porous Silicon by Temperature Programmed Desorption Method".

3. A copy of the publication is included